MASTER'S DISSERTATION

A STUDY OF VCR MULTI-REEF REMNANT EXTRACTION IN THE CARLETONVILLE AREA

Johann Christoff Esterhuyse

A dissertation submitted to the Faculty of Engineering and Built Environment, University of the Witwatersrand, Johannesburg, in fulfillment of the requirements for the degree of Master of Science in Engineering. 2017

DECLARATION

I declare that this dissertation is my own unaided work. It is being submitted for the degree of Master of Science in Engineering to the University of the Witwatersrand, Johannesburg. It has not been submitted before for any degree or examination to any other University.

_____

J.C. Esterhuyse

_____ day of _____ year_____.

ABSTRACT

Even after years of mining, a vast gold resource remains in the Carletonville area of the Witwatersrand basin. Mining in this area nevertheless predates 1934 and the accessible ore-reserves on the primary reefs are being depleted. Mining of secondary reefs and remnants has therefore become important in recent years. Of particular interest is multi-reef mining as it will become much more prevalent in this part of the gold mining industry. Very little rock engineering research on multi-reef mining scenarios at great depth is available in the literature. Owing to the lack of proper understanding and guidelines for remnant selection and extraction in a multi-reef environment, a study was conducted by the author of this dissertation. The key references of earlier work are discussed in the literature survey.

This study compared two displacement discontinuity boundary element codes, MINSIM and TEXAN, to simulate multi-reef environments. The preliminary analysis proved to be valuable and indicated that a small middling with a large overlap of mining is required to achieve a significant effect on ERR and average pillar stress on the remnant pillar. Care should be exercised with the so-called “45° rule” when destressing pillars and modelling is required in all cases. The study found that there is no significant difference between the results obtained from the two numerical modelling codes.

To better understand the process of understoping, a simplified geometry of a pillar being understoped was investigated. An analysis of the incremental stress evolution in the middling between two reef horizons, as the pillar was being incrementally understoped, revealed valuable information. A zone of very high major principal stress and low minor principal stress develops between the two reefs. This indicates a high risk of violent shear failure between the two reefs. The reason for successful historic extractions of actual multi-reef remnants was therefore explored in more detail.

As part of this analysis, an “extended” ERR concept introduced by Napier in 1991, was investigated. It was found that bedding planes and lithology played a crucial part in the stable dissipation of energy in these multi-reef remnant geometries. The study indicated that the stope convergence and the various energy components are affected by the presence, position and properties of a bedding plane. The energy solutions are very complex and sometimes counterintuitive. Care should be exercised when modelling specific cases. The modelling was nevertheless valuable to indicate that energy dissipated on weak layers, such as bedding planes, may reduce the risk of violent failure in a multi-reef mining scenario. This is an important novel contribution of this study.

As a further step, actual multi-reef remnants were selected and back analysed to verify the hypothesis of weak layers being useful to make multi-reef mining less hazardous. Aspects such as seismic history, numerical modelling and photographic records were studied. From the analysis it was found that multi-reef extraction was successful in cases where a weak rock type was present in the immediate stratigraphy or where pertinent bedding planes were found. This supported the hypothesis as presented above.

An important practical outcome of this study is that much greater emphasis needs to be placed on studying the rock mass surrounding multi-reef environments at depth to determine the risk of extraction in these conditions. This should be added to the list of remnant selection criteria.

ACKNOWLEDGEMENTS

I would like to thank Professor Francois Malan for all the guidance and support he has given me, as well as for the time that he invested in this study, because without it this study would not have been possible.

I would also like to thank Mine A for the opportunity to use the data and information presented in this dissertation.

TABLE OF CONTENTS

DECLARATION ii
ABSTRACT iii
ACKNOWLEDGEMENTS v
TABLE OF CONTENTS vi
LIST OF FIGURES viii
LIST OF TABLES xviii

1. INTRODUCTION
1.1. Background 1
1.2. Objective and Scope 3
1.3. Methodology 3
1.4. Overview of Dissertation 4

2. LITERATURE REVIEW
2.1. Mining in the Witwatersrand 5
2.2. Geological setting of the Witwatersrand 8
2.3. Pillar and Remnant Mining 13
2.3.1. Period up to 1952 13
2.3.2. Research in the period from 1952 up to 1995 15
2.3.3. Research from 1996 onwards 19
2.4. Factors influencing remnant stability 20
2.5. Conventional acceptable risk methodology 24
2.6. Deep level multi-reef mining and de-stressing 30
2.7. Operations at Mine A 37
2.8. Example of current remnant precautions at Mine A 43
2.8.1. Work area classification 48

3. COMPARISON OF CODES TO SIMULATE MULTI-REEF MINING
3.1. Numerical modelling codes 51
3.2. Effect of element size on APS 53
3.3. General layout for a multi-reef comparison 57
3.4. Results from the simulations 59
3.4.1. Middling 59
3.4.2. ERR values and the process of understoping 62
3.5. Conclusions and recommendations 66

4. INVESTIGATING MULTI-REEF MINING USING AN EXTENDED ERR CONCEPT
4.1. Stress analysis of multi-reef mining using TEXAN 67
4.2. Analysis using an extended ERR concept 72
4.3. Examples and hypothesis for the mechanism of successful understoping 74
4.4. Summary 85

5. CASE STUDY AND BACK ANALYSIS OF REMNANT A: (VC25-23) 86

6. CASE STUDY AND BACK ANALYSIS OF REMNANT B: (VC22-30) 119

7. CASE STUDY AND BACK ANALYSIS OF REMNANT C: (VC20-31) 146

8. CASE STUDY AND BACK ANALYSIS OF REMNANTS D and E 169

9. CONCLUSIONS AND RECOMMENDATIONS
9.1. Conclusions 177
9.2. Recommendations 181
9.3. Future work 182

REFERENCES 184

APPENDIX A 190

APPENDIX B 216

APPENDIX C 237

LIST OF FIGURES

Figure	Page
2.1.1 The Witwatersrand ridge. The Witpoortjie waterfall is visible in this photograph (after Viljoen, 2009).	6
2.1.2 The discovery site with the outcrop of the Main Reef Leader (MRL) and Main Reef (MR) visible (after Viljoen, 2009).	6
2.1.3 The Langlaagte discovery site during 1886 and at present (after Viljoen, 2009).	7
2.2.1 Schematic of the deposition of the Witwatersrand Basin (after Wilson and Anhaeusser, 1998).	8
2.2.2 Geological map showing the principal gold fields (after Wilson and Anhaeusser, 1998).	10
2.2.3 Location of mines in and around the Central Rand (after Wilson and Anhaeusser, 1998).	11
2.2.4 Location of mines in the West Wits Line (after Wilson and Anhaeusser, 1998).	12
2.3.1 Layout of a typical gold mine (after Cook et al., 1966). Note the remnants illustrated in the diagram.	13
2.3.2 Types of abutments (after Stacey et al, 2006).	17
2.4.1 Typical continuous stope closure of a VCR panel (after Malan, 1999).	23
2.5.1. Risk evaluation process (after Stacey et al, 2006)	27
2.5.2 Schematic indicating a risk estimation process (after Rangasamy et al, 2003).	29
2.6.1 Conditions encountered when mining of a secondary reef (after Jager and Ryder, 1999).	30
2.6.2 De-stressing of the VCR by understoping (after Du Plessis and Talu, 1997).	33
2.6.3 The Hennings method (after Du Plessis and Talu, 1997).	34
2.6.4 Stress changes when approaching a pillar (after Singh et al, 2005).	36
2.7.1 Typical layout of an underground gold mine (after Hoover, 1909).	38
2.7.2 Section through some of the Mine A shafts (after Anon., 2012).	39

2.7.3 Generalised stratigraphy at the Mine A operations (after Anon., 2012). 40
2.7.4 Simplified geomorphological model indicating the slope terrace model (after Wilson and Anhaeusser, 1998). 41
3.2.1 Cross-section of two parallel sided panels with a central pillar. 53
3.2.2 Average stress acting on a central pillar compared to grid size. 55
3.2.3 Layout used for the circular pillar analysis (after Napier and Malan, 2011). 56
3.2.4 Average stress acting on a circular pillar compared to grid size. 56
3.3.1 Geometry used for the initial simulations (A similar geometry has been used by Napier and Malan, 2011). 58
3.3.2 The extent of the understoping of the first pillar. 58
3.3.3 Sequence of understoping the first pillar. 59
3.4.1 Schematic section illustrating the “45° rule”. 60
3.4.2 MinSim screenshot of the modelled layout. 61
3.4.3 Effect of middling on the stress on Pillars 1 and 2. Both the MinSim and TEXAN results are shown. 61
3.4.4 MinSim screenshot of the modelled layout. 62
3.4.5 ERR of the understoping face when mined incrementally below Pillar 1. 63
3.4.6 ERR on Pillar 1 while it is being incrementally extracted. This shows scenarios for when the pillar is understoped and not understoped. 64
3.4.7 APS of Pillar 1 while it is being incrementally understoped. 65
4.1.1 Major principal stress below the VCR Pillar 1 prior to any mining on the Libanon Reef. The region of very high principal stress is found at the edge of the pillar, but confined to localised regions. The stress convention is compressive stresses are negative. 68
4.1.2 Major principal stress below the VCR Pillar when the Libanon Reef stope is below the first pillar abutment. The disruption of the stress field is minor at this stage. 68

4.1.3 Major principal stress below the VCR Pillar when the Libanon Reef stope face is halfway below the VCR pillar. Note the region of very high principal stress between the edges of the two stopes. 68

4.1.4 Major principal stress below the VCR Pillar when the Libanon Reef stope position is below the second VCR abutment. The region of very high principal stress between the edges of the two stopes persists at this stage. The average stress in a 3 m wide vertical zone between the edges of the two stopes is 395 MPa. 69

4.1.5 Major principal stress below the VCR Pillar when the understoping is complete. The regions of high principal stress have disappeared and it is clear that mining on the VCR pillar will now occur in a lower stress regime. Above the centre of the Libanon Reef stope, a large region of tensile stress has developed. 69

4.1.6 Minor principal stress in the middling between the two reefs when the Libanon stope crosses the second VCR abutment. Note the low minor principal stress above the active Libanon face, forming an additional tensile region. 70

4.1.7 Large seismic events generated when the Middelvlei Reef mining approaches the Carbon Leader Reef abutments. Events as large as M3.1 was generated and for this geotechnical area it seems as if it will be difficult to do understoping of remnants safely. This behaviour is supported by the modelling described above. 71

4.3.1 Cumulative released energy during the understoping at a 30 m middling with the presence of a strong bedding plane. DWRT is the TEXAN notation for ΔW_R. This is the "extended" ERR and higher values would indicate more hazardous conditions. 75

4.3.2 Cumulative released energy during the understoping at a 30 m middling with the presence of a weak bedding plane. DWRT is the TEXAN notation for ΔW_R. This is the "extended ERR" and higher values would indicate more hazardous conditions. 76

4.3.3 Cumulative released energy during the understoping at a 30 m middling. This is parameter ΔW_R in equation 4.2.4. This is the

"extended" ERR and higher value would indicate more hazardous conditions. 77

4.3.4 Cumulative work done during the understoping at a 30 m middling. This is parameter ΔW in equation 4.2.4. 77

4.3.5 Cumulative strain energy during the understoping at a 30 m middling. This is parameter ΔU in equation 4.2.4. 78

4.3.6 Cumulative dissipated energy during the understoping at a 30 m middling . This is parameter ΔW_D in equation 4.2.4. 78

4.3.7 Major principal stress during the understoping at a 30 m middling. 80

4.3.8 Minor principal stress during the understoping at a 30 m middling. 80

4.3.9 Major principal stress with bedding plane in the hangingwall of the VCR reef during the understoping at a 30 m middling. 81

4.3.10 Minor principal stress with bedding plane in the hangingwall of the VCR reef during the understoping at a 30 m middling. 81

4.3.11 Energy released (ΔW_R) during the understoping at a 60 m middling. 82

4.3.12 Energy released (ΔW_R) during the understoping at a 90 m middling. 82

4.3.13 Work done (ΔW) during the understoping at a 30 m middling. 83

4.3.14 Energy released (ΔW_R) during the understoping at a 30 m middling. 84

5.1 Locality plan view of the VC25-23 area. The VCR target areas are indicated by the black outline. The blue areas are mined VCR and the purple is mining on the Libanon reef. 87

5.2 1:200 Plan view of the LI25-23A stope. The black line indicates the mined Libanon Reef (mining planned on the Libanon) and the red line indicates the VCR pillars. 88

5.3 Simplified section through the VC25-23 depicting multiple reef bands and the inclined access ways. 89

5.4 Plot of all events greater than M_L0.0 in a 300 m radius. 90

5.5 Activity rate in the VC25-23 area. 92

5.6 Hourly distribution of events in the VC25-23 area. 93
5.7 Annual energy release for the VC25-23 area. 93
5.8 Cumulative seismic moment of the VC25-23 area for 8 years. 94
5.9 Summary of the seismic events in the VC25-23 area. 94
5.10 Seismic response to production of the VC25-23 area. 95
5.11 Number of seismic events compared to cumulative production of VC25-23. 96
5.12 Magnitude distribution of seismicity in the VC25-23 area. 97
5.13 Seismic statistics of the VC25-23 area. 98
5.14 Comparative plot of the number of seismic events and production statistics of the VC25-23 area. 98
5.15 Plot of production and seismic magnitude statistics of VC25-23. 99
5.16 Photograph depicting the shale footwall below the LI 25-23 Libanon stope (courtesy of D.F. Malan). 100
5.17 Condition of the shale footwall in the LI25-23 stope (courtesy of D.F. Malan). 101
5.18 Condition of the quartzite hangingwall in the LI25-23 stope (courtesy of D.F. Malan). 101
5.19 Condition of the quartzite hangingwall adjacent to the face of the LI25-23 stope (courtesy of D.F. Malan). 102
5.20 Condition of the quartzite hangingwall, where the bedding planes were exposed in the back area of the LI25-23 stope (courtesy of D.F. Malan). 102
5.21 Condition of quartzite between the two reef elevations as seen in the sidewall of a newly developed ore pass. The observed movement and dilation contributes to the energy dissipated as described in Chapter 4.3 (courtesy of D.F. Malan). 103
5.22 Unravelling of the hangingwall in the back area of the Libanon where the VCR overstoping was completed. This damage can be attributed to the tensile zone as seen in the modelling illustrated in Figure 4.1.5 (courtesy of D.F. Malan). 103
5.23 Sequenced layout for the modelling of VC25-23. 104

5.24 Outline of the modelled layout of the VC25-23, prior to mining (2006) 105
5.25 ERR results indicating the effect of the de-stressing at LI25-23. 107
5.26 ERR values of an area at the VC25-23 stope before understoping the VCR. The VCR stope is shown in green while the modelled mining face of the Libanon reef is shown by the ERR values. 108
5.27 ERR values of an area at the VC25-23 stope after understoping the VCR. The VCR stope is shown in green while the modelled mining face of the Libanon reef is shown by the ERR values. 108
5.28 Stress contour plot indicating the location of on-reef sections for a modelled layout on the VCR elevation. The green shows the mined VCR, the blue lines shows the modelled VCR faces and the dotted black lines shows the modelled Libanon mining. 109
5.29 Plot of the stresses along section A- A' on the VCR elevation. 109
5.30 Plot of the stresses along section B- B' on the VCR elevation. 110
5.31 Average ERR and cumulative production comparison for the 25-23 area. 111
5.32 Location of an analysed dip section on the Libanon reef elevation. 112
5.33 Location of an analysed strike section on the VCR reef elevation. 112
5.34 Contour plot of the major principal stress prior to any mining on the Libanon reef. 113
5.35 Contour plot of the principal stress during the understoping. 114
5.36 Contour plot of the principal stress during the continued understoping on the Libanon reef. 114
5.37 Contour plot of the principal stress during the completion of the de-stress mining on the Libanon reef. 115
5.38 Contour plot of the principal stress on strike before mining on the Libanon reef. 115
5.39 Contour plot of the principal stress on strike during the introduction of the mining on the Libanon reef. 115
5.40 Contour plot of the principal stress on strike when mining on the Libanon reef is halfway underneath the pillar. 116

5.41 Contour plot of the principal stress on strike during the continued de-stress mining on the Libanon reef. 116
5.42 Contour plot of the principal stress on strike during the completion of the de-stress mining on the Libanon reef. 116
5.43 Contour plot of the principal stress on strike during the de-stressed mining on the VCR reef. 117
6.1 Locality plan view of the VC22-30 area. 119
6.2 Stoping plan view of a portion of the VC22-30 stope. 120
6.3 Simplified section through VC22-30 depicting the waste cut access way. 121
6.4 Plot of all events greater than M_L0.0 in a 300 m radius around the VC22-30 area. 123
6.5 Hourly distribution of events in the VC22-30 area. 124
6.6 Activity rate in the VC22-30 area. 125
6.7 Seismic energy release per year of the VC22-30 area. 126
6.8 Cumulative seismic moment of the VC22-30 area for 2 years. 127
6.9 Summary of the seismic events in the VC22-30 area. 127
6.10 Seismic response to production of the VC22-30 area. 128
6.11 Number of seismic events compared to cumulative production of VC22-30. 128
6.12 Magnitude distribution of seismicity in the VC22-30 area. 129
6.13 Seismic statistics of the VC22-30 area. 129
6.14 Comparative plot of the number of events and production for the VC22-30 area. 130
6.15 Plot of production and seismic magnitude data for VC22-30. 130
6.16 Closure measurements in the VC22-30 area. 131
6.17 Travelling way developed in the shale below the VC22-30 area. 133
6.18 Inclined development to reef in the VC22-30 area. 134
6.19 On reef hangingwall conditions at the understoped VC22-30. 135
6.20 Hangingwall conditions of the ground that was not understoped in the VC22-30 area. 136
6.21 Outline of the modelled layout of the VC22-30 area. 137
6.22 Sequenced layout for the modelling of VC22-30 area. 137

6.23 ERR results indicating the effect of the de-stressing at VC22-30. 138
6.24 Location of on reef sections for a modelled layout. 138
6.25 Plot of stress along section A-A'. 139
6.26 Plot of the stress along section B- B'. 139
6.27 Slickensided movement along the 20 m fault. 140
6.28 Mining sequence of VC22-30. 140
6.29 ERR and cumulative production comparison for VC22-30. 141
6.30 Position of an apparent dip section of the VC22-30 area. 142
6.31 Contour plot of the principal stress prior to any mining on the de-stressing cut. 143
6.32 Contour plot of the principal stress during the understoping. 143
6.33 Contour plot of the principal stress during the continued understoping on the de-stressing cut. 143
6.34 Contour plot of the principal stress during the mining of the VCR in the understoped area. 144
6.35 Contour plot of the principal stress during the mining of the VCR in the understoped area. 144
7.1 Locality plan view of the VC20-31 area. 146
7.2 Plan view of the VC20-31 stope. The outline of a portion of the waste cut is indicated by the blue line. 147
7.3: Simplified section through the VC20-31 depicting the waste cut access way. 148
7.4 Plot of all events greater than M_L0.0 in a 300 m radius around VC20-31. 149
7.5 Activity rate of the VC20-31. 150
7.6 Hourly distribution of events at the VC20-31. 150
7.7 Cumulative seismic moment of the VC20-31 area for 2 years. 151
7.8 Summary of the seismic events in the VC20-31 area. 151
7.9 Seismic response to production of the VC20-31 area. 152
7.10 Number of seismic events compared to cumulative production of VC20-31. 152
7.11 Magnitude distribution of seismicity in the VC20-31 area. 153

7.12 Seismic statistics of the VC20-31 area. 153
7.13 Production and the number of events of the VC20-31 area. 154
7.14 Production and the Mmax in the VC20-31 area. 154
7.15 Number of events and production comparison for VC20-31. 155
7.16 Closure measurements in the VC20-31 area. 155
7.17 Ground conditions in an inclined travelling way into the VC20-31 area. 157
7.18 Ground conditions of an inclined travelling way to reef at VC20-31. 157
7.19 Inclined development to reef in the VC20-31 area. 158
7.20 Fall of ground in the inclined travelling way below the VC20-31 area. 159
7.21 Hangingwall conditions of the ground not de-stressed in the VC20-31 area. 160
7.22 Ground conditions of the hangingwall and face of the de-stressed ground in the VC20-31 area. 161
7.23 On reef hangingwall conditions in the de-stressed area of VC20-31. 161
7.24 Outline of the modelled layout of the VC20-31. 162
7.25 Sequenced layout for the modelling of VC20-31. 163
7.26 ERR results indicating the effect of the de-stressing at VC20-31. 164
7.27 Positions of sections for the modelled layout. 164
7.28 Plot of the stresses along section A- A'. 165
7.29 Plot of the stresses along section B- B'. 165
7.30 ERR and cumulative production plot for VC20-31. 166
7.31 Location of a section on the waste cut at VC20-31. 166
7.32 Contour plot of the major principal stress prior to any mining on the waste cut. 167
7.33 Contour plot of the major principal stress during the understoping. 167
7.34 Contour plot of the major principal stress during the continued understoping on the waste cut. 167
6.35 Contour plot of the major principal stress during the mining of the VCR through the abutment of the understoped area. 168

6.35 Contour plot of the major principal stress during the continued mining of the VCR past the abutment of the waste cut. 168
8.1 Locality plan of the KL23-48 stope. 170
8.2 Locality plan of the MB 24-43 stope. 170
8.3 Plot of recorded seismic activity at KL23-48. 171
8.4 Plot of recorded seismic activity at MB24-43. 171
8.5 Indication of historic seismic activity at KL23-48. 172
8.6 Indication of historic seismic activity at MB24-43. 172
8.7 Seismic statistics of the KL23-48 area. 173
8.8 Seismic statistics of the MB24-43 area. 173
8.9 ERR plot of Kl23-48 area on the Kloof reef elevation. 174
8.10 ERR plot of the Main reef elevation at MB24-43 area. 174
8.11 ERR plot of the MB24-43 area on the Carbon leader elevation. 174
8.12 Rock properties of Stratigraphic profiles found in the Carletonville area. a- Main Reef, b- MVR and Carbon leader, c- VCR and d- Vaal Reef (after Schweitzer and Johnson, 1997). 176

LIST OF TABLES

Table	Page
3.1. Numerical modelling parameters used in the numerical codes.	54
3.2. Numerical modelling parameters used in the numerical codes.	57
4.3.1 Energy components during the understoping at a 30 m middling for the last step.	79
4.3.2 Closure and energy parameters for a stiff system.	84
8.1 Summary of the seismic events in the KL23-48 area.	172
8.2 Summary of the seismic events in the MB24-43 area.	173
8.3 Rock strengths at Mine A.	175

CHAPTER 1

INTRODUCTION

"*You ask me my opinion with regard to the future? Well I am not a clairvoyant. But I regard the outlook a bright one. South Africa is one of the wealthiest and most fortunate countries of the world. We are lucky to be living here!"* (Albu Bart, 1935)

1.1. BACKGROUND

The discovery of the world's largest gold deposit in South Africa had a profound impact on the country's economy. It assisted with the development of the most advanced and one of the largest economies in Africa. Even today, South Africa is one of the leading mineral producing countries in the world. The production of precious metals accounts for more than 50% of the South Africa's exports (This is Gold, 2015).

As the accessible ore-reserves are diminishing and the value of the remaining resources increases in line with the higher gold price (in Rands), it is clear that remnant mining is a topical issue in the South African gold mining industry. There is currently a significant potential to include some of the remaining remnants in the reserve base of the mines.

A 2012 study by the Department of Mineral Resources indicates that South Africa's gold reserves are worth 3.29 Trillion Rand (SAPA, 2012). Situated within the heart of the Witwatersrand basin is the Carletonville mining area. Mining in the Wits Basin precedes 1886 and more than 2.0 billion ounces of gold has already been extracted from the mines in this area (This is Gold, 2015).

According to Jager and Ryder (1999), a remnant is an unmined block of ground surrounded by extensive mining, while a pillar is an isolated block of ground. Pillars are generally left for one or more of the following purposes – barrier,

boundary, bracket, buttress, crush, dip, in-panel, non-yield, stabilizing or water barrier.

The majority of the current remnants or pillars are the result of rock engineering designs to control Energy Release Rates (ERR) and seismicity. In the past, grade and mining conditions mostly dictated the mining layout.

To ensure the required levels of safety, the risk involved with mining a specific remnant should be identified and evaluated. Since the early 1900s, the risk of mining remnants has been recognised and various guidelines has been published. However, these publications only provided general guidelines and hence the fundamental question of which remnants can be safely extracted is still not clear. This requires specific local knowledge, usually passed on between practitioners, in-depth analyses as well as site investigations. As a further complication, very few of the guidelines are related to the extraction of multi-reef remnants.

Up to a quarter of the current mining at the Mine A operations in the Carletonville area can be classified as remnant mining. A substantial portion of the remnant mining as well as proposed mining on secondary reefs would classify as multi-reef mining. To better understand multi-reef pillar extraction, a literature review was conducted followed by numerical analysis and back analysis of successfully extracted remnants at this mine.

In general, a significant amount of literature is available on pillar mining and pillar mining guidelines owing to the increasing numbers of remnants being extracted. When the available information is assessed, it is clear that very little practical guidelines are given with respect to multi-reef remnants.

1.2. OBJECTIVE AND SCOPE

Owing to the lack of current multi-reef remnant selection criteria, the objective of this dissertation was to develop a better understanding of multi-reef remnant extraction, the effect of using a de-stressing cut and when another mined reef band is present. It also investigated the use of ERR, as well as an extended generalised ERR concept as part of the tools to provide improved pillar analysis techniques.

To meet these objectives, the following items were investigated:

- Past and current definitions and regulations
- Current methods of ensuring safe remnant extraction
- The value of ERR and other concepts computed using numerical modelling
- Back analysis of extracted remnants

1.3. METHODOLOGY

- Literature survey

  A literature survey was conducted to investigate successful extraction as well as past and current definitions and regulations. This was useful to better understand the extracting of multi-reef remnants.
- Theoretical concepts derived from numerical modelling

  A basic understanding of the value of numerical modelling codes as well as the extended ERR concept was obtained in this step.
- Back analysis

  Historic multi-reef remnant extractions were analysed, comparing physical conditions observed with simulated conditions.
- Use of the de-stressing mining cut and multi-reef mining was investigated. This work focused on:
  - Numerical modelling: This step compared the modelling results and the successfully extracted remnants in the area.

  - Monitoring: In order to compare the results of the numerical modelling to the prevailing underground conditions, monitoring data was analysed.

- Recommendations for multi-reef remnant selection and extraction

  The results obtained during this study were analysed to investigate if significant parameters can be identified that can assist with improved multi-reef extraction.

1.4. OVERVIEW OF DISSERTATION

The discovery of gold in South Africa had a big impact on the country and its economy. Owing to the diminishing accessible ore reserves, remnant mining and multi-reef remnant mining in particular, will become a significant part of future gold mining. The dissertation topic was chosen as almost no literature is available on specific practical guidelines as to the selection or assessing of multi-reef remnants. Chapter 1 deals with some background, the problem statement and methodology. Chapter 2 is a literature survey that deals with aspects relevant to mining in the Witwatersrand, geological setting and historic mining. The focus topics namely pillars, remnants and multi-reef mining are also discussed in this chapter.

Chapter 3 focuses on numerical modelling. This chapter gives a history and comparison of numerical modelling codes readily available to conduct multi-reef analysis. Chapter 4 continues with the numerical analysis and describes the Extended ERR concept. This concept builds on one of the most common design criterion used since the 1960s. The concept is then applied to number of theoretical scenarios. Chapters 5 to 8 seek comparisons between underground observations to the numerically modeled concepts shown in Chapter 4. The study is summarised in Chapter 9 where the recommendations and future work is noted.

CHAPTER 2
LITERATURE REVIEW

2.1. MINING IN THE WITWATERSRAND

The deposits of the Witwatersrand Basin are one of the most important gold mining districts in the world. It is a major contributor to sustained economic growth in South Africa. In Sir John Barrow's journey to Leerakoo in 1806, a map was published that indicates "high mountains supposed to contain gold". Very little is recorded on any further discoveries or mining until the late - 1800s (Letcher, 1936). Mining activities of vein quartz only commenced in 1885 by Fred and Henry Struben on the farms Zwartkranz, Sterkfontein and Wilgespruit along a prominent quartzite ridge known as the "Witwatersrand" (Wilson and Anhaeusser, 1998).

During 1885, two wanderers, George Harrison and George Walker, were employed to erect a stamp mill for Fred Struben and build a house on the farm Langlaagte (Viljoen, 2009).

These two recognized the gold bearing nature of the conglomerate on the farm, which eventually became known as the Main Reef Leader. The Langlaagte farm was initially 2260 morgen, but was subdivided by the granting of prospecting rights. The farm and ownership changed numerous times as the prospecting continued (Wilson and Anhaeusser, 1998). Eventually, the land was consolidated and sold off to the Johannesburg Consolidated Investment Co.Ltd. (JCI) during 1915.

President Kruger officially opened the Witwatersrand goldfields in September 1886 by proclaiming nine farms along the quartzite ridge as public gold diggings (Wilson and Anhaeusser, 1998).

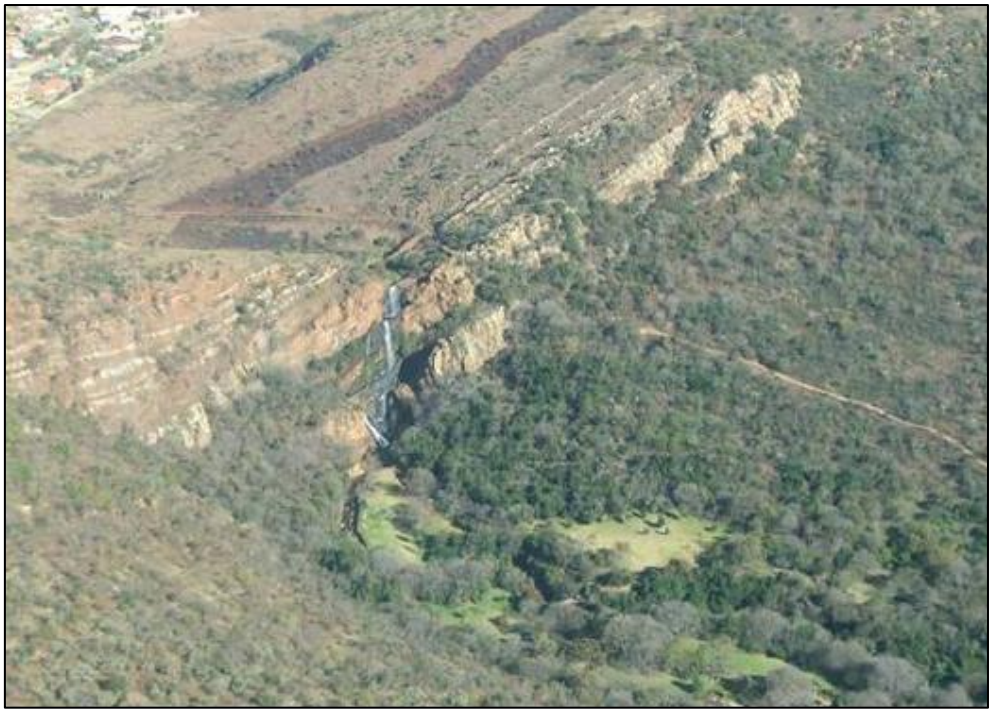


Figure 2.1.1 The Witwatersrand ridge. The Witpoortjie waterfall is visible in this photograph (after Viljoen, 2009).

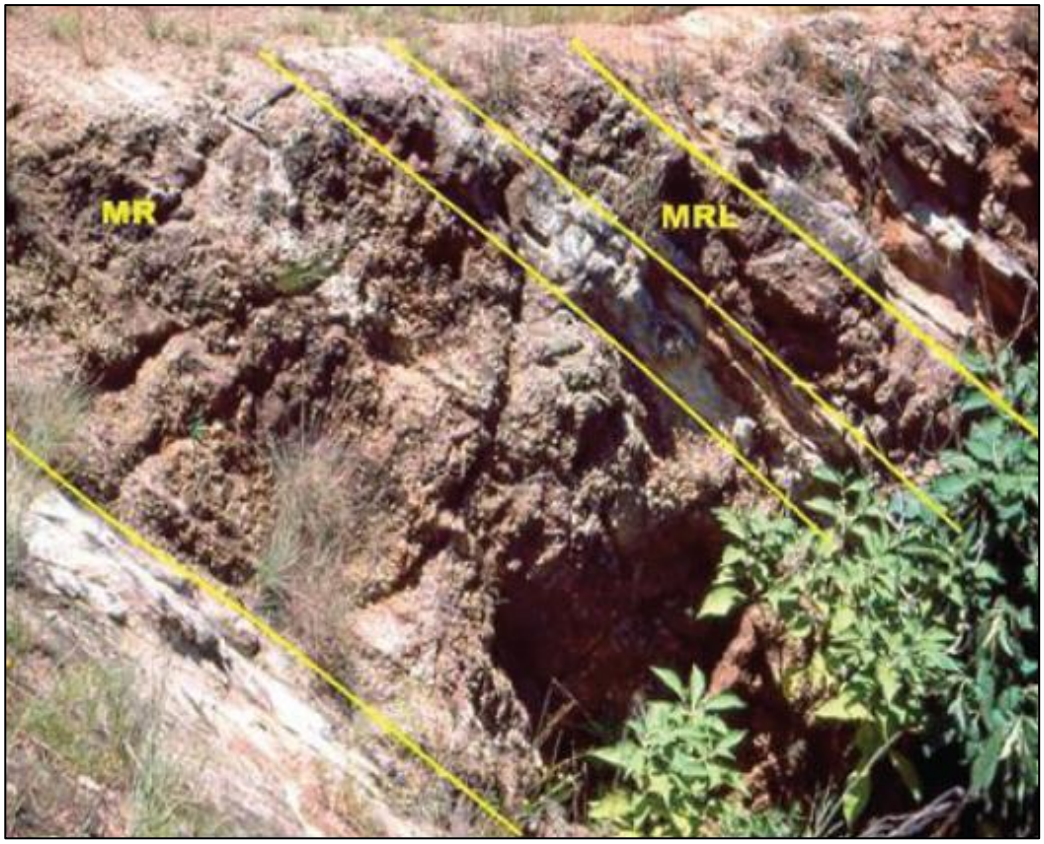


Figure 2.1.2 The discovery site with the outcrop of the Main Reef Leader (MRL) and Main Reef (MR) visible (after Viljoen, 2009).

Prospecting spread rapidly from the Central Witwatersrand along the conglomerate outcrops. The majority of the capital that drove the rapid development of the Witwatersrand gold fields was provided by diamond mining magnates. In order to control the settlement of the mining camps that were informally set up around the mining operations, the government declared a number of plots on the Randjeslaagte farm. This village was officially named Johannesburg in October 1886 after Veldcornet Johannes Meyer (Wilson and Anhaeusser, 1998).

During the years that followed, many challenges arose in terms of mining profitability. A key challenge was the gold extraction from the unweathered ore as the depth of mining increased. The improvements and innovations originating from the Witwatersrand mining are still applied worldwide.



Figure 2.1.3 The Langlaagte discovery site during 1886 and at present (after Viljoen, 2009).

During the latter years, large companies such as Rhodes' Goldfields started acquiring large blocks of ground to the south of the outcrop. During 1889 to 1892, geological exploration by drill holes at a depth of 170 m to 1489 m (Viljoen, 2009) at Turffontein, a pioneering and unparalleled technological feat at the time, was used to prove the extension of the reef at even deeper levels. This also encouraged renewed exploration efforts in the Klerksdorp area (Viljoen, 2009).

2.2. GEOLOGICAL SETTING OF THE WITWATERSRAND BASIN

Owing to the importance of the Witwatersrand Basin, this sedimentary sequence is one of the most intensely studied geological areas in the world. Many theories regarding the origin of the gold exist, but it is commonly agreed that the gold deposition was due to an alluvial system as depicted in Figure 2.2.1.

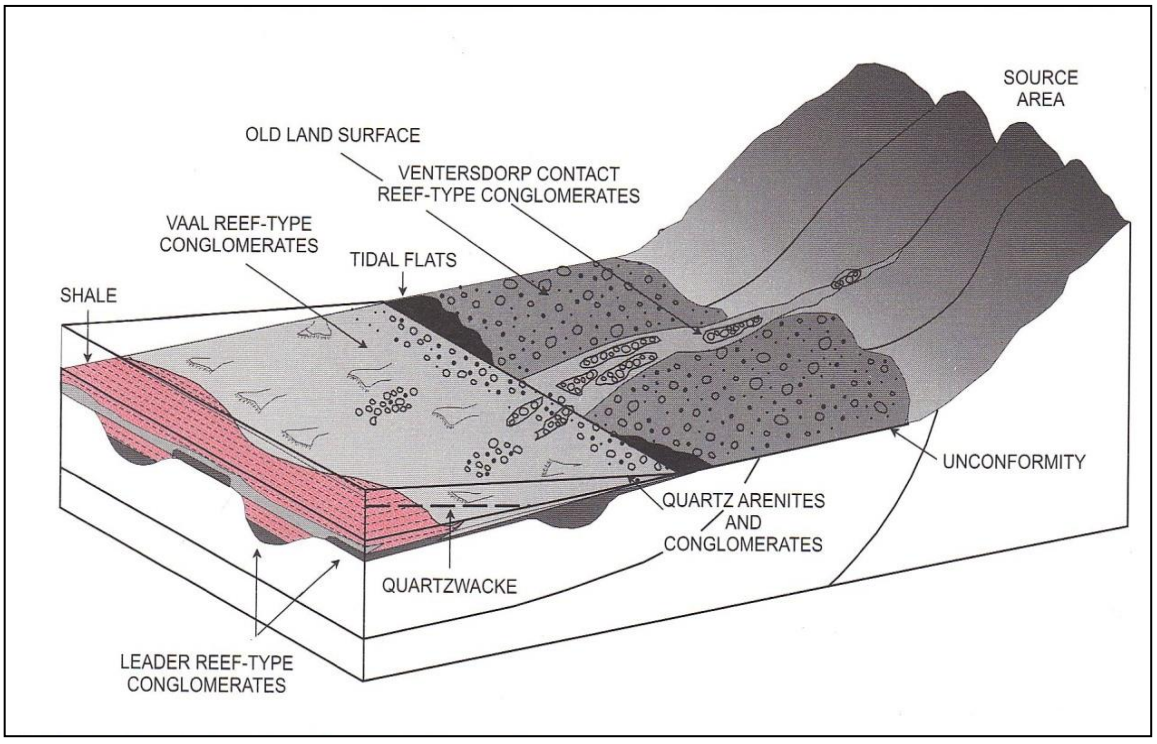


Figure 2.2.1 Schematic of the deposition of the Witwatersrand Basin (after Wilson and Anhaeusser, 1998).

It is estimated that approximately 3 billion years ago several braided rivers flowed into an inland sea. These rivers carried and deposited material into the deltas

surrounding the sea, this area of deposition s depicted in Figure 2.2.2. Materials such as pebbles and heavy minerals were deposited first, while finer sand, clay and silt were carried further into the sea. This deposition was covered with sand and clay due to flooding, upheavals, changes and movements which created movements of the shorelines and unconformities. The deposition cycle was repeated several times in order to form multiple reef bands. The sedimentary sequences that are present within the lake are shale formations, quartzites and conglomerates. No limestones are present (Durrheim et al., 2005).

The deposition cycle was unexpectedly stopped during the formation of the VCR reef band when the lake was filled up by volcanic events with outpourings of basalts and flow lavas. This lava accumulated up to a thickness of 8 km and in the process terminated any further sedimentation within the lake (Durrheim et al, 2005). The structure of the basin was affected by at least four major deformation periods, the early Dominion rifting, syn-Witwatersrand compression, mid-Ventersdorp extension as well as the Vredefort meteoric impact that further folded, thrusted, shattered and covered the lake area (Viljoen, 2009).

The Witwatersrand gold field is subdivided into smaller principal gold fields relative to the location in relation to Johannesburg, geological setting (eg. major faulting) as well as overall mine-ability as depicted in Figure 2.2.3. The West Wits Line, also known as the Carletonville gold field, is subdivided by the bank fault as depicted in Figure 2.2.4. This fault displaces the sub outcrops by 9 km and terminates on the West Rand fault, which separates the West Wits and West Rand goldfields (Viljoen, 2009).

When considering the major geological structures within the Witwatersrand, the sequences are dominated by the West Rand and Panvlakte horst blocks. These blocks are superimposed over broad folding associated with the southwest dipping Westrand Syncline, the northern limb of the syncline dips in a southwesterly direction and the southern limb dips in an east-southeasterly direction.

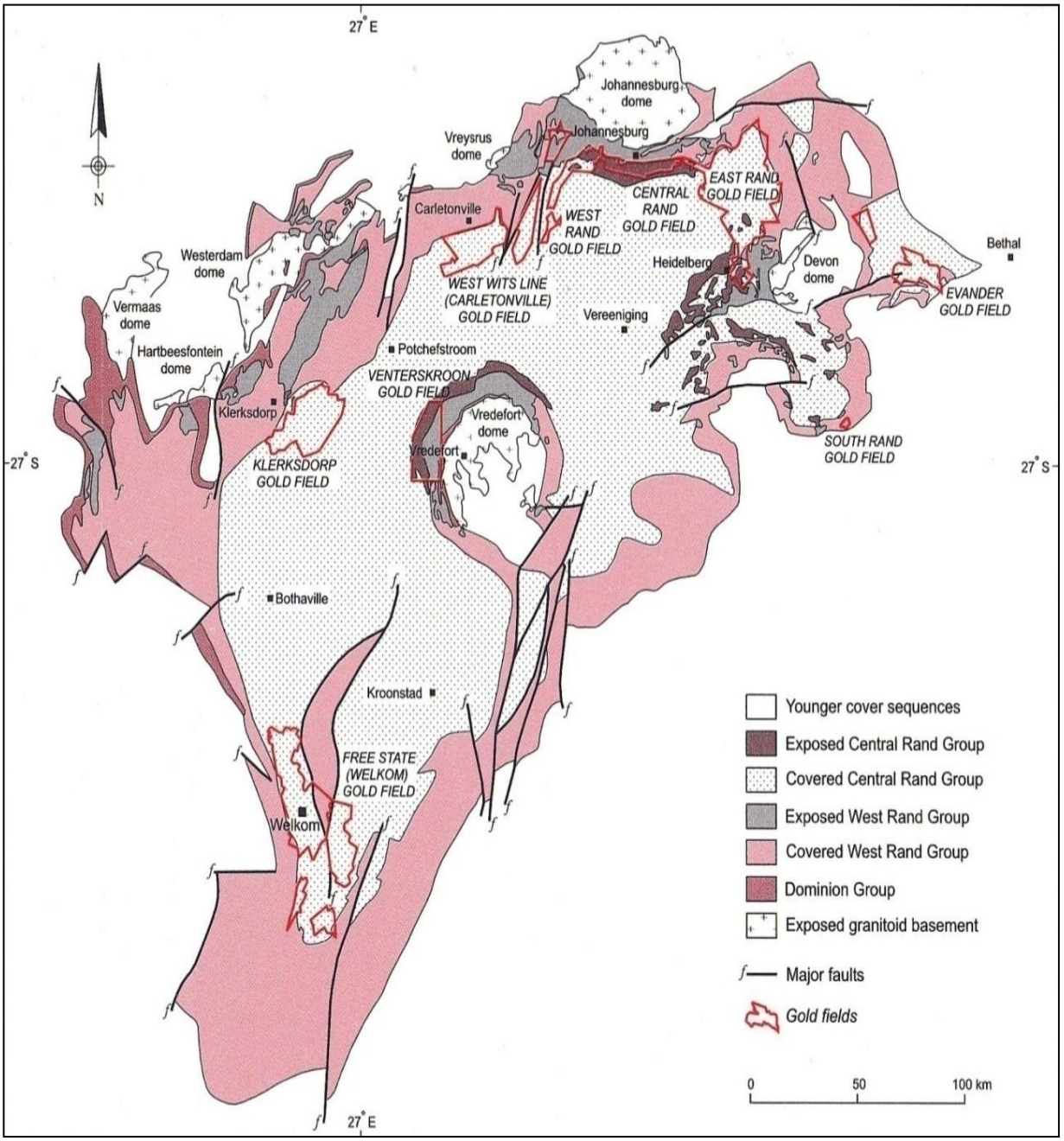


Figure 2.2.2 Geological map showing the principal gold fields (after Wilson and Anhaeusser, 1998).

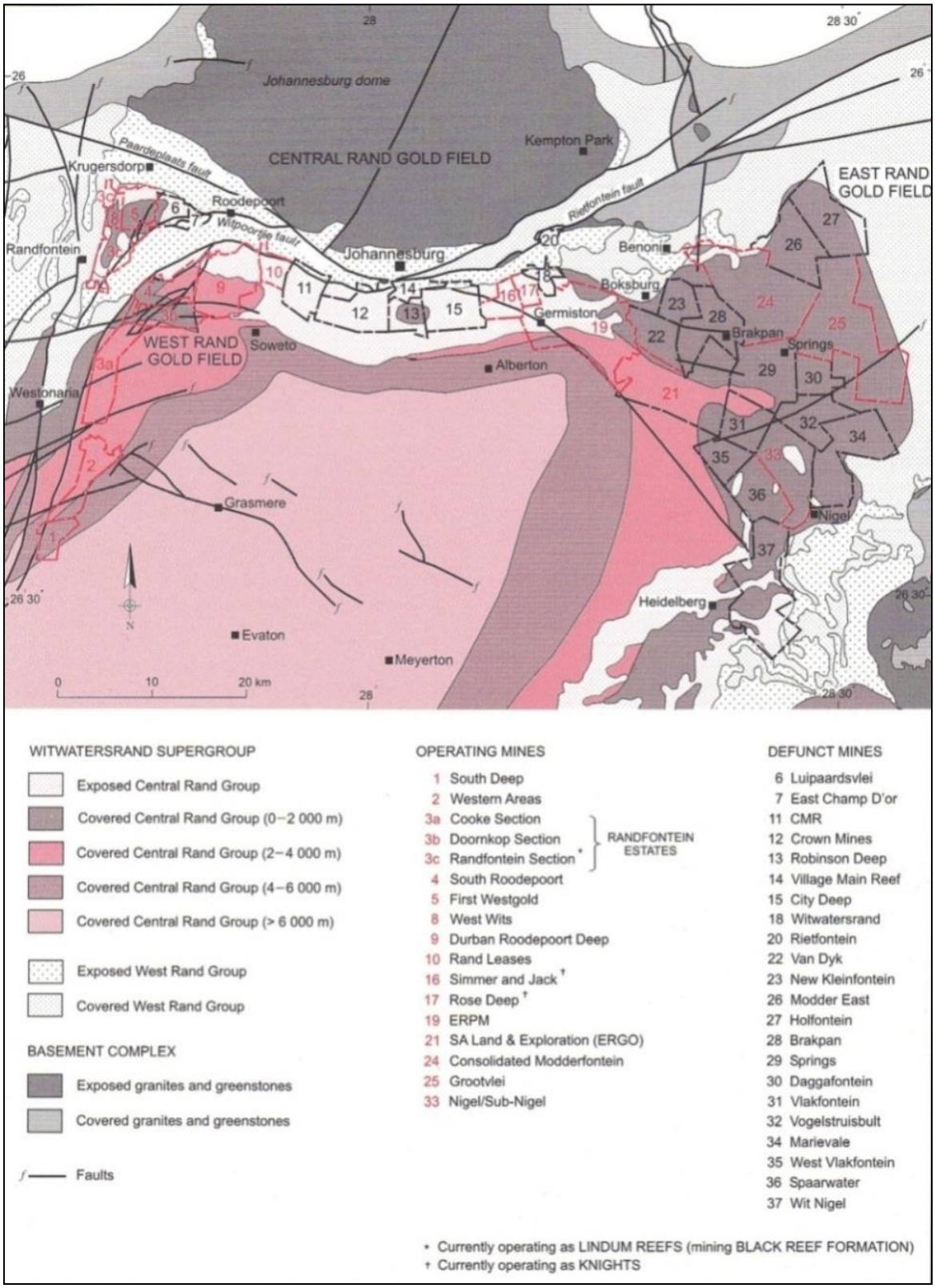


Figure 2.2.3 Location of mines in and around the Central Rand (after Wilson and Anhaeusser, 1998).

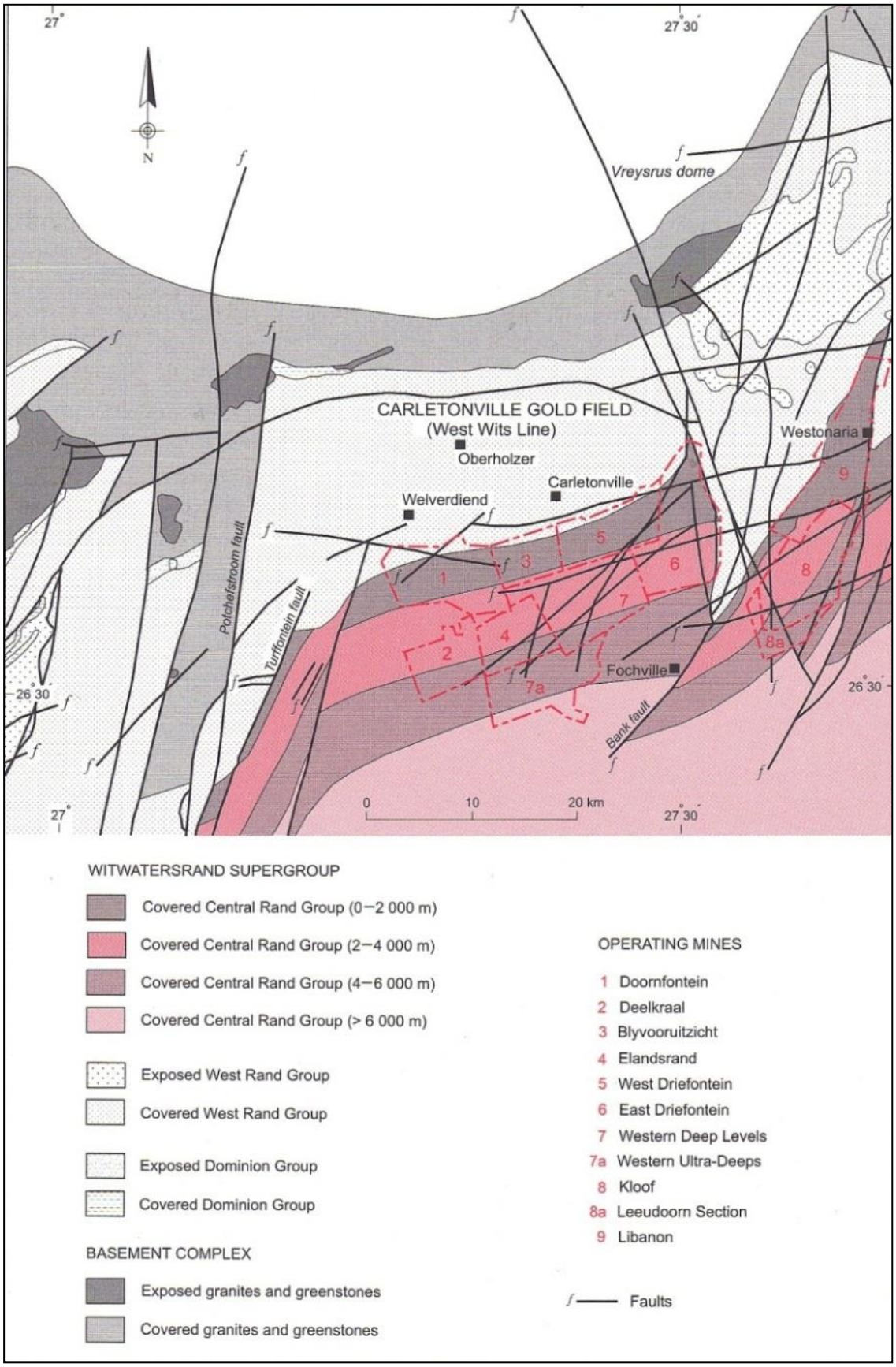


Figure 2.2.4 Location of mines in the West Wits Line (after Wilson and Anhaeusser, 1998).

2.3. PILLAR AND REMNANT MINING

Many ideas have been formulated regarding the concepts of pillars and remnants. The classifications can be summarised in three distinct periods.

2.3.1 Period up to 1952:

During the early 1900s, remnants, formed by the practice of scattered mining layouts, had such a significant effect on seismicity that numerous task teams were appointed during this period.

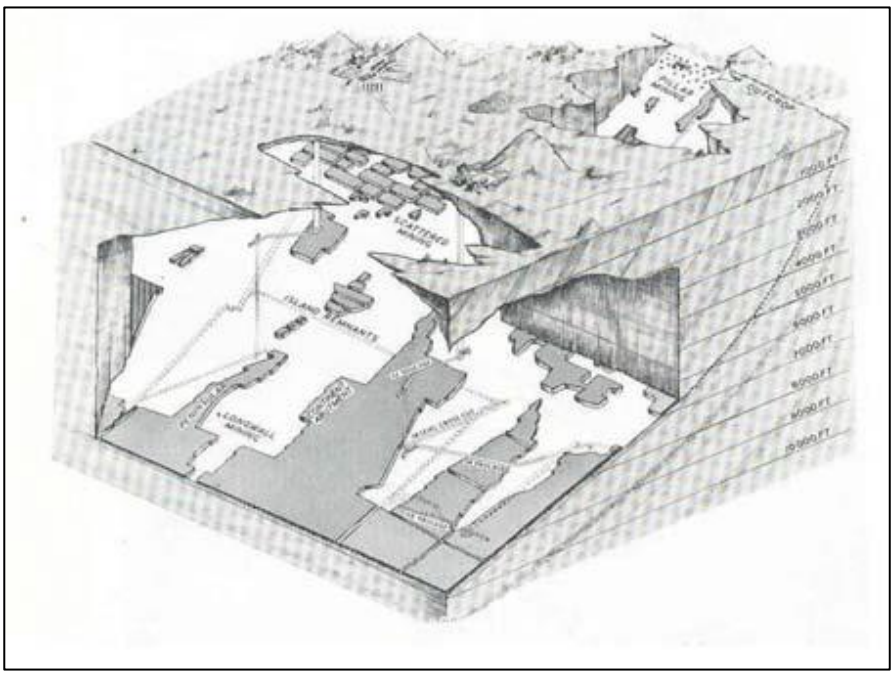


Figure 2.3.1 Layout of a typical gold mine (after Cook et al., 1966). Note the remnants illustrated in the diagram.

As the industry expanded, the severity of rock bursting increased, hence additional research was conducted by state appointed task teams, Figure 2.3.1 depicts a typical gold mine layout. The task teams made various recommendations of which some were adopted and accepted as best practice up to today. Some of the early conclusions and recommendations were that tremors were due to the shattering of pillars, large protection pillars should be left around vertical shafts,

rapid face advance and a single advance direction should be used when mining remnants, travelling ways should be protected and that pillars should be eliminated by installing extensive artificial support (Rangasamy and Jager, 2002).

The early tremor and rockburst task teams that made the recommendations are summarized below (Brown, 2011):

- During 1908 some minor damage was experienced in Ophirton and a task team was appointed to investigate the origin and effect of these tremors.
- During 1915, the Witwatersrand Earth tremors committee was tasked to report on the origins, effects of tremors on surface and underground workings and means of preventing tremors experienced in the Johannesburg and Witwatersrand areas.
- During 1924, the Witwatersrand Rockburst Committee was tasked to report on the occurrence and control of rockbursts.

In 1924 the Witwatersrand Rockburst Committee published recommendations. The following list contains some of the most prominent recommendations (Stacey et al., 2006):

- No pillars and remnants should be left during the mining operations as far as practically possible.
- Multiple reef bands should not be mined simultaneously.
- In remnants, mining faces should be advanced daily.
- The number of employees in a remnant should be limited.
- In a remnant area, the support density should be increased.
- The mining layout of a remnant should be suitable for the conditions.

The earliest documented definition for a remnant was during 1944, when the "pressure burst" problem at East Rand Proprietary Mines was investigated (Hill, 1944). Hill made a statement that almost 90% of the pressure bursting was

associated with remnants. “A portion of unstoped ground detached from the main body of ore and of such a size that the stresses accumulating in it may precipitate a burst” (Hill, 1944). Hill (1944) applied this theory at ERPM by declaring all island blocks smaller than 3344 m^2 as a remnant. He found that remnants smaller than this size tended to burst. At Blyvooruitzicht during 1952, blocks with a smallest dimension of 45 m was defined as a remnant. These areas were defined as “special areas” (Brown, 2012).

2.3.2 Research in the period from 1952 up to 1995:

Owing to the failure of the earlier attempts to solve the rockburst problems associated with remnants, a formal research program was initiated by the Council for Scientific and Industrial Research (CSIR) in 1952 (Stacey et al., 2006). The Chamber of Mines (COM) took over the sponsorship of all the research initiatives conducted on rockbursts in 1953. A comprehensive report “Recommendations of the Rockburst Committee” was published in 1964 (Rangasamy and Jager, 2002). This report reviewed the recommendations made in 1924 and included a study on the sources and mitigating factors of rockbursts. The following recommendations were made:

- Remnants should be identified, either as Listed, Support or Special Remnant and rockburst precautions implemented. A remnant was defined as:
    - An area that is not de-stressed by mining, and with an area of less than 3344 m^2, at a depth between 609 to 1672 m. In some cases a remnant may be declared earlier. The remnant should be situated between mined out areas or geological structures.
    - A stope that would be passing through the abutment of a secondary reef.
- When mining a remnant, mining should take place towards the largest or closest solid.
- If the remnant is elongated, mine in the direction of elongation.
- Do not split a remnant or mine it in two different directions.

- Stoping faces should not approach each other within a remnant.
- Leads and lags should be kept to a minimum.
- Mining should take place at an oblique angle towards a geological structure or away from a structure if possible.
- Stoping faces should be advanced regularly, and the face advance should not exceed 0.6 times the stoping width.
- A second escape way should be present and kept open.

The report published by Stacey et al. (2006) identified eight abutment types as indicated in Figure 2.3.2:

- Continent abutment is an area where the unmined ground extends for more than 304 m at right angles through the general strike of the face.
- Cape abutment is a part of an abutment that projects into an excavated area with an angle.
- Island Abutment is similar to a continent abutment but smaller and is totally surrounded by mined out areas.
- Peninsula abutment is almost surrounded by mining except for an area that is joined to an un-mined area by a portion that is not wider than 304 m.
- Strip abutment is an abutment that is at least five times the length of the average width, hence elongated and roughly rectangular in shape.
- Isthmus abutment is an area that joins two larger abutments.
- Pillar abutment is a type of island abutment that would be left for the life of mine as per design.
- Remnant is an area or part of an area that is deemed to be dangerous or highly stressed.

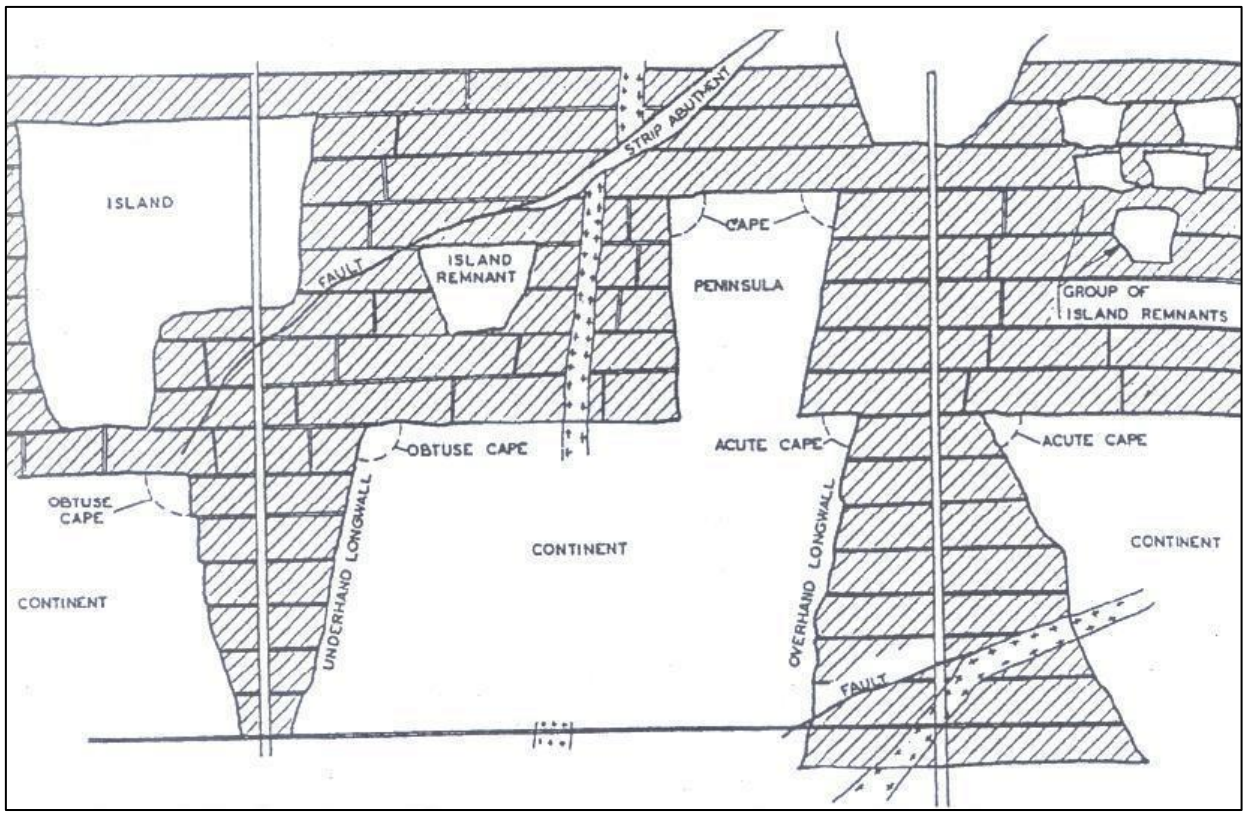


Figure 2.3.2 Types of abutments (after Stacey et al, 2006).

The research in this period also yielded proof that rockbursts were much more common while mining in a dyke. Observed underground movements were in agreement with elastic theory, the application of the Energy Release Rate (ERR) as well as critical span concept in 1966. The influence of stoping width, depth, abutments and layouts were also investigated. Cook et al. (1966) summarised past research and presented an approach to mitigate the rockburst problem. The recommendations were to:

-Observe.

-Amalgamate traditional and documented experience in order to develop a hypotheses.

-Combine hypotheses to develop a mechanism that suits the observations.

-Test the mechanism with controlled underground experiments.

Cook et al. (1966) concluded that the “existence or otherwise of the rockburst hazard depends on whether the geometrical rate at which energy must be released, is greater or less than the rate at which energy can be dissipated non-violently as the excavation is enlarged” .

During 1983 Salamon summarised the work of the research done by the Rockburst committee and suggested that the improvements in support systems, design layouts and reduction in convergence will result in a reduced rockburst hazard (Rangasamy and Jager, 2002).

In 1988, The Chamber of Mines Research Organization (COMRO) published the “Industry guide to methods of ameliorating the hazards of rock falls and rockbursts”. In this guide remnants were defined as “blocks of ground surrounded by extensive mining” (Jager and Ryder, 1999).

The guide by Starfield and Cundall (1988) also specified the following recommendations for special remnant situations:

- Increased support density.
- Reduced support-to-face distances.
- Increased temporary support density.
- Increased areal coverage by using headboards and umbrellas.
- Use of pre-stressed units.
- Using larger and stiffer support units.
- Use of rockburst resistant support units.

During 1987 a dedicated micro-seismic system was employed to investigate the formation and extraction of remnants. During this study, an increase in the

B-value was noted during the formation of a remnant in the Klerksdorp area (Legge and Spottiswoode, 1987). This work was followed up by Minney and Naismith (1993). They concluded that the only reliable indicator of stress change in a pillar is a plot of the cumulative B-value (Legge and Spottiswoode, 1987).

COMRO (1988) published a special issue of Mining Survey and indicated the following focus areas for rockburst research (Brown, 2012):

- Mining layouts should be of such a nature that stress concentrations are limited by correct planning. The research produced the elastic boundary element modelling program, MINSIM.

- Support systems should be designed to reduce the extent of rockburst damage and falls of ground. The research resulted in the development of the rapid yielding hydraulic prop and some advances in backfill.

- Rockburst control by engineering out the risks and monitoring seismicity.

Johnson (1994) defined a remnant as a block of highly stressed ground in which the stresses exceed approximately a half of the host rock Uniaxial Compressive Strength (UCS). He found that no conclusive correlation could be found between some typical rock engineering parameters and remnant stability. He also mentioned his disappointment with the small number of remnant back analysis studies conducted.

2.3.3 Research from 1996 onwards

During 1996, The Health and Safety Act No 29 was promulgated. This act prescribed a risk assessment system as a necessity. The method promoted by the act limited the use and further development of a generic remnant mining methodology. The prescribed code of practice and bylaws do not adequately capture the risk involved nor provide any insight into the best practice methodologies of mining remnants. However the risk assessment method, if

applied effectively, does provide useful input into all the stages of remnant extraction.

Rangasamy and Jager (2002) indicated that continuous closure measurements are imperative for improved support design, hazard assessments and quantifying the effect of seismicity in remnant situations. The value of this monitoring technique was highlighted by the analysis of closure rates of various remnants. Indications were that the closure ratio can be utilized in order to identify site response and possible hazards of remnants in different geotechnical areas.

2.4. FACTORS INFLUENCING REMNANT STABILITY

Remnants are usually left because of adverse or difficult mining conditions, such as complications caused by geological structures, poor ground conditions, low grade or rockburst damage (Durrheim, 1997). Adverse conditions are usually amplified once the remnant is cut and the final pillar has been formed.

Cook and Salamon (1966) discussed the similarities in risks between ultra deep mining and remnant mining. Mining of remnants poses problems as high rates of closure, ground mobility, increased rock bursting and siting of access development has to be addressed (Johnson, 1994).

From an industry survey, Rangasamy and Jager (2002) concluded that in the Far West Rand region, the classification of remnants based on size and seismic history is favoured. The shape, block stress and geology are considered secondary selection criteria. In the Klerksdorp and Free State regions, stress, geology and seismic history of the area feature prominently in the classification of remnants (Stacey et al., 2006).

When considering the stability of a remnant various factors such as the location, geology and rock properties have an influence. Dominant factors include the

mining depth, reef package and lithology, as well as other mining and extent of mining in the vicinity, hence also the size and shape of the remnant in question.

The presence of geological structures create adverse mining conditions in terms of rock falls as well as rockbursts. The geological structures as well as the associated sympathetic structures create poor hangingwall conditions. The presence of structures within a panel therefore presents the opportunity for large collapses as well as deeper fracturing and weakening. A geological structure may also be the source of seismicity or may act as a channel through which seismic energy is transmitted to a nearby mining face.

The local ground conditions as well as the site response would be dictated by the rock properties. Some of the properties are the strength, modulus, brittleness, viscosity, rock quality, discontinuities and properties of the discontinuities. An example of the influence of the properties on the site response would be that the strength and modulus of the rock control the amount of strain energy released during a rockburst, while the orientation and intensity of fracturing would be determined by the strength of successive layers and by the properties of discontinuities.

In order to gain insight and anticipate expected underground conditions, certain rock mass models and their mathematical descriptions were explored. Usually the calculations are done using the assumption that the system will behave elastically and is homogeneous and isotropic. This is done in order to simplify the problem. Some of the parameters that are typically considered are the major principal stresses, Average Pillar Stress (APS), Energy Release Rates (ERR), Excess Shear Stress (ESS), width to height ratios and failure criteria.
The parameters mentioned above can be calculated using numerical modelling. Since the 1960s, the formulation and application of numerical methods has been researched and applied (Brown, 2011). The successful application of numerical modelling nevertheless depends on the quality of the geometry and input parameters. The mining problems are typically data-limited and cannot be

modelled easily. A vast amount of knowledge and experience has been accumulated during recent years as the technology evolved and became more accessible. Many practitioners nevertheless still regard the software as a black box and they do not give sufficient attention to the mechanisms of failure. Numerical modelling should be regarded as an aid to thought, rather than a substitute for thinking (Starfield and Cundall, 1988).

As part of the analysis and selection of remnants, the determination of the rock mass properties is critical as this would provide valuable insight into the underground conditions as well as the expected behaviour of the rock mass.
Several criteria and constitutive laws has been developed utilizing the peak strength. The two most widely utilized are the Mohr Coulomb and Hoek Brown criteria (Brady and Brown, 2005). Both criteria have their deficiencies and several adaptions have been proposed. The criterion by Christensen originally used for ceramic material may have a lot of potential for application in deep level or remnant mining (Brown, 2012).

One of the most important but almost unpredictable factors to consider would be seismicity. The South African subcontinent is situated in a reasonably stable tectonic region and the majority of the prevailing stress regime are lithostatic in nature and very little natural seismicity occurs. In contrast, mining induces seismicity due to changes within the stress field. This may trigger movement on faults or even rupture the rock mass in order to release some of the stored strain energy. The amount of strain energy released is largely controlled by the rock properties, the prevailing stress regime as well as the mining geometry (Brown, 2012). The stability of affected pillars would be influenced by the source mechanism as well as the other seismic parameters of such an event, as well as the rock mass properties, while the peak ground velocity would also have a bearing on the stability of the area as the support designs are generally based on the thickness of the hangingwall beam moving downwards and the ground movements indicated by peak ground velocities (Brown, 2011). Seismicity also affects the stiffness of a rock mass and repeated seismic events in an area would

soften the rock mass and allow additional deformation to occur (Jager and Ryder, 1999). Minney and Naismith (1993) found that the b-value and cumulative seismic data is the most reliable indicators of stress change. This result is similar to that recorded by Legge and Spottiswoode in 1987 while monitoring the formation of a remnant in the Klerksdorp area (Johnson, 1994).

Owing to the change in stress as a mining face advances, the readjustment to equilibrium may cause instantaneous or gradual re-adjustments. Associated with the re-adjustment is stope closure. The ideal would be to have a regular or decaying closure rate with no instantaneous releases as this will indicate an efficient redistribution of stresses and a lower risk of damaging rockbursts. This concept was proven in the coal mines by Linkov (Malan, 1999). Malan (1999) determined that on a normal advancing VCR panel with a hard lava hangingwall there are at least three phases of closure occurring. The observed time dependent closure as well as observed phases are depicted in Figure 2.4.1.

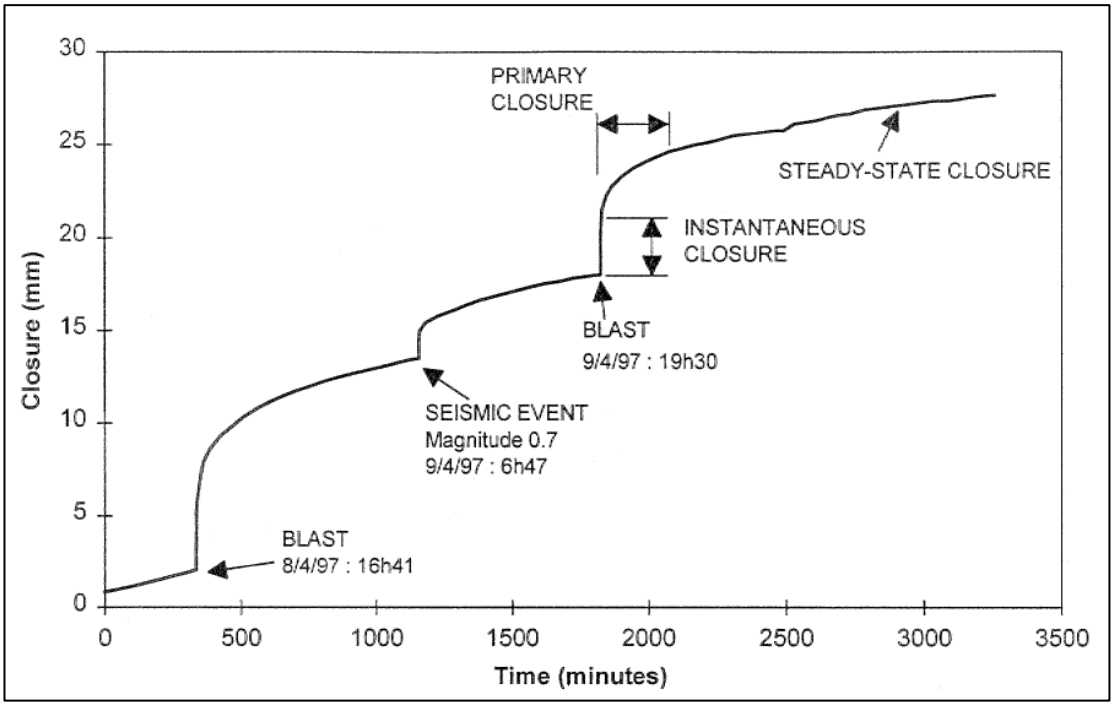


Figure 2.4.1 Typical continuous stope closure of a VCR panel (after Malan, 1999) .

From Figure 2.4.1 it can be seen that a large increase in the closure rate is present following a blast. A low steady state closure follows the primary closure phase. The large instantaneous change can be interpreted as the removal of the confining influence of the portion of the face during the blast. Thus a higher face stress would probably lead to a higher instantaneous closure and indicate a burst prone area (Malan, 1999).

Remnants are particularly common and dangerous when mining multiple longwalls. The danger lies in the creation of a remnant between two advancing faces. If an L shaped remnant is formed, the potential exists for the whole remnant to fail in a single event. The correct layout would be to form a triangular remnant where the last mining would take place along the largest solid, and the apex of the remnant would then crush continually as the face advances. Another alternative is to mine the remnant in a up-dip fashion. The creation of a heading in a high stress environment will nevertheless create hazardous conditions (Durrheim, 1997).

The height to width ratio of a pillar also affects the stability of a remnant. If the unconfined height of a remnant is increased it would have a detrimental effect on the strength of the pillar (Durrheim, 1997).

2.5. CONVENTIONAL ACCEPTABLE RISK METHODOLOGY

Owing to the high risk involved with mining operations, the risk / reward relationship should be utilized to the benefit of the owners, the employees and the company. This is especially true in remnant mining, as the conventional acceptable risk methodology and limits are seldom met. The classical field of engineering has a focus on excellence and risk avoidance which is in contrast to the practice of mining because of the uncertainties and the probability that the rock mass will not behave as expected (Stacey et al., 2006).

In order to make a decision as to the mining of a certain area, the following list shows some of the risks that should be considered (Brown, 2012);

- Support and excavation performance
    - Mining layout and sequence
    - Mining under previously mined area
    - Mining over previously mined area
    - Effects of blasting
    - Applicability of numerical modelling results
- Mechanical properties of the rock mass
    - Elasticity of the rock mass
    - Rock mass strength
    - Rock mass classification
    - Rock brittleness and rockbursting
    - Pillar strength
    - Rock weathering or other weaknesses
- Estimation of stress regime
    - Effect of rock mass itself on the stress field
    - Effect of geological structures on the stress field
- Behaviour of the rock mass under high stress
    - Effect of rock strength
    - Effect of squeezing – ductile and viscous behaviour
- Seismicity
    - Natural seismicity
    - Mining-induced seismicity
    - Effect of geological structures
    - Site response

- Geology
    - Hydro-geology
    - Presence and properties of jointing
    - Presence and properties of geological structures
    - Known and unknown geological boundaries
    - Mining under geological structures

The unstructured risk-only approach does not yield acceptable results as some of the major risks may be overlooked (for instance in this case proximity of other mining and grade).

As a result, various design processes were developed throughout the years in order to determine and define acceptable risk when mining. Bieniawski (1991) defined six core principals of rock engineering design. These principals were summarised into a methodology by Stacey et al. (2006) as depicted in Figure 2.5.1.

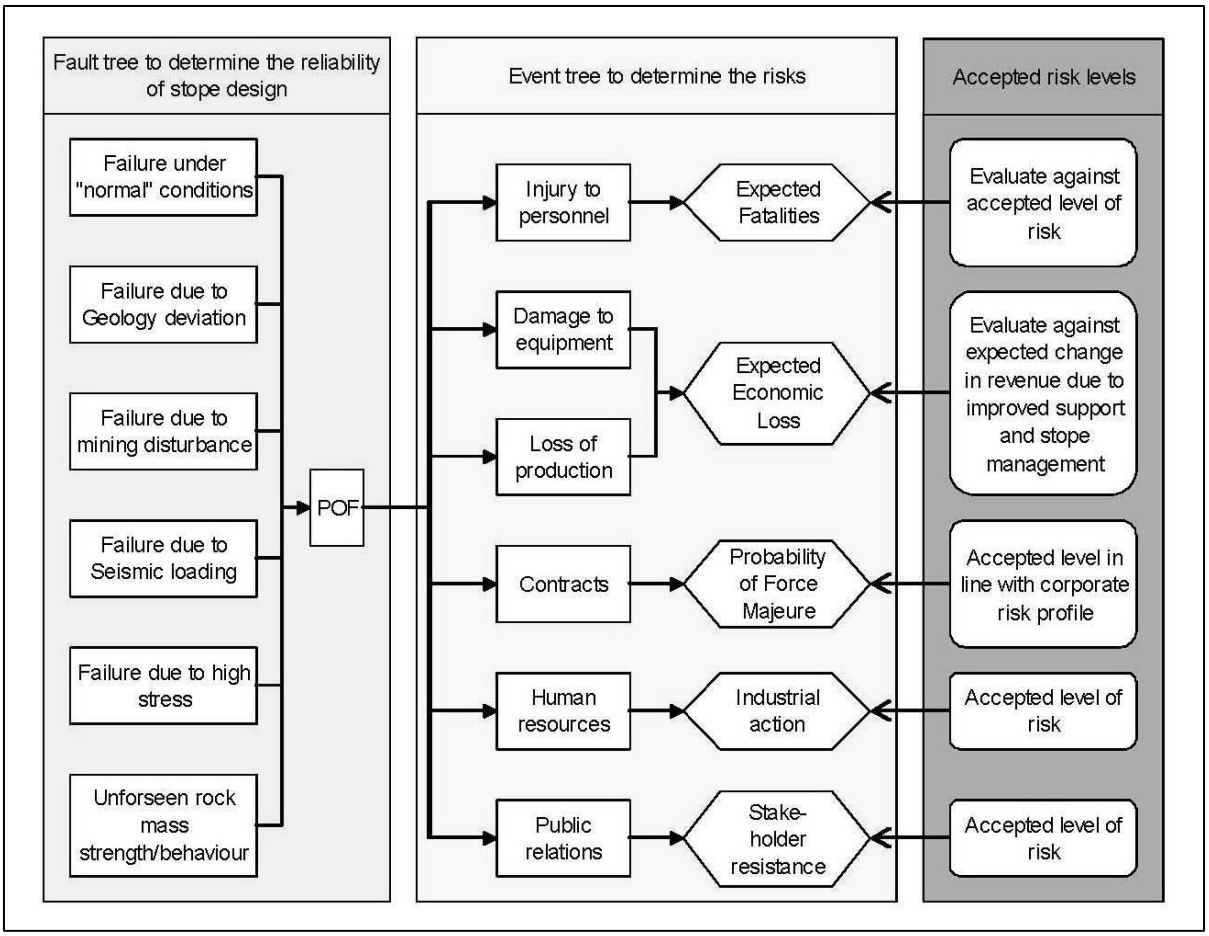


Figure 2.5.1 Risk evaluation process (after Stacey et al, 2006).

If the methodology is carefully studied, it reveals that the availability of reliable information to conduct the risk evaluation is problematic. In practice, the risk assessment approach is used to reduce and minimize the levels of risk as well as residual risks. The situation is further complicated as the risk is usually multi-layered as described by Hebblewhite as noted by Brown in 2012;

- The day-to-day operational risks.
- Site and condition-specific risks.
- Core risks associated with the mining method (Brown, 2012).

The risk assessment approach does, however, have a number of shortcomings. The list of shortcomings mentioned below is not necessarily complete or all the elements mentioned does not necessarily apply to all operations (Brink et al., 2002):

- Resistance to change – such as a new risk assessment system
- The lack of sufficient resources – trained and certified personnel
- The lack of follow-ups done on recommendations made
- Availability and quality of information – such as geological information
- Quantification of risks – such as rockbursting
- Subjectivity and consistency

As part of an effort to determine the viability of extracting remnants, Rangasamy et al. (2003) developed a simple process, a risk estimation matrix, to outline the decision making process when dealing with high risk mining. The process followed to estimate the risk involved is depicted in Figure 2.5.2:

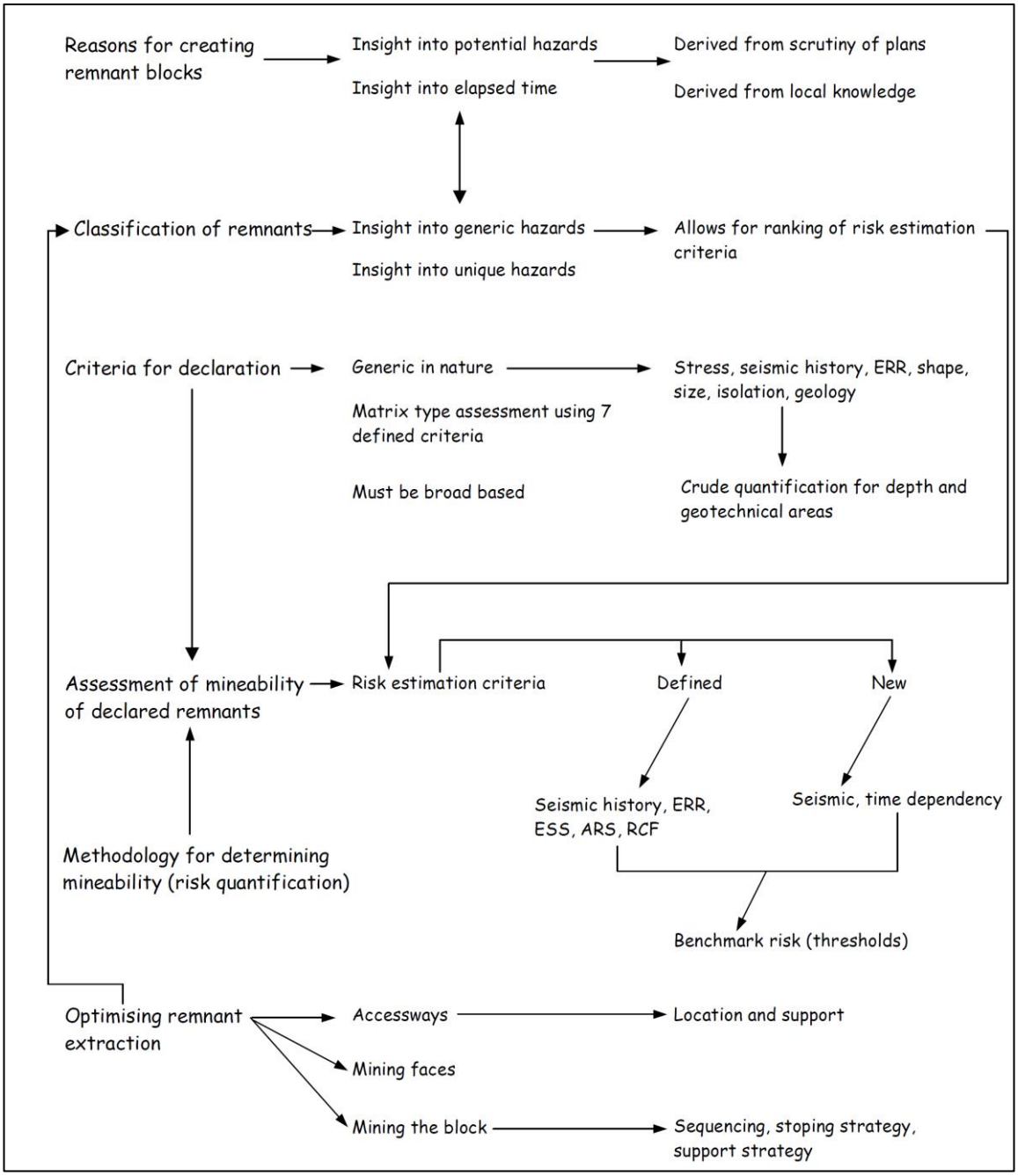


Figure 2.5.2 Schematic indicating a risk estimation process (after Rangasamy et al, 2003).

2.6. DEEP LEVEL MULTI-REEF MINING AND DE-STRESSING

A large number of reefs are present within the Witwatersrand Basin, many of which can be economically exploited. The Central Rand goldfield has three predominant reefs, Main Reef, Main Reef Leader and South Reef. These reef bands are situated in close proximity to one another. Multi-reef mining is therefore common within the Basin. Plans dating from 1946 shows stoped areas on the Main Reef group with middlings in the order of a few metre (Riemer and Durrheim, 2011).

According to Maritz (2014), the complex nature of multi-reef environments are not well understood, hence no clear design methodology is available. Design methodologies from other accepted methods are therefore adopted. He continued to illustrate that the stress and loading regime of pillars are influenced by many factors such as dip of the reef, depth below surface as well as the presence of multi-reef mining.

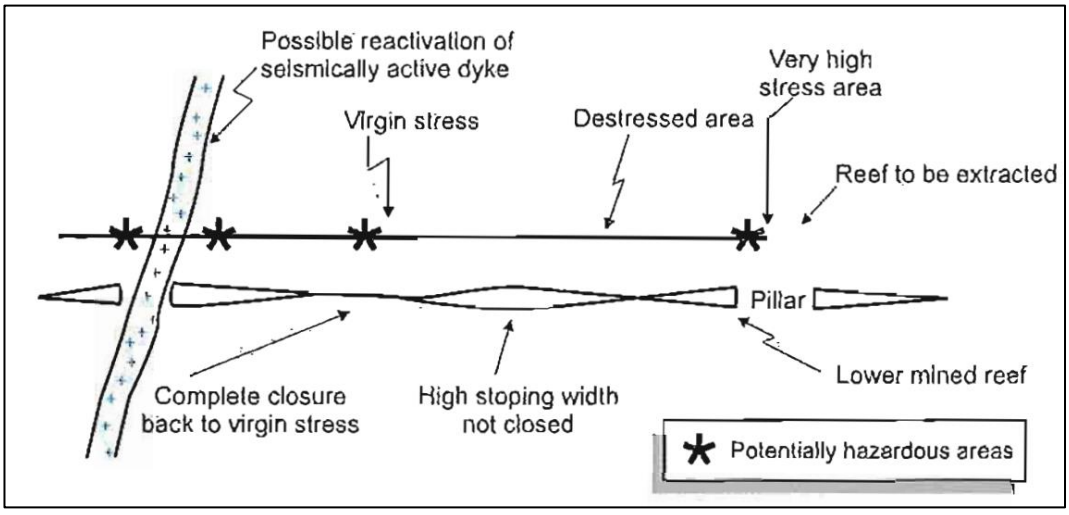


Figure 2.6.1 Conditions encountered when mining a secondary reef (after Jager and Ryder, 1999).

It is difficult to determine the parameters influencing the rock behaviour in multi-reef tabular layouts, especially when the middling is small. The majority of the knowledge available on multi-reef mining is based on empirical data and past

experience. According to Jager and Ryder (1999), designing layouts or support for multi-reef mining should be approached as a unique problem. Such designs requires the consideration of additional variables, such as mining depth, middling, effect of pillars and remnants, as well as the influence of surrounding rock types.
There are two sub categories of multi-reef mining: Simultaneous and subsequent extraction. Each category would involve a different set of considerations that should be met to successfully extract the planned area.

In shallow multi-reef mining conditions it is important to consider the stability of the middling between superimposed stability pillars. As a general rule the stability of the middling reduces as the span increases on the secondary reef during multi-reef extraction as subsequent extraction under shallow mining conditions. Thus it is very important to limit the spans on the lower reef, by leaving pillars or placing cemented backfill. The installed support on the upper reef may encounter stability problems due to footwall movement, in turn reducing support resistance. It is thus advised by Jager and Ryder (1999) to mine the lower reef subsequent to mining the upper reef.

Figure 2.6.1 shows the typical conditions that would be experienced in an intermediate to deep level mine during multi-reef extraction. Stope closure can occur over large areas and the magnitude as well as orientation of regenerated stresses can differ significantly from the original configuration. If the middling between the two reef elevations is sufficiently small – stress fractures can be intersected by the subsequent mining. According to Jager and Ryder (1999) unmined areas or total closure would also significantly affect the mining conditions of the subsequent mining, in severe cases a superimposed pillar should be left as stress levels may be high. Geological structures may also pose a risk in the form of reactive seismic energy when mining in close vicinity or when transecting. Seismicity on some structures may be reinitiated by the subsequent mining.

Simultaneous extraction poses the same risks as was discussed with subsequent extraction but the interaction of the stress concentrations also becomes important. In order to avoid such stress interactions the mining layouts should be similar and one of the reefs should lead by a distance sufficient not to affect the face of the trailing reef. According to Jager and Ryder (1999) the lead distance should be determined for every situation by numerical modelling and, in deep conditions, by additional closure measurements on the leading reef.

It has been documented by Jager and Ryder (1999), that mining faces in close proximity to each other pose increased risk. Other contributing factors include the under-and-over stoping of solid pillars and remnants as well as the fact that the majority of the layouts were never optimized or designed for multi-reef mining. Even at shallow depths, these less-than-ideal layouts can exacerbate the problem of pillar failures, as well as lead to the creation of large shear stresses and higher than expected energy releases. Multi-reef mining also creates the potential for larger closures and has a greater potential for hangingwall collapse in weak strata (Napier and Malan, 2008).

For multi-reef mining, it is expected that the formation of excess shear stresses and high energy releases can be controlled when considering some of the methods discussed in the DeepMine research program namely (Riemer and Durrheim, 2011):

- The mapping of geological structures ahead of mining with the use of borehole radar.

- The design, selection and planning of mining methods to be most appropriate for the expected conditions.

- The design of mining using parameters such as Excess Shear Stress (ESS); Energy Release Rate (ERR); Rockwall Condition Factor (RCF) and Average Pillar Stress (APS).

To analyse the stress distributions around mining excavations, various numerical modelling techniques have been developed. During the early 1960s, Salamon suggested the use of the technique later called the Displacement Discontinuity Boundary Element Method in the mining industry (Napier and Malan, 2008). Initially, due to the limitations of hardware and technology, only small portions of single reef excavations were analysed. With time, the techniques were improved and today the analysis of multi-reef excavations can be conducted. Large scale multi-reef problems are nevertheless cumbersome to analyse (Napier and Malan, 2007).

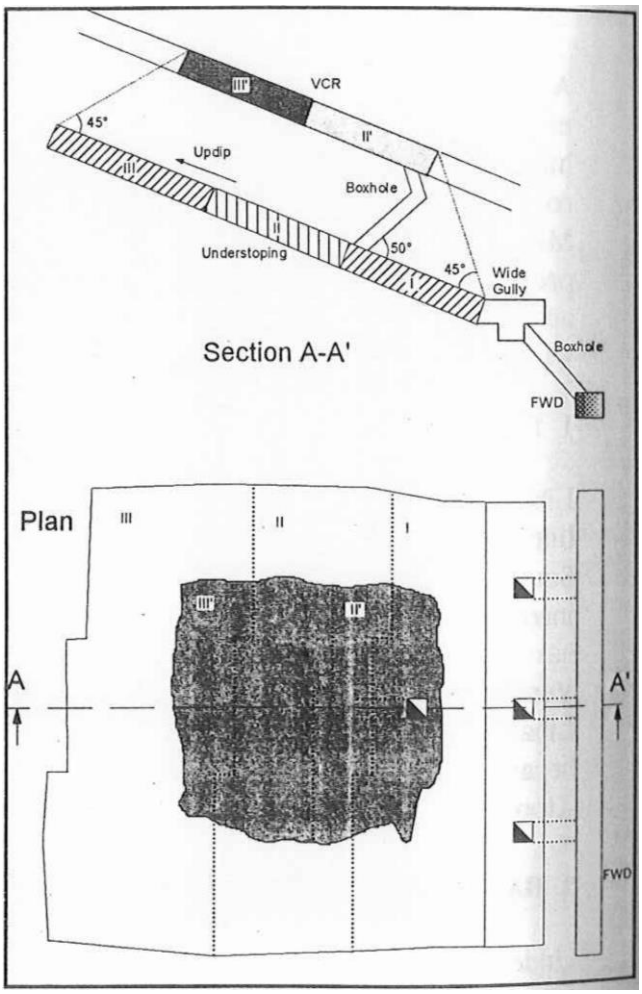


Figure 2.6.2 De-stressing of the VCR by understoping (after Du Plessis and Talu, 1997).

Du Plessis and Talu (1997) recorded their pillar mining experiences of multi-reef mining on a deep level gold mine in the West Wits, based on local lithology. In their paper, the influence of the rock type, middling as well as critical rock engineering parameters are highlighted. The authors mention that problems were encountered when the middling was too small as this causes the middling to collapse. When de-stressing was done on the Kloof Reef, poor ground conditions were encountered when reduced middlings were mined due to the multi-layered reef package. Another problematic area is when the VCR mining followed too far behind. Significant strata control problems were encountered, probably due to the area being de-stressed and the formation of a tensile zone above the stope. They mentioned that if the VCR mining was conducted too close to the waste cut, very high closure rates were experienced. If no waste cut was carried, the closure rates within the stope were very high. The hangingwall of the VCR deteriorated and even mined itself out in front of the reef face (Du Plessis and Talu, 1997).

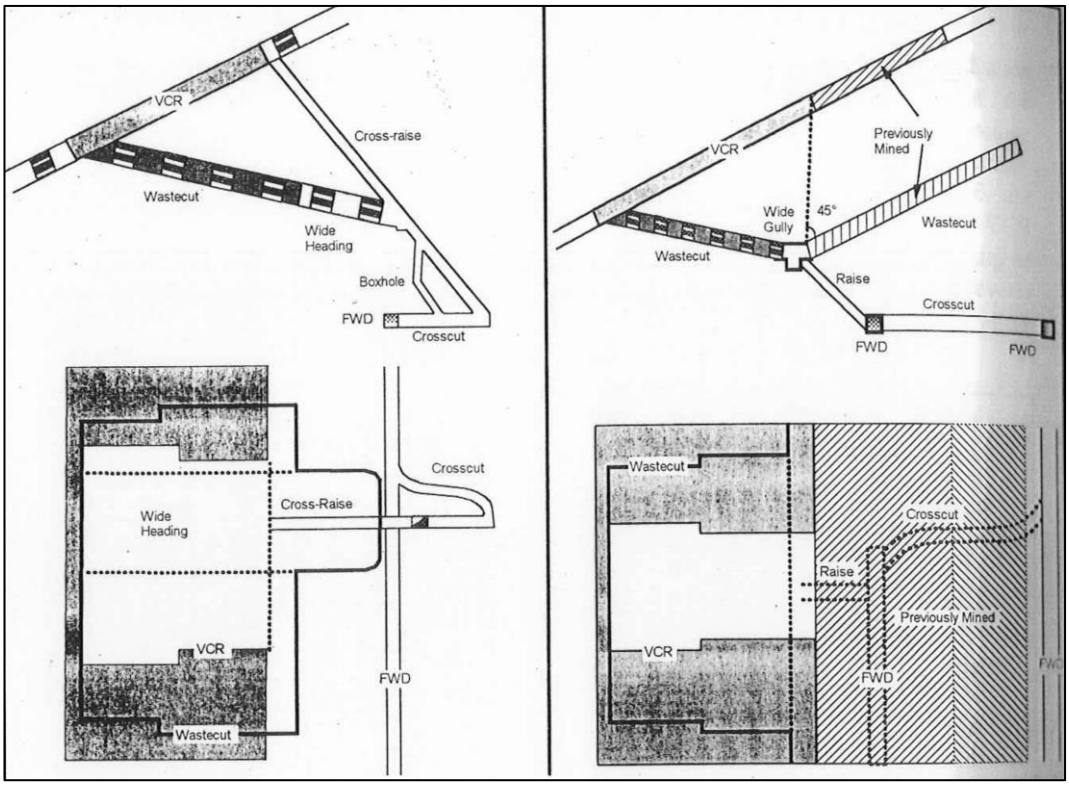


Figure 2.6.3 The Hennings method (after Du Plessis and Talu, 1997).

The preferred mining method was indicated as up-dip mining, from a single side, due to the orientation of the stress fractures. They also mention that an acceptable

middling is between 6 m and 30 m of which 10 m is the ideal. The paper introduces a novel understoping layout called the Hennings method (Figure 2.6.3) and continues to describe support strategies and mining layouts that were developed to combat the rockburst problems experienced when mining remnants and pillars on Libanon gold mine.

Some work has been conducted on the platinum mines with specific reference to multi-reef room-and-pillar mining in shallow conditions. Napier and Malan (2008) illustrated the value of the TEXAN modelling code to analyse multi-reef mining conditions. The specific problems experienced on the platinum mines may be different to that of the deep level gold mines where the de-stress cut or primary reef has been extensively and continually extracted. Due to different layouts, infrastructure, middling and geological structures, the superimposing or matching of supporting pillars may not be the major influencing factor when considering multi-reef or de-stress mining in the gold mines. In general, a significant reduction in the vertical stress component is achieved in the deep mines without significantly affecting the horizontal clamping component. The change in the stress field will affect the rock mass and the fracturing patterns, thereby increasing the support requirements. Other associated problems include bed-separation when understoping or the complete closure and stress-regeneration when overstoping (Hustrulid, 2001).

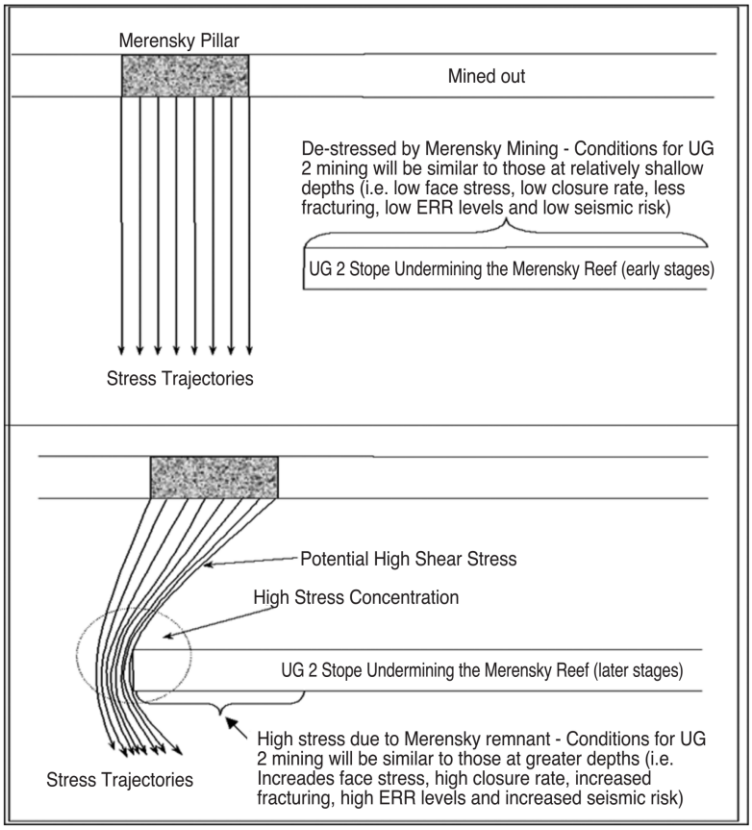


Figure 2.6.4 Stress changes when approaching a pillar (after Singh et al, 2005).

An analysis to determine the influence of pillars in a multi-reef mining environment on the platinum mines by Singh et al. (2005), indicated the significant influence of middling and the presence of tensile horizontal skin stresses. The study concluded that mining conditions of a shallow operation may be similar to that of deep level mining when mining below remnants. The study also found by means of underground observations and closure measurements that stress relaxation would rather take place in the form of mobilizing of joint-bound blocks rather than fracturing on the UG2 reef.

Maritz (2014) also illustrated by means of elastic numerical modelling that the geometry, such as reef dip and multi-reef mining, has a profound influence on stress and loading regime of pillars. The complex stress interaction is due to the introduction of a shear component even if the pillars are perfectly superimposed (Maritz et al., 2012).

In certain cases as proved by Singh et al. (2005), horizontal tensile stresses may be induced as the mining moves out of the de-stressed zone (Figure 2.6.4. The horizontal tension has been shown to persist for up to 8 m into the hangingwall and were as high as 5 MPa. The combined effect of high horizontal tension and large elastic convergence is very unfavorable for hangingwall stability, requiring upgraded support systems.

It can be concluded that only limited empirical guidelines are available, when considering the available literature on multi-reef mining. The notion that local knowledge and know-how is passed on to rock engineering practitioners on the operations are evident. Very few of these experiences were published.

2.7. OPERATIONS AT MINE A

This MSc study was conducted using data from Mine A and some background information regarding this mine is therefore included in the literature study.

Mine A is situated in the West Wits, Carletonville goldfield and lies approximately 50 km west of Johannesburg and 15 km from Carletonville. Mine A is situated between the Witpootjie fault to the east and Bank fault to the west (Anon., 2012). Mining started during 1939. The mining done in this area was shallow and conformed to the typical layout depicted in Figure 2.7.1.

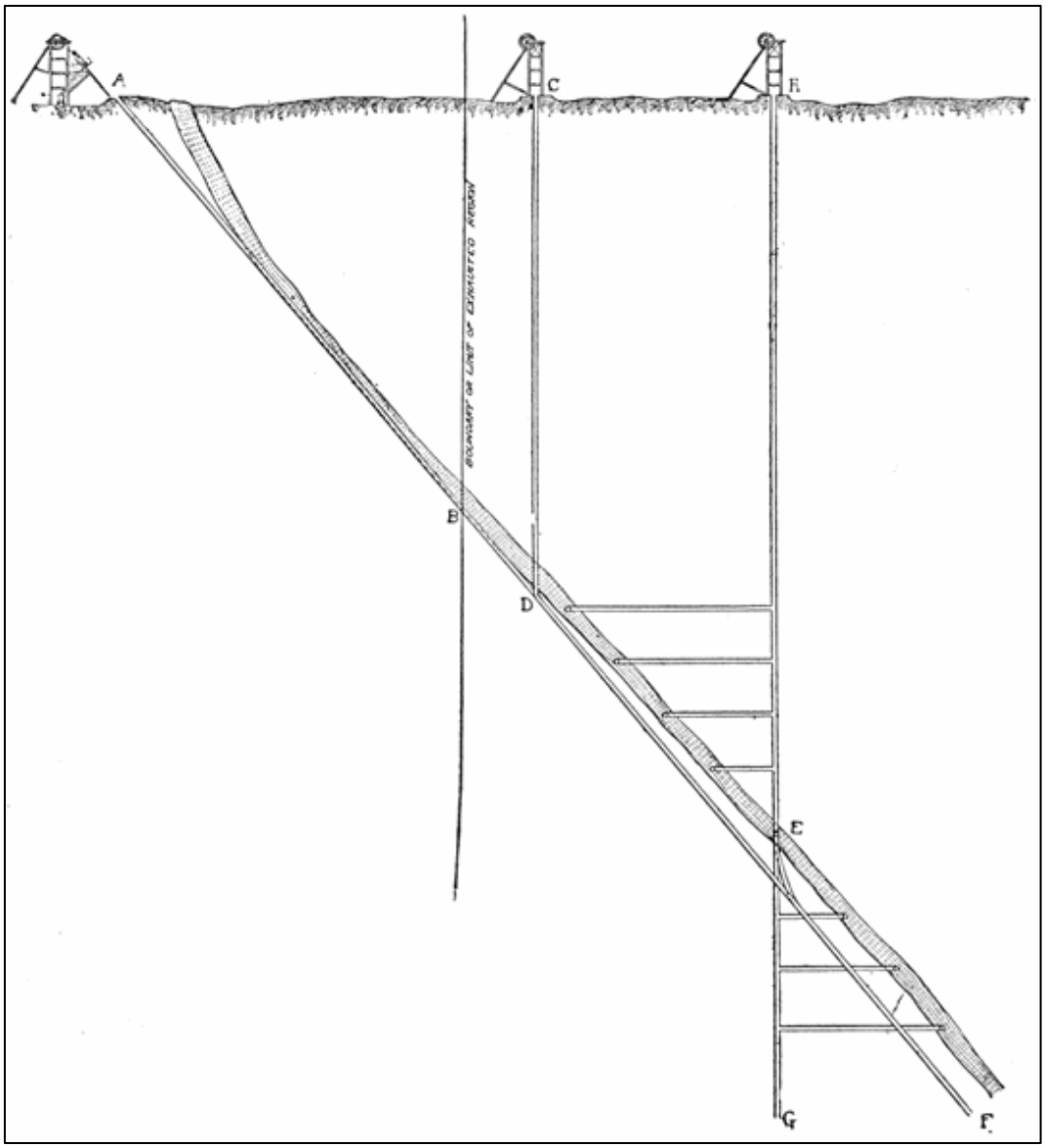


Figure 2.7.1 Typical layout of an underground gold mine (after Hoover, 1909).

Five different reefs exist within the area, namely the Ventersdorp Contact Reef (VCR) situated at the top of the Central Rand Group, the Libanon Reef, the Kloof Reef, the Carbon Leader Reef (CLR) and the Middelvlei Reef (MR). Many of these reefs are not extensively mined due to localized areas of playability. Figure 2.7.2 depicts a section through some of the Mine A shafts and Figure 2.7.3 depicts the local stratigraphy at these operations.

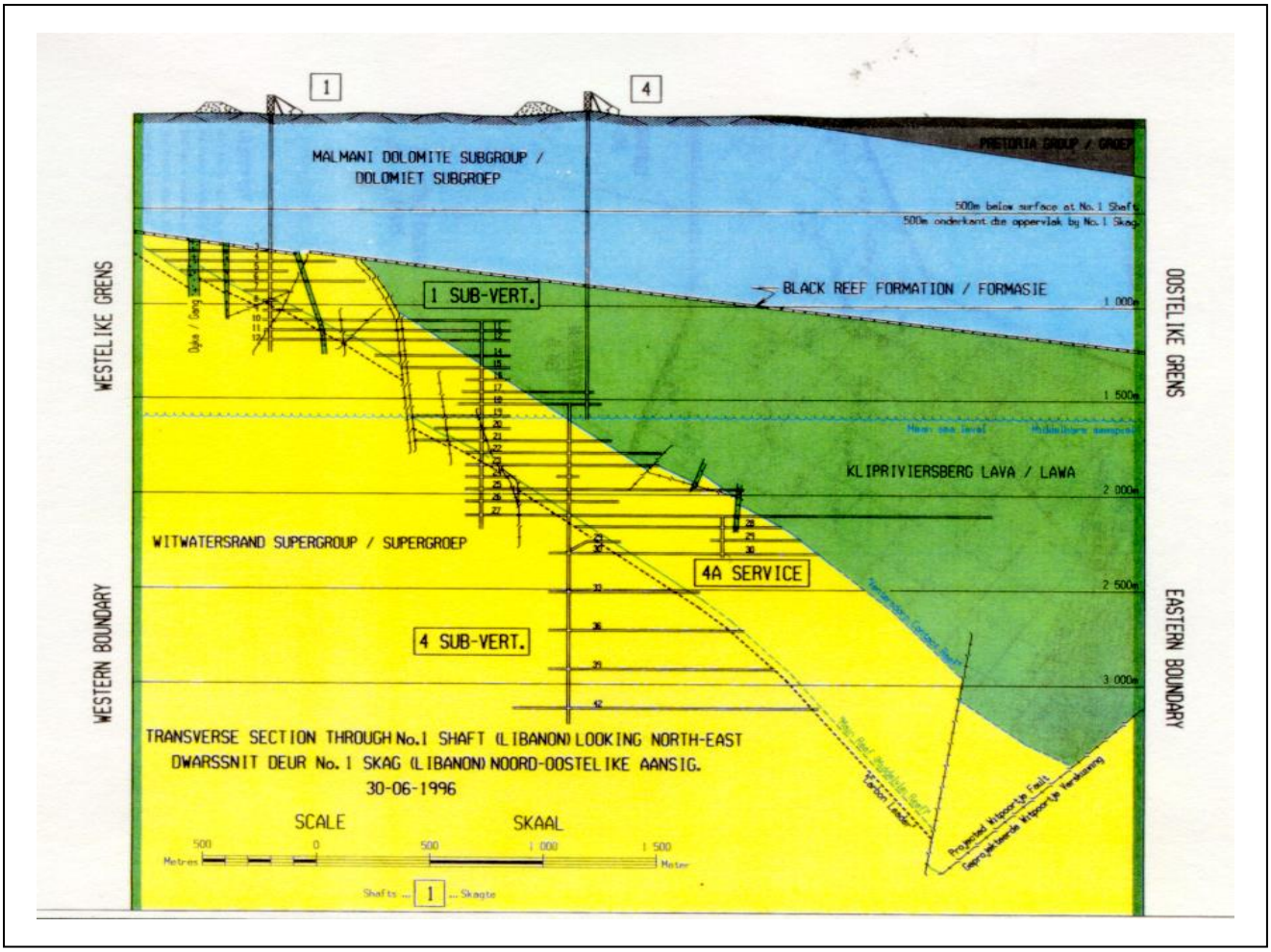


Figure 2.7.2 Section through some of the Mine A shafts (after Anon., 2012).

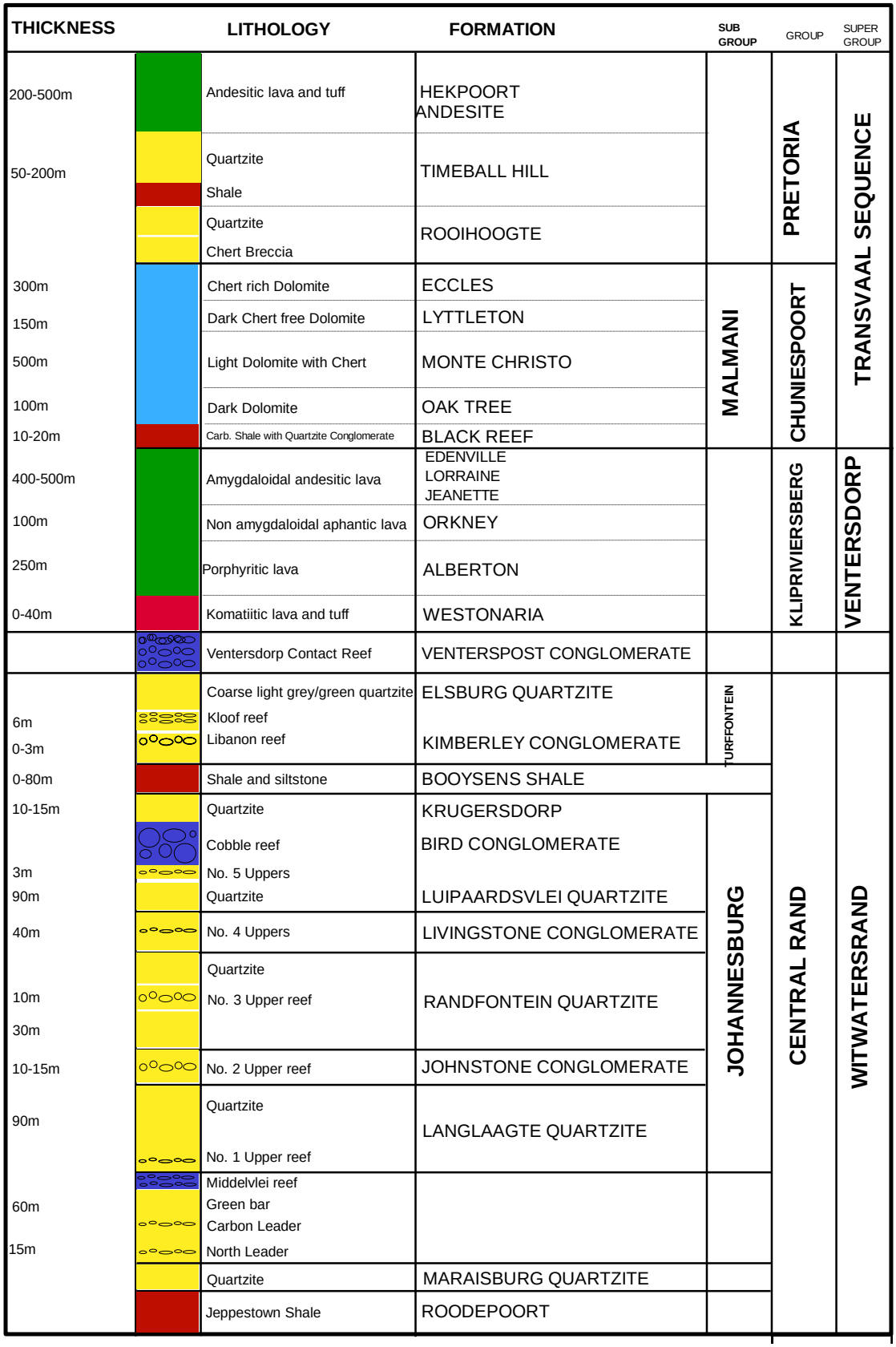


Figure 2.7.3 Generalised stratigraphy at the Mine A operations (after Anon., 2012).

The primary reef extracted at these operations is the VCR. The VCR is an unconformity with regards to the regional strike and dip. The VCR generally strikes East-Northeast with a dip of 21º. The dip varies largely due to the paleomorphic slope-terrace model as depicted in Figure 2.7.4. The secondary reefs dip at a steeper angle than that of the VCR and the middling between the reef bands thus increase when moving away from the sub-outcrop positions (Anon., 2012).

The mine has adopted the terrace and slope model for the VCR. The model suggests that river terraces and their associated deposits were developed on a relatively flat surface. These terraces formed on the river valley floors and were formed as part of an eroding fluvial environment. This type of system is characterized by paired terraces and the deepening of successive deposits depicted in Figure 2.7.4. The slopes that are referred to are weathered areas inter-connecting the different terraces and are usually found at a steep incline with poor mineralization.

The terrace model for Mine A consists of a complex system of terraced areas with alluvial fanning, braiding and other fluvial related depositional characteristics, which is further complicated by the uneven footwall lithology.

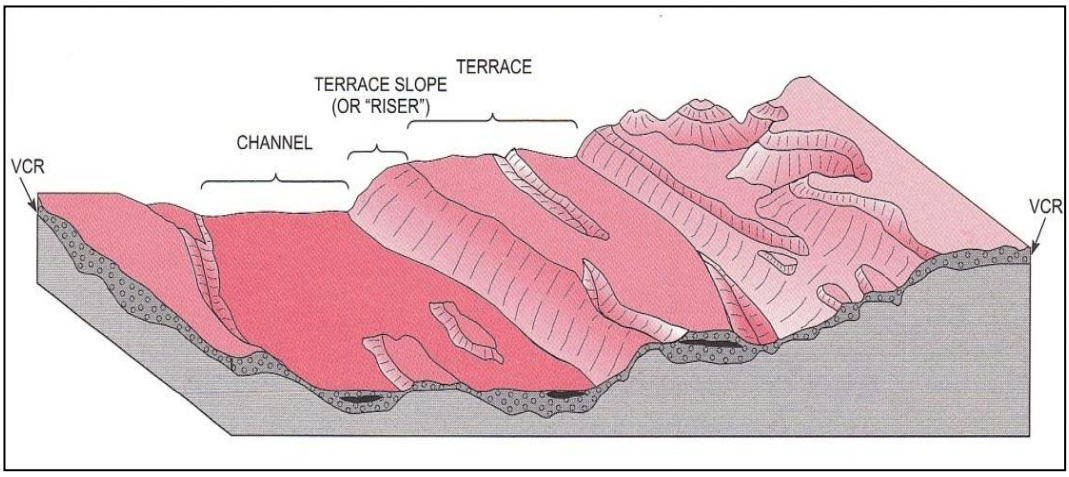


Figure 2.7.4 Simplified geomorphological model indicating the slope terrace model (after Wilson and Anhaeusser, 1998).

The area is further disturbed by a series of North-Northeast striking faults. These faults are generally high angle normal faults with throws of less than 70 m, whereas the dolomitic dykes in the area strike in a Northerly direction.

Because of the unconformity of the VCR, the VCR hangingwall consists of lavas, whereas the footwall consists of quartzites or fairly competent shales. The reef itself is a coarse grained conglomerate with a UCS of approximately 200 MPa. The hangingwall lavas are found as two types namely the Westonaria formation (WAF) and the Alberton lava. The Westonaria formation sub-outcrops onto the Alberton formation on the shallower portions of the lease area, below 2500 m. The Alberton lava is a fine grained basaltic lava and is usually amygdaloidal. This lava has a compressive strength in excess of 220 MPa and thus results in fair hangingwall conditions. Owing to its strength, it is prone to seismicity and will tend to form blocky conditions if exposed. The WAF on the other hand is a fine grained komatite, ultramafic lava with a compressive strength as low as 40 MPa. The WAF usually results in poor hangingwall conditions due to its weak strength, presence of quartz veining and parting plane faulting. The WAF will mine itself if exposed or damaged during mining operations. This situation is further complicated by the presence of pillowing within the formation, as well as the thinning of the WAF layer as the sub outcrop is approached (Anon., 2012). The other rock types that is found in the immediate vicinity of the reef includes;

- Mylonite occurs on the contact between the VCR and WAF with a thickness of up to half a metre, creating very poor conditions.
- Khaki shale, a fine grained altered shale found within the reef package resulting in laminated conditions with a low strength.
- Elsburg quartzite is usually found in the footwall and generally has a UCS of more than 220 MPa. This rock type is laminated with various bedding planes, but it is nevertheless very competent.

2.8. EXAMPLE OF CURRENT REMNANT PRECAUTIONS AT MINE A

As multi-reef mining is frequently associated with remnant conditions, the current remnant precautions at Mine A are discussed below for the benefit of the reader. The adopted risk management and fall-of-ground prevention initiatives at Mine A, does not differ significantly from the recommendations made by the Rockburst committees of 1915 and 1924. These strategies include the following aspects that are considered during the design and planning of remnant mining;

- a background overview,
- planning of the extraction of the block of ground and
- documentation.

During the background overview of a block of ground, the following aspects should be considered:

- mine design,
- underground investigations,
- geological report and
- seismic analysis.

To determine the optimal mining design and layout, the following should be considered:

- Determine why the block was not mined during the primary phase.
- Collect and collate all known information and damage reports.
- Determine if any extraordinary events such as fires, flooding or bursting occurred in the past.

- Review the plans and consider the position relative to other remnants, the geological setting, the lithology, the geotechnical area and associated risks, the access development and associated risk with the development.

During the underground investigations, the following should be examined:

- Off-reef excavations, access ways and escape routes in order to determine areas that should be re-supported, re-opened or re-developed.
- Conditions of the areas surrounding the block to be mined.

The geological information report should include the following:

- The description of the geology.
- The relevant stratigraphy of the area, including possible changes in dip, strike or folding and potential planes of weakness.
- Expected grades of the block of ground.
- Information on the geological structures (and infilling) present in the area, including the trends and nature of the structures.
- The location certainty of the structures as well as work required to establish their positions.
- Possible sources of water, flammable or noxious gas.
- Sections of the block of ground.

The seismic report should contain at least:

- Detail such as the M_{max}, peak particle velocities (PPV), diurnal distributions and mean return periods for certain magnitude ranges.
- The source mechanisms of the larger events should be analysed.
- The potential of seismicity on geological structures should be assessed.

- The seismic network status, coverage and accuracy should be stated as well as required future expansions.
- A seismic hazard classification for the mining area.

The following activities are related to the planning of the block of ground:

The first step is to determine practical and viable alternatives using all the information gathered during the first step of the process as well as by taking cognisance of access and egress, transport, cleaning, ventilation and material transportation. The layout should also conform as far as practically possible to the rock engineering best practices, such as:

- Mining towards the largest solid,
- Mining away from geological structures,
- Mining at an oblique angle towards geological structures,
- Mining remnants in the direction of elongation,
- Consideration of the orientation of cross jointing and fracturing caused by previous mining,
- Avoid the mining of multiple remnants in close proximity,
- A limited extraction rate.

To assess the options proposed above, the alternatives should be numerically modelled and compared. In the modelling report, the program used, input parameters, intention of the model and all assumptions should be stated as to ensure that the results contained in the report is not misinterpreted. Some of the parameters that could be compared are:

- ERR
    - Compare different extraction sequences.
- ESS
    - Compare possibility and expected potential of slip on geological structures and abutments for the different extraction sequences.
- APS
    - Compare the APS to the strength ratios of the different sequences to determine the potential for pillar punching.
    - The width-to-height ratio as well as effective width to height ratio should also be considered.
- Field stress acting on off-reef excavations
    - Compare the stress to the strength ratios applicable to the access development for the different sequences to determine probable failure potential of the extraction sequences.
    - From past experience, it was found that a major principal stress in excess of 120 MPa requires the installation of ringset support, while a major principal stress in the range between 60 and 120 MPa requires the installation of secondary support and in a major principal stress field of less than 60 MPa, primary support should suffice.

The final step would be to formalize the mining sequence by documenting the selection criteria and results of the previously mentioned steps. This would also entail the drawing up of a Master Plan in order to visually explain the optimum sequence. Once again all the relevant geological structures, access ways and egress ways, remnants and planned pillars should be identified on such a plan (Anon., 2012).

Even if all the industry best practices and the previously mentioned methodology are diligently followed, the mining of a block of ground can still pose a risk. The residual risk should be mitigated by adhering to some generic practices. In general the following risk mitigating factors should be implemented (Anon., 2012);

- Regular advance of the stope face.
- Leads and lags should be controlled.
- Stope faces should be pre-conditioned.
- Rock conditions should be monitored by obtaining feedback from production personnel as well as site investigations.
- Exposure of the workforce to risks should be minimised.
- Seismicity should be monitored and a system implemented to identify elevated seismic risks.
- Longer term seismic hazards should be identified and incorporated into the planning.
- Systems should be put in place in order to monitor and record damage to the workings.
- Compliance to mitigating instructions should be investigated during collective planning meetings and the compliance monitored on an ongoing basis.
- Support systems should be designed using units capable of dynamic deformation, taking into account ground conditions, failure mechanisms and anticipated stresses.
- In some cases, the area coverage of support should be increased by reducing support spacing, introducing more units or increasing the area of contact in order to reduce the fall of ground risk in an area.

While not all the risk conditions will be included in the generic practices, the more site-specific risks should be addressed during the detailed planning session.

2.8.1 Work area classification

The first part of the planning session should revolve around the area classification with the options of Normal, Precautionary Special or Restricted Special Areas. Each of these classifications may have additional generic precautions in order to reduce or mitigate risks while mining.

The detailed planning should then focus on the following areas, Cleaning arrangements, access and egress ways, on-reef travelling ways and areas of refuge (Anon., 2012).

- In order to ensure that no accumulations of ore is present in high risk areas, the planning of gullies, gully depth, routing of service systems and pulling distances should be considered.

- To secure the access and egress ways to a high risk area, the travelling ways should preferably be from two independent levels. The travelling ways should also not be routed so as to traverse the same geological structure. In general, the travelling ways should be supported with secondary support if possible.

- On-reef travelling ways should be clearly demarcated, supported with support units that are able to absorb dynamic deformation and long axis packs in order to ensure long-term stability.

- The waiting place and refuge chamber should be situated in areas that are not likely to be affected by stress changes or affected by geological structures.

When the generic precautions alone will not suffice, an area should be declared as a Special Area. Special Areas can be divided into two classes – Precautionary and Restricted where the latter is seen of one of the highest risk classifications for a

mineable block of ground. To classify the working area, various factors should be considered in the form of a hazard ranking. The factors should include results from numerical modelling, risk derived from a seismic back analysis, risk posed by the physical conditions underground, the potential for instability and the collapse of access ways to the area as well as the nature of major and minor geological structures in the proximity of the working area.

When an area is classified as a special area, additional written communication is required to ensure that the supervision is aware of the classification, as well as the specific instructions regarding decisions, layouts and precautions. Start, stop and offline-notes should be prepared by the surveyor in order to properly guide the mining and layouts. Some of the additional measures should be as follows (Anon., 2012):

- Geology to be updated on the 1:200 survey plan following the monthly measurements.
- A detailed planning session should be held after this in order to review the proposed mining.
- The minutes and the site specific special recommendations of the planning meeting should be captured and distributed on a Special area control sheet.
- All relevant parties, Mining (day and night shift), Safety, Geology, Ventilation, Rock Engineering and Management should agree to the special recommendations to be carried out in the area by signing off the special area control sheet.
- A signed copy of the special area control sheet, in conjunction with the applicable support standards, should be displayed on the waiting place notice board.

- The working area should be identified underground and on the 1:200 plans displaying notices stating “Special Area”.

- If adverse ground conditions are experienced, the Rock Engineering Department should issue a report stating the additional recommendations to rectify or improve the conditions or to reduce the potential risk associated with the condition.

- The Safety Department and Rock Engineering should visit these panels more frequently, at least once a month, in order to gauge compliance and monitor conditions.

CHAPTER 3
COMPARISON OF CODES TO SIMULATE MULTI-REEF MINING

Jager and Ryder (1999) indicated that it is difficult to determine the parameters influencing multi-reef mining. Numerical modelling is nevertheless valuable in this regard. Napier and Malan (2007) illustrated that a displacement discontinuity code can simulate multi-reef environments. The limitations of existing modelling codes nevertheless needs to be carefully considered when interpreting data from such an analysis.

A difficulty with displacement discontinuity codes is that numerical instability can be experienced when simulating multi-reef environments in close proximity. This is particularly problematic if the reefs are closer than 3 element lengths for constant strength elements.

Maritz (2014), Napier and Malan (2007) and Maritz, Malan and Piper (2012) illustrated that the TEXAN code is suitable to simulate multi-reef environments when assuming an elastic rock or material. TEXAN can currently solve 2D and 3D problems with multiple interacting tabular reef planes and planar fault planes. The rock is assumed to be elastic and isotropic. Of particular interest for this current study and the multi-reef geometries that need to be simulated when doing remnant de-stressing, is the ability of the code to use higher order elements. This allows for the simulation of closely spaced reefs and accurate calculation of the tensile zones above the stopes. The author compared two codes available for this study and a series of numerical runs were conducted using both TEXAN as well as
MinSim 2000.

3.1 NUMERICAL MODELLING CODES

Historically, numerical modelling tools were developed for the quantitative analysis and design of tabular mine layouts. These tools had their origins in the

United Kingdom during the 1950s and 1960s. For simple geometries, analytical solutions are available, but the problems are usually too complex and numerical approximations are required (Salamon, 1964).

The underlying principle is the use of a discontinuity in the rock mass to represent a "jump" in the displacement field. This underpinned further developments made by a number of researchers and was captured in a paper by Hackett (1959). He studied an analytical model of narrow width parallel-sided coal mine panel excavation. Closed form analytical solutions of longwall excavations with stabilising pillars were not available due to the complexity of these problems.

Stress distributions around complicated tabular layouts were later developed using a number of analogue and digital computational approaches. The construction of a purpose-built analogue device, such as the electrolytic tank in 1964, was one such development. Subsequently, further analogue computers were developed which comprised of resistor arrays (Salamon et al., 1964, Cook et al., 1966).

During the 1960s, Salamon proposed the so-called "face element principle" (Plewman et al., 1969). He described this principle in a series of papers published in 1964 and 1965. This was the forerunner of the numerical modelling technique known today as the displacement discontinuity method. Salamon's method provides a basic building block to solve a complicated mine layout geometry. Compared to other methods, by only discretising the boundaries rather than the full fabric of the rock mass, it leads to major gains in computing efficiency. Boundary element methods are, however, not suited to model inelastic rock mass behaviour.

Deist developed one of the first versions of MINSIM ('MINing SIMulator') during 1960 (Plewman et al., 1969). Moris subsequently enhanced the program during 1970 in order to allow for the analysis of shallow areas with a free surface. The code was further developed as MINSIM-D by Ryder and Napier (1985). This code was designed to analyse multiple interacting reef and fault slip problems. TEXAN (Tabular EXcavation ANalyser) is a more recent development by Napier to

accurately simulate pillar stresses on a large number of pillars over an extensive mining area (Napier and Malan, 2007).

Both MINSIM and TEXAN are boundary element codes and therefore possess greater computing efficiency and can be easily applied over a large range of problems such as stopes or planes of weakness when compared to finite element codes. The actual mining problem, when using MINSIM, is solved by superimposing a grid of elements over the mined areas. TEXAN can employ a number of higher order triangular or square elements to more accurately simulate the geometry, whereas MINSIM only superimposes a square grid.

3.2 EFFECT OF ELEMENT SIZES ON APS

To investigate the differences between the numerical codes and theoretical calculations, the relationship between APS and element size was investigated. Errors can arise when determining the average stress, depending on geometry, layout, element size and shape. In order to benchmark the two numerical codes, a simple single strip pillar between two parallel-sided panels was analysed as depicted in Figure 3.2.1.

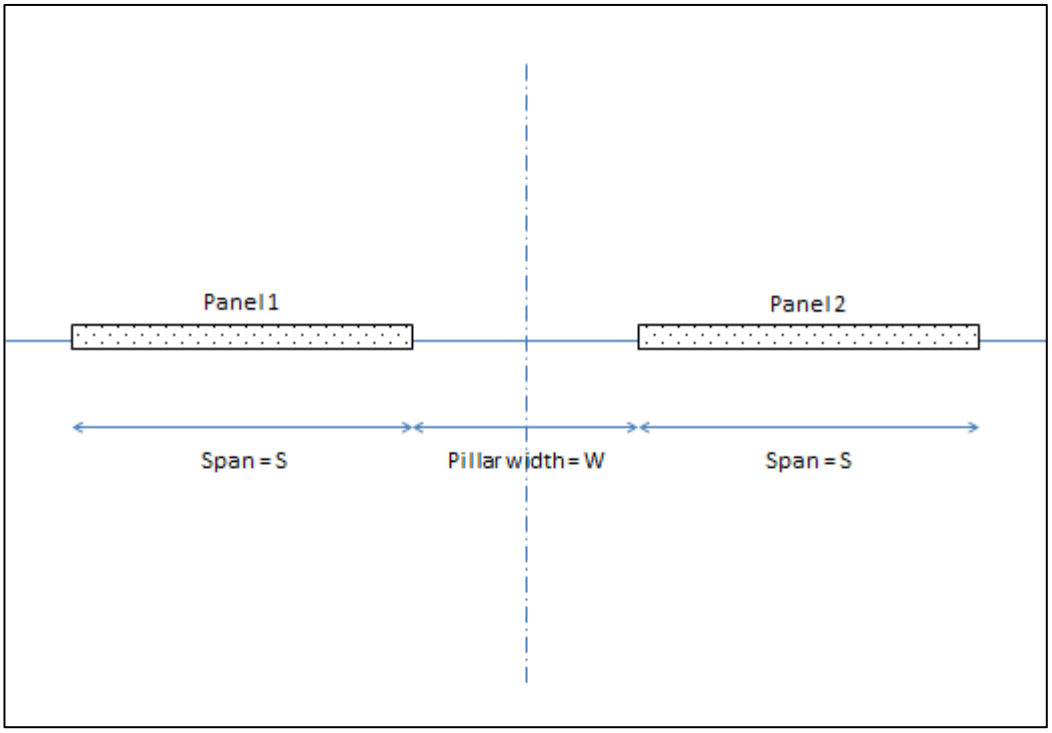


Figure 3.2.1 Cross-section of two parallel sided panels with a central pillar.

The analysis was conducted using the generic parameters listed in Table 3.1.

Table 3.1 Numerical modelling parameters used in the numerical codes.

Parameter	**Value**
Virgin stress	100 MPa
Young's modulus	72 GPa
Poisson's Ratio	0.2
k-ratio	0.5
Span	120 m
Pillar width	24 m

The analytical expression to determine the average stress of this scenario is: (Salamon, 1968).

$$\frac{\sigma_{zz}}{\sigma_{vzz}} = \frac{\pi}{2K(k)\sqrt{1-k^2}} \tag{3.2.1}$$

Where K(k) is the integral defined as;

$$K(k) = \int_0^{\pi/2} (1 - k^2 \sin^2\theta)^{-1/2}\ d\theta \tag{3.2.2}$$

and k is given by;

$$k^2 = 1 - \left(\frac{w}{w+2s}\right)^2 \tag{3.2.3}$$

The equation can be solved by assuming constant elastic convergence and by setting the total stress at the centre of each panel element to zero (Napier and Malan, 2011). This will however cause some error depending on the choice of element size. Figure 3.2.2 plots the values derived by Napier and Malan (2011) and a MinSim solution conducted for this study on one graph for comparison.

From this figure it can be seen that the MinSim values are 1% lower, but the trend is the same.

When analysing square or circular excavations, errors are generated as shown by Napier (1983). When assessing ERRs in slits, linear displacement discontinuity elements are ineffective and erratic errors of more than 40% can result due to the size of the grid used. To minimise the errors, the grid size can be reduced, but the most efficient method to overcome this would be to use higher order elements. Alternatively the grid could be adjusted by a fraction and this process is referred to as the quarter grid correction. This adjustment bring the error from a possible ¾ to 1/16th of the original grid. This correction has been built into the MinSim modelling code (Ryder and Napier, 1985). The difference in APS observed in Figure 3.2.2 can be attributed to the quarter grid correction built into the MinSim analysis.

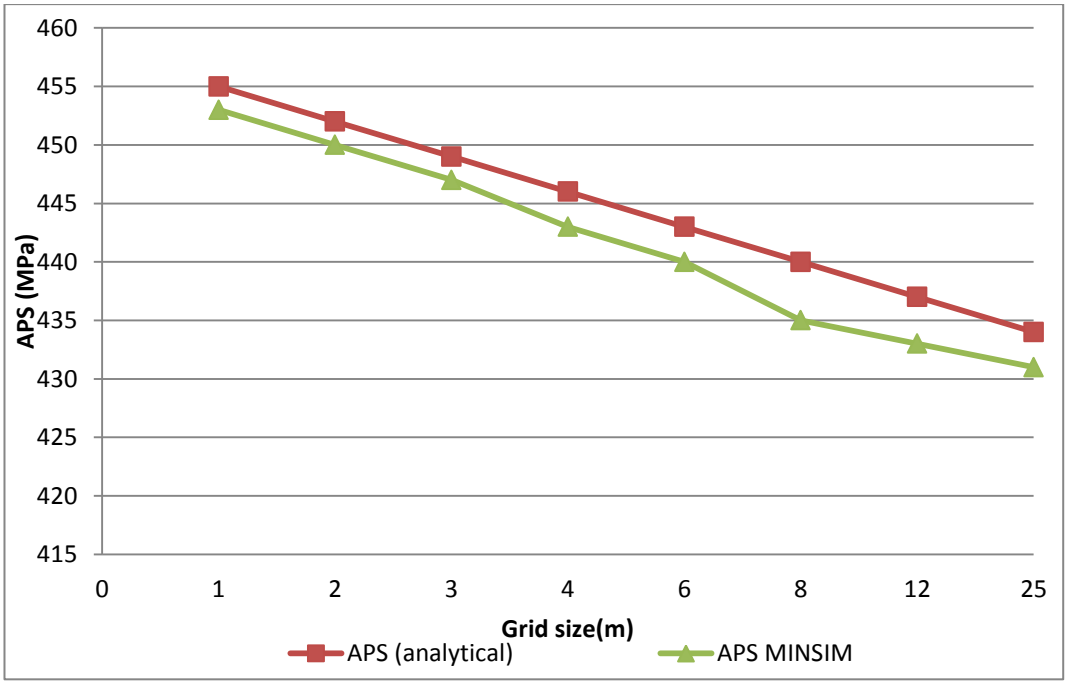


Figure 3.2.2 Average stress acting on a central pillar compared to grid size.

The analysis can be expanded to a circular pillar in the centre of an annular excavation as depicted in Figure 3.2.3. The analytical solution is given in Napier and Malan (2011).

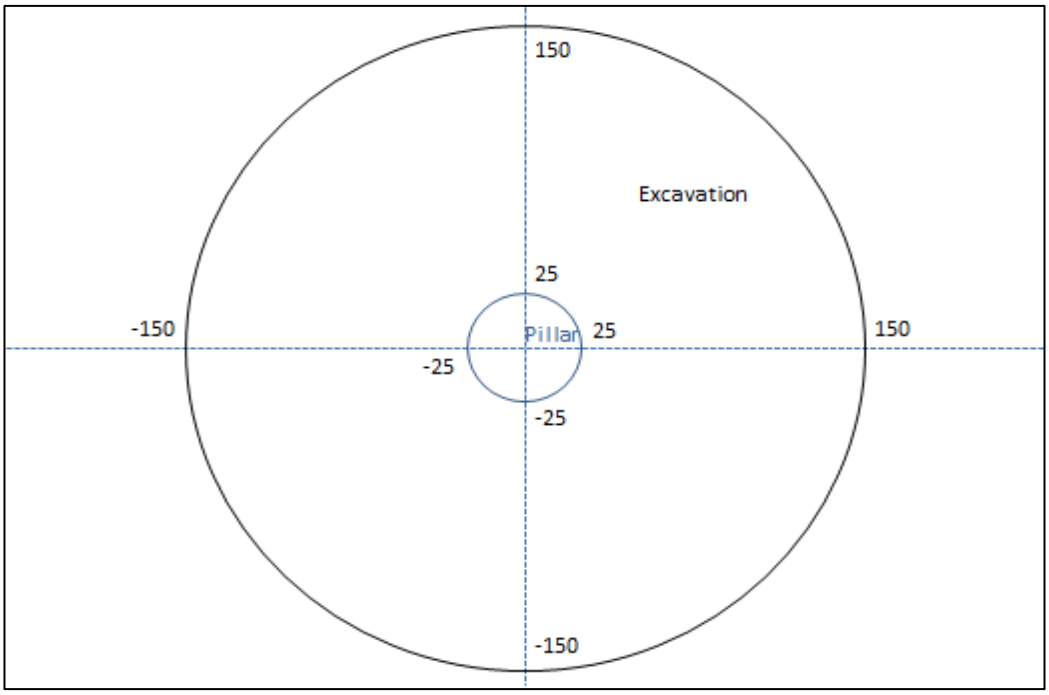


Figure 3.2.3 Layout used for the circular pillar analysis (after Napier and Malan, 2011).

From Figure 3.2.4 it can be seen that the MinSim calculations done for this study have the same trends for the two different types of analyses.

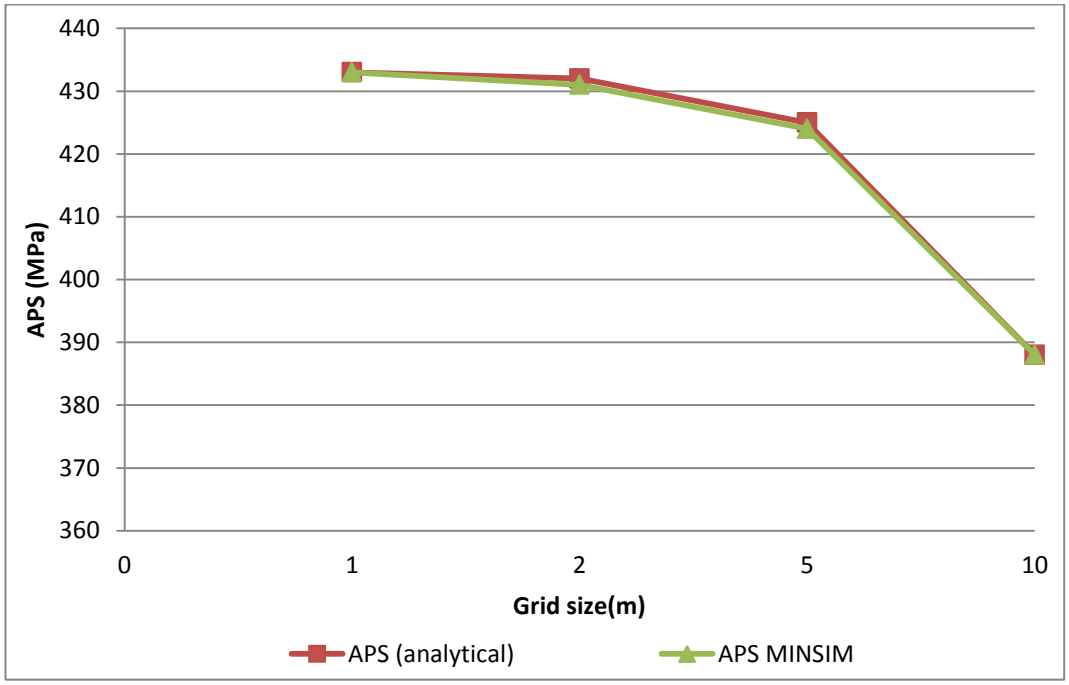


Figure 3.2.4 Average stress acting on a circular pillar compared to grid size.

In both Figures 3.2.2 and 3.2.4 it can be seen that the stress values follow a similar trend. Malan and Napier (2011) noted that the analytic solution for the simulation depicted in Figure 3.2.1 has a value of 455.91 MPa and that the TEXAN code extrapolated value have an error of only 0.03%. This was estimated by using evenly sized and finer elements and a number of runs to examine the trend.

3.3 GENERAL LAYOUT FOR A MULTI-REEF COMPARISON

The numerical modelling parameters used for the preliminary multi-reef simulations are given in Table 3.2. To investigate the mechanism of overstoping, a simplified geometry was used for the initial simulations (Figure 3.3.1). It was simulated with no dip and the depth was 2000 m. Although only one pillar was understoped, a second pillar was included in the simulation to illustrate the increase of stress on this second pillar after the first pillar was extracted. Figure 3.3.2 illustrates the extent of the understoping on a different reef and Figure 3.3.3 the sequence in which this understoping was simulated.

Table 3.2 Numerical modelling parameters used in the numerical codes.

Parameter	Value
Depth	2000 m
Young's modulus	70 GPa
Poisson's Ratio	0.2
Rock density	2700 kg/m^3
k-ratio	0.5
Element size	5 m

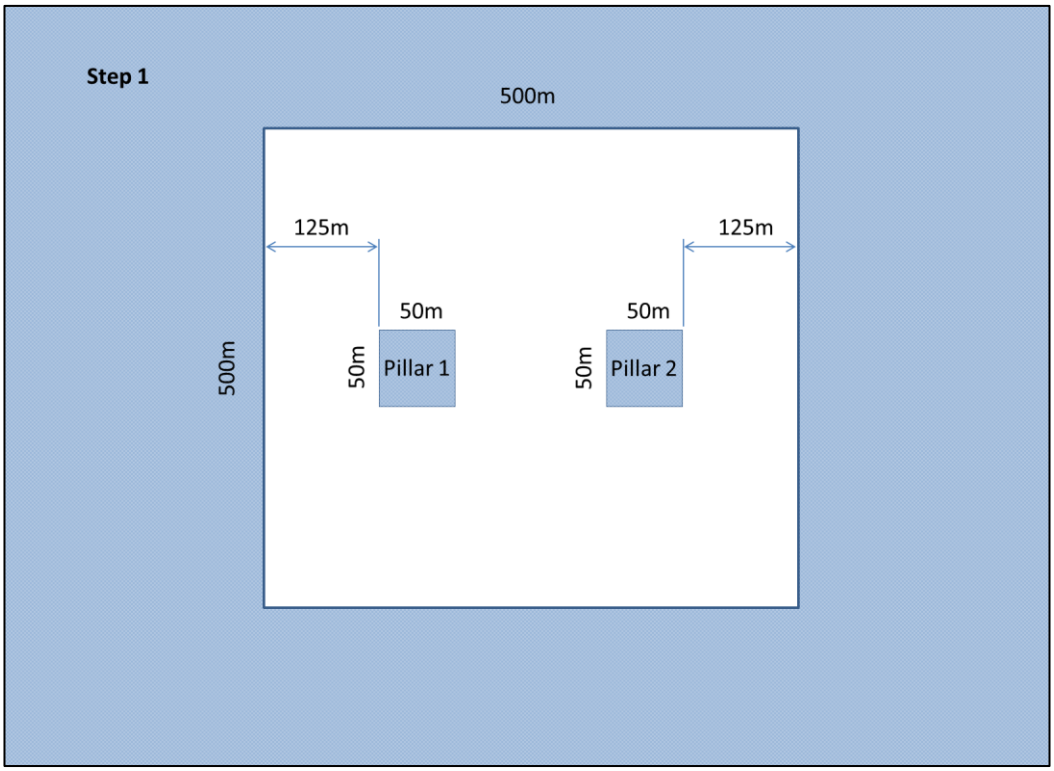


Figure 3.3.1 Geometry used for the initial simulations (A similar geometry has been used by Napier and Malan, 2011).

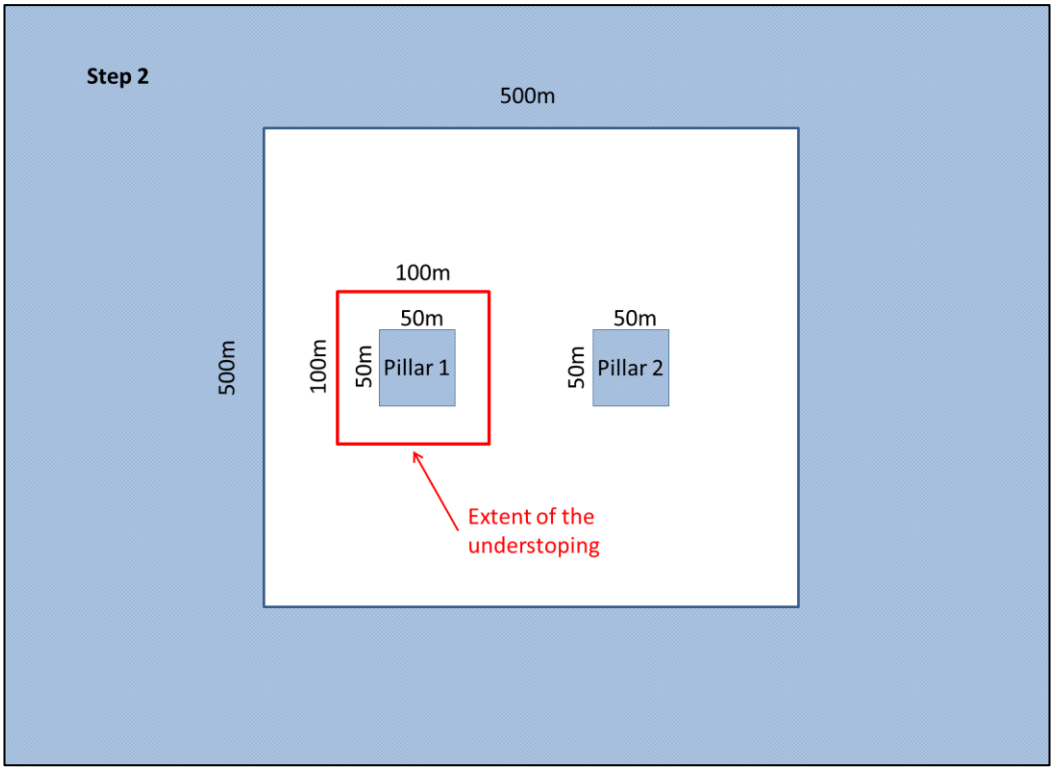


Figure 3.3.2 The extent of the understoping of the first pillar.

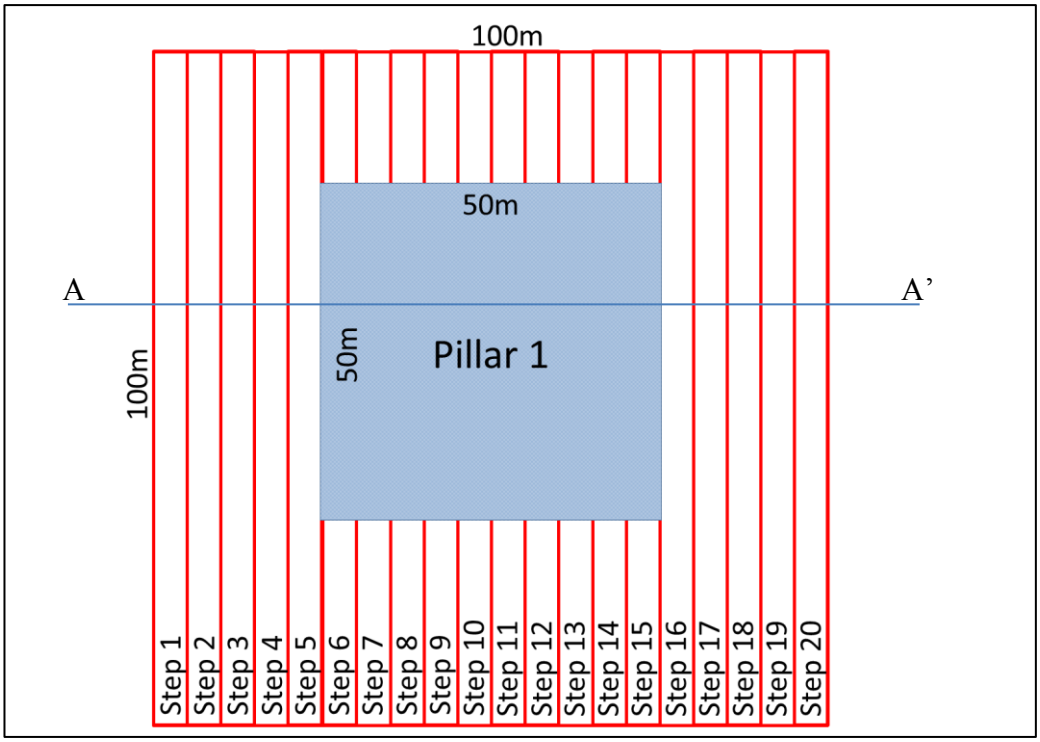


Figure 3.3.3 Sequence of understoping the first pillar.

3.4 RESULTS FROM THE SIMULATIONS

In order to investigate the similarity between the two numerical codes, a number of key parameters were investigated for comparison and analysis.

3.4.1 Middling

For the first few simulations, the geometry shown in Figures 3.3.2 and Figure 3.3.3 was used and the effect of middling was investigated. Figure 3.4.2 illustrates this geometry in the MinSim code. The size of the de-stressing cut was kept constant at 100 m x 100 m and a middling of 25 m, 20 m, 15 m and 10 m was investigated. The maximum middling of

25 m was not exceeded in the model as this resulted in the so-called "45° rule" (Figure 3.4.1) still being met by the size of the understoping. The concept of the "45° rule" entails that if the mining overlap on the understoping is more than the vertical middling, it is expected that the pillar between the mined out areas should be de-stressed.

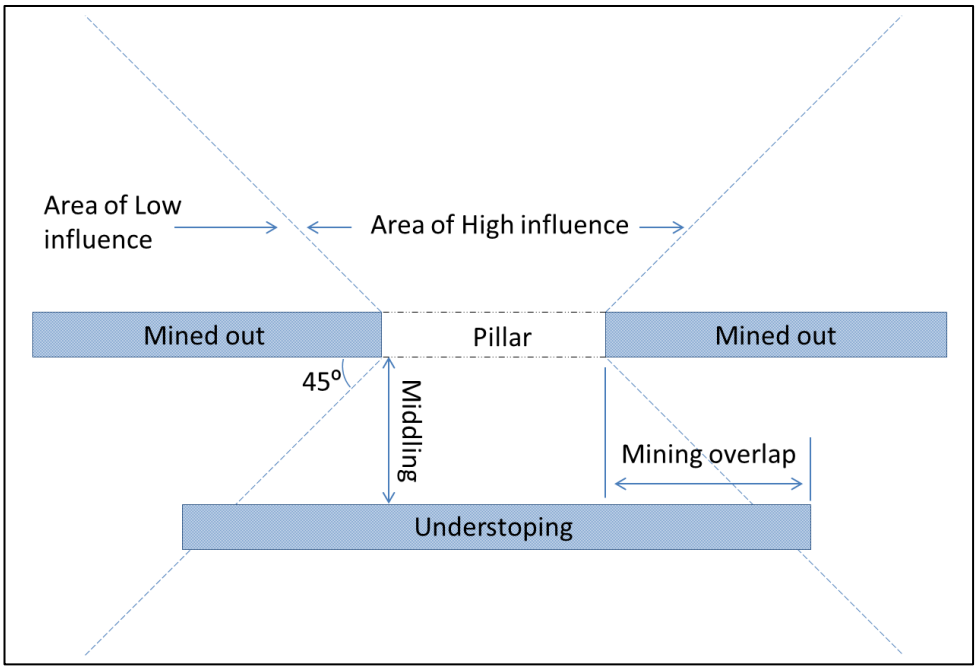


Figure 3.4.1 Schematic section illustrating the "45° rule".

Figure 3.4.3 illustrates the pillar stresses as a function of middling. For the pillar which is understoped, the stress decreases with decreasing middling. This reduction in stress must be transferred elsewhere and for Pillar 2, the stress increases slightly as Pillar 1 is being de-stressed. This increase in stress on Pillar 2 is not in proportion to the reduction in Pillar 1 as the abutments also carry a significant portion of the increase in stress. Surprisingly, the 25 m middling still resulted in a high stress on the pillar that was understoped (Pillar 1) and care should therefore be exercised with the 45° rule.

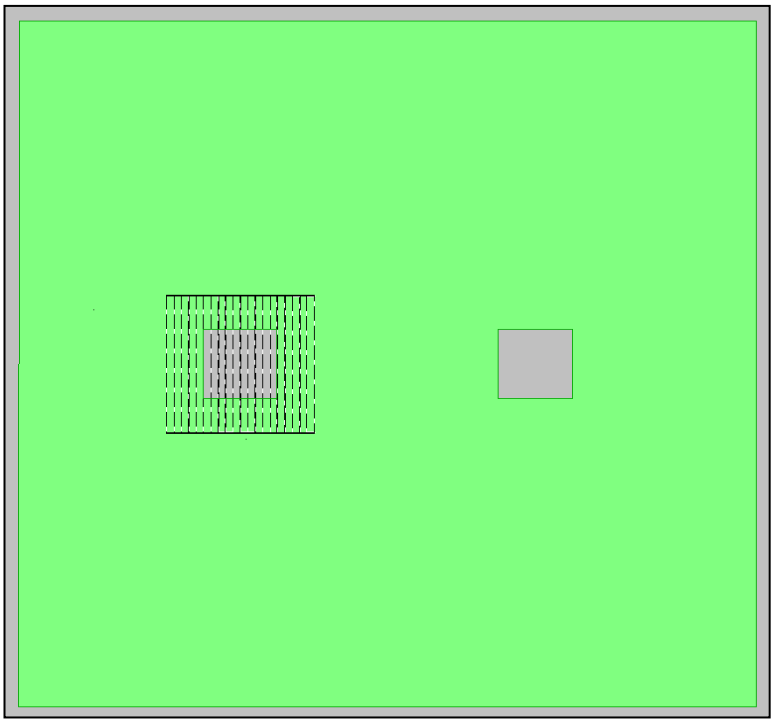


Figure 3.4.2 MinSim screenshot of the modelled layout.

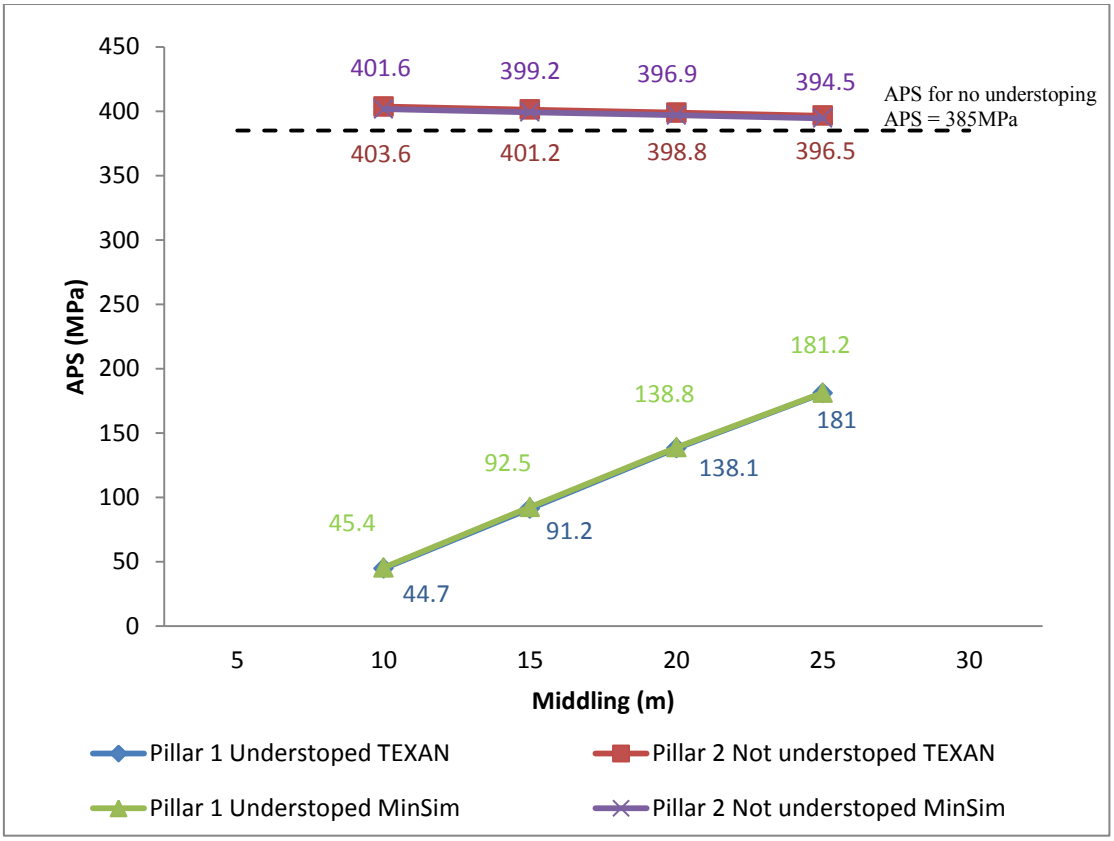


Figure 3.4.3 Effect of middling on the stress on Pillars 1 and 2. Both the MinSim and TEXAN results are shown.

3.4.2 ERR values and the process of understoping

ERR is a useful indicator of stress concentration and in some cases there is a good correlation between ERR levels and seismicity (Ryder and Jager, 2002). In numerical codes, the ERR is typically calculated as

$$ERR = \frac{1}{2}\sigma_b S_a \quad (3.4.1)$$

where;

σ_b = normal stress acting on the stope face

S_a = convergence behind the face

Figure 3.4.4 illustrates the sequence of understoping in order to compare the ERR on the de-stressing cut as it is being mined incrementally below the pillar. The middling was simulated as 25 m. The ERR for the TEXAN run was calculated using the ERR equation shown above.

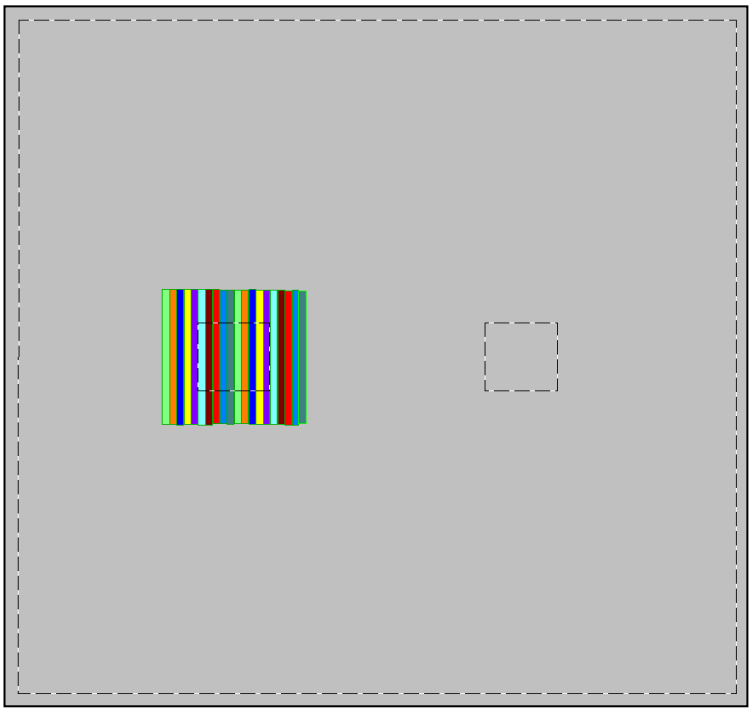


Figure 3.4.4 MinSim screenshot of the modelled layout.

When comparing the results obtained from the two codes in Figure 3.4.5. it can be seen that the values obtained are very similar, however it seems like the MinSim values are "lagging" when compared to the TEXAN results. The different MinSim results are caused by the quarter grid correction which is not implemented in TEXAN. Note that the peak ERR is observed when the understoping is almost completed and when the understoping face is close to the second abutment. The peak value for this geometry and depth is approximately 20 MJ/m².

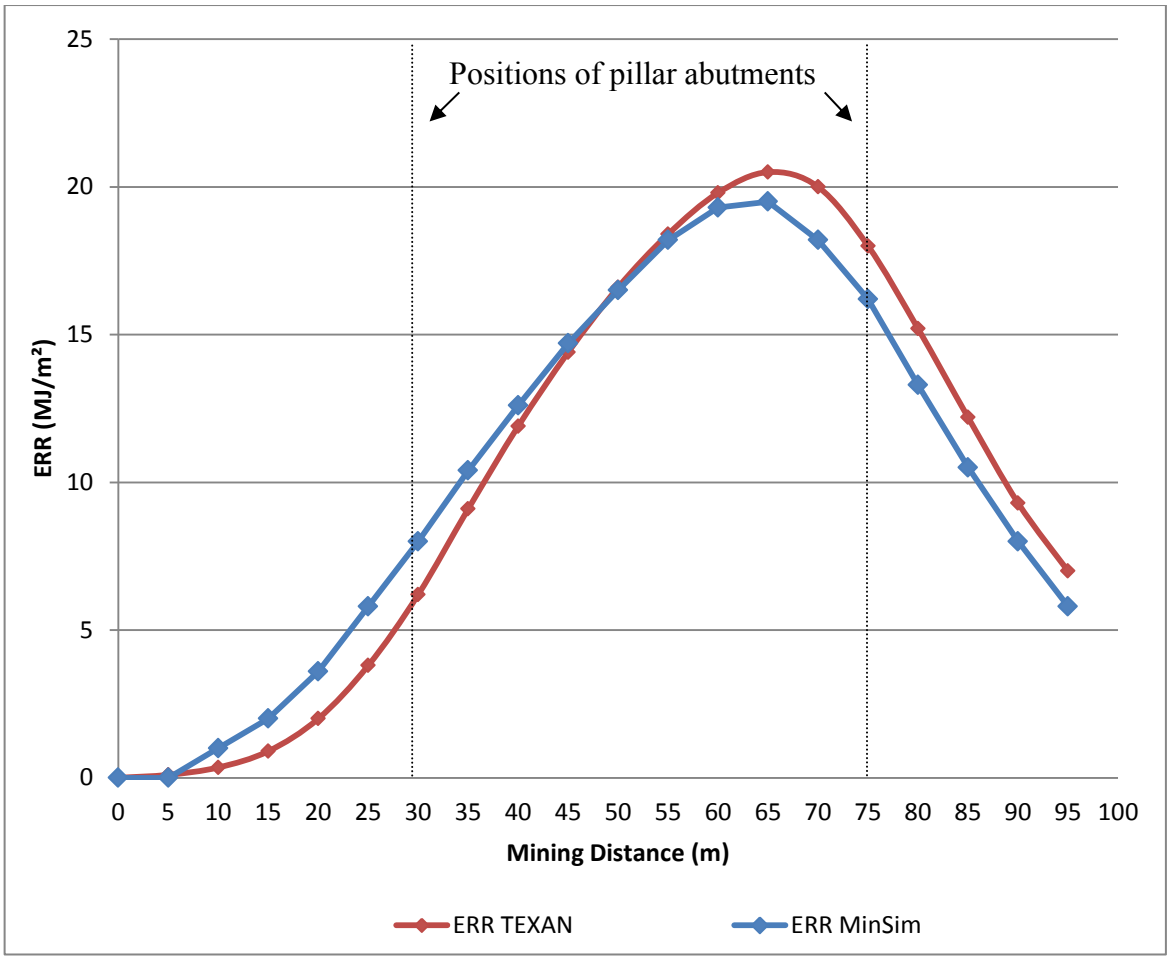


Figure 3.4.5 ERR of the understoping face when mined incrementally below Pillar 1.

Compared to the ERR on the understoping reef plane, Figure 3.4.6 illustrates the ERR on the plane of Pillar 1 when mining this particular pillar. The width of the pillar is 50 m and as expected, the ERR increases

very rapidly for the last few mining steps. When the pillar is already understoped, the ERR values on the pillar are much lower, although there is still a spike in values for the last few mining steps.

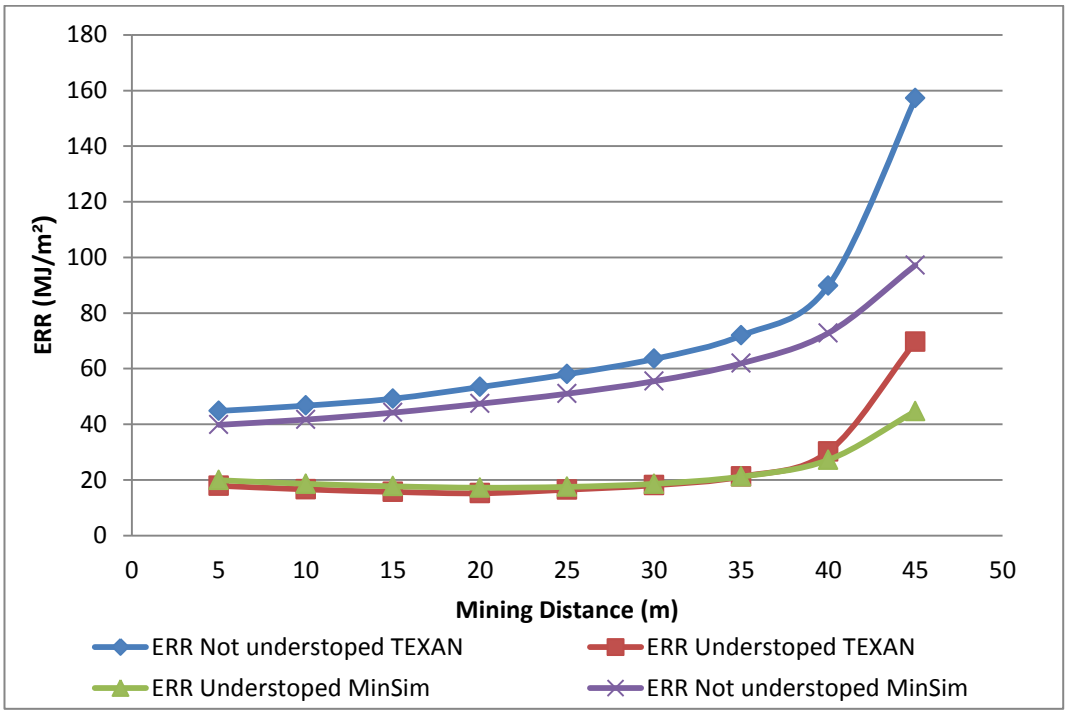


Figure 3.4.6 ERR on Pillar 1 while it is being incrementally extracted. This shows scenarios for when the pillar is understoped and not understoped.

Figure 3.4.7 illustrates the decrease in APS of pillar 1 during the process of understoping. The rate of APS reduction per metre advance (and stress redistribution) occurs much more rapidly when undermining the second abutment compared to the first abutment. Intuitively, it therefore appears that most problems (if any) during the understoping process would be experienced when the understoping crosses the second abutment. This is in qualitative agreement with the ERR calculations.

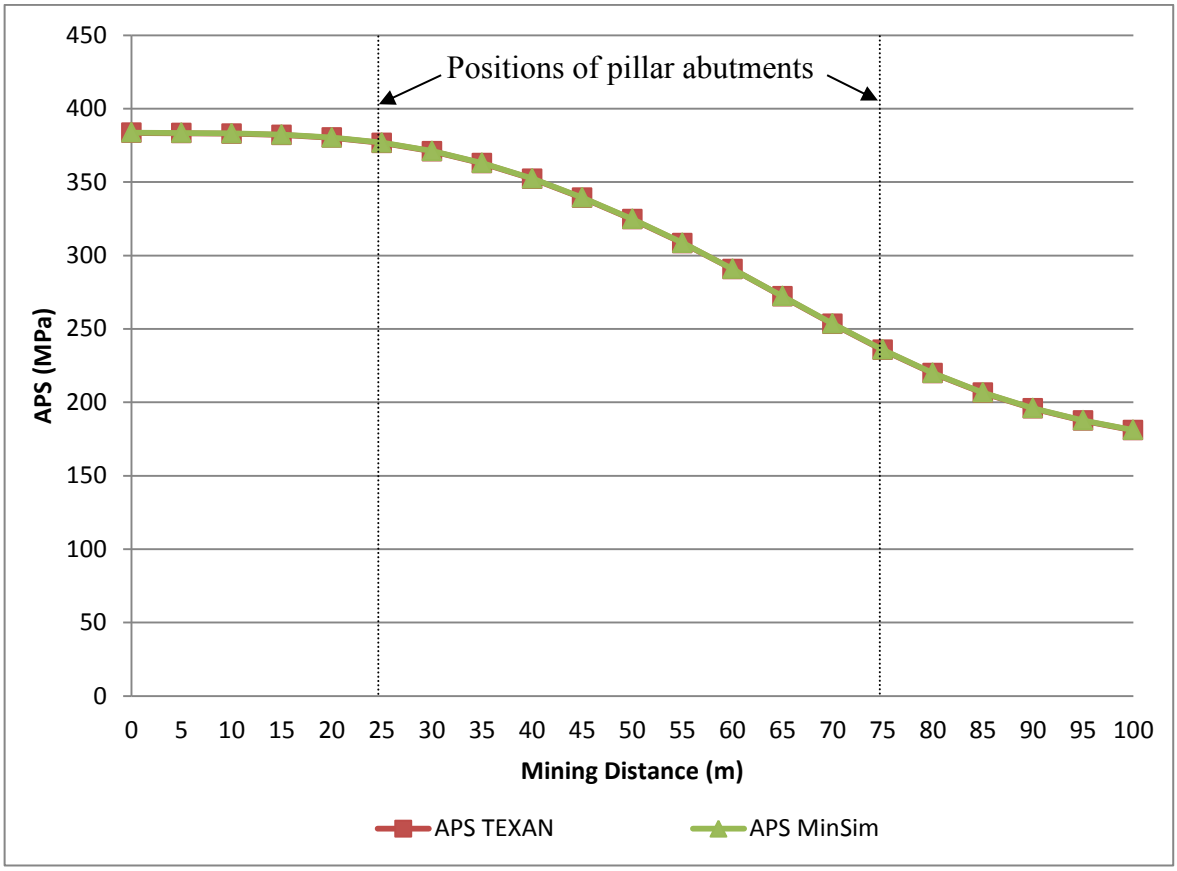


Figure 3.4.7 APS of Pillar 1 while it is being incrementally understoped.

From the results presented in this chapter it can be seen that there are no significant difference between the two modelling codes and they compare well to the analytical solutions in terms of APS if small elements are used. There were, however, a slight difference between results obtained with the two codes. The difference observed was small and is caused by the quarter grid correction in the MinSim code which is not implemented in TEXAN.

The effect and benefit of de-stressing was demonstrated in this chapter in terms of reduced ERRs and stresses. The effect of middling was also very evident in the analyses.

3.5 CONCLUSIONS AND RECOMMENDATIONS

Following a numerical analysis of a simplified multi-reef scenario, the key findings were:

- The effect of middling is important to consider when planning to mine a multi-reef remnants. Numerical modelling results indicate that care should be exercised with the application of the 45º rule. It appears that only a 50% reduction in stress is achieved when an overlap of 45º are applied – hence a low middling with a large overlap should be preferred.
- The numerical analysis indicated that although the understoping is slightly deeper than the remnant that is targeted for extraction, the ERR values of this de-stress mining are lower than that of the on-reef mining itself. A possible reason for the lower values are the small span of the de-stress cut.
- It is clear that the de-stressing cut has a significant effect in reducing the on-reef ERR values, when mining the targeted pillar on the primary reef.
- From the results, there are no significant difference between the modelling codes and both are used where applicable in the rest of the dissertation. MinSim was preferred for the actual geometries as it was easier to digitize the complex layouts.

CHAPTER 4

INVESTIGATING MULTI-REEF MINING USING AN EXTENDED ERR CONCEPT

To gain a better understanding of potential rock failure during understoping, a further study using the TEXAN code was conducted. Preliminary modelling described in this chapter indicates that a zone of very high major principal stress and low minor principal stress develops between the two reefs during the mining of the de-stressing cut. As described by Du Plessis and Talu (1997), this is considered to be hazardous and the reason why understoping is nevertheless done successfully in practice is not clear. The reason for the success is therefore further explored in this chapter. The study was conducted by using an "extended ERR" concept proposed by Napier (1991).

4.1 STRESS ANALYSIS OF MULTI-REEF MINING USING TEXAN

To understand the process of understoping, an analysis of the incremental stress evolution in the middling between the two reef horizons was conducted. The same model and parameters as described in Section 3.3 (Chapter 3) was used for this analysis. The plots illustrate a section through the centre of Pillar 1 and the stresses between the VCR and Libanon Reef horizons.

The Major Principal stresses along Section A-A' (see Figure 3.3.3) are plotted in Figures 4.1.1 to 4.1.5. All these simulations were conducted for a middling of 25 m. A series of simulations at 60 m and 90 m was also conducted.

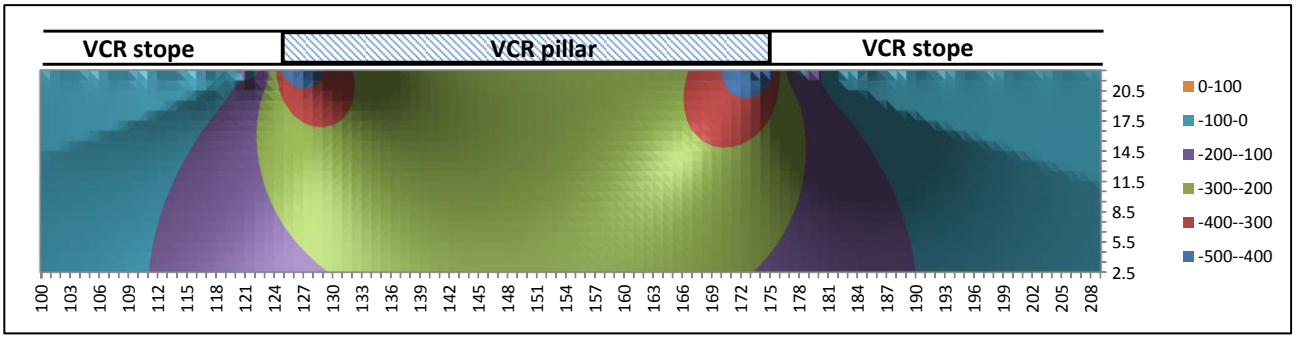


Figure 4.1.1 Major principal stress below the VCR Pillar 1 prior to any mining on the Libanon Reef. The region of very high principal stress is found at the edge of the pillar, but confined to localised regions. The stress convention is compressive stresses are negative.

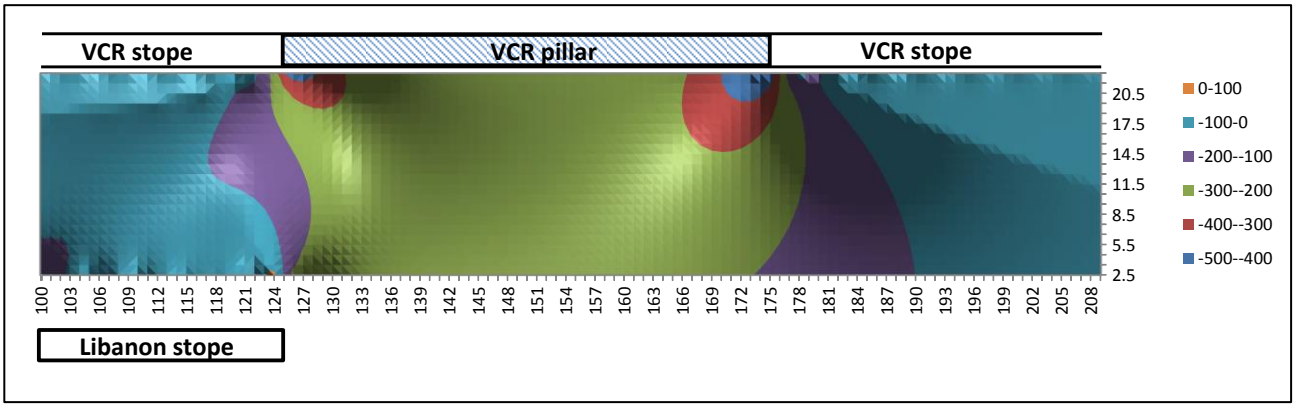


Figure 4.1.2 Major principal stress below the VCR Pillar when the Libanon Reef stope is below the first pillar abutment. The disruption of the stress field is minor at this stage.

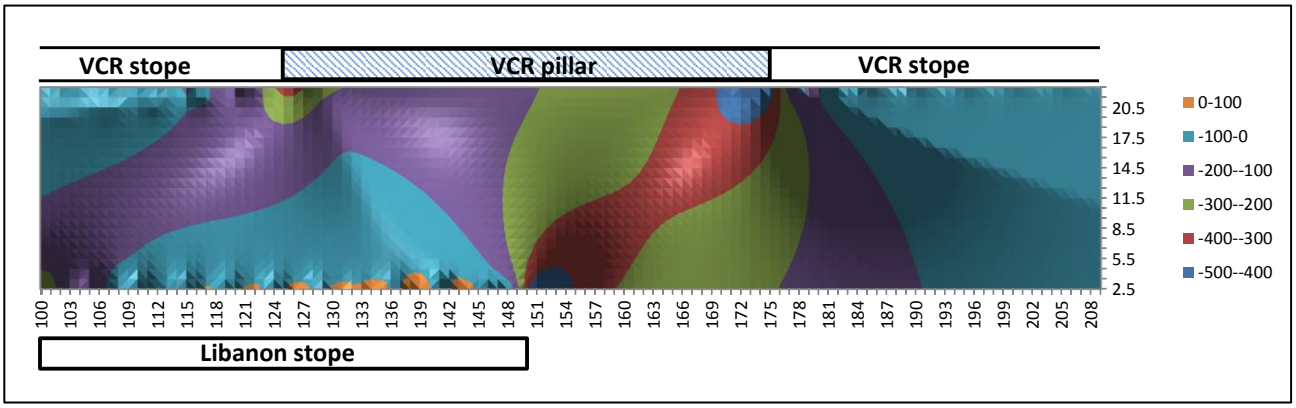


Figure 4.1.3 Major principal stress below the VCR Pillar when the Libanon Reef stope face is halfway below the VCR pillar. Note the region of very high principal stress between the edges of the two stopes.

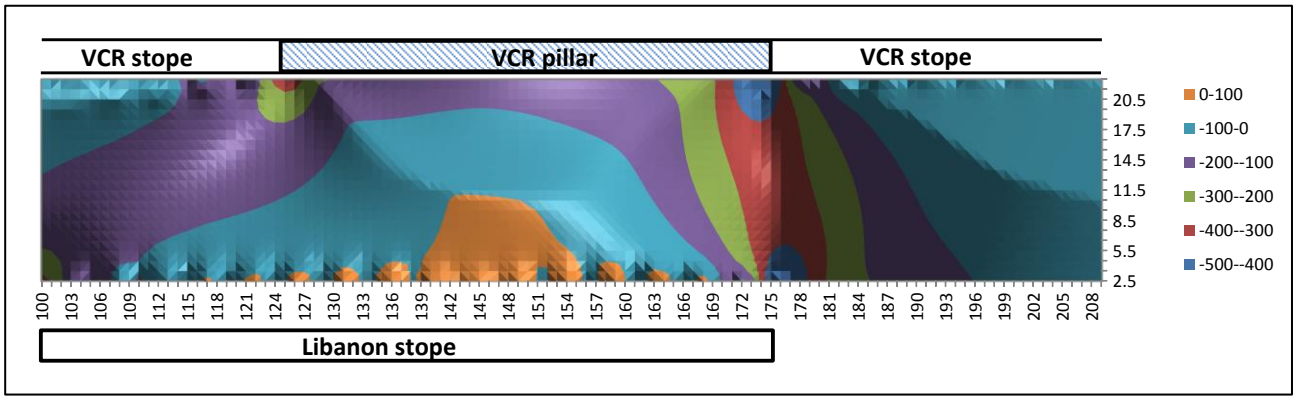


Figure 4.1.4 Major principal stress below the VCR Pillar when the Libanon Reef stope position is below the second VCR abutment. The region of very high principal stress between the edges of the two stopes persists at this stage. The average stress in a 3 m wide vertical zone between the edges of the two stopes is 395 MPa.

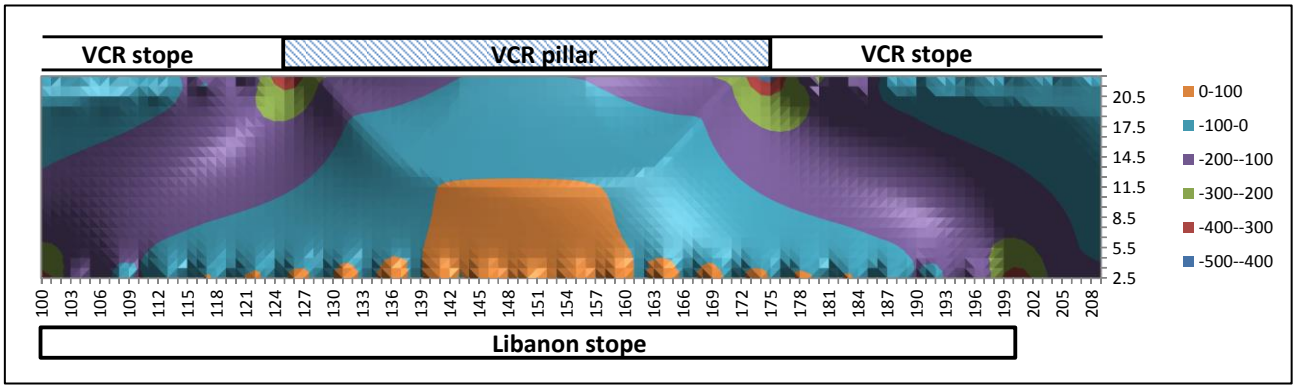


Figure 4.1.5 Major principal stress below the VCR Pillar when the understoping is complete. The regions of high principal stress have disappeared and it is clear that mining on the VCR pillar will now occur in a lower stress regime. Above the center of the Libanon Reef stope, a large region of tensile stress has developed.

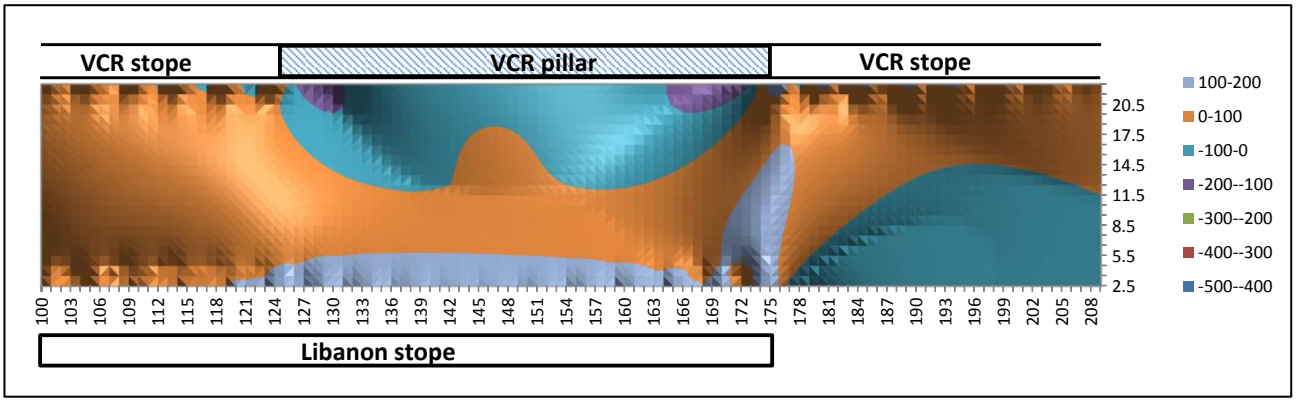


Figure 4.1.6 Minor principal stress in the middling between the two reefs when the Libanon stope crosses the second VCR abutment. Note the changes of the low minor principal stress above the active Libanon face, forming an additional tensile region.

Considering the Mohr-Coulomb failure criteria in σ_1-σ_3 space (equation 4.1.1 below):

$$\sigma_1 = \sigma_c + \beta_0 \sigma_3 \qquad (4.1.1)$$

where

$$\beta_0 = \frac{1+sin\phi_i}{1-sin\phi_i} \qquad (4.1.2)$$

and

σ_1 = major principal stress

σ_3 = minor principal stress

σ_c = uniaxial compressive stress of the rock

ϕ_i = coefficient of friction

Figures 4.1.4 and 4.1.6 in conjunction with equation (4.1.1) illustrate that the likelihood of shear failure in the middling between the reefs is very high. If for example it is estimated that the minor principal stress in this zone above the face of the Libanon stope is 0 MPa (it is in fact tensile in some areas making it worse), equation (4.1.1) reduces to:

$$\sigma_1 = \sigma_c \qquad (4.1.3)$$

Failure will therefore occur if the major principal stress is larger than the uniaxial compressive stress of the rock. For a hard brittle quartzite, it is estimated that the UCS = 220 MPa. The simulated major principal stress from Figure 4.1.4 is 395 MPa. Failure will therefore definitely occur.

A key finding from this study is that if the rock is an intact, hard brittle material, the likelihood of dynamic shear rupture is high and large seismic events can be expected. This is confirmed by multi-reef mining in a different mine where Carbon Leader Reef and Middelvlei Reef are extracted. The middling between the reefs consists of a hard brittle quartzite and very large seismic events are generated when mining the Middelvlei Reef up to the abutment of the Carbon Leader Reef. An example of this seismicity is shown in Figure 4.1.7. The Middelvlei Reef is found above the Carbon Leader Reef and the middling in this area is approximately 60 m.

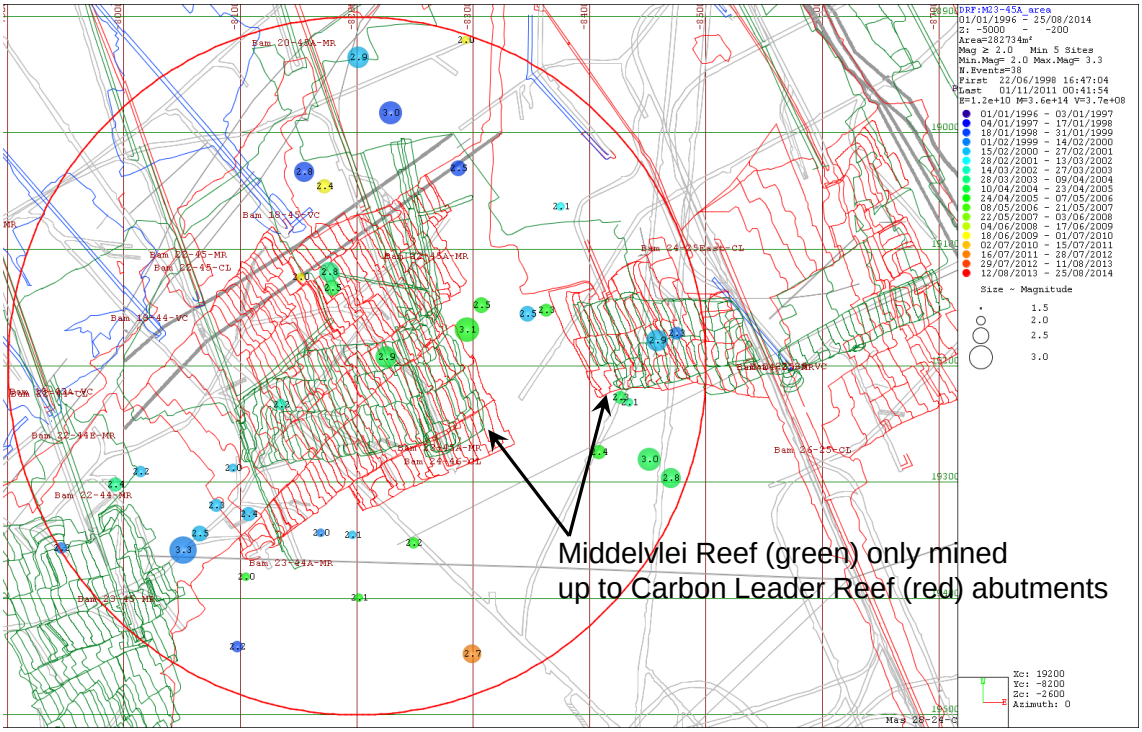


Figure 4.1.7 Large seismic events generated when the Middelvlei Reef mining approaches the Carbon Leader Reef abutments. Events as large as M3.1 were generated and for this geotechnical area and it seems as if it will be difficult to do understoping of remnants safely. This behaviour is supported by the modelling described above.

The preliminary elastic modelling conducted in this section appears to contradict the case studies in the following chapters which indicates that the understoping of VCR pillars on the Libanon Reef horizon can be successfully done. The key objective of this study is to investigate a simple numerical model indicating why under- or overstoping seem feasible in some geotechnical areas, but not in others.

4.2 ANALYSIS USING AN EXTENDED ERR CONCEPT

Ryder and Jager (2002) provides an extensive treatise of the ERR concept. They define ERR as "the spatial rate of release of 'unaccounted-for' energy (frictional heating plus kinetic energy) per m^2 mined". Since the 1960's, it has been the most common criterion that has been used in the design of deep level mining layout sequencing in South Africa. According to the authors, ERR should be considered as a measure of stress concentration and underground conditions at mining faces. Boundary element displacement discontinuities methods are well suited to calculate ERR values for irregular mining layouts.

The use of ERR as a design criterion for layout sequencing and to determine extraction ratios has been described in many papers (for example, Salamon, 1984; Napier, 1991). It nevertheless has practical shortcomings as a measure of the rockburst hazard. The most significant drawback of the criterion is that no dissipative mechanisms are incorporated into the model to allow for face crushing, failure and shear on bedding planes and other discontinuities. To address this shortcoming, Napier and Malan (2014) investigated an extended criterion to include an energy dissipation term. The basis of this work was a paper by Napier (1991) wherein which was published a set of formulae to compute energy changes in an elastic rock mass containing an arbitrary number of fractures. The key aspects of this approach are illustrated below. The formulae to calculate these energy components in a displacement discontinuity framework is not presented here as it is considered beyond the scope of this study.

In the extended criterion, the "energy release" increment, ΔW_A represents the difference between the incremental work done by gravity forces acting on the rock mass, ΔW, and the incremental change in the strain energy, ΔU, that is stored in (or released from) the rock mass when the excavation boundary is extended during a mining step. ΔW_A is therefore given by:

$$\Delta W_A = \Delta W - \Delta U \tag{4.2.1}$$

If the incremental area mined is designated by ΔA then the "classical" energy release rate or ERR is defined to be

$$ERR = \lim_{\Delta A \to 0} \Delta W_A / \Delta A \tag{4.2.2}$$

As described above, ERR values are computed for mine layouts using programs such as MINSIM (Plewman et al., 1969; Deist et al., 1972; Ryder and Napier, 1985) which uses the displacement discontinuity boundary element method. An enhanced criterion is proposed by Napier (1991) by modifying equation (4.2.1) to include an energy dissipation term ΔW_D. The term represents the work dissipated by reaction forces at the discontinuity interfaces. If this dissipation term is appropriately assessed, a general measure of incremental mining "stability", designated as ΔW_R, can be defined as follows:

$$\Delta W_R = \Delta W_A - \Delta W_D \tag{4.2.3}$$

and by inserting equation (4.2.1):

$$\Delta W_R = \Delta W - \Delta U - \Delta W_D \tag{4.2.4}$$

The incremental stability measure or "extended" ERR, as defined by equation (4.2.3), is associated with an incremental change to the excavation shape and may, in addition, include released energy from explicitly modelled fractures or bedding planes.

4.3. EXAMPLES AND A HYPOTHESIS FOR THE MECHANISM OF SUCCESSFUL UNDERSTOPING

Inelastic rock behaviour cannot be simulated in displacement discontinuity boundary element codes, except when discontinuities such as bedding planes and fractures are explicitly included in the model. The approach followed in this section was to use a geometry similar to that described in Section 4.1. Multiple runs were conducted with the bedding plane in different positions as well as different middlings between the mining excavations. The discontinuity included in the model was a weak or strong bedding plane. The ERR calculations were extended by using equation 4.2.4 to take energy dissipated by the bedding plane into account. The objective was to use this simplistic model to provide some insight as to why understoping can be successfully used in some areas to extract pillars, but not in others. The energy calculations described above in Section 4.2 are built into the TEXAN framework and the models were therefore simulated with this code.

The energy that is released during the understoping process, as governed by equation 4.2.4, is depicted in the figure. The numerical model used a 5 m grid with a 30 m middling between the reefs. A bedding plane was introduced 15 m from the excavations similar to that described in Section 3.3 (Chapter 3). The layout was similar to Figure 3.3.3. To investigate the effect of the bedding plane "parameters", the simulations were conducted with parameters that simulate a weak bedding plane, with no cohesion and low strength, as well as a strong bedding plane.

The cumulative released energy for 4 scenarios are plotted in Figures 4.3.1 and 4.3.2. The figures depicts the possible positions of the bedding plane and also differentiates between a weak bedding plane and a strong bedding plane.
From these figures, it can be seen that the cumulative released energy for a bedding plane, if it is situated in the hangingwall of the top reef or footwall of the bottom reef, is less than that if no bedding plane is present. It is also clear that the presence of a bedding plane between the two reef horizons has a much higher

released energy component. This illustrates that if an appropriate mechanism exists to dissipate energy in a stable manner, the understoping process will be less hazardous than that predicted by the elastic model in Figures 4.1.1 to 4.1.5.

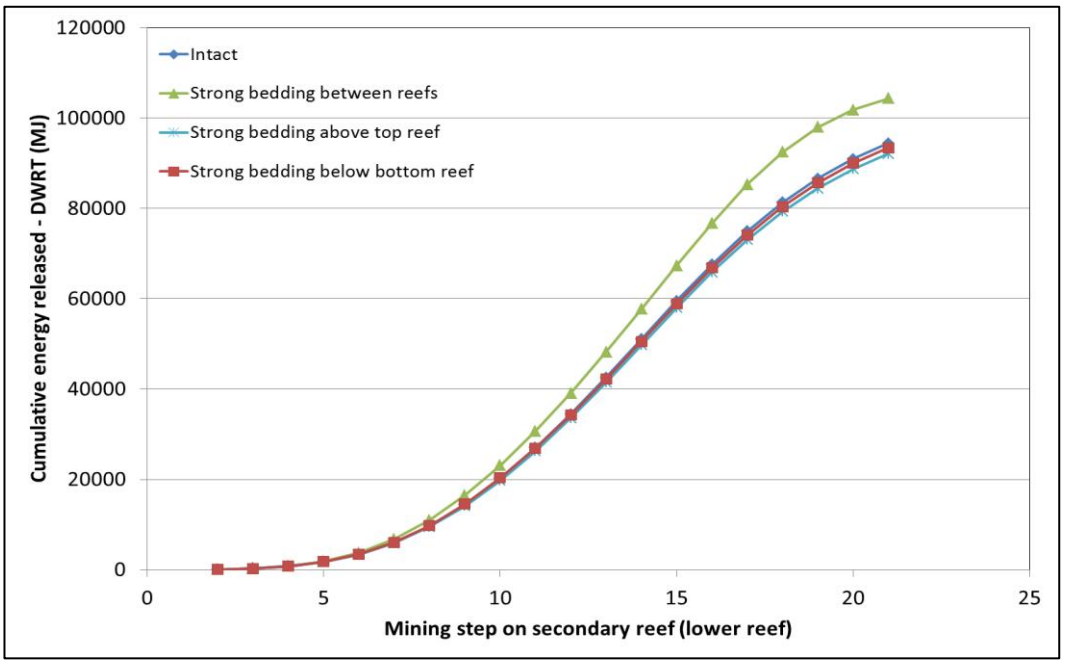


Figure 4.3.1 Cumulative released energy during the understoping at a 30 m middling with the presence of a strong bedding plane. DWRT is the TEXAN notation for ΔW_R. This is the "extended" ERR and higher values would indicate more hazardous conditions.

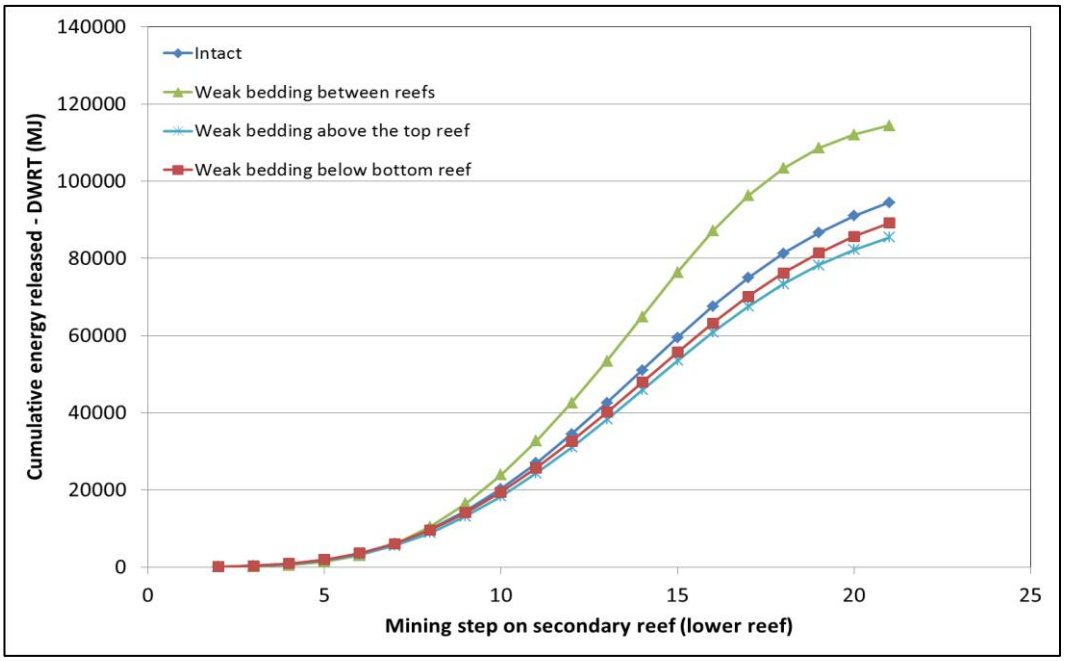


Figure 4.3.2 Cumulative released energy during the understoping at a 30 m middling with the presence of a weak bedding plane. DWRT is the TEXAN notation for ΔW_R. This is the "extended ERR" and higher values would indicate more hazardous conditions.

From the previous results, it appears that a weak bedding plane, if correctly positioned, reduces the energy released and the risk when doing the understope mining. To investigate why this is the case, all the energy components as described in equation 4.2.4 is examined in Figures 4.3.3 to 4.3.6 for 4 scenarios. The bedding between the reefs increase all the energy components when compared to the other scenarios.

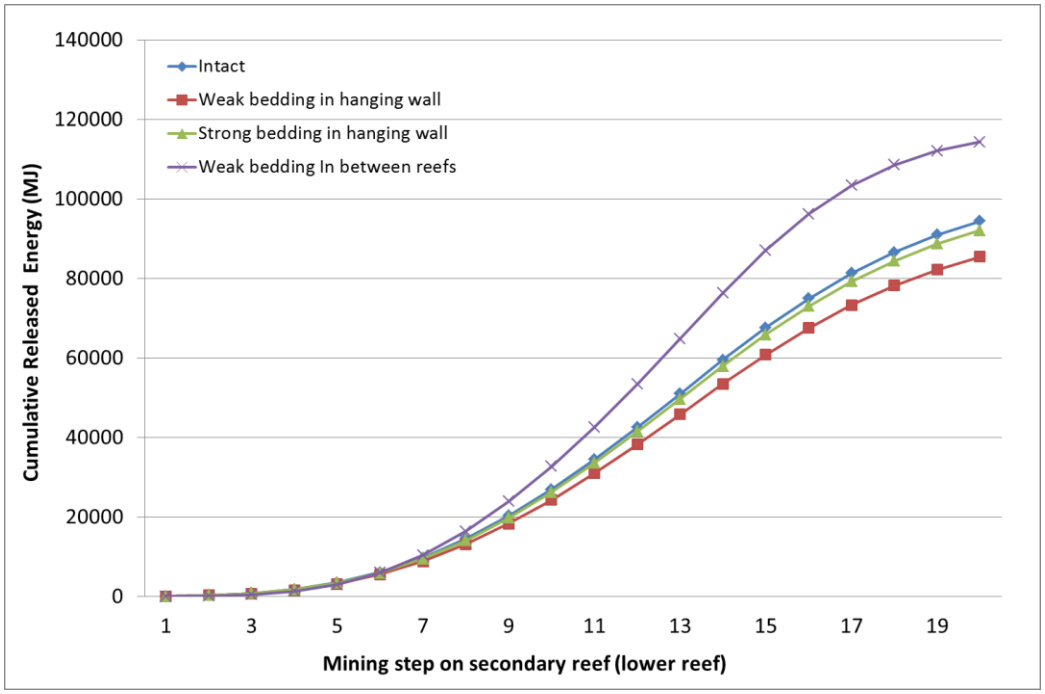


Figure 4.3.3 Cumulative released energy during the understoping at a 30 m middling. This is parameter ΔW_R in equation 4.2.4. This is the "extended" ERR and higher value would indicate more hazardous conditions.

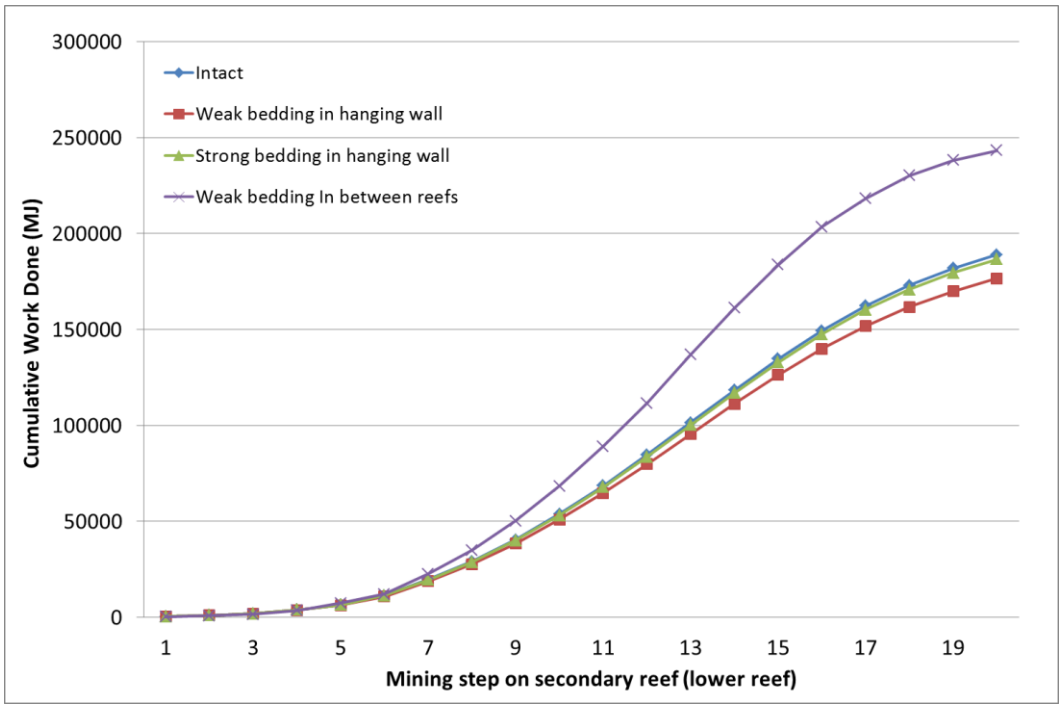


Figure 4.3.4 Cumulative work done during the understoping at a 30 m middling. This is parameter ΔW in equation 4.2.4.

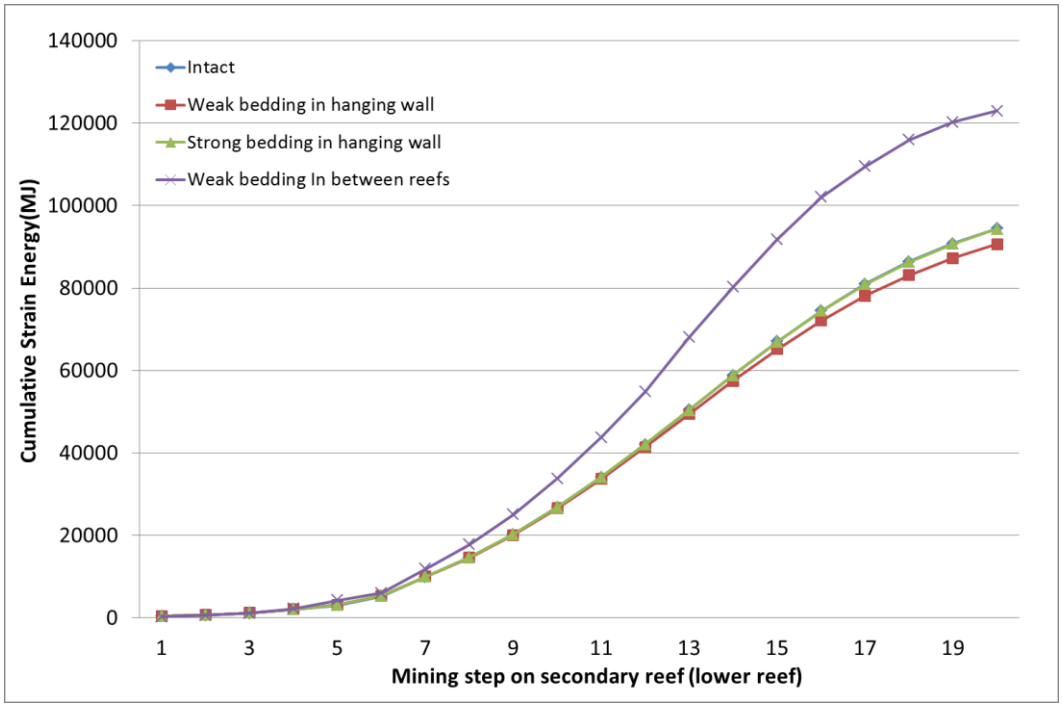


Figure 4.3.5 Cumulative strain energy during the understoping at a 30 m middling. This is parameter ΔU in equation 4.2.4.

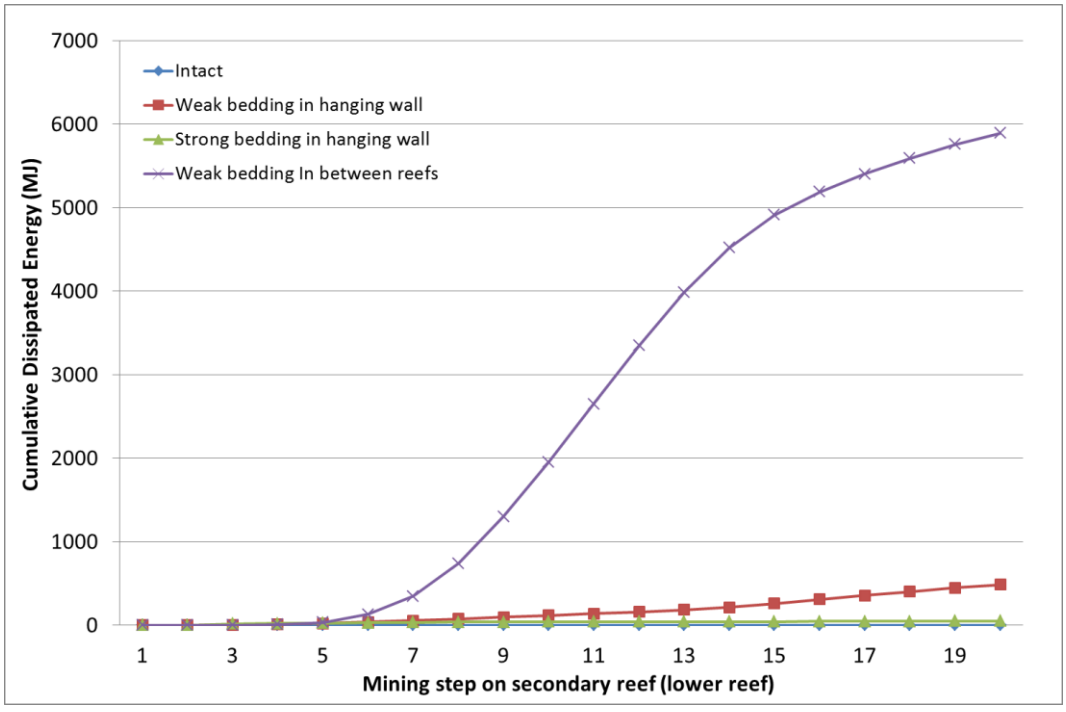


Figure 4.3.6 Cumulative dissipated energy during the understoping at a 30 m middling . This is parameter ΔW_D in equation 4.2.4.

To understand why and how the energy components are affected, a table was compiled showing the average closure on the two reef planes compared to the energy components for the 4 scenarios. This is given as Table 4.3.1 and shows values for the last mining step. From this table, it can be seen that the energy dissipated for the intact scenario is zero due to the absence of a bedding plane. By comparing the closure and the cumulative work done, it can be seen that the components are related. For the weak bedding between the reefs, the closure is higher and the result is the largest cumulative work done. For this case the energy dissipated is also the highest, but it cannot compensate for the greater cumulative work done and therefore this presents a higher released energy and the greatest risk.

From the data in the table an increase in dissipated energy can be seen in the presence of a bedding plane. Even though the released energy is more with the presence of a bedding plane between the two reef horizons, the dissipated energy is more than tenfold that of the other scenarios, indicating the value of a bedding plane to dissipate some of the energy and thereby reducing the released energy and the potential for violent energy release. It should also be considered that this modelling is the first evidence that energy stably dissipated on discontinuities can reduce the effect of violent energy release. The energy dissipated component ΔW_D will be larger if a greater number of discontinuities are included in the model. It is however considered beyond the scope of this study.

Table 4.3.1 Energy components during the understoping at a 30 m middling for the last step.

	Average closure VCR	Average closure Libanon	Cum. Released energy (DWRT) (ΔW_R)	Cum. Work done (DWT) (ΔW)	Cum. Strain energy (DUT) (ΔU)	Cum. Energy dissipated (DWDST) (ΔW_D)
Intact	284.17	156.08	94 441	188 893	94 452	0
Weak bedding in hangingwall	284.45	154.19	85 441	176 515	90 587	488
Strong bedding in hangingwall	285.04	150.16	92 107	186 533	94 374	52
Weak bedding in between reefs	289.16	173.73	114 363	243 225	122 971	5 892

To further investigate the effect of the bedding plane, the major and minor principal stresses were plotted when the Libanon mining face was below the middle of the VCR remnant. In Figure 4.3.2 it was illustrated that a weak bedding plane in the hangingwall of the upper reef reduces the energy released compared to the geometry with no bedding plane, hence the plots are for this layout.

Figure 4.3.7 is a plot of the major principal stress while Figure 4.3.8 illustrates the minor principal stress when no bedding plane is present. As a comparison Figure 4.3.9 is a plot of the major principal stress while Figure 4.3.10 illustrates the minor principal stress of the solution when a weak bedding plane is present in the hangingwall. When comparing the two sets of plots it seems that they are identical but under closer scrutiny of the data, when the detailed result data was investigated it was found that values of the solution with the bedding plane is lower. It is therefore deduced that the bedding plane in the hangingwall only has a very small effect on the stress between the reefs. Future work using different codes that can simulate rock failure such as FLAC is required to further investigate the effect of energy dissipation by weak layers of fracturing.

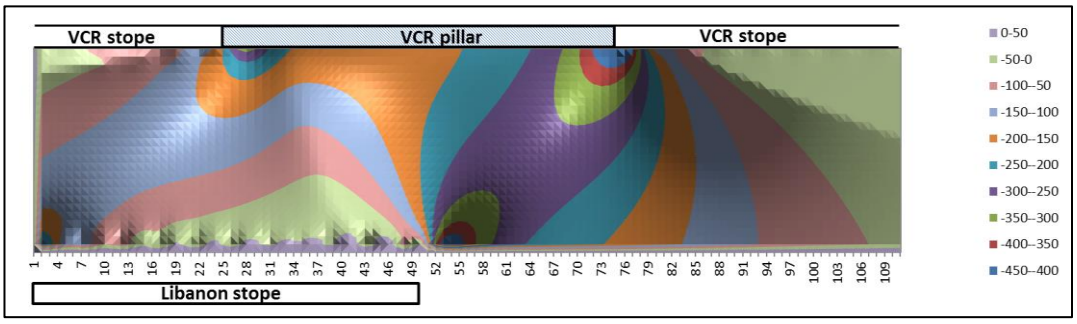


Figure 4.3.7 Major principal stress during the understoping at a 30 m middling.

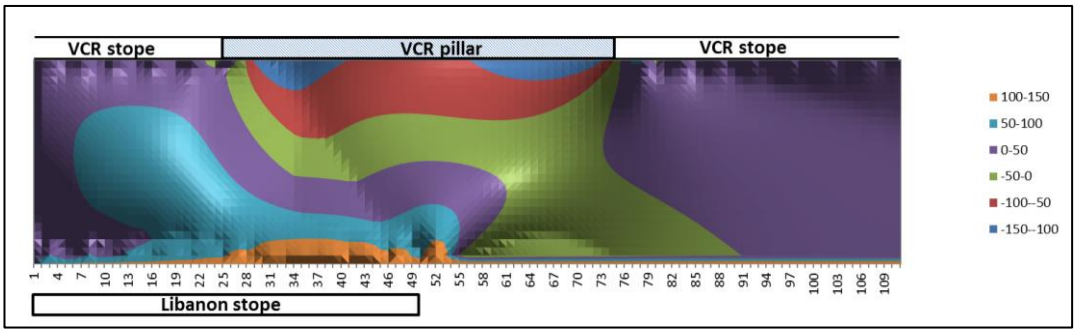


Figure 4.3.8 Minor principal stress during the understoping at a 30 m middling.

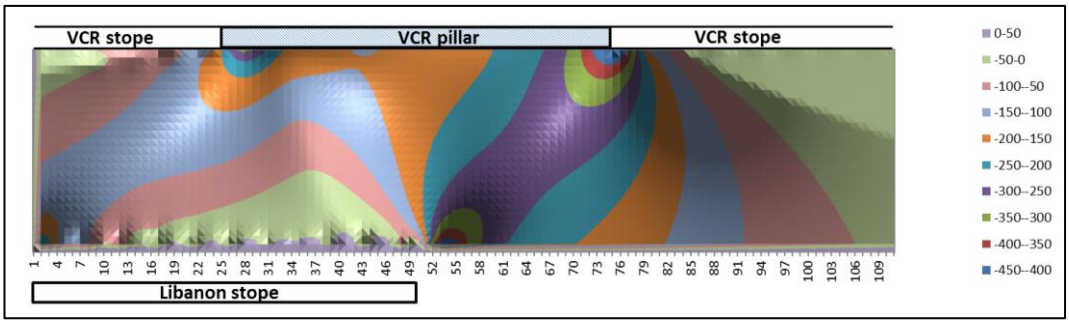


Figure 4.3.9 Major principal stress with bedding plane in the hangingwall of the VCR reef during the understoping at a 30 m middling.

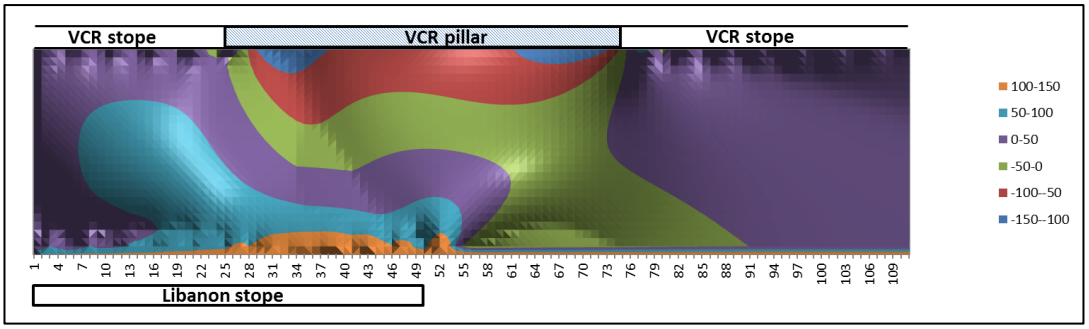


Figure 4.3.10 Minor principal stress with bedding plane in the hangingwall of the VCR reef during the understoping at a 30 m middling.

To investigate the effect of the middling between the reefs, the intact scenario as well as the scenario with a weak bedding plane in the hangingwall was simulated with a 60 m and 90 m middling between the reef planes. For these simulations the released energy was calculated and these are depicted in Figure 4.3.11 for a middling of 60 m and Figure 4.3.12 for a middling of 90 m.

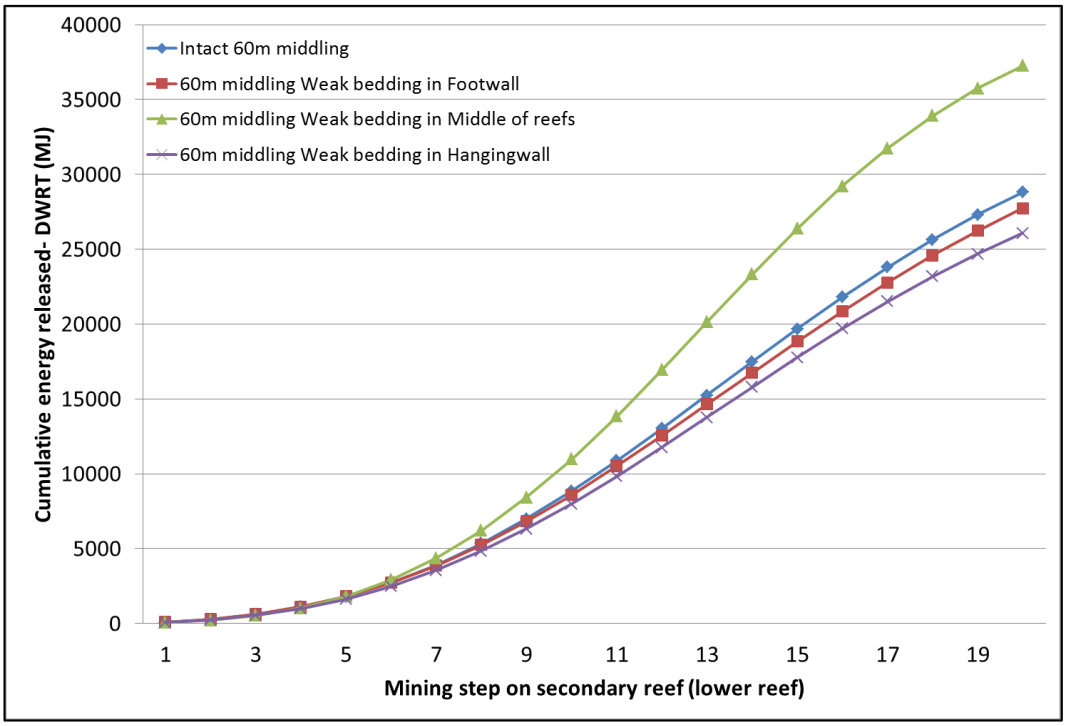


Figure 4.3.11 Energy released (ΔW_R) during the understoping at a 60 m middling.

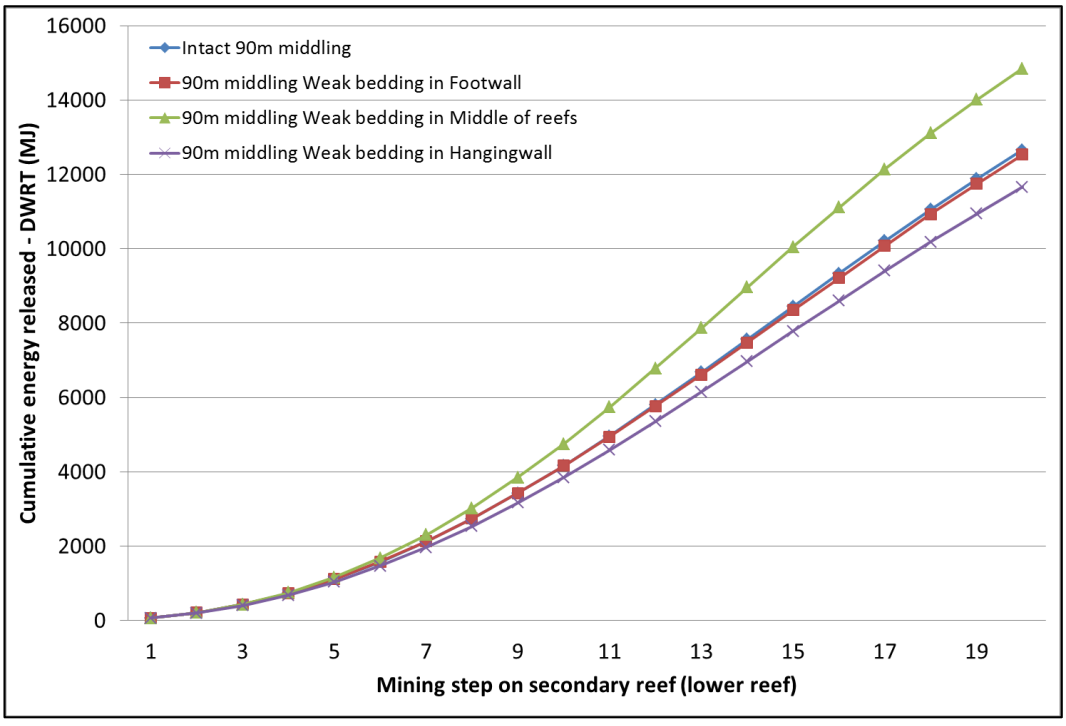


Figure 4.3.12 Energy released (ΔW_R) during the understoping at a 90 m middling.

Figures 4.3.9 and 4.3.10 shows similar trends to that of Figure 4.3.2, although the amount of energy released is reduced significantly as the middling is increased. This can most probably be attributed to the reduced influence of the two excavations on each other as the excavations is moved further apart.

Figures 4.3.13 and 4.3.14 and Table 4.3.2 compares the energy of solutions for a stiff system with a Young's modulus of 90 GPa compared to that of a softer system with a modulus of 70 GPa. From Figure 4.3.13 and Table 4.3.2 can be seen that the total energy or work done is fairly similar to that of a softer system. The stiffer system does have significantly more energy available but less closure were indicated.

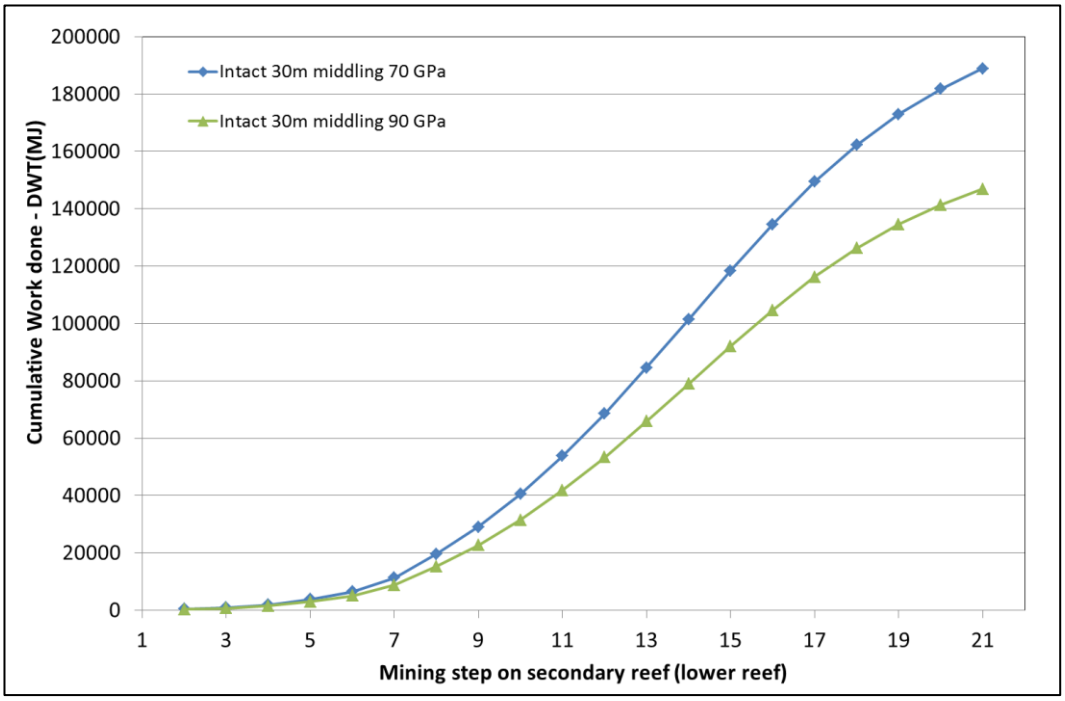


Figure 4.3.13 Work done (ΔW) during the understoping at a 30 m middling.

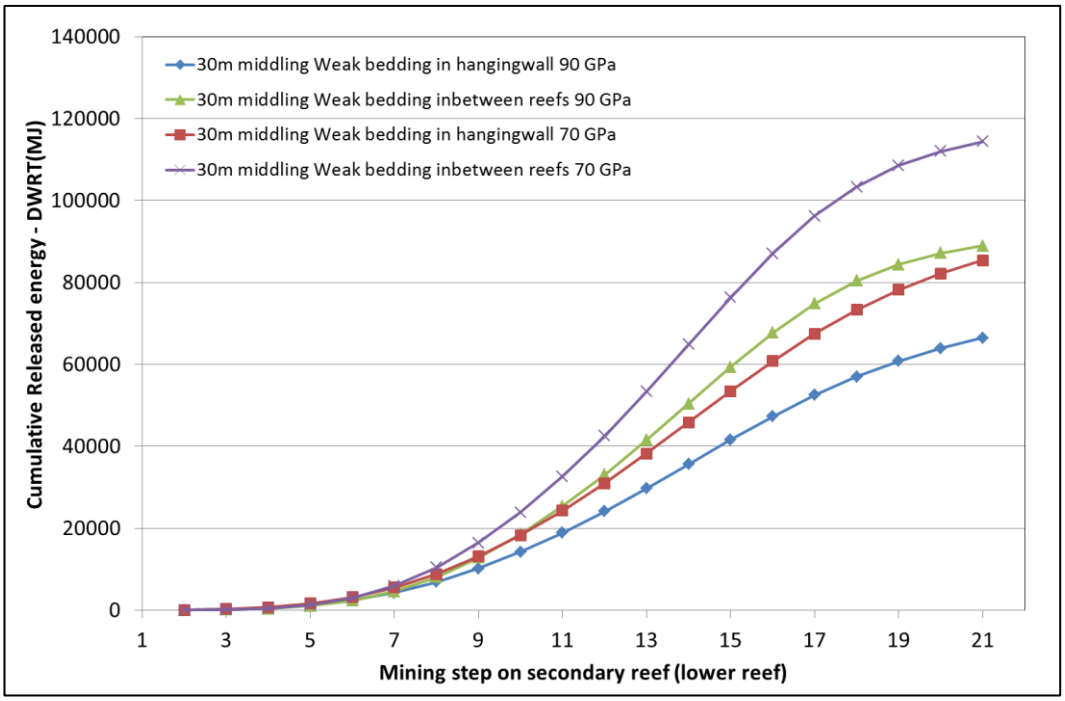


Figure 4.3.14 Energy released (ΔW_R) during the understoping at a 30 m middling.

Table 4.3.2 Closure and energy parameters for a stiff system.

	Average closure VCR	Average closure Libanon	Cum. Released energy (DWRT) (ΔW_R)	Cum. Work done (DWT) (ΔW)	Cum. Strain energy (DUT) (ΔU)	Cum. Energy dissipated (DWDST) (ΔW_D)
Intact 70 GPa	284.17	156.08	94 441	188 893	94 452	0
Intact 90 GPa	221.02	121.39	73 453	146 916	73 462	0
Weak bedding in hangingwall 90 GPa	221.70	116.79	66 454	137 290	70 456	379
Weak bedding in hangingwall 70 GPa	284.45	154.19	85 441	176 515	90 587	488
Weak bedding in-between reefs 90 GPa	224.90	135.13	88 949	189 175	95 644	4 582
Weak bedding in-between reefs 70 GPa	289.16	173.73	114 363	243 225	122 971	5 892

4.4. SUMMARY

Considering the information presented in tables as well as the figures in Section 4.3, it is clear that the bedding plane is useful to dissipate energy. The total energy and closure is affected by the presence of the bedding plane and the response is therefore very complex. Care should therefore be exercised when modelling specific cases.

As a further step, actual multi-reef mining remnants with readily available records were selected and observations from these sites were compared in the next chapters. The aspects that were investigated are the seismic history, numerical modelling results as well as photographic records. This enabled the evaluation and back analysis of the remnants.

Five remnants were selected for this study. The remnants were all from the Carletonville area, however they were located at different shafts at different depths, but with a similar lithology as described in Figure 2.7.3.

From the background information and preliminary modelling described in Chapters 3 and 4, shear failure when over stoping is likely. Attempts were made to identify signs of shear failure or energy dissipation in these case studies.

CHAPTER 5

CASE STUDY AND BACK ANALYSIS OF REMNANT A : VC25-23

The stopes of this remnant are located to the south west of the shaft, and the LI25-23A stope is overlain by the VC25-23 stope. The middling between the two reef bands is 15 m. Both the VCR and Libanon reef bands are a quartzitic conglomerate, the immediate footwall of the VCR reef are quartzite, whereas the footwall of the Libanon is shale. The hangingwall of the VCR consists of weak lava.

The most recent mining in the area commenced on the Libanon reef to understope the VCR block which was the primary mining objective to be mined. Very little stoping has occurred on the Libanon reef in this area prior to the commencement of the understoping. The VCR target area contained two pillars on either side of a raise with mining on all 4 boundaries and it had an initial size of 17000 m^2. According to the mine plans, no major geological structure is present in this block of ground. A fault and dyke is present in the general vicinity of the area, but these structures were extensively stoped through in the past.

The block of ground on the VCR reef had a high gold content and subsequent to starting the de-stressing on the Libanon reef, it was found that the gold content on this secondary reef was also high. Access development is situated deep in the footwall of the VCR and large portions had been extensively overstoped. In the bottom level crosscut, the Libanon reef is traversed before intersecting the VCR reef. The target block of ground is above the level reef intersection and extends to above the next levels' reef intersection. Access is gained through secondary development from the stoping on the Libanon reef, implying that the access routes were de-stressed from the time of development.

The face shapes of the stoping operations on both reef elevations was fairly well controlled, although it is evident that some difficulty was experienced on various

occasions to control the face shapes as well as to maintain the original layout. Changes in the face orientation and face length was therefore observed. There were no stabilising pillars or crush pillars left on either of the reef horizons during the extraction. The locality of the block of ground can be seen in Figures 5.1 and 5.2 below.

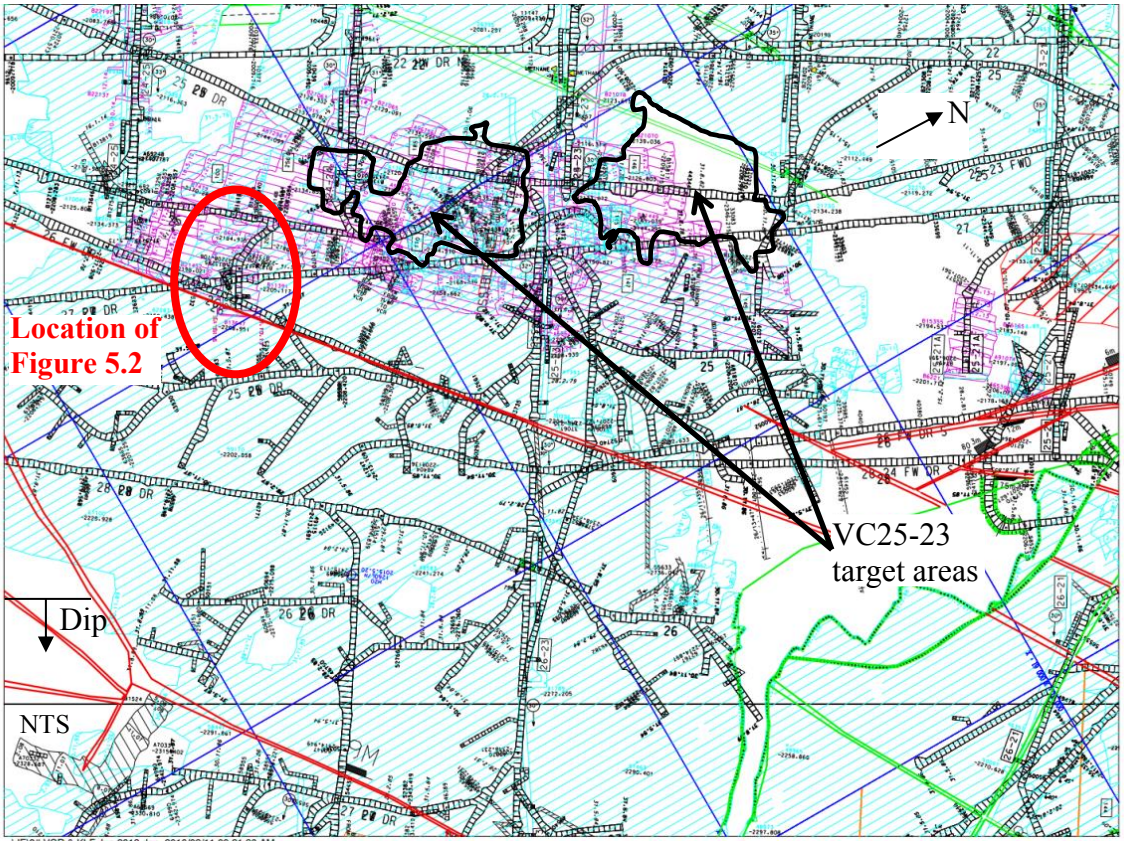


Figure 5.1 Locality plan view of the VC25-23 area. The VCR target areas are indicated by the black outline. The blue areas are mined VCR and the purple is mining on the Libanon reef.

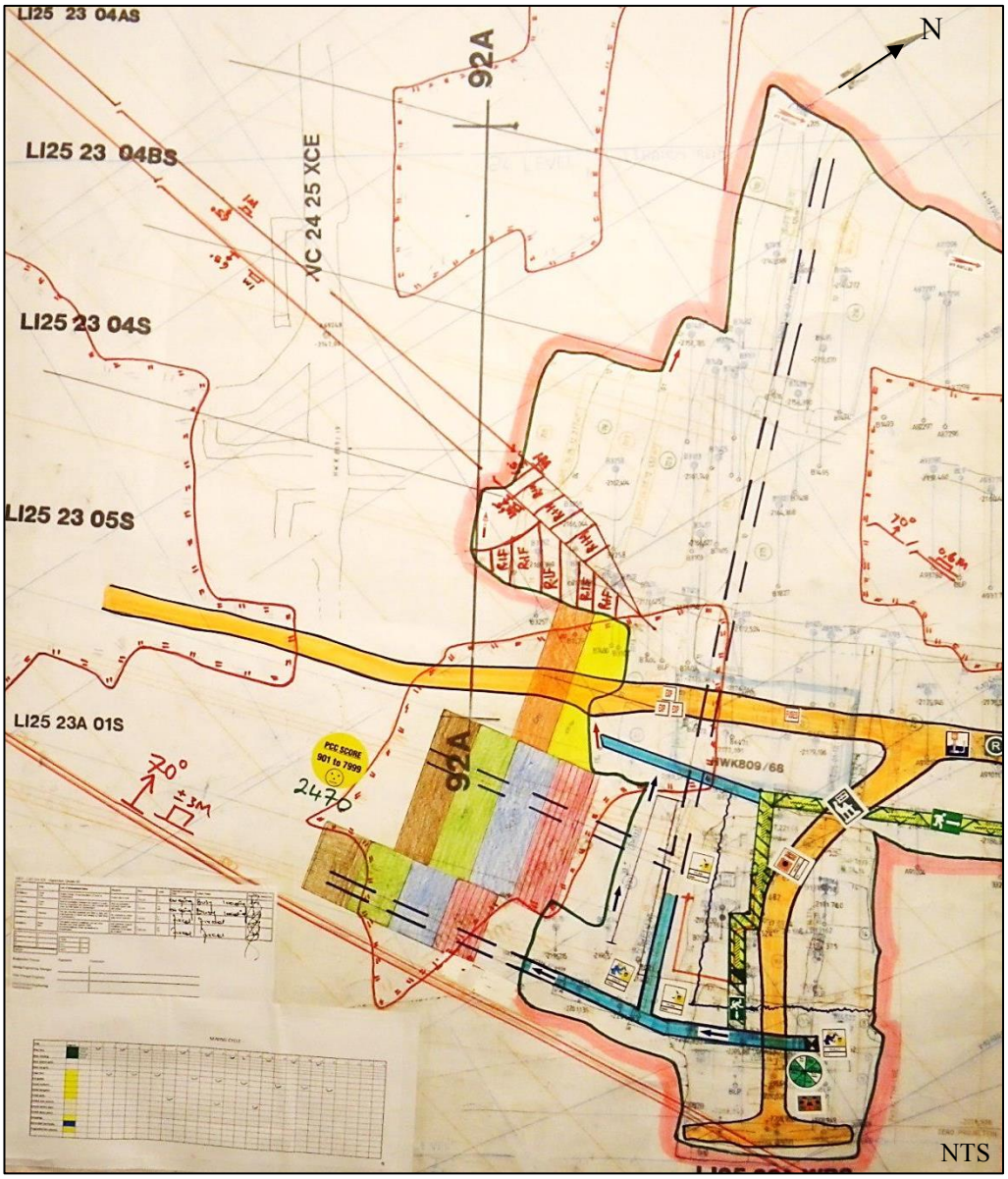


Figure 5.2 1:200 Plan view of the LI25-23A stope. The black line indicates the mined Libanon Reef (mining is planned on the Libanon) and the red line indicates the VCR pillars.

Figure 5.3 depicts a simplified section. The VCR was understoped on the Libanon Reef. From the Libanon Reef inclined development was developed to the VCR elevation and from this access points the understoped area was extracted first.

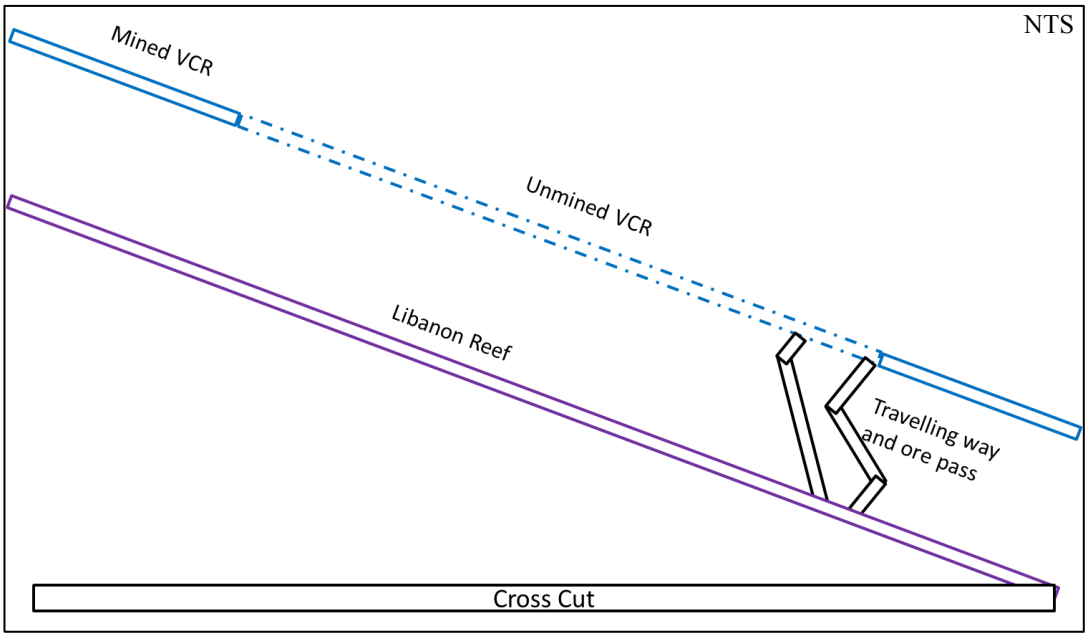


Figure 5.3 Simplified section through the VC25-23 depicting multiple reef bands and the inclined access ways.

As part of the Special Area precautions, the seismicity was monitored by the mine network consisting of 39 geophones located across an area of 56 km^2. The seismic network has been in operation since late 1996. The seismic network coverage of the shaft is of such a nature that M_L -0.25 seismic events can be reliably recorded and the system is capable to provide the location of a M_L 0.0 seismic event with an accuracy of up to 45 m. Figure 5.4 depicts a seismic plot of all events greater than a zero magnitude during the last 17 years within a 300 m radius of the stope. The event plots in this figure is coloured based on the date of occurrence, while the size of the plot is an indication of the magnitude. Potentially damaging events with a magnitude greater than M_L 1.5 are plotted together with the magnitude.

The largest recorded seismic event was M_L= 2.5, while the expected M_{max} was M_L 2.7. The seismic information indicates that the majority of the events were slip-type events and there was a probability of less than 60% that an event of magnitude M_L 1.0 will occur during any given month.

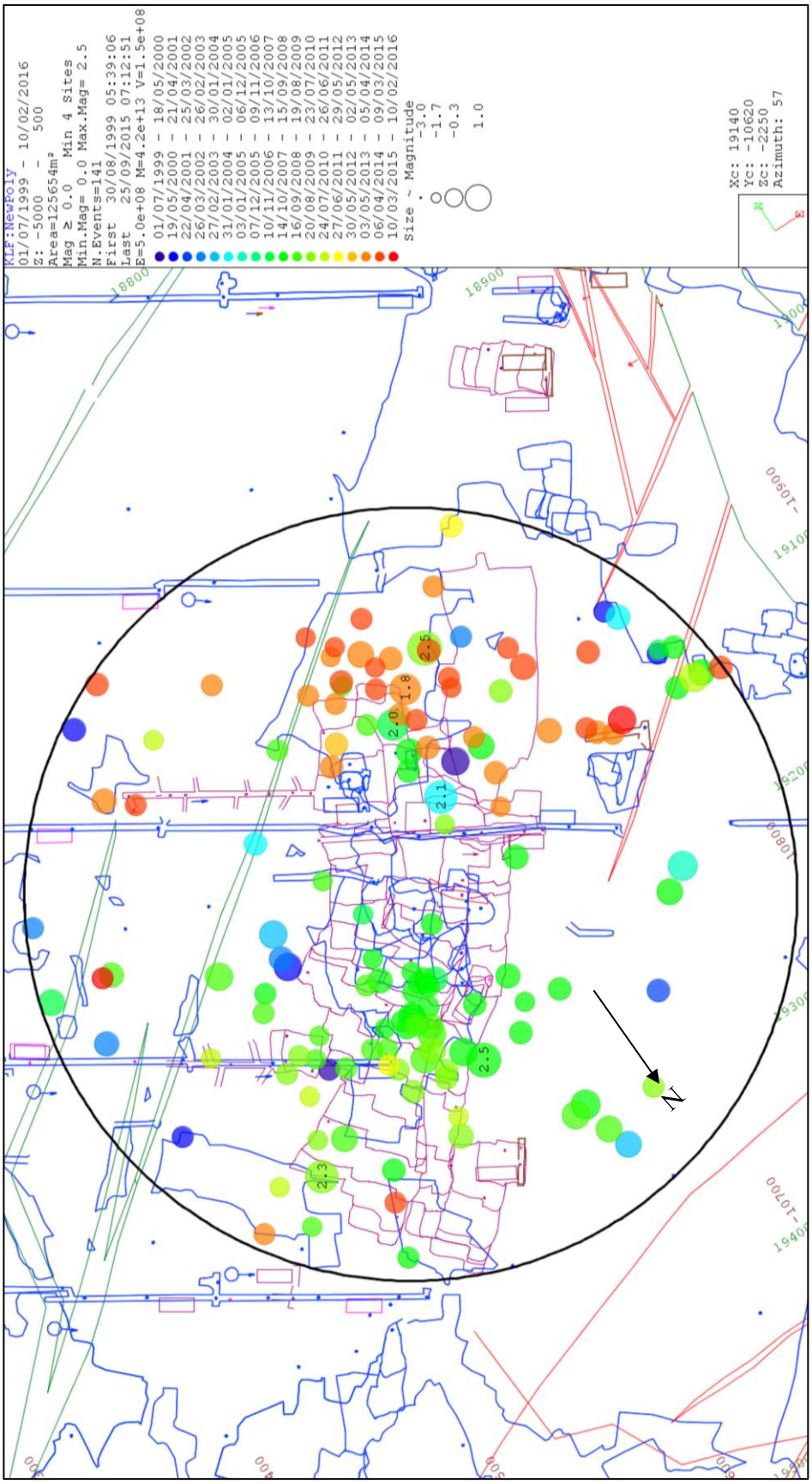


Figure 5.4 Plot of all events greater than M_L0.0 in a 300 m radius.

The activity rate of the area is shown in Figure 5.5. From this figure it can be seen that the seismic activity appears to be linked to the mining of the area. Figure 5.4 shows that the majority of the $M_L > 1.5$ events (numbered events) occurred in the Northern block. It can be argued that this block is the smaller of the two, extraction of the Libanon de-stressing is not complete and the mining of the Southern side is complete, hence shifting the load to the remaining block. From the figure, time periods of no or decreased production can also be identified.

Figure 5.6 depicts the hourly distribution for the recorded events, this also has no clear trend, however peaks were observed at 11h00 and 3h00. The shaft did not have a centralized blasting system until 2011 and operated without night shift in the VCR section. Therefore the 11h00 peak may be associated with blasting, while the other peaks can only be attributed to aftershocks following large events. The ideal for this figure would be a peak during the 3 hour blasting window. This would result in the decrease of exposure of the working crews.

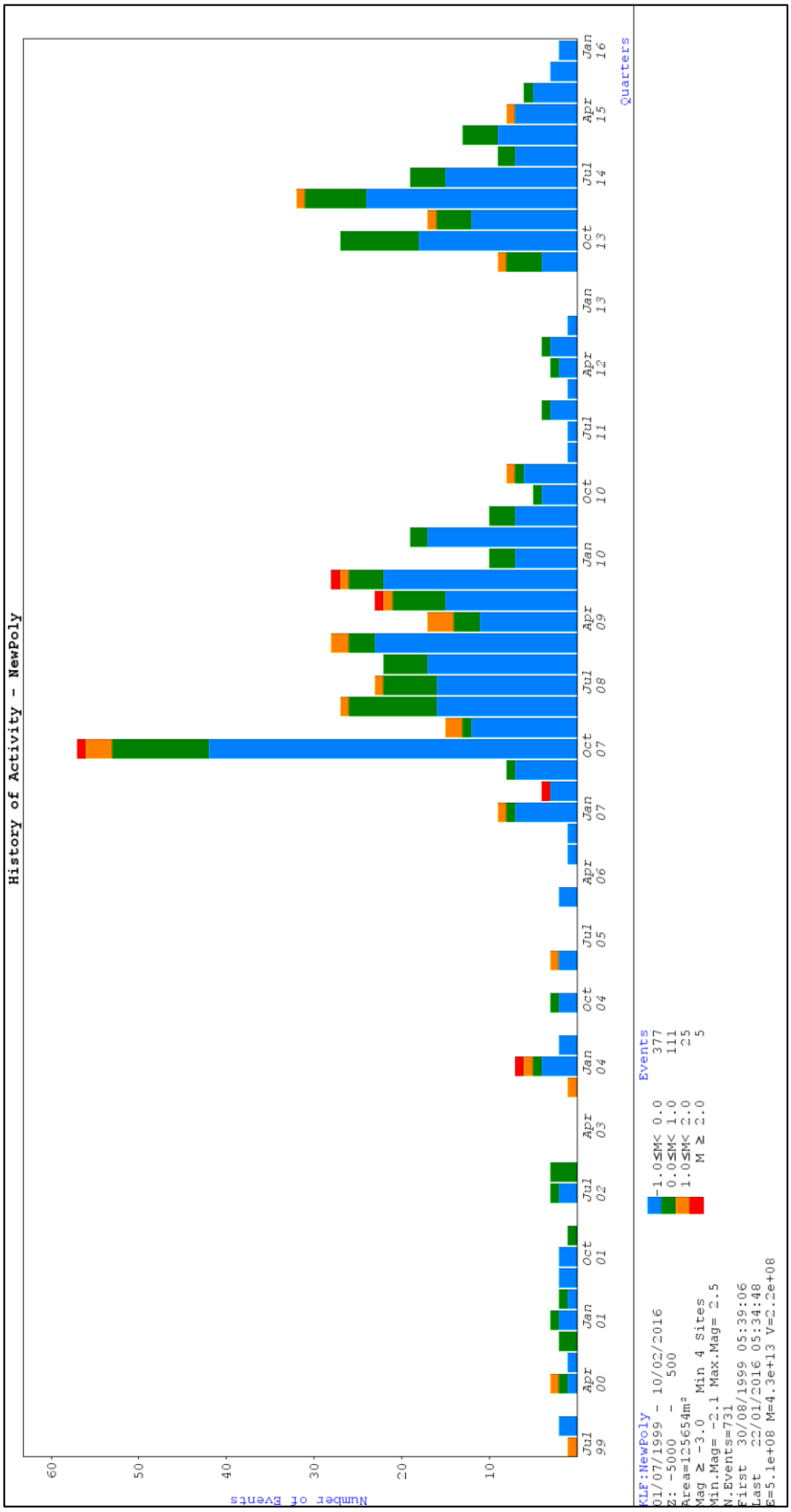


Figure 5.5 Activity rate in the VC25-23 area.

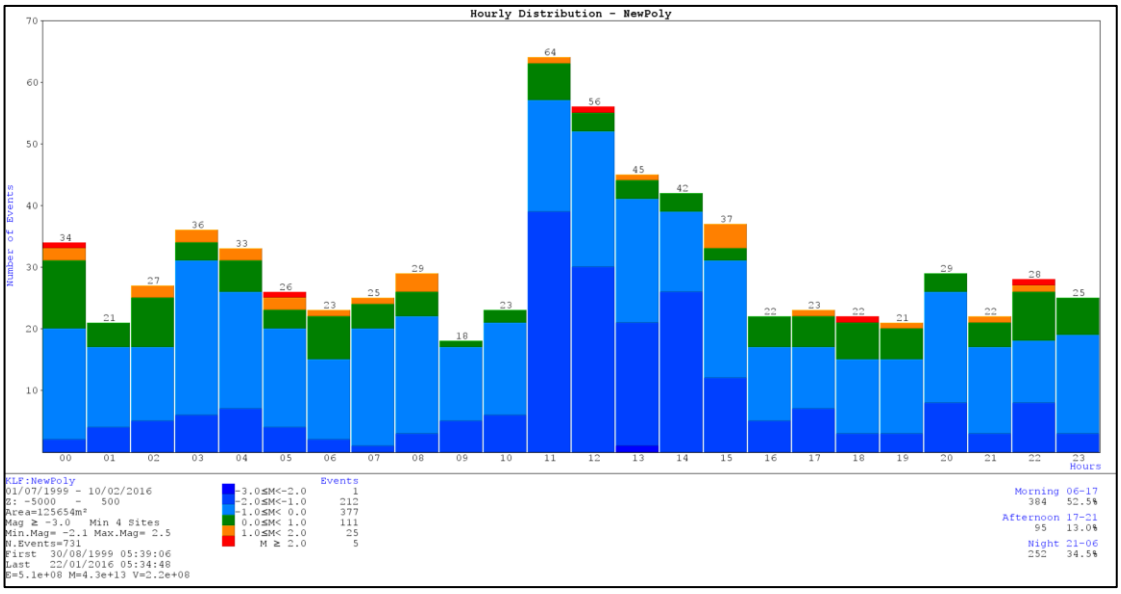


Figure 5.6 Hourly distribution of events in the VC25-23 area.

Figure 5.7 depicts the energy released in MJ per annum of this area. Owing to the very large energy release of the larger events, it appears that the majority of the years indicated comparatively insignificant seismic energy releases. The VCR stoping to the South was started during September 2011 and the stoping on the North was started in June 2015. The Libanon understoping was mined through abutments areas where stress concentrations can be expected. The breast mining on the South started during November 2008 and on the North during August 2013. In general, the majority of the energy was released during the understoping on the Libanon reef.

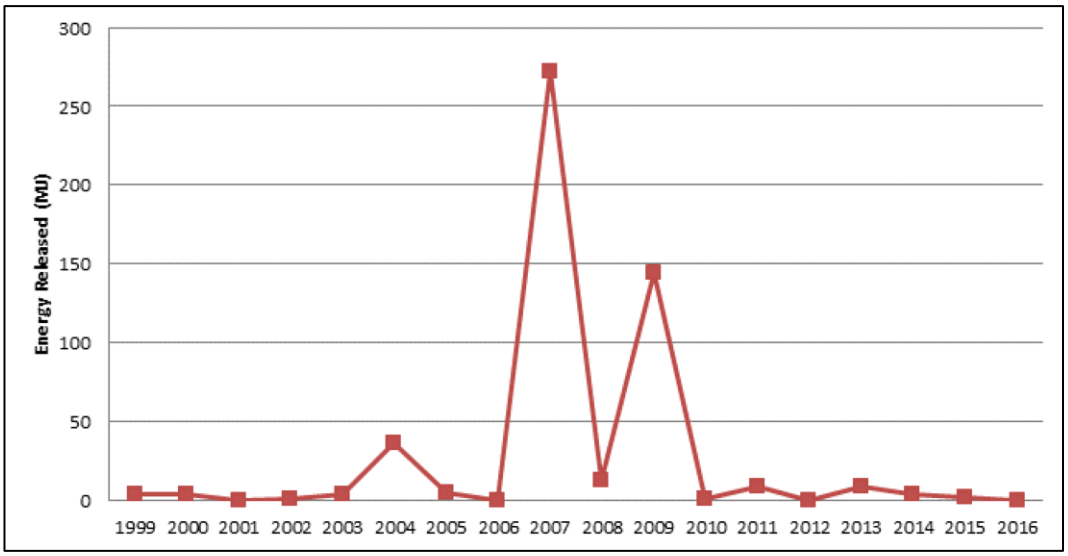


Figure 5.7 Annual energy release for the VC25-23 area.

Figure 5.8 shows the cumulative seismic moment for the VC25-23 area. The figure is divided into 4 distinct periods of mining. The figure clearly shows the effect of de-stressing as very little energy is released during the VCR mining. Figure 5.9 provides more detail as to the seismicity in the area, as depicted in Figures 5.7 and 5.8.

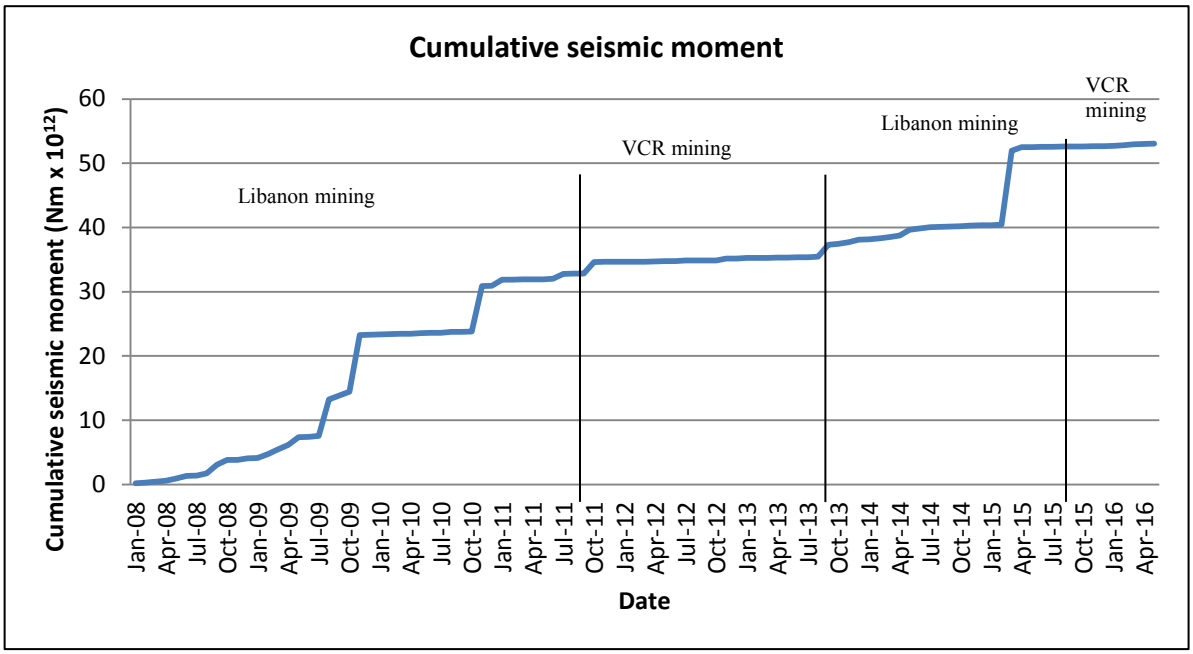


Figure 5.8 Cumulative seismic moment of the VC25-23 area for 8 years.

Year	Number of Events						Max. Mag.	Energy MJ	Moment 10^{12} Nm
	M<0	0≤M<1	1≤M<2	2≤M<3	3≤M	Total			
1999	2	0	1	0	0	3	1.5	4.09	0.69
2000	2	3	1	0	0	6	1.4	3.38	0.55
2001	7	2	0	0	0	9	0.3	0.17	0.08
2002	3	5	0	0	0	8	0.9	1.23	0.37
2003	0	0	1	0	0	1	1.4	3.61	0.48
2004	8	2	1	1	0	12	2.1	36.50	2.83
2005	3	0	1	0	0	4	1.6	5.30	0.75
2006	4	0	0	0	0	4	-0.1	0.04	0.01
2007	173	13	4	2	0	192	2.5	272.01	8.79
2008	82	22	4	0	0	108	1.7	12.82	3.35
2009	120	16	7	2	0	145	2.5	143.90	18.68
2010	45	9	0	0	0	54	0.3	0.51	0.38
2011	11	2	1	0	0	14	1.7	8.53	0.98
2012	8	2	0	0	0	10	0.6	0.21	0.17
2013	23	13	1	0	0	37	1.8	9.16	2.71
2014	65	17	2	0	0	84	1.0	3.83	1.63
2015	32	5	1	0	0	38	1.3	1.82	0.85

Figure 5.9 Summary of the seismic events in the VC25-23 area.

Figure 5.10 is a plot of the cumulative production and the cumulative seismic moment. This figure can be summarised as the seismic response to production. It can also be seen that at least two average gradients are present for the seismic moment. These coincide with the de-stressing cut on the Libanon reef and the mining on the VCR. The slope of the first VCR mining is flatter than that of the second period of mining on the Libanon reef. Similarly Figure 5.11 plots the number of events as a function of the cumulative area mined. From this figure the different mining areas can be identified, as well as the time periods when understoping or de-stressed mining took place. It should however be noted that the de-stressed mining did not take place in isolation as mining on the Libanon reef continued and was done during the majority of the time that the de-stressed mining took place.

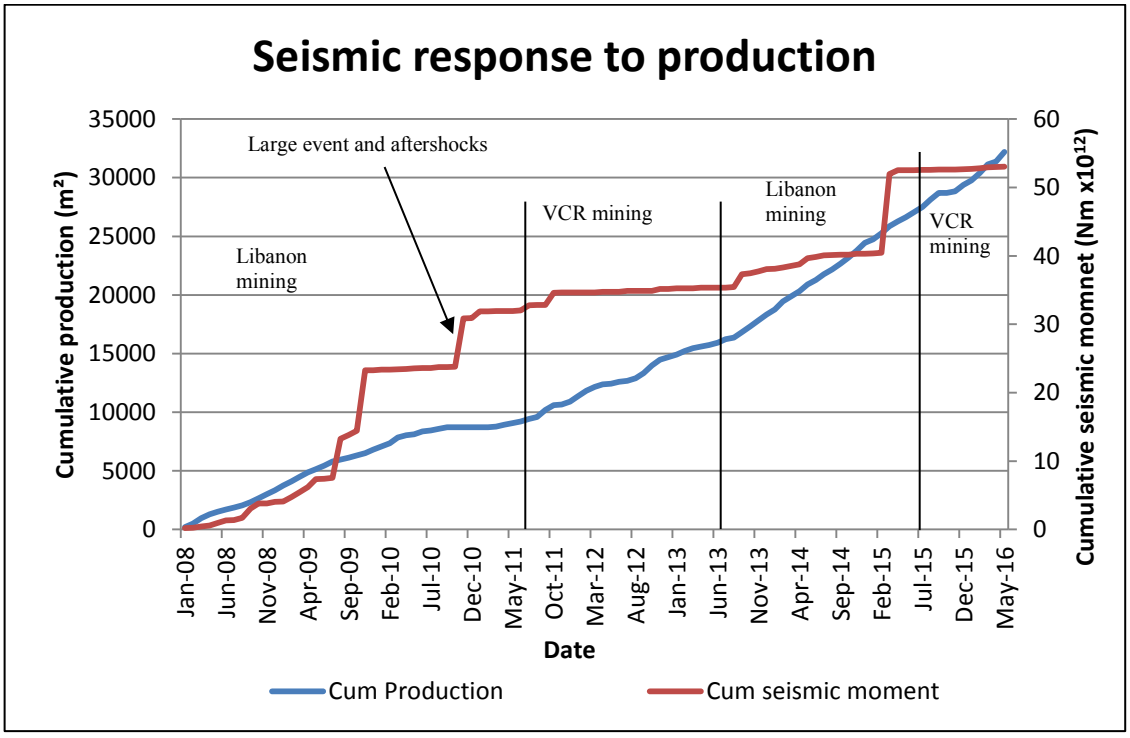


Figure 5.10 Seismic response to production of the VC25-23 area.

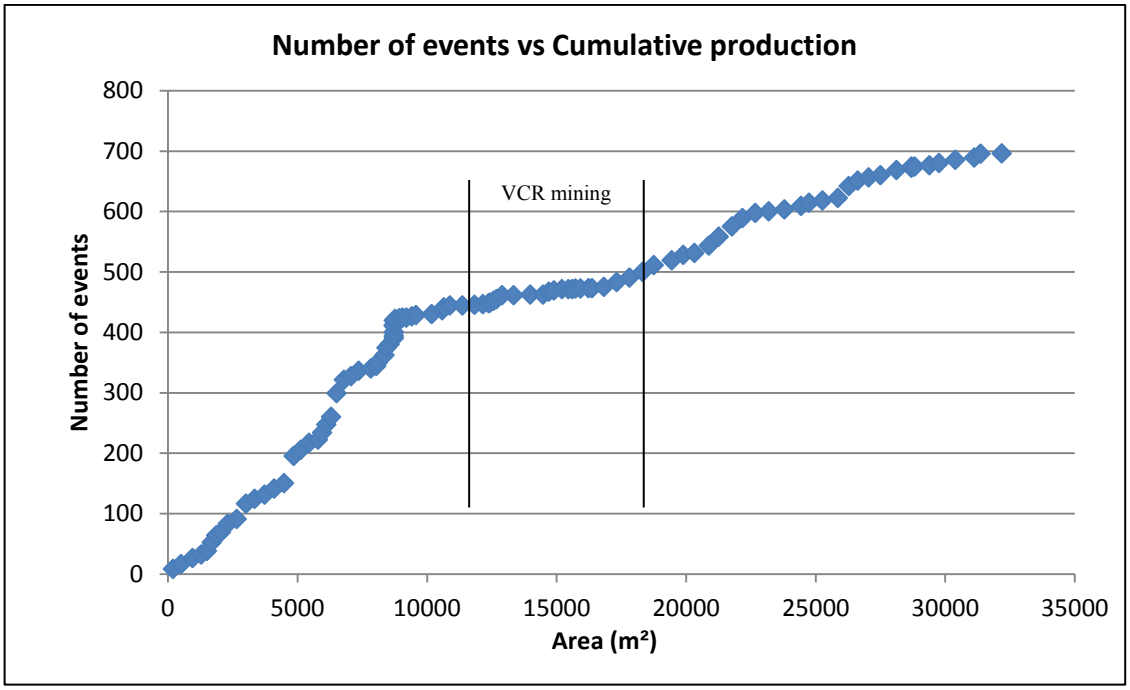


Figure 5.11 Number of seismic events compared to cumulative production of VC25-23.

The magnitude distribution of all events since 1999 is depicted in Figure 5.12. The green distribution indicates the given magnitude distribution while the cumulative distribution larger than the given magnitude is indicated by the blue.

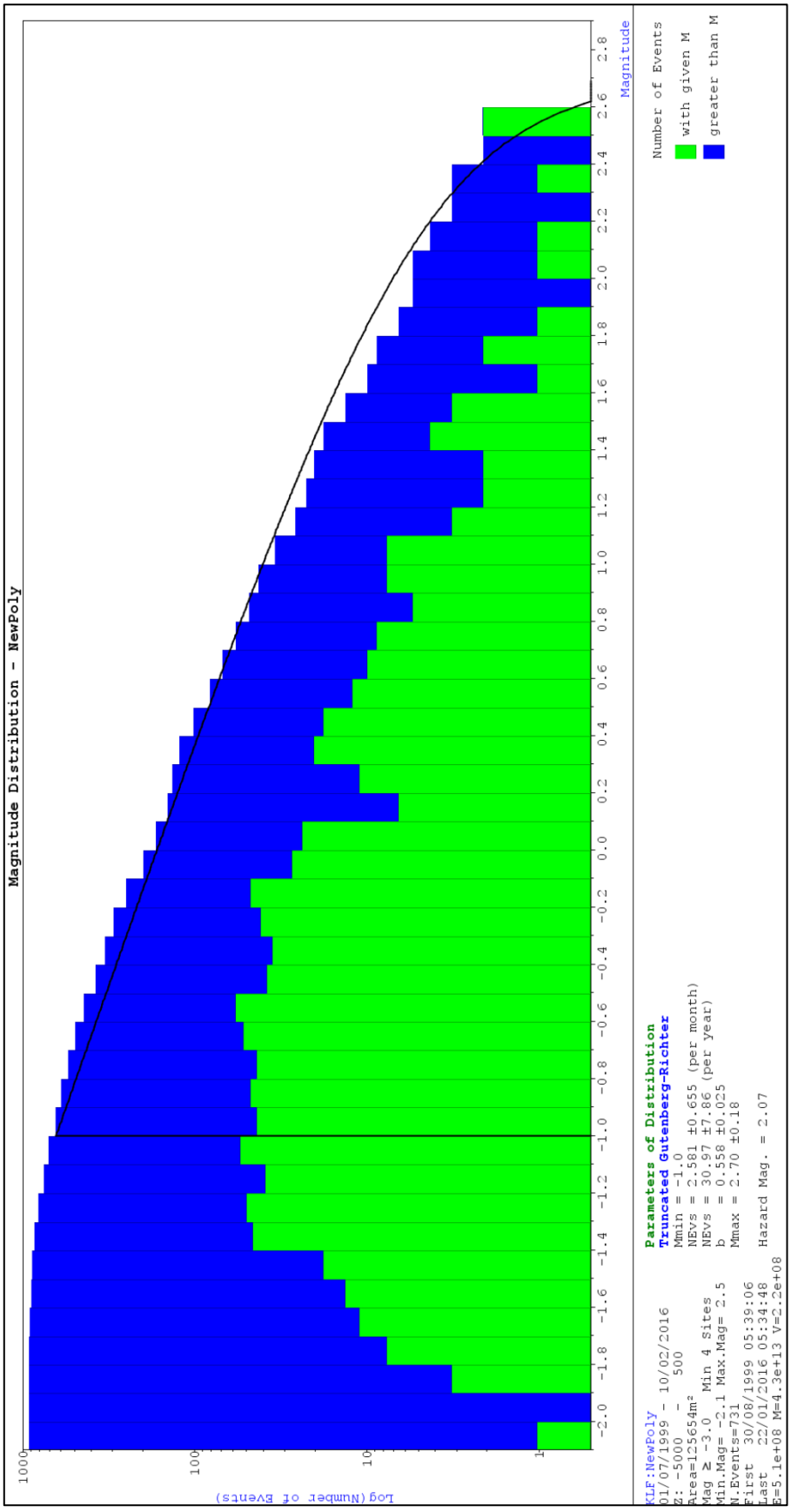


Figure 5.12 Magnitude distribution of seismicity in the VC25-23 area.

Probabilities of Seismic Event

Mag.	1 month	3 months	6 months	1 year	2 years	5 years
-1.0	92.4%	100.0%	100.0%	100.0%	100.0%	100.0%
-0.5	74.0%	98.2%	100.0%	100.0%	100.0%	100.0%
0.0	50.2%	87.7%	98.5%	100.0%	100.0%	100.0%
0.5	29.9%	65.6%	88.2%	98.6%	100.0%	100.0%
1.0	16.2%	41.1%	65.3%	88.0%	98.6%	100.0%
1.5	7.9%	21.9%	38.9%	62.7%	86.1%	99.3%
2.0	3.2%	9.3%	17.8%	32.4%	54.3%	85.9%
2.5	0.7%	1.9%	3.9%	7.6%	14.6%	32.5%

Figure 5.13 Seismic statistics of the VC25-23 area.

Figure 5.14 and Figure 5.15 illustrates the production and number of seismic events as well as M_{max}. From these figures it seems that there is more seismic activity during sustained production. The general trend observed is an increase in seismic activity when a high extraction rate is sustained in ground that is not de-stressed. The graphs also suggests a threshold as to the limitation of events as well as M_{max} when the extraction rate is limited.

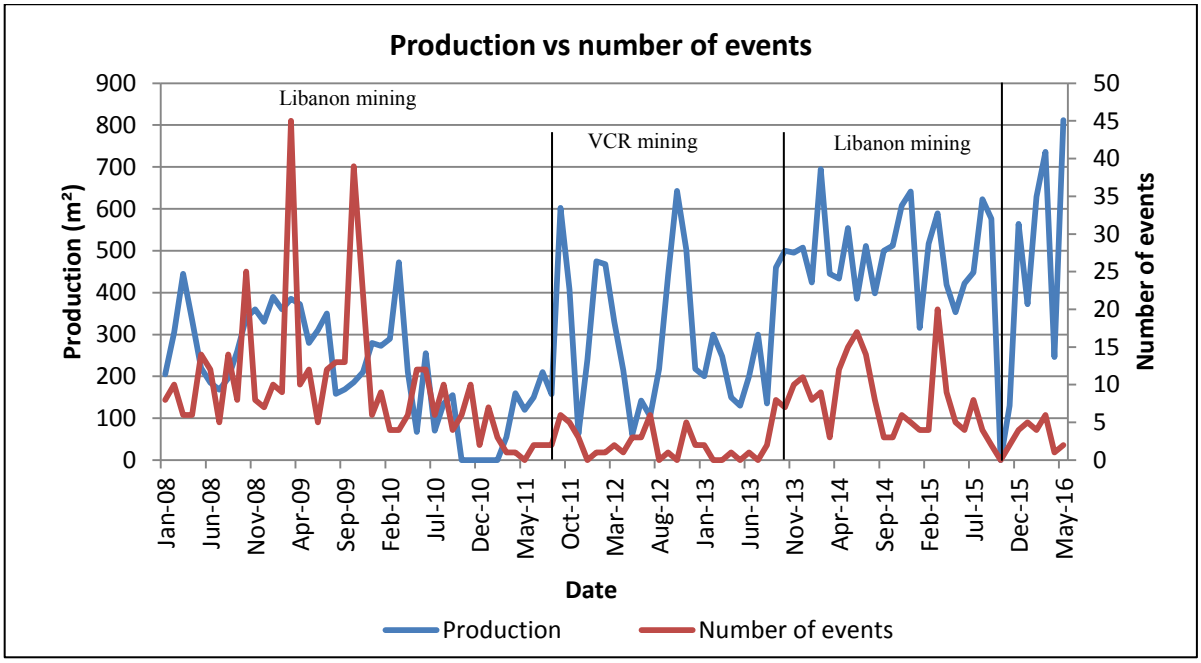


Figure 5.14 Comparative plot of the number of seismic events and production data of the VC25-23 area.

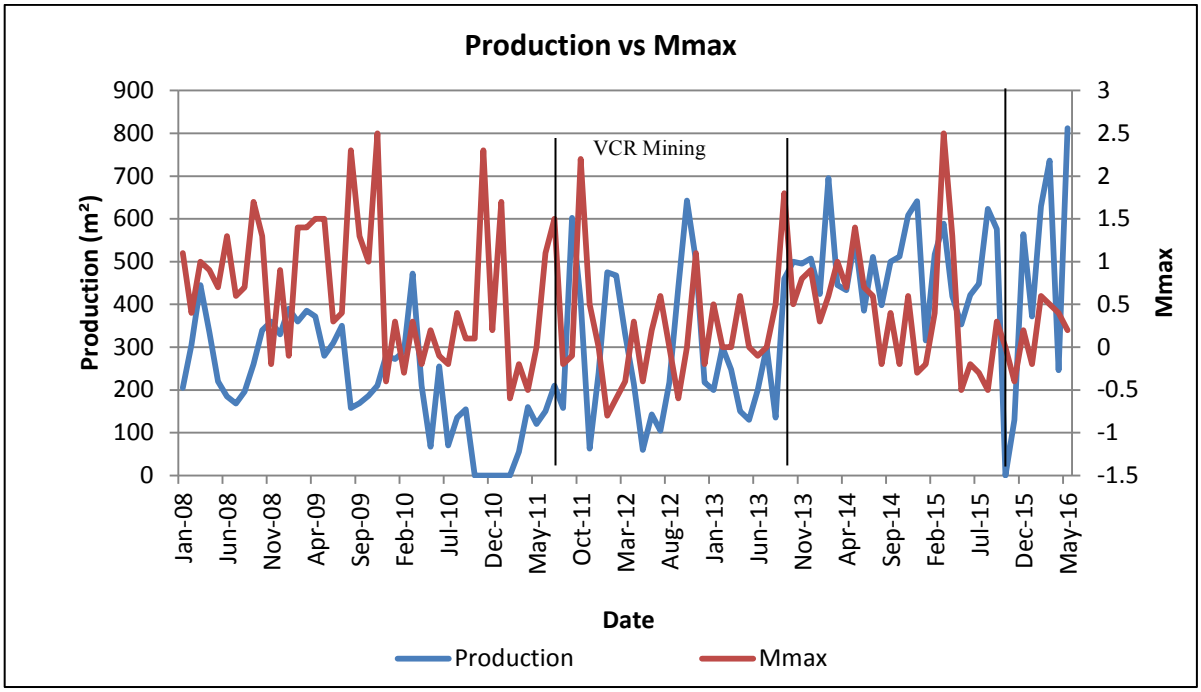


Figure 5.15 Plot of production and seismic magnitude data for VC25-23.

Figure 5.16 is a visual record of the observed underground conditions of the off-reef excavations. These excavations were mined through the strata layers to intersect the reef. Poor, fractured ground was observed as the bedding planes were broken and it exposed multiple joint sets and other geological discontinuities. The areas that were inspected did not show any abnormal deformation or shear.

Figures 5.17 to 5.20 depicts the ground conditions of the Libanon stope prior to overstoping. Figures 5.21 and 5.22 depicts the typical ground conditions in areas where the overstoping was completed. The observed unravelling can be attributed to the formation of a tensile zone. A tensile zone was also observed in Section 4.1 (Figure 4.1.5) when overstoping was complete. These observations support the modelling results.

Stress fracturing and joint sets are clearly visible in both the on-reef and off-reef excavations. The footwall of the Libanon stope consisted of shales, which dilates in the presence of moisture and oxygen, resulting in the rapid deterioration of this rock mass. Figure 5.18 and 5.19 depicts a hangingwall in proximity to the VCR abutment with very few stress fractures.

In Figure 5.20 closely-spaced bedding planes in the quarzitic Libanon hangingwall is seen. This layered stratigraphy is a common feature for quartzite on Gold Mine A. During the investigation, a newly developed ore pass, Figure 5.22, between the Libanon and VCR stoping indicated that some of the parting planes were mobilized, creating open discontinuities. This damage can be related to the dissipated energy component of equation 4.2.4 as described in Chapter 4. This is an important observation as it is supporting evidence for the mechanism of energy dissipation. This reduces the amount of energy that may be released violently. Although it is not shown in one of the figures it is worth mentioning that the back areas were subjected to a significant amount of closure. In some areas it is estimated as to be as much as a metre.



Figure 5.16 Photograph depicting the shale footwall below the LI 25-23 Libanon stope (courtesy of D.F. Malan).



Figure 5.17 Condition of the shale footwall in the LI25-23 stope (courtesy of D.F. Malan).



Figure 5.18 Condition of the quartzite hangingwall in the LI25-23 stope (courtesy of D.F. Malan).



Figure 5.19 Condition of the quartzite hangingwall adjacent to the face of the LI25-23 stope (courtesy of D.F. Malan).



Figure 5.20 Condition of the quartzite hangingwall, where the bedding planes were exposed in the back area of the LI25-23 stope (courtesy of D.F. Malan).



Figure 5.21 Condition of quartzite between the two reef elevations as seen in the sidewall of a newly developed ore pass. The observed movement and dilation contributes to the energy dissipated as described in Chapter 4.3 (courtesy of D.F. Malan).



Figure 5.22 Unravelling of the hangingwall in the back area of the Libanon where the VCR overstoping was completed. This damage can be attributed to the tensile zone as seen in the modelling illustrated in Figure 4.1.5 (courtesy of D.F. Malan).

In Appendix A, the simulated ERR is presented for selected mining steps. The mining layout that was modelled is shown in Figures 5.23 to Figure 5.25. In Figure 5.23, the solid green is previously mined areas, blue lines indicates the on-reef VCR mining and the dotted black lines the off-reef understoping. All the ERR plots that is in this analysis displays an offset between the mined faces and the ERR value location. This offset can be attributed to the way the program calculates the ERR, projection of the plot as well as the way the program selects blocks of the grid to be analysed.

The parameters used in the model were those suggested by the SIMRAC GAP 332 report: a Young's modulus of 60 GPa, Poisons ratio of 0.27, cohesion of 0 MPa, friction angle of 30º, k-ratio of 0.5 and a vertical stress increase of 0.0275 MPa/m. Due to the limitations of boundary element numerical modelling with regards to low middling multi-reef mining, the model was run using a 2 m grid size.

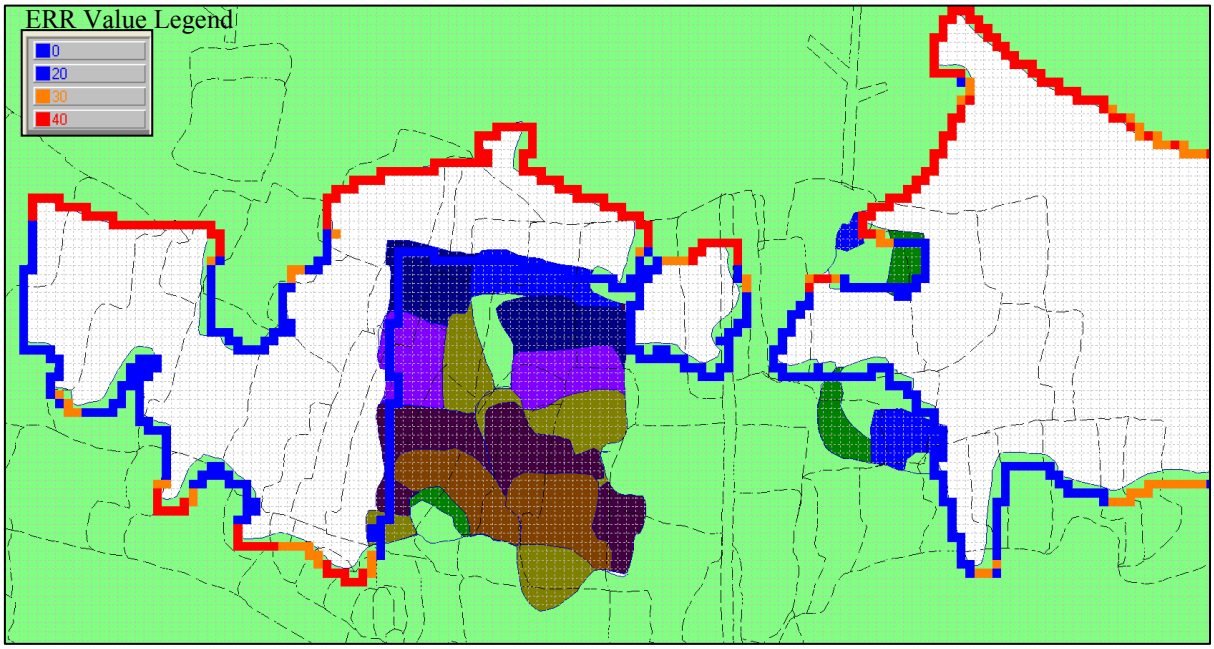


Figure 5.23 Sequenced layout for the modelling of VC25-23.

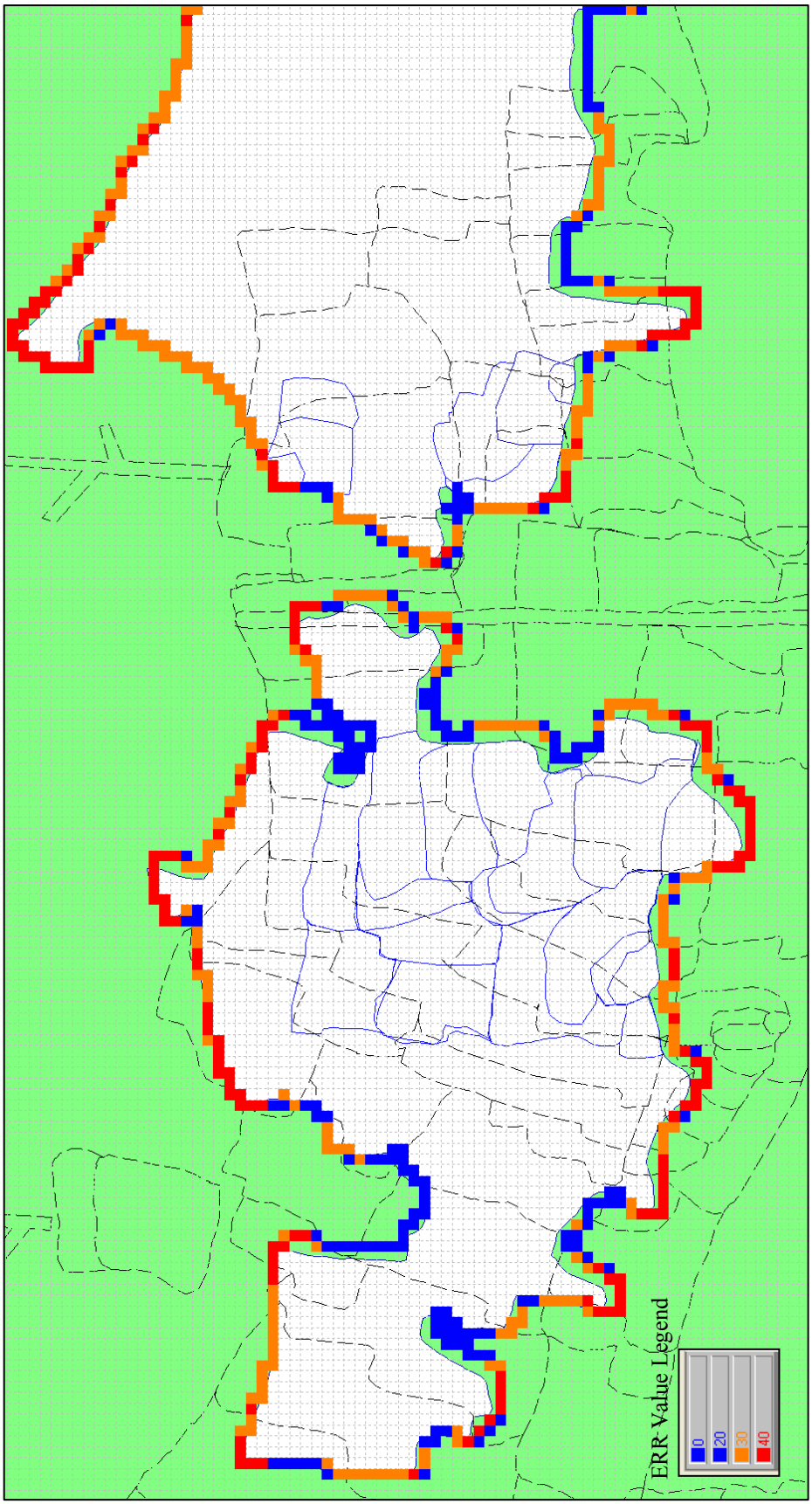


Figure 5.24 Outline of the modelled layout of the VC25-23, prior to mining (2006).

Figure 5.24 and 5.25 depicts the ERR values obtained from the numerical model. The particular step shown in the figures are during the period when the last mining is conducted on the VCR horizon in understoped (de-stressed) conditions. The middling of the stopes were modelled as 15 m. Figure 5.24 shows favorable ERR values in the de-stressed area, although some areas have high peak values when unmined blocks of ground is left or when poor face shapes or layouts are present.

Figure 5.25 depicts the ERR on the Libanon reef, at the end of the mining. The other steps are given in Appendix A. The step shown here is the worst case scenario as the VCR area that is not understoped is reduced substantially and many of the poor mining layouts formed abutments, sharp corners and isolated pillars. Figures 5.26 and 5.27 depicts the ERRs where a abutment was breached in this area. This figure shows a similar picture as Figure 5.24, where areas with elevated values indicate the presence of abutments and areas where overstoping is not complete or where poor layouts are present.

Figure 5.28 indicates a stress contour plot of the major principal stress on the VCR reef elevation as reference for the locations of two line plots of the stress as indicated. Figures 5.29 and 5.30 depicts the two line plots. From these plots can be seen that the stress levels are high. The trend of the figures indicates that the principal stress would increase as the face advances, it is however evident that this increase is not linear as the face advances. It can also be seen that a stress concentration is present towards the end of the plot, this can be associated with a abutment on the VCR elevation that is partially de-stressed. The stress indicated is well above the strength of the host rocks and hence intense fracturing of the VCR hangingwall and footwall is expected in the area close to the abutment.

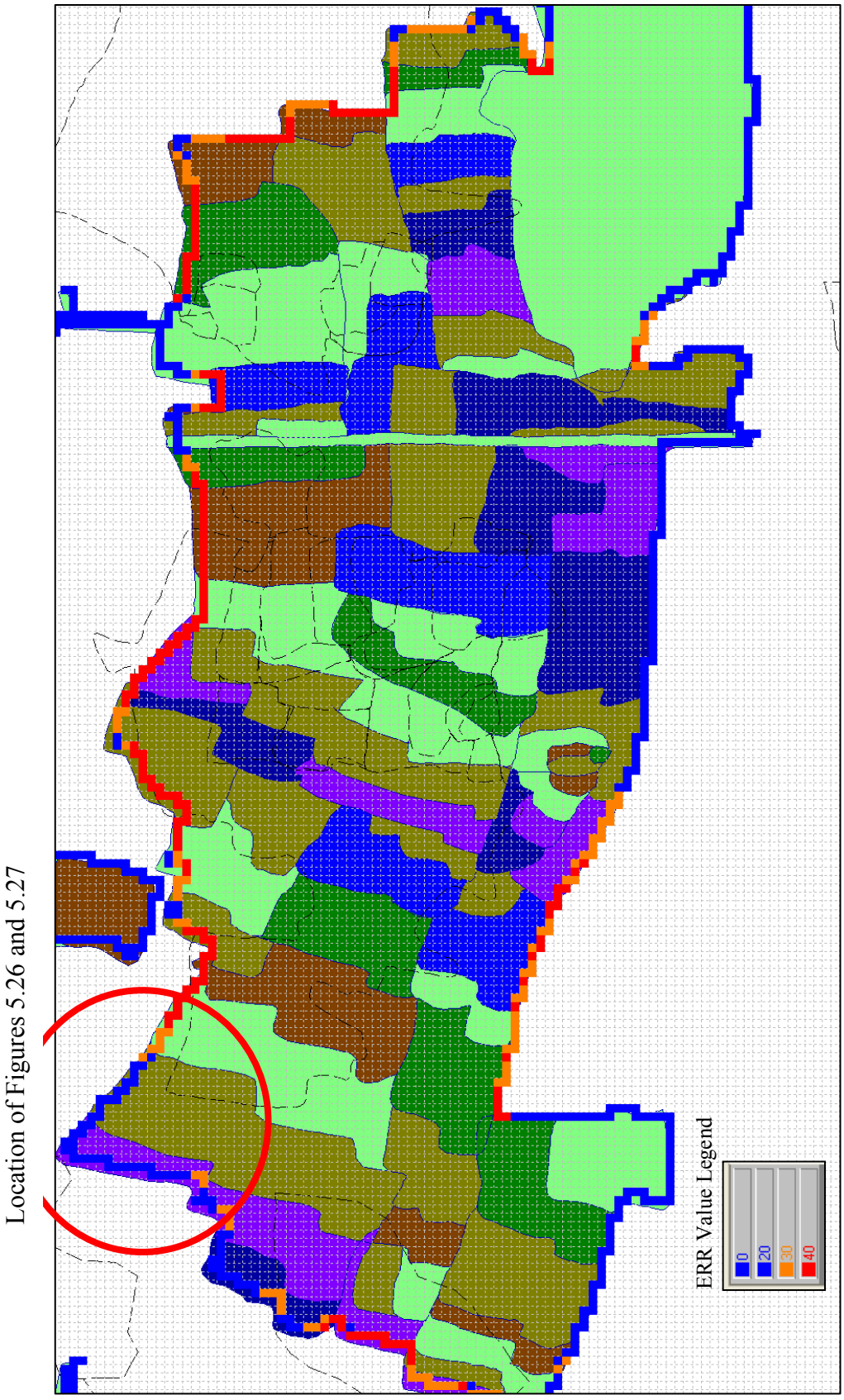


Figure 5.25 ERR results indicating the effect of the de-stressing at LI25-23.

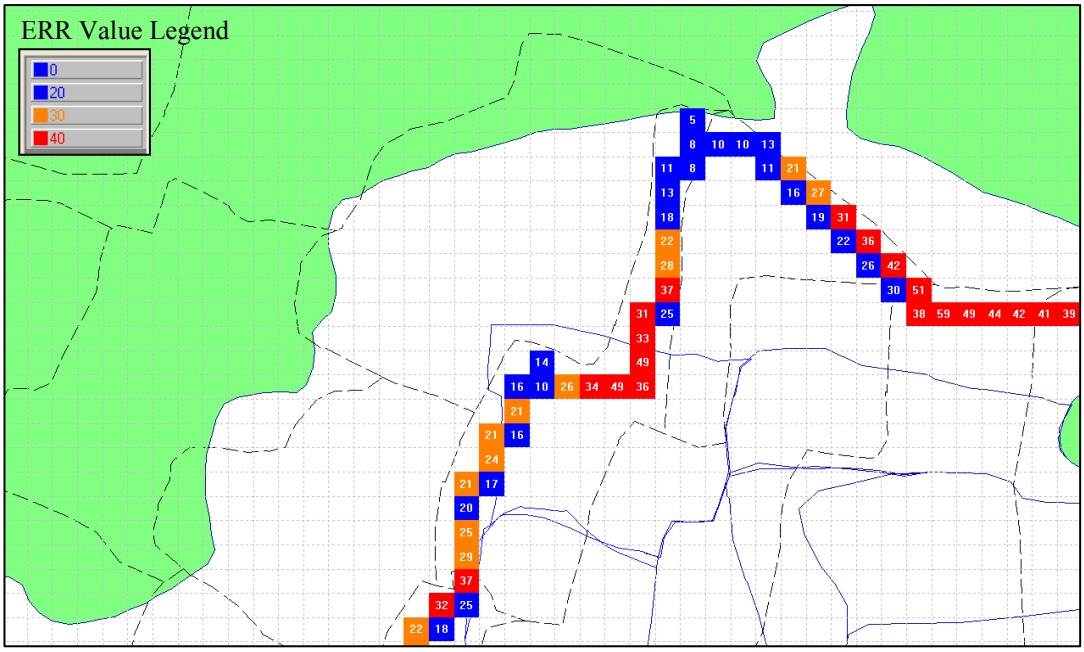


Figure 5.26 ERR values of an area at the VC25-23 stope before understoping the VCR. The VCR stope is shown in green while the modelled mining face of the Libanon reef is shown by the ERR values.

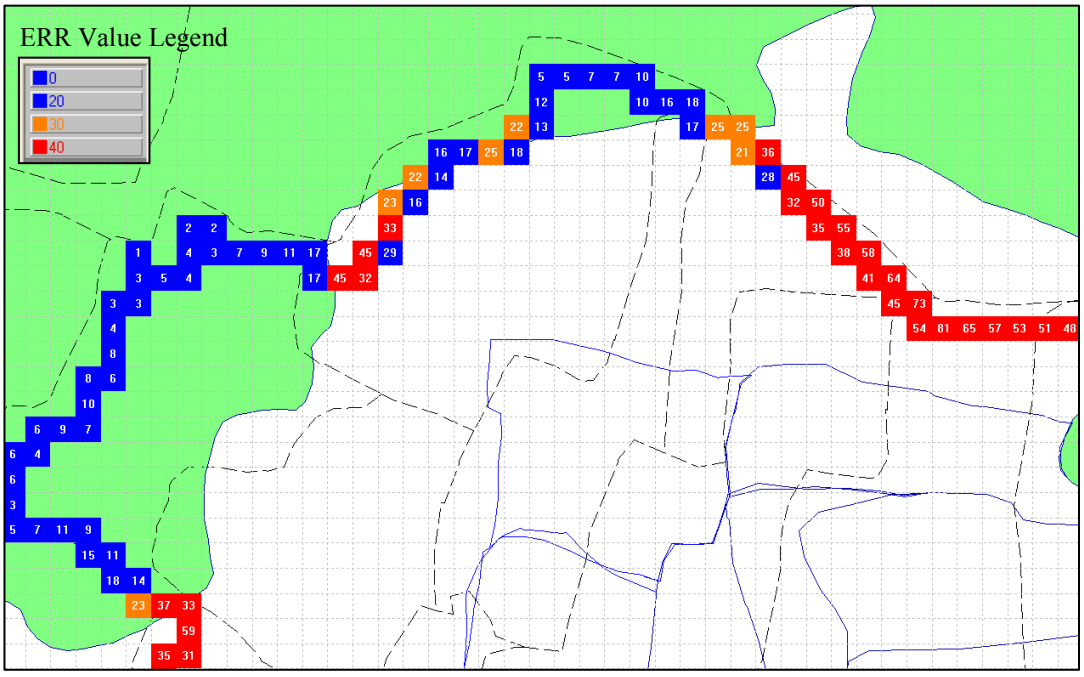


Figure 5.27 ERR values of an area at the VC25-23 stope after understoping the VCR. The VCR stope is shown in green while the modelled mining face of the Libanon reef is shown by the ERR values.

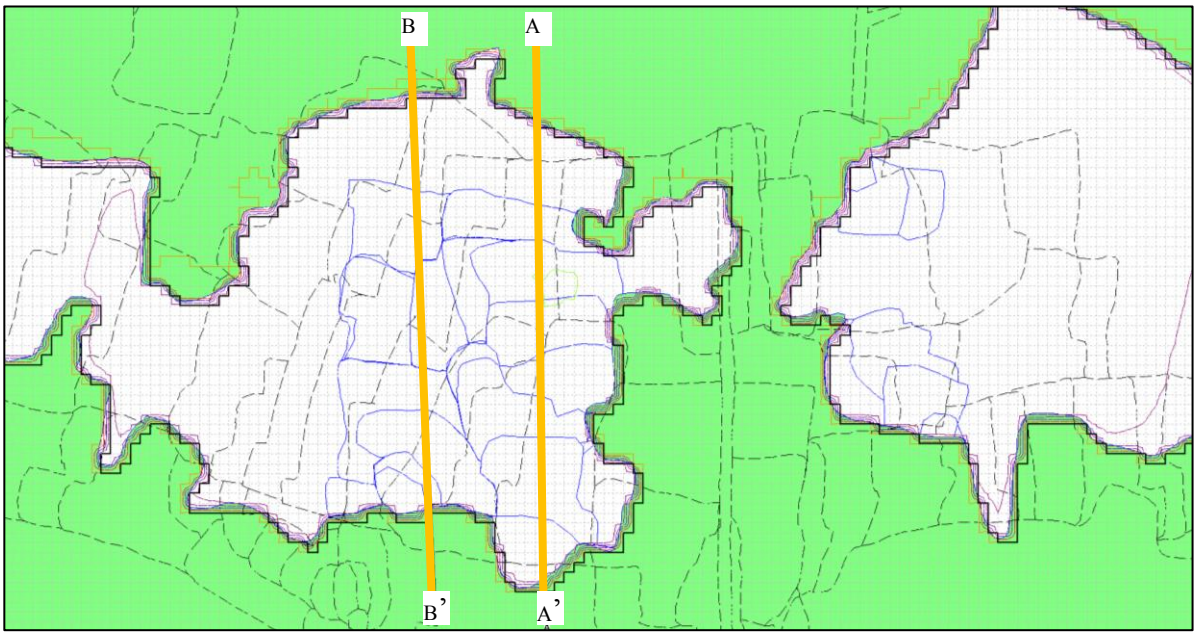


Figure 5.28 Stress contour plot indicating the location of on-reef sections for a modelled layout on the VCR elevation. The green shows the mined VCR, the blue lines shows the modelled VCR faces and the dotted black lines shows the modelled Libanon mining.

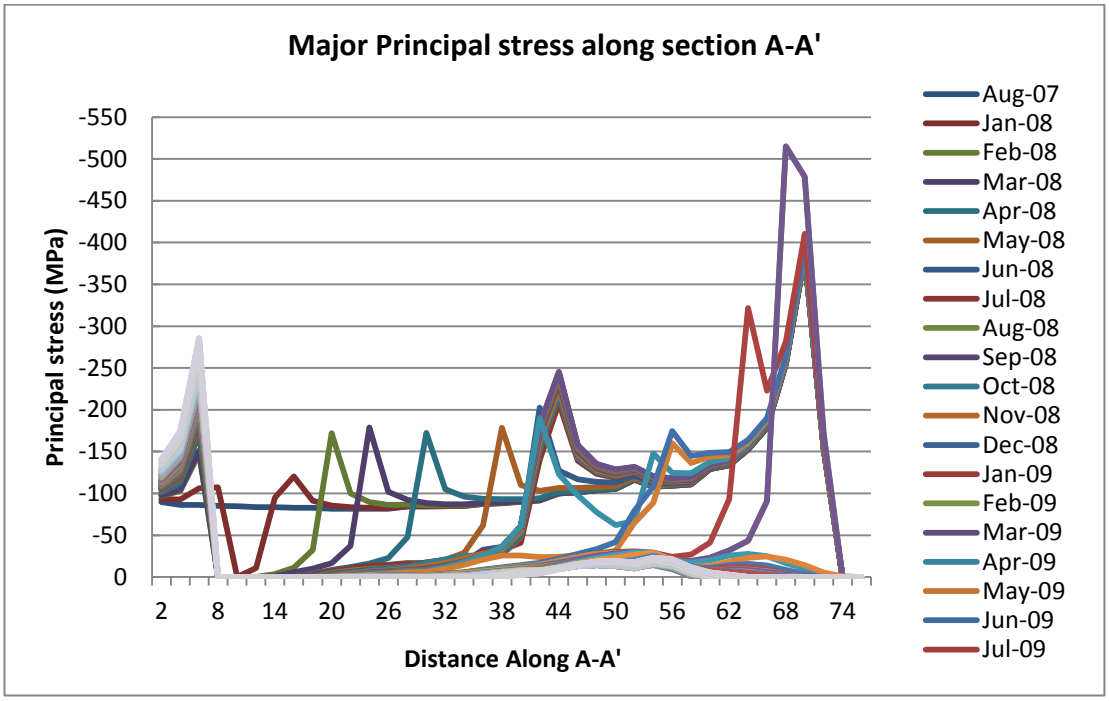


Figure 5.29 Plot of the stresses along section A- A’ on the VCR elevation.

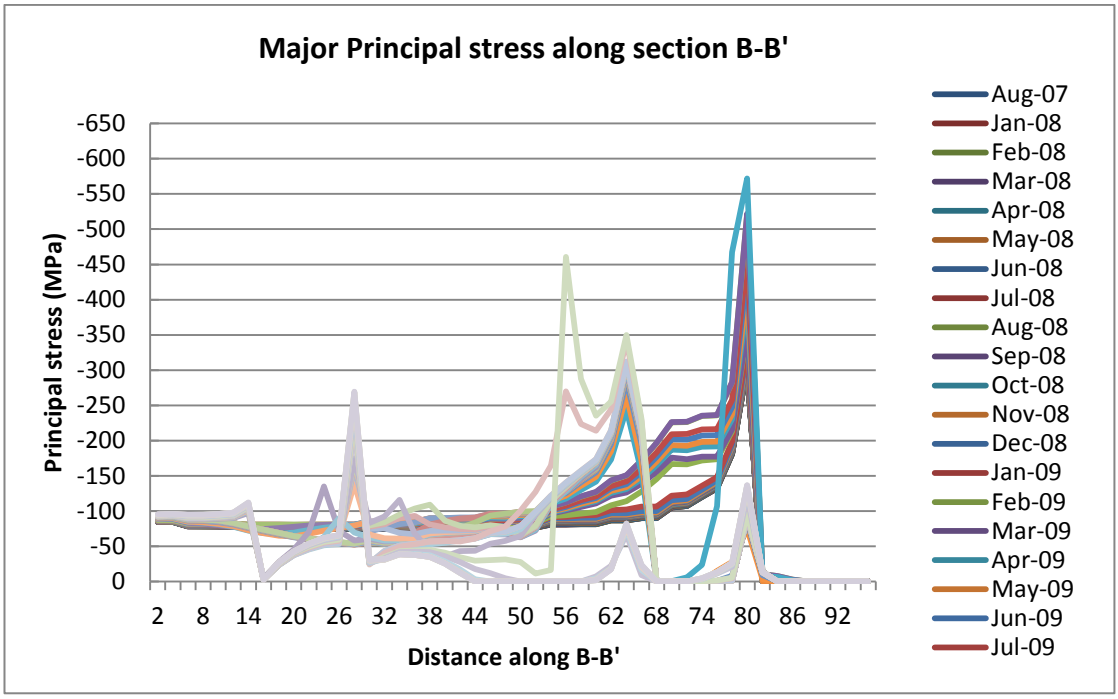


Figure 5.30 Plot of the stresses along section B- B’ on the VCR elevation.

Figure 5.31 depicts the average ERR values plotted against the cumulative production of the area. It is clear that there are 2 distinct mining periods. The first period was towards the end of the original layout when Libanon mining occurred up to the final position. The second period is during the VCR mining when the ERR values were very low. Elevated vales are also observable as the abutments were reached.

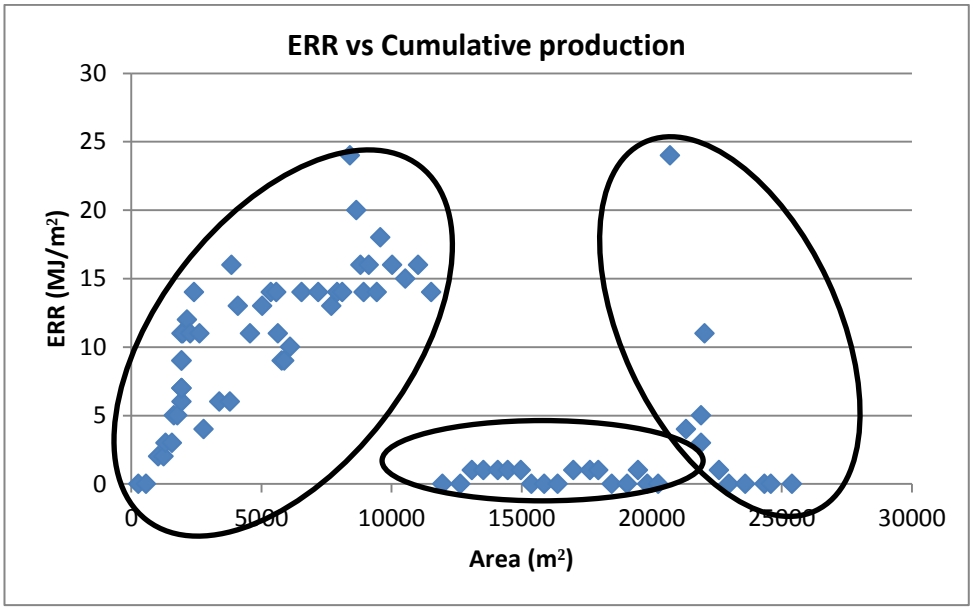


Figure 5.31 Average ERR and cumulative production comparison for the 25-23 area.

To determine the effect of de-stressing on stress between the two mining horizons, sections were plotted and analysed. Owing to the mined layout and configuration, sections were plotted on dip and strike to better understand the influencing factors (Figures 5.32 and 5.33). Figures 5.34 to 5.37 depicts a selection of major principal stress plots for a section on-dip through the model as depicted in Figure 5.32. Figures 5.38 to 5.42 depicts the major principal stress on a strike section as depicted in Figure 5.33.

The figures clearly shows the interaction of the abutment stresses as the faces advance, and the effect of de-stressing is also visible. These results confirm the modelling using a simplified model is Chapter 4 that illustrate the zones of high principal stress as the Libanon mining faces mines below the VCR abutments.

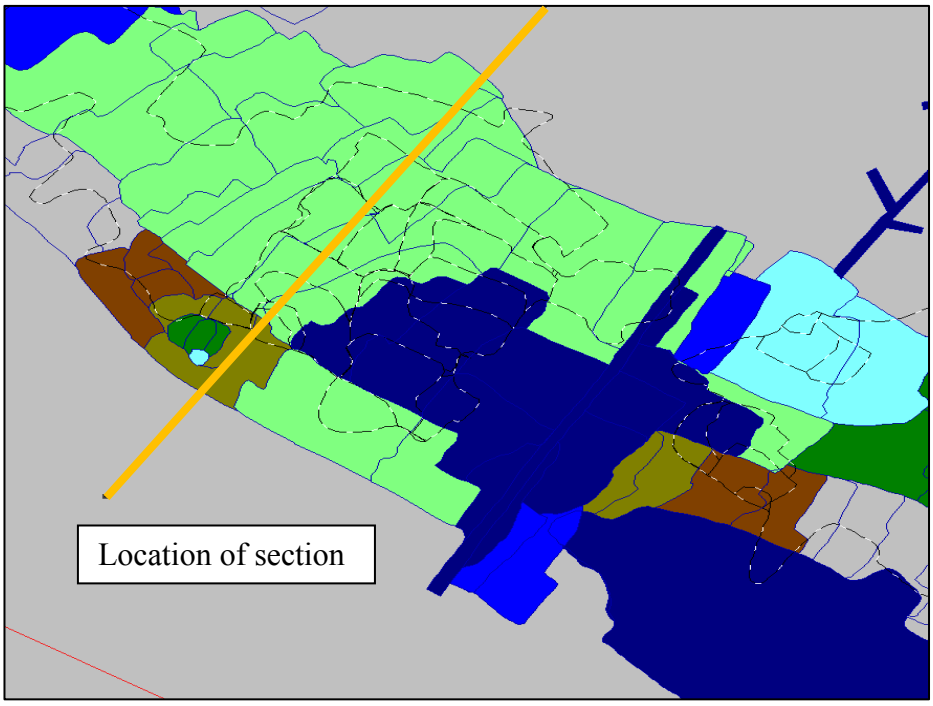


Figure 5.32 Location of an analysed dip section on the Libanon reef elevation.

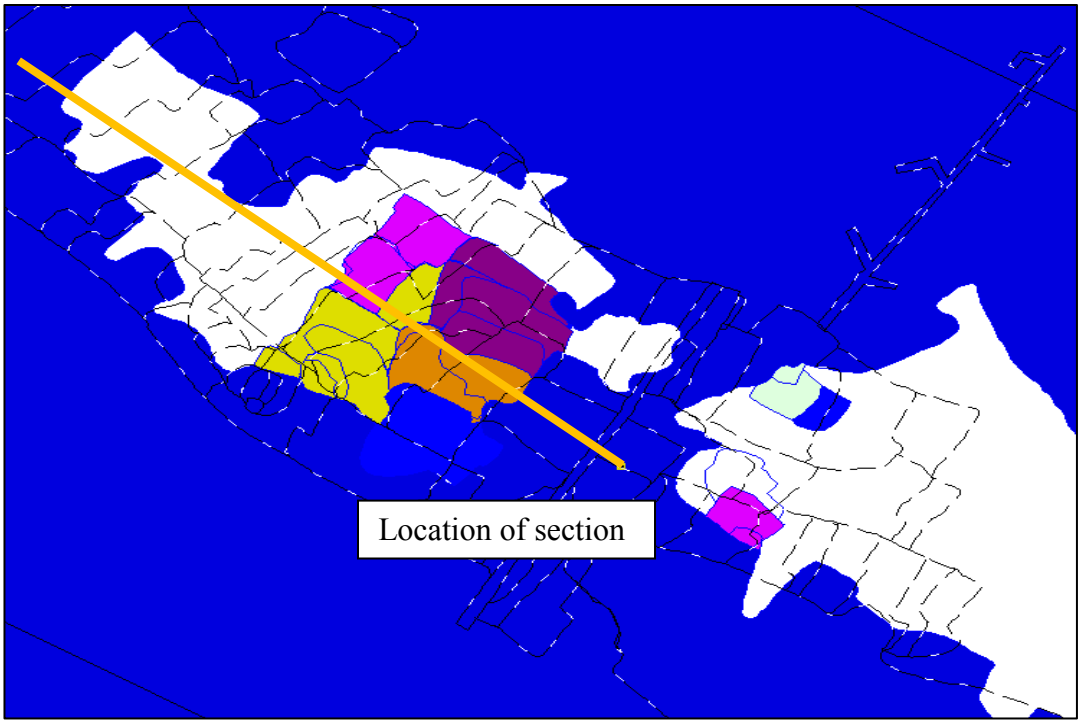


Figure 5.33 Location of an analysed strike section on the VCR reef elevation.

Figure 5.34 and 5.38 shows a region of very high major principal stress on the edges of the stoped out area. These concentrations are confined to very localized areas. Areas of zero stress are also seen along the stoped out area.

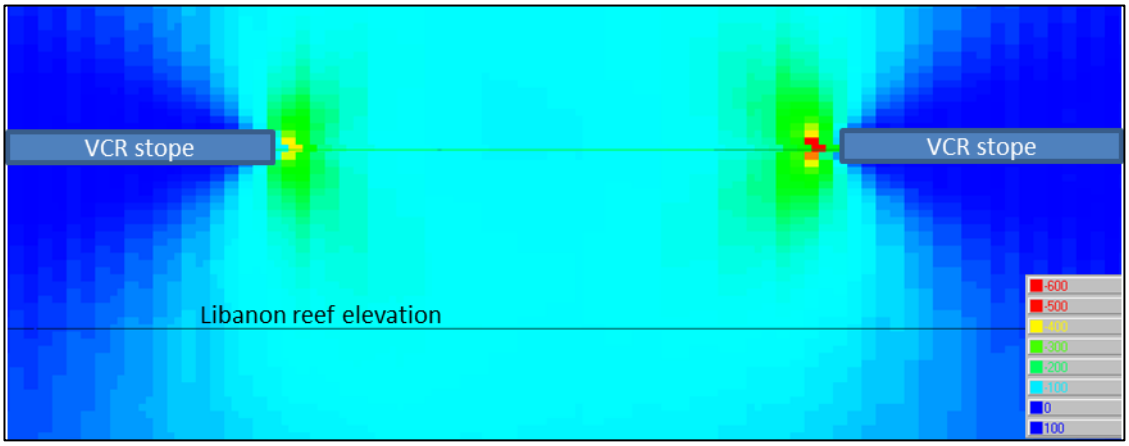


Figure 5.34 Contour plot of the major principal stress prior to any mining on the Libanon reef.

Figures 5.35 to 5.42 illustrates the stress contours after the introduction of the Libanon mining. From the figures it is clear that the additional stope has a significant disruptive effect on the stresses and the interaction between the edges of the two stopes. Figure 5.36 also indicates the partial de-stressing of the VCR reef elevation as the overlap between the reef horizons is increased. From Figure 5.40 it is evident that the stress on the VCR is reduced as the area is partially understoped.

Considering the figures as described above it can be seen that stress concentrations are present on the abutments. It is also clear that there are significant interaction between the two reef horizons. This interaction of the concentrations on the abutments will induce failure as well as shear as mentioned in Chapter 4. When comparing the released energy (Chapter 4.3) to the seismicity as described earlier in this chapter there seems to be a disconnect, as the modelled ERR figures are very high in many areas on the Libanon reef elevation. The levels of seismicity in the specific areas where elevated ERR values are present do not appear to be excessive or elevated. However when the other forms of energy dissipation as mentioned in Chapter 4, are considered, it may be possible that

energy is being dissipated on bedding planes in response to the high abutment stresses associated with high ERR.

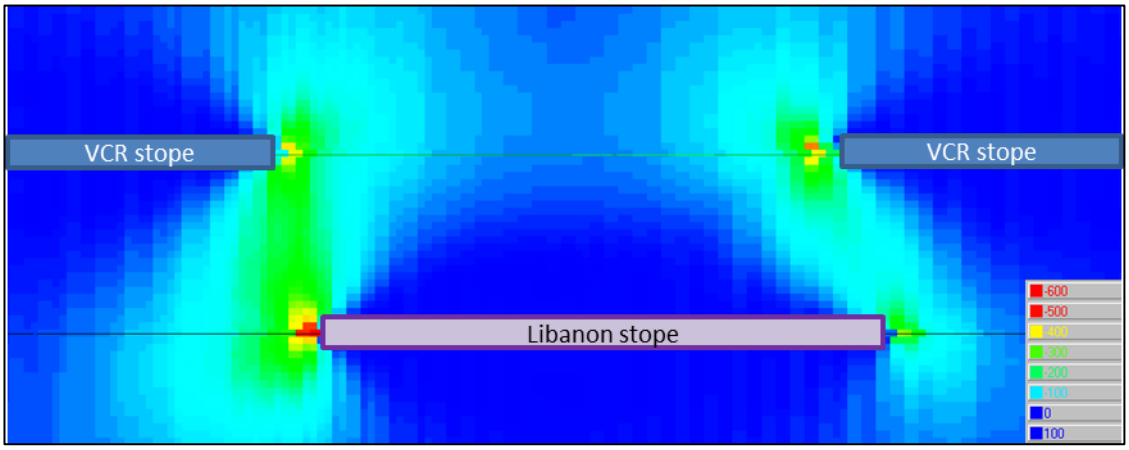


Figure 5.35 Contour plot of the principal stress during the understoping.

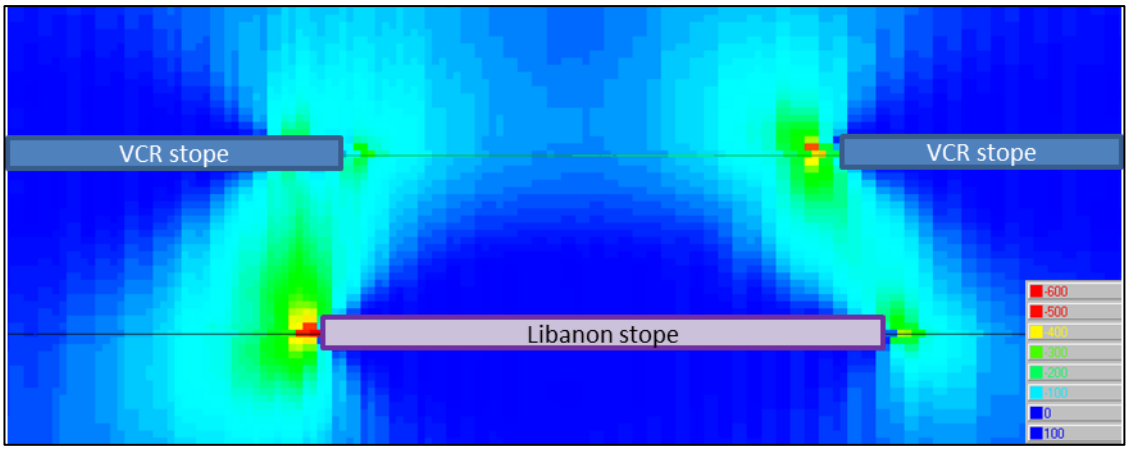


Figure 5.36 Contour plot of the principal stress during the continued understoping on the Libanon reef.

Figure 5.37 sees a portion of both the VCR and Libanon stopes de-stressed as the overlap of mining on the two reef horizons are enlarged. This would mean that some of the stoping on the VCR would take place at a lower stress.

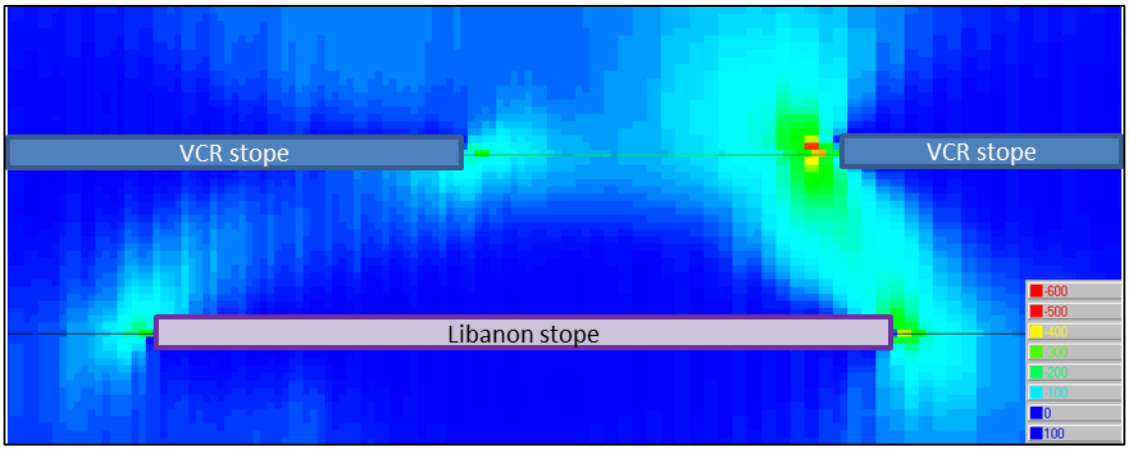


Figure 5.37 Contour plot of the principal stress during the completion of the de-stress mining on the Libanon reef.

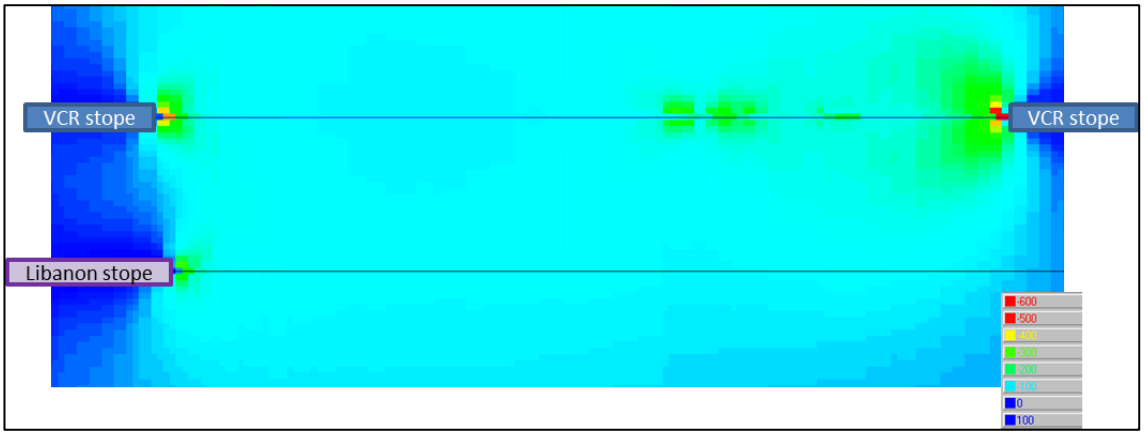


Figure 5.38 Contour plot of the principal stress on strike before mining on the Libanon reef.

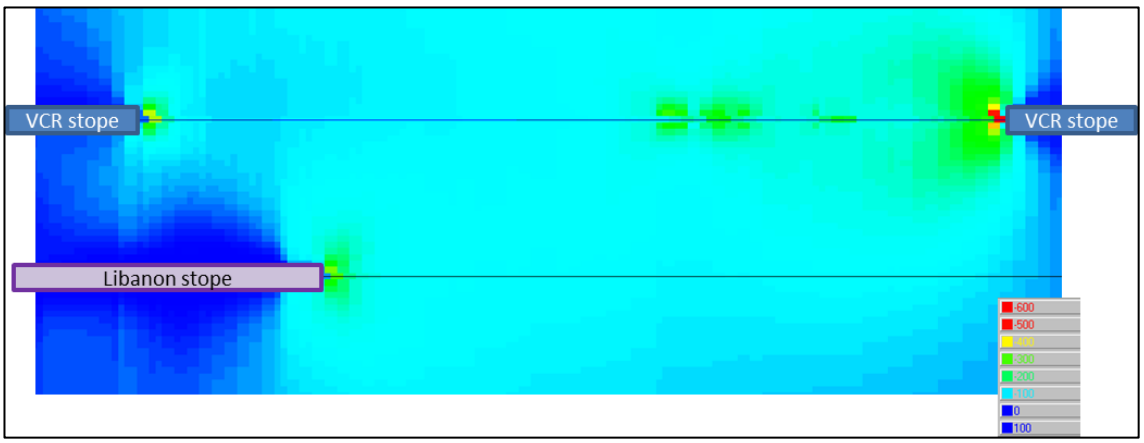


Figure 5.39 Contour plot of the principal stress on strike during the introduction of the mining on the Libanon reef.

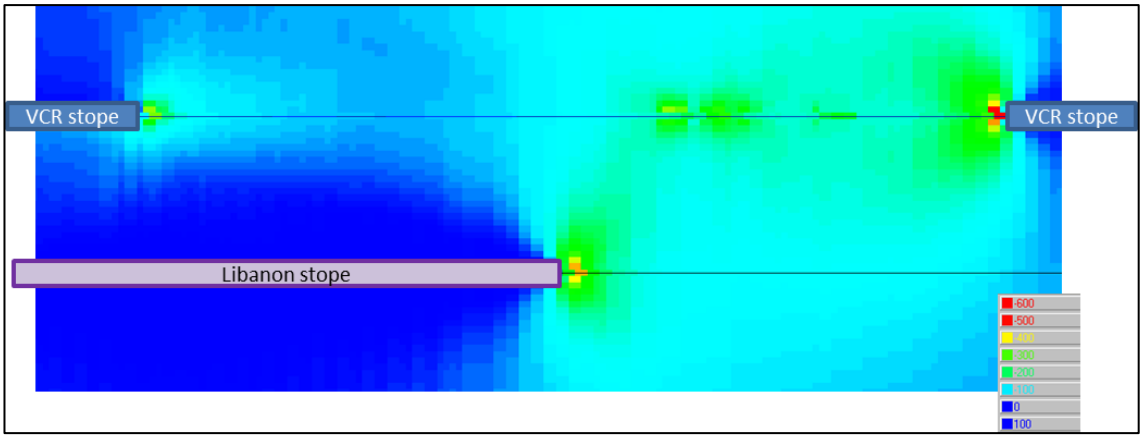


Figure 5.40 Contour plot of the principal stress on strike when mining on the Libanon reef is halfway underneath the pillar.

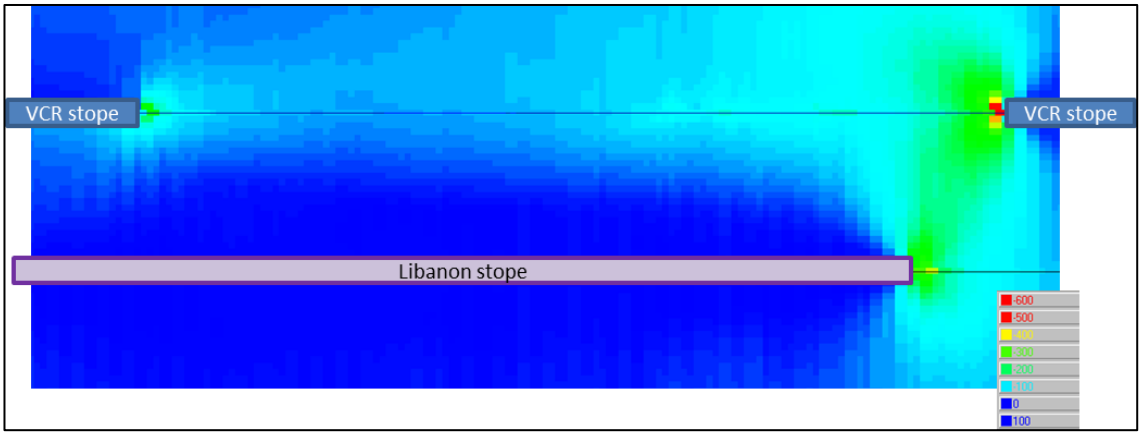


Figure 5.41 Contour plot of the principal stress on strike during the continued de-stress mining on the Libanon reef.

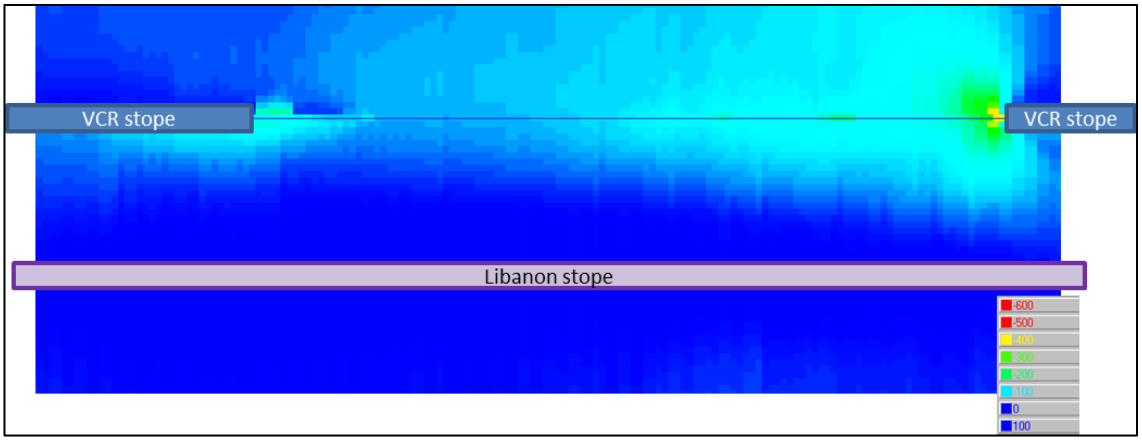


Figure 5.42 Contour plot of the principal stress on strike during the completion of the de-stress mining on the Libanon reef.

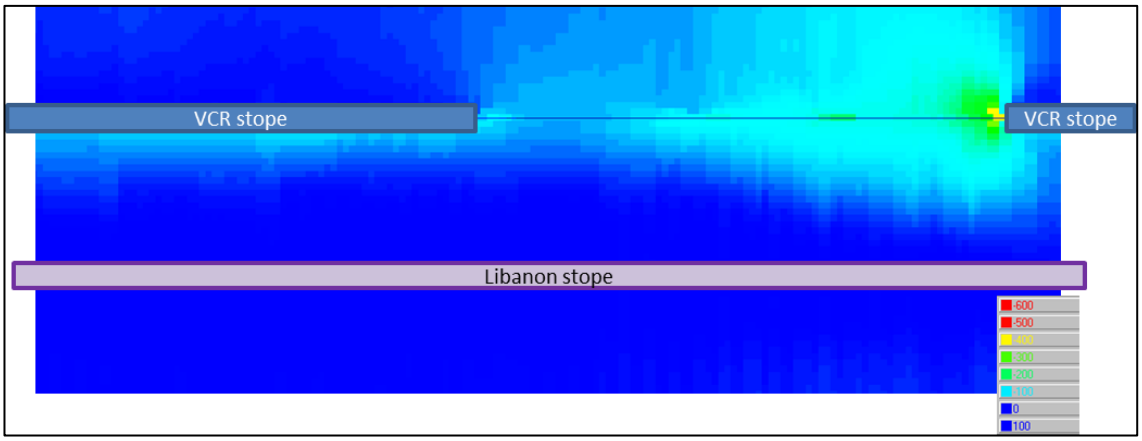


Figure 5.43 Contour plot of the principal stress on strike during the de-stressed mining on the VCR reef.

SUMMARY

In summary, the analysis in Chapter 5 indicated that the multi-reef mining in reasonably close proximity of 15 m of pillars in a large area were mined successfully. The lithology of the area included a weak shale in the footwall of the Libanon reef and a weak hangingwall lava above the VCR.

The seismicity seemed to be mining related for stopes that were not de-stressed. From the numerical modelling, the ERR values and major principal stress were elevated in many areas. The areas where de-stressing was not complete and where poor mining layouts or sharp corners were present were identifiable by elevated ERR levels. This creates the risk of potential pillar failure and abutment breaches when mining on a different elevation. The numerical modelling indicated that fracturing will be present as peak principal stress is expected to be greater than the rock strength. This was confirmed during the underground investigations. It was also shown that as the pillar size is reduced the stress increases hence creating an increasing risk of failure as the pillar size is reduced. The modelling indicated that the principal stresses are significantly impacted upon by the multi-reef mining. This was also confirmed as tensile cracks and unravelling were observed in the back areas of completely overstoped areas. The modelling indicated that the principal stresses interacts when the faces of the reefs are in close proximity and this creates the potential for shear failure. Shear failure was observed between the

two excavations in the form of bedding plane slip and dilation as observed in the ore pass. This was an important observation as it supports the hypothesis presented in Chapter 4 that shear slip on bedding planes may dissipate energy and reduce the energy that can be violently released. The levels of seismicity in the specific areas of elevated ERR values were not excessive or elevated. This could also be due to energy being stably dissipated on bedding planes. It should however be noted that the site response may be affected by the nature of failure of different rocktypes, for example violent failure of brittle quatzites.

CHAPTER 6

CASE STUDY AND BACK ANALYSIS OF REMNANT B :VC22-30

This block of ground is located to the North-East of the shaft (Figure 6.1). The target area is bound and cut by a dyke and a 20 m throw fault. The dyke is an offshoot of a seismically active dyke. The parent dyke is classified as high-risk and has a M_{max} of 3.5. The fault is also an offshoot from a high-risk seismically active fault. The fault splits the original remnant into two areas and has a 20 m throw. Only the southern portion of the remnant was mined. The dyke has a 6 m throw with a reverse dip of 55°. Further to the West, the 50 m throw Tear fault (not in this figure) traverses the area and seismic events plot around the fault, even with no mining in the vicinity.

The southern side of the block of ground was successfully extracted starting 2005 until 2011. Mining ceased when a 20 m throw fault was exposed, leaving the northern side of the block of ground unmined. The locality of the block of ground can be seen in Figure 6.1 below.

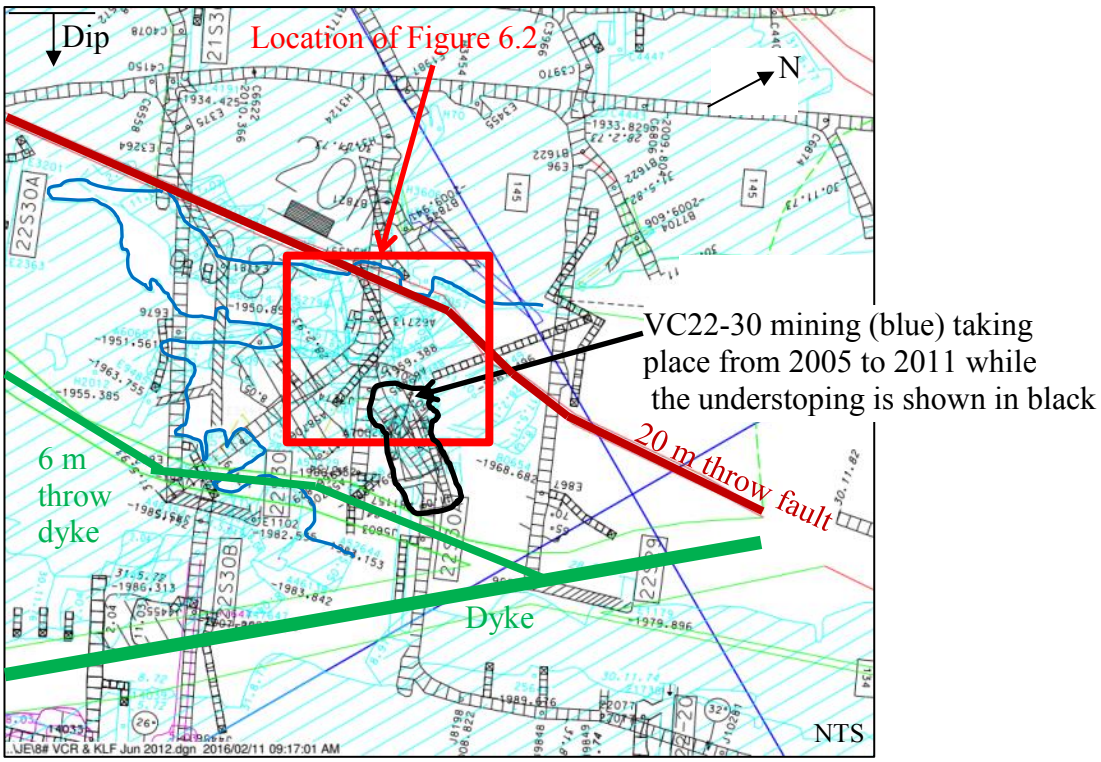


Figure 6.1 Locality plan view of the VC22-30 area.

The immediate hangingwall of the VCR is a weak lava and the footwall consists of a quartzite down to the Libanon Reef elevation. Below the Libanon Reef the footwall consists of shale. No mining has been done on the Libanon Reef in this area, although the reef is present 10 m below the VCR. The reason for not mining the Libanon is that the understoping was conducted to provide access rather than de-stress the block.

The VCR target area was an isolated block of ground with mining on 3 boundaries and had an initial size of 8000 m^2. Adjacent to the block towards the south, the mined span was in excess of 600 m. According to the mine plans, various major geological structures are present in and around this block of ground. Many of the structures present in the vicinity of the area were extensively stoped through and stripped against. In the vicinity of this block of ground are various other blocks where extraction was attempted in the last 10 years. From the mine plans it can be seen that the majority of these blocks were successfully extracted.

To show the complexity regarding the mining layout of this area, a small portion of the stoping plan is shown in Figure 6.2. In this plan the VCR is indicated in red and blue and the off reef waste cut is shown in black.



Figure 6.2 Stoping plan view of a portion of the VC22-30 stope.

The block of ground on the VCR had an extremely high gold content. Access development is situated deep in the footwall of the VCR and large portions had been extensively overstoped. The block was accessed by means of a waste cut that was mined from the footwall development situated 70 m below the block. This resulted in a complex layout where the waste cut was blasted with multiple sections overlapping each other until the reef was intersected. Figure 6.3 depicts a simplified section of the geometry. From this position, the understoped area was extracted first.

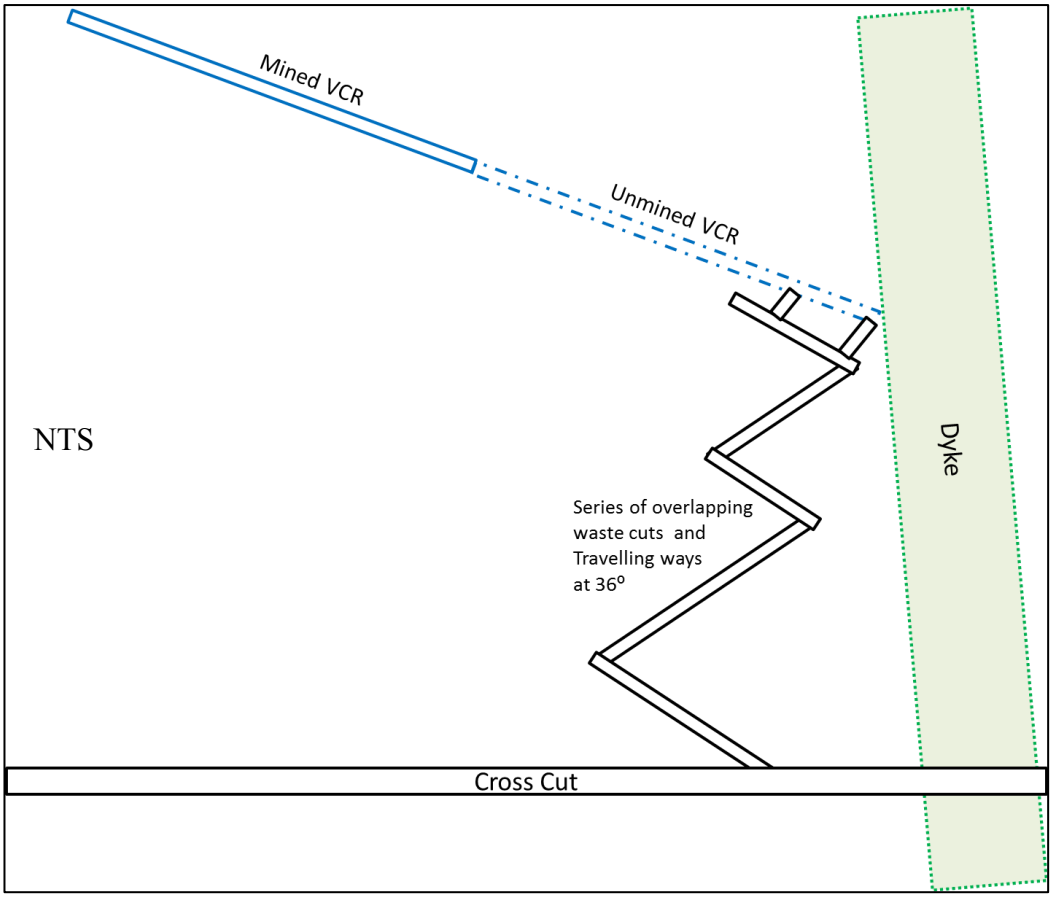


Figure 6.3 Simplified section through VC22-30 depicting the waste cut access way.

Seismicity was recorded since 1996 by the mine's network of 39 geophones located across an area of 56 km^2. The seismic network coverage of the shaft is of such a nature that M_L -0.4 seismic events can be reliably recorded. The system is capable of providing the location of a M_L 0.0 seismic event with an accuracy of 45 m.

Figure 6.4 depicts a seismic plot of all events greater than a zero magnitude for the last 17 years within a 300 m radius of the stope. The events in this figure are coloured based on the date of occurrence, while the size of the plot is an indication of the magnitude. It appears that a few large seismic events occurred on the major geological structures in the vicinity of this block of ground, even when very little or no mining occurred. The largest observed seismic event was M_L= 2.9, while the expected M_{max} is M_L 3.1.

The seismic information indicated that the majority of the events are slip-type events and there was a probability of less than 30% that an event of magnitude M_L 1.0 will occur during any given month.

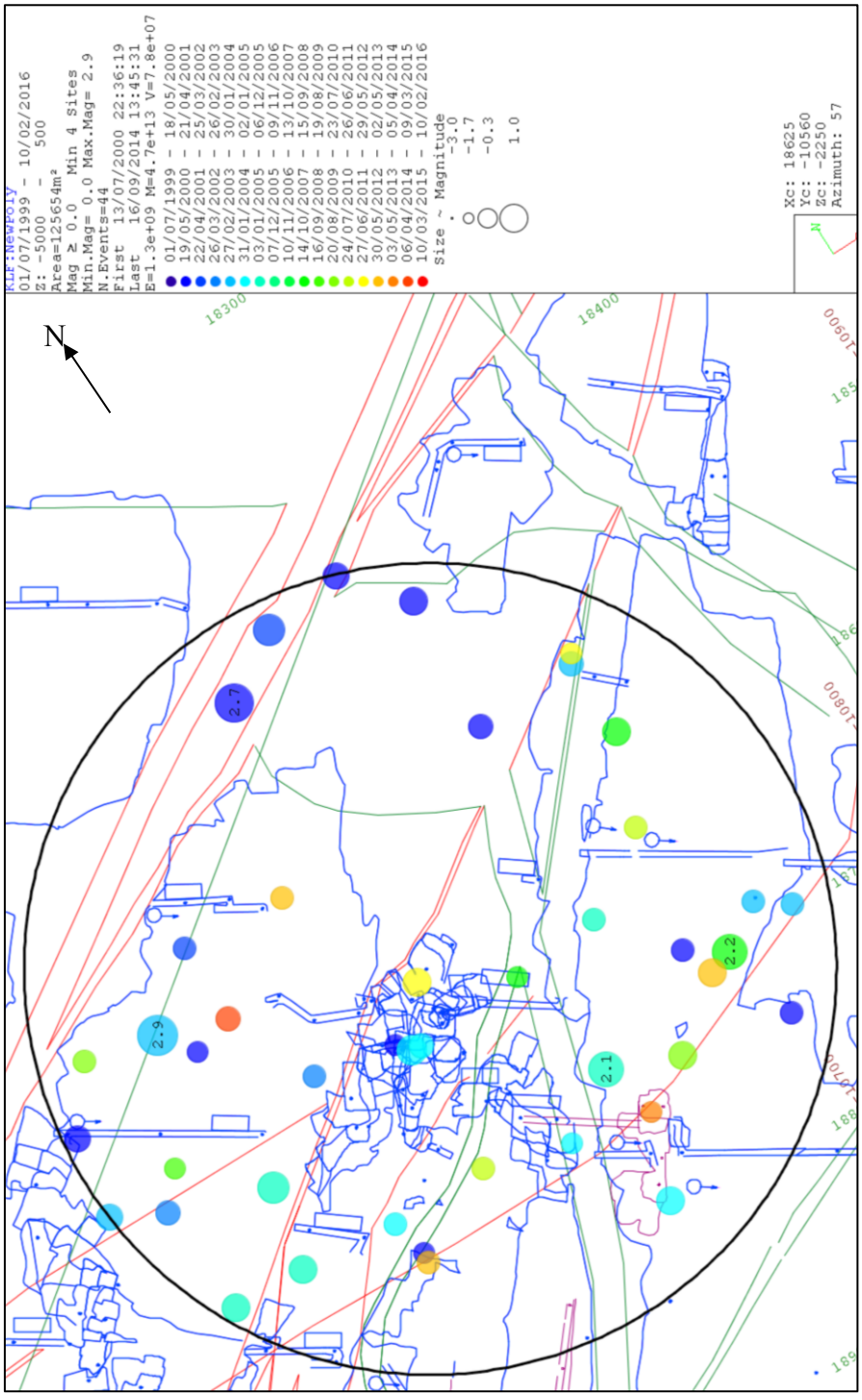


Figure 6.4 Plot of all events greater than M_L0.0 in a 300 m radius around the VC22-30 area.

Figure 6.5 depicts the hourly distribution for the recorded events. This has no clear trend, although peaks were observed at 13h00 and 23h00. The shaft did not have a centralized blasting system until 2010 and operated without night shift in the VCR section. The 13h00 peak may therefore be associated with blasting, while the other peaks can only be attributed to aftershocks following large events.

The activity rate of the area is shown in Figure 6.6. From this figure it can be seen that the seismic activity appears random and that M_L> 2.0 events occurred every 5 months until the drop off in seismicity when all mining in the area was stopped.

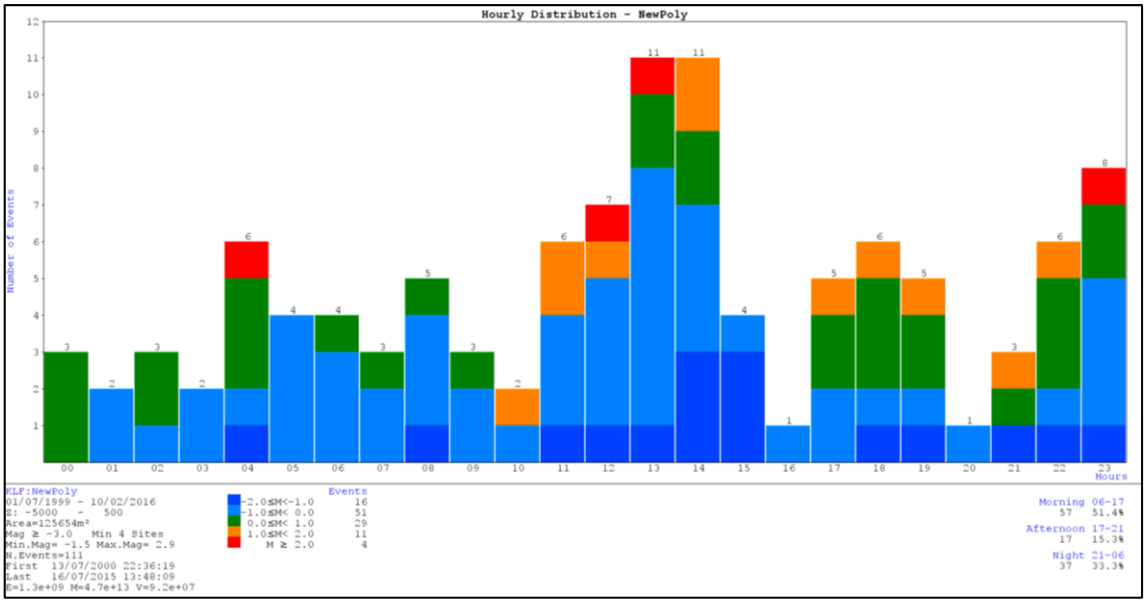


Figure 6.5 Hourly distribution of events in the VC22-30 area.

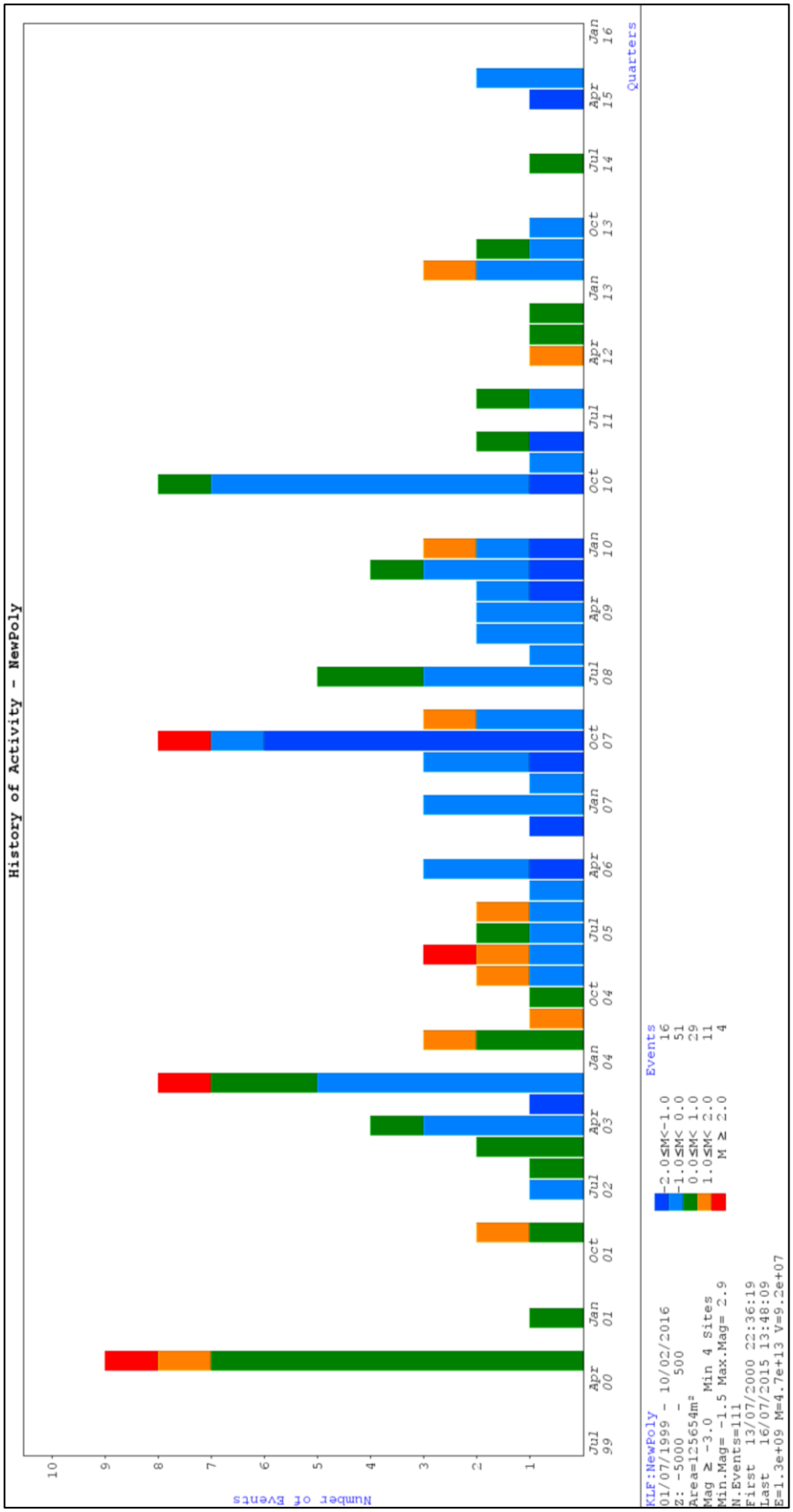


Figure 6.6 Activity rate in the VC22-30 area.

Figure 6.7 depicts the energy released in MJ per annum of this area. Taking into consideration the time periods of mining, the peaks observed appears to be linked to the simultaneous extraction of multiple blocks of ground in the area. If only the time period from 2009 to 2011 is considered, a slightly different picture emerges. From Figures 6.8 and 6.9 it can be seen that only one significant peak is present during the extraction of the block during the end of 2008. This can be associated with the change from understoping to stoping on reef, as well as breaching of the de-stressed abutment.

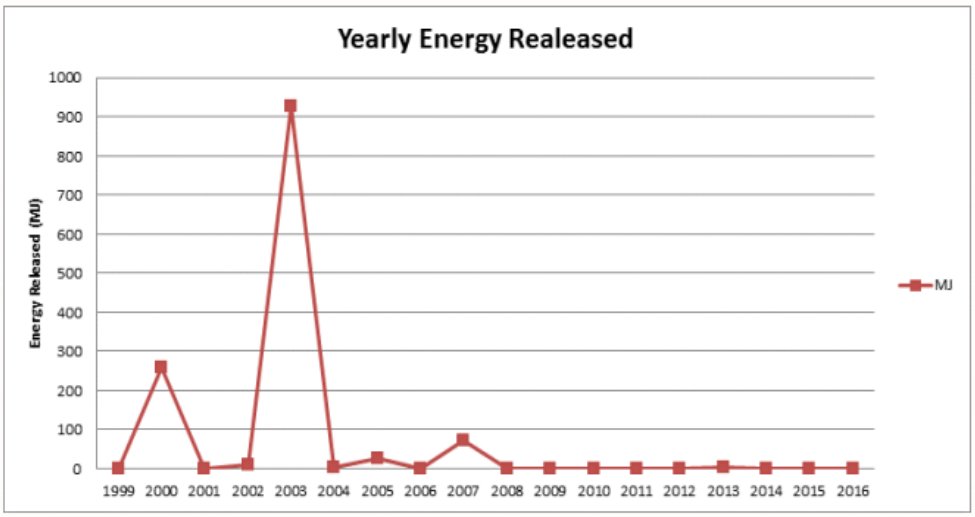


Figure 6.7 Seismic energy release per year of the VC22-30 area.

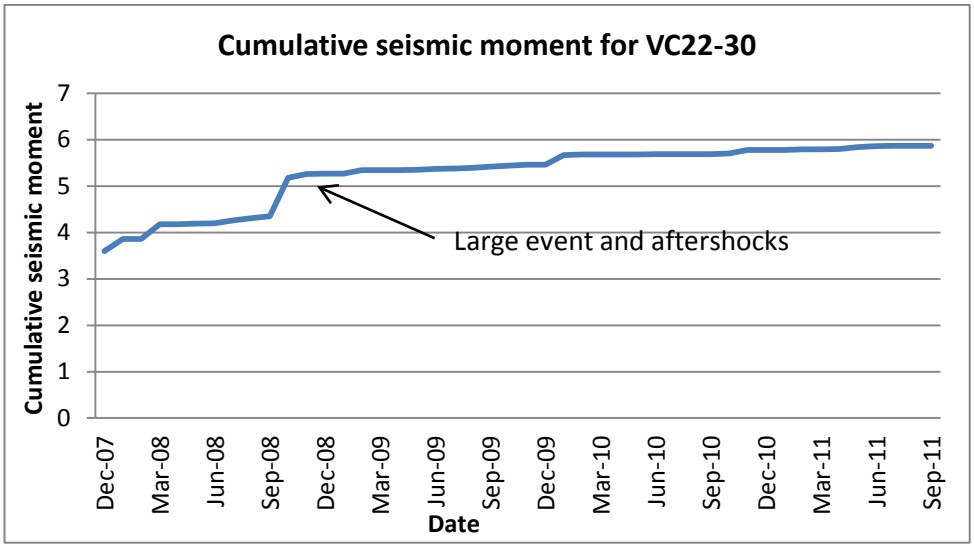


Figure 6.8 Cumulative seismic moment of the VC22-30 area for 2 years.

Year	Number of Events						Max. Mag.	Energy MJ	Moment 10^{12} Nm
	M<0	0≤M<1	1≤M<2	2≤M<3	3≤M	Total			
1999	0	0	0	0	0	0	-	0.00	0.00
2000	0	7	1	1	0	9	2.7	258.08	17.23
2001	0	1	0	0	0	1	0.0	0.02	0.02
2002	1	2	1	0	0	4	1.7	9.16	1.01
2003	9	5	0	1	0	15	2.9	926.61	18.44
2004	0	3	2	0	0	5	1.3	2.40	0.89
2005	4	1	3	1	0	9	2.1	24.31	5.22
2006	5	0	0	0	0	5	-0.7	0.00	0.01
2007	14	0	0	1	0	15	2.2	72.44	3.16
2008	6	2	1	0	0	9	1.1	0.65	0.37
2009	9	1	0	0	0	10	0.2	0.09	0.05
2010	9	1	1	0	0	11	1.1	1.04	0.30
2011	3	2	0	0	0	5	0.4	0.16	0.07
2012	0	2	1	0	0	3	1.0	0.63	0.26
2013	4	1	1	0	0	6	1.2	1.38	0.29
2014	0	1	0	0	0	1	0.7	0.35	0.06
2015	3	0	0	0	0	3	-0.1	0.01	0.02
2016	0	0	0	0	0	0	-	0.00	0.00
Total	67	29	11	4	0	**111**	**2.9**	**1297.35**	**47.39**

Figure 6.9 Summary of the seismic events in the VC22-30 area.

Figure 6.10 is a plot of the cumulative production and the cumulative seismic moment. This figure is the seismic response to production. Figure 6.11 illustrates the number of events to the cumulative area mined. It can be seen that two distinct periods were present. This coincides with the off-reef and on-reef mining that was conducted. The slope of the graph representing the off reef mining is steeper than that of the on reef. Considering the mining layout shown in Figure 6.1 and section presented in Figure 6.3, the difference in slope can possibly be explained by the mining taking place in or above the shales, or the presence of multiple bedding planes affecting the energy release hypothesis as described in Chapter 4.

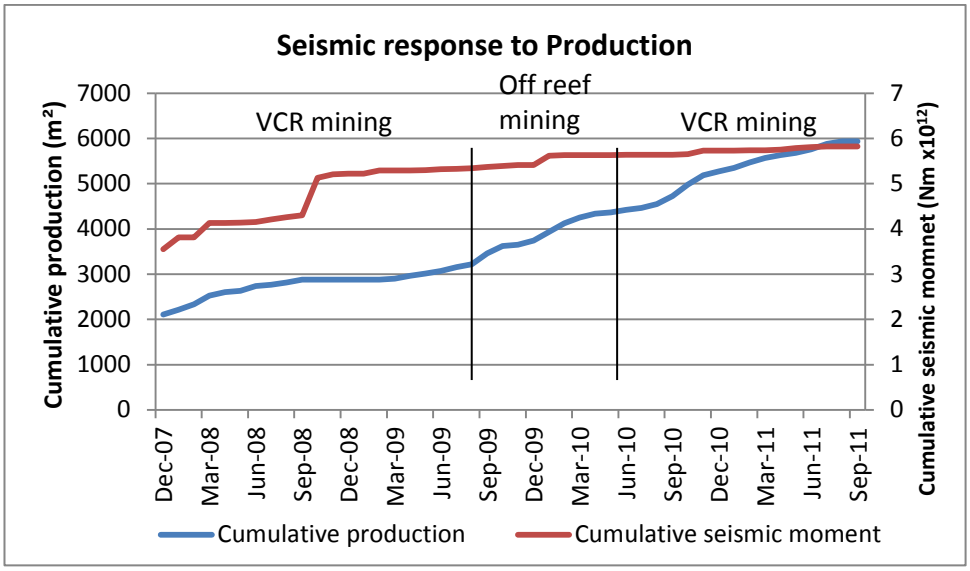


Figure 6.10 Seismic response to production of the VC22-30 area.

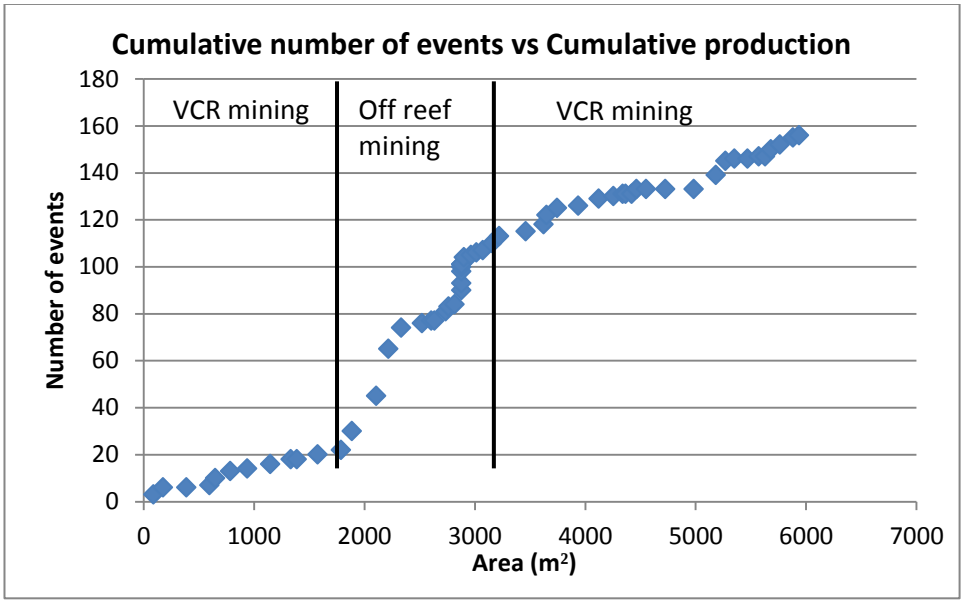


Figure 6.11 Cumulative number of seismic events compared to cumulative production of VC22-30.

The magnitude distribution of all events since 1999 is depicted in Figure 6.12. The incomplete nature of the data set may be because of the network characteristics, while the recurrence period of the larger magnitude events also plays a role. The green distribution indicates the given magnitude distribution while the cumulative distribution is indicated by the blue.

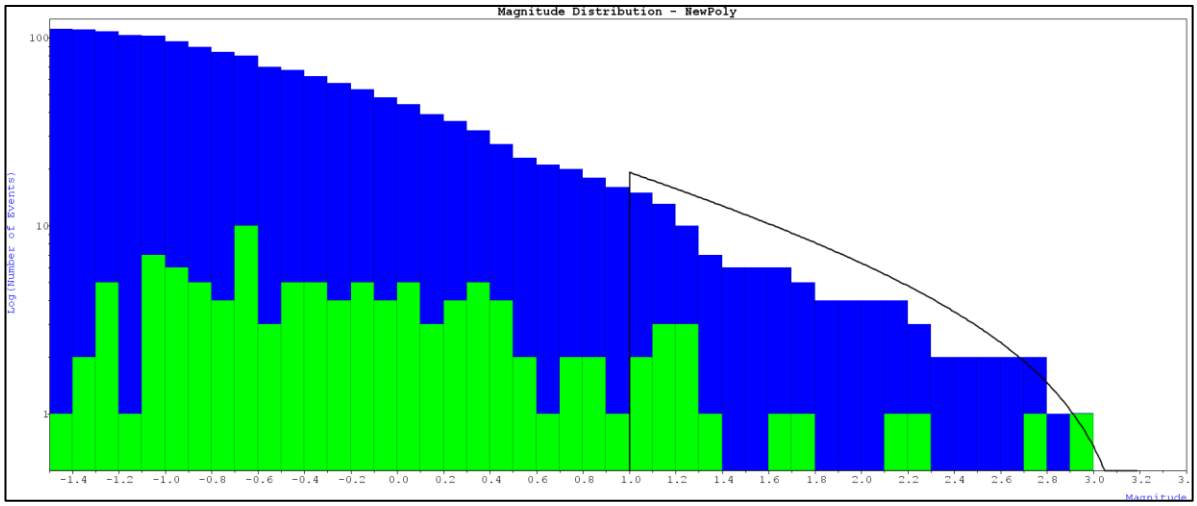


Figure 6.12 Magnitude distribution of seismicity in the VC22-30 area.

Summary of Data

KLF:NewPoly
01/07/1999 - 10/02/2016
Z: -5000 - 500
Area=125654m²
Mag ≥ -3.0 Min 4 Sites
Min.Mag= -1.5 Max.Mag= 2.9
N.Events=111
First 13/07/2000 22:36:19
Last 16/07/2015 13:48:09
E=1.3e+09 M=4.7e+13 V=9.2e+07

Mean Return Periods

Mag.	Number of Events /Month	/Year	Return Period months	years
1.0	0.10	1.2	10.374	0.86
1.5	0.06	0.7	17.402	1.45
2.0	0.03	0.4	31.544	2.63
2.5	0.01	0.2	68.264	5.69
3.0	0.00	0.0	297.441	24.79

Maximum Expected Magnitude

In 1 year M = 1.15
In 2 years M = 1.78
In 5 years M = 2.43

Seismic Events Distribution

Magn >	1.0	1.5	2.0	2.5	3.0
Theor.	19	11	6	3	0.7
Observed	15	6	4	2	0

Hazard Magnitude

Hazard Mag. = 2.22
SumEnergy = 1.30E+09 J SumEnergy/Year = 7.81E+07 J
SumMoment = 4.74E+13 Nm SumMoment/Year = 2.85E+12 Nm

Figure 6.13 Seismic statistics of the VC22-30 area.

Figure 6.14 and 6.15 illustrates the production and number of seismic events as well as M_{max}.

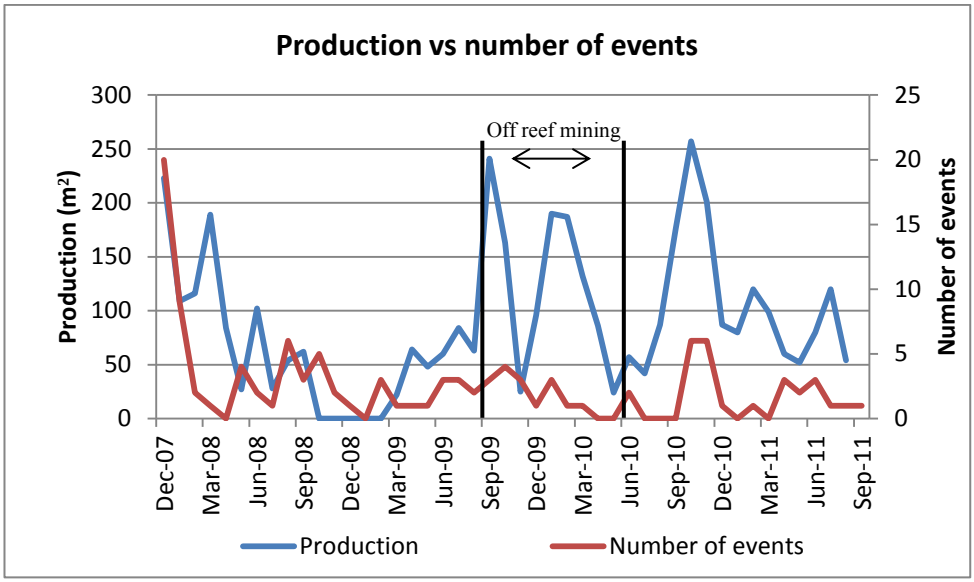


Figure 6.14 Comparative plot of the number of events and production for the VC22-30 area.

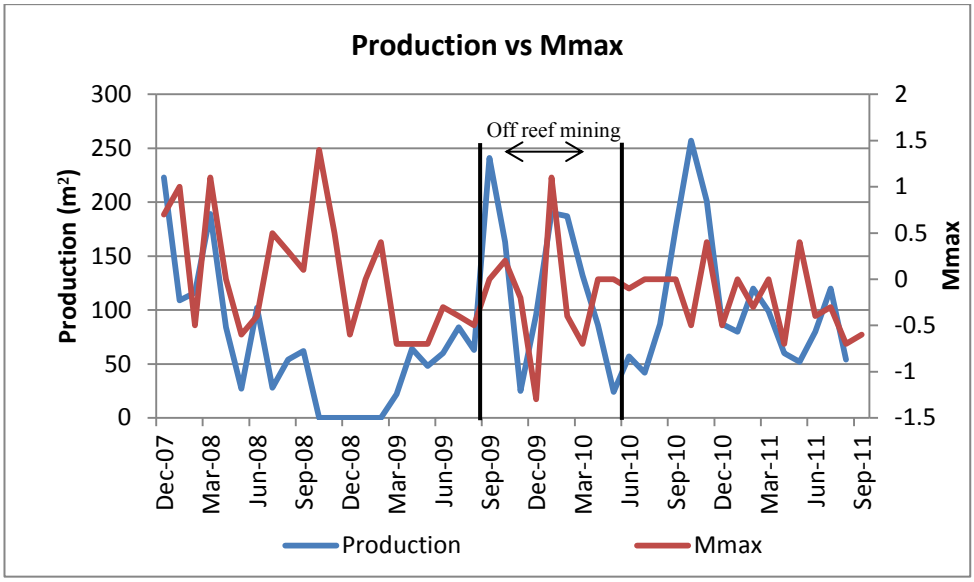


Figure 6.15 Plot of production and seismic magnitude data for VC22-30.

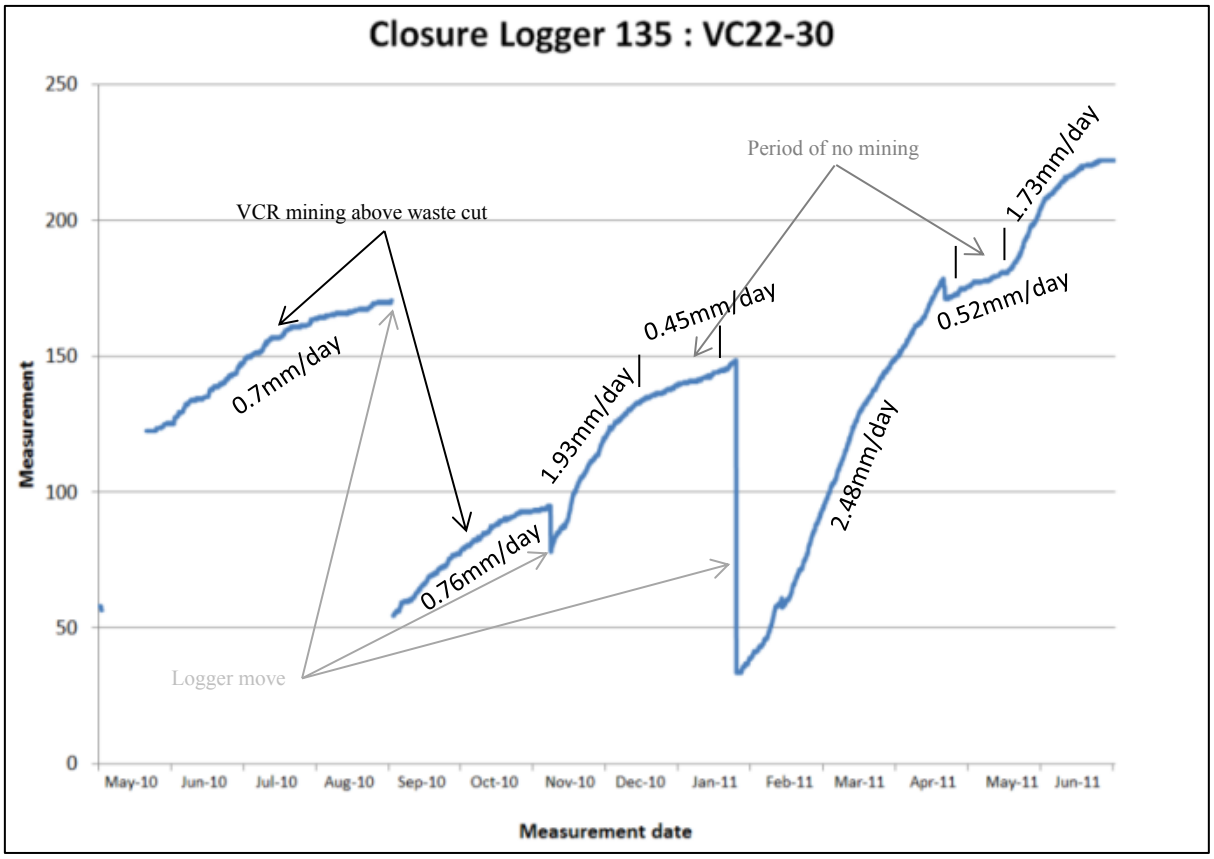


Figure 6.16 Closure measurements in the VC22-30 area.

Figure 6.16 is a closure measurement graph of the VC22-30 working area. The measurements were recorded electronically at a set interval. The station was re-installed 4 times during the mining operations for various reasons, such as accessibility. The logger was re-installed each time at the second line of packs behind the mining face. Mining in the area was conducted on the VCR horizon during the measurement period although no mining occurred towards the end of December nor during the end of April. The graph does show the change in closure rate (slope of the graph) when the mining was stopped. The graph also distinctly shows (slope of graph) the difference between stoping in de-stressed ground and in areas that were not de-stressed. Chapter 4 alluded to the influence of closure on the available energy that can be released or dissipated.

Figures 6.17 to 6.21 are visual records of the observed underground conditions. The underground conditions were fair, but some areas were highly fractured with up to 3 joint sets present in the strata. The off-reef excavations mined through the

strata layers in order to intersect the reef and were extremely fractured as the bedding planes were broken. It exposed multiple joint sets and other geological discontinuities (seen in Figure 6.17 and 6.18). The footwall consisted of shales, which swells in the presence of water, further aggravating the poor conditions (Figure 6.17). This creates a risk when the areas are left standing unattended for an excessive time period. This usually resulted in self-mining and eventual collapse of the excavation between the installed support units. Figure 6.18 also depicts the mining along and breaking through distinct bedding planes within the inclined development between the waste cut and reef. The photo was taken after the overstoping of the excavation and no additional damage or shearing was observed in the excavation. The effect of such bedding planes were shown in Chapter 4.



Figure 6.17 Travelling way developed in the shale below the VC22-30 area.



Figure 6.18 Inclined development to reef in the VC22-30 area.

Figure 6.19 depicts the ground conditions of the de-stressed area whereas Figure 6.20 depicts the ground conditions of the stoping in the “virgin” area. Stress fracturing and joint sets are clearly visible in both the excavations. Figure 6.19 depicts the fallouts that occurred due to a lack of confinement or resisting stresses within the host rock in the de-stressed area, as can be expected in shallow mining (described in Chapter 4).



Figure 6.19 On reef hangingwall conditions at the understoped VC22-30.



Figure 6.20 Hangingwall conditions of the ground that was not understoped in the VC22-30 area.

In Appendix B, the simulated ERR is presented for selected mining steps. The mining layout that was modelled is shown in Figures 6.21 and 6.22. In Figure 6.21, the solid green is previously mined areas, blue lines indicates the on-reef VCR mining and the dotted black lines the off-reef understoping. The parameters used in the model was similar to that used for the modelling in

Chapter 5. A offset in the plotted ERR values and the modelled face positions are also observed in the presented results similar to the description of Chapter 5.

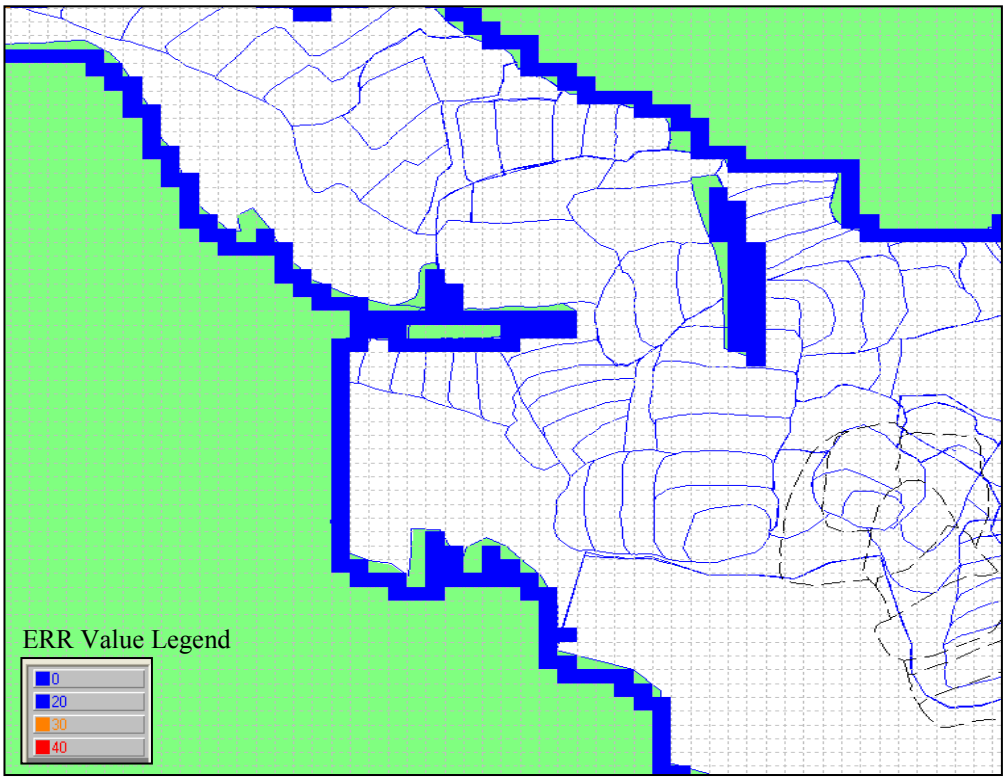


Figure 6.21 Outline of the modelled layout of the VC22-30 area.

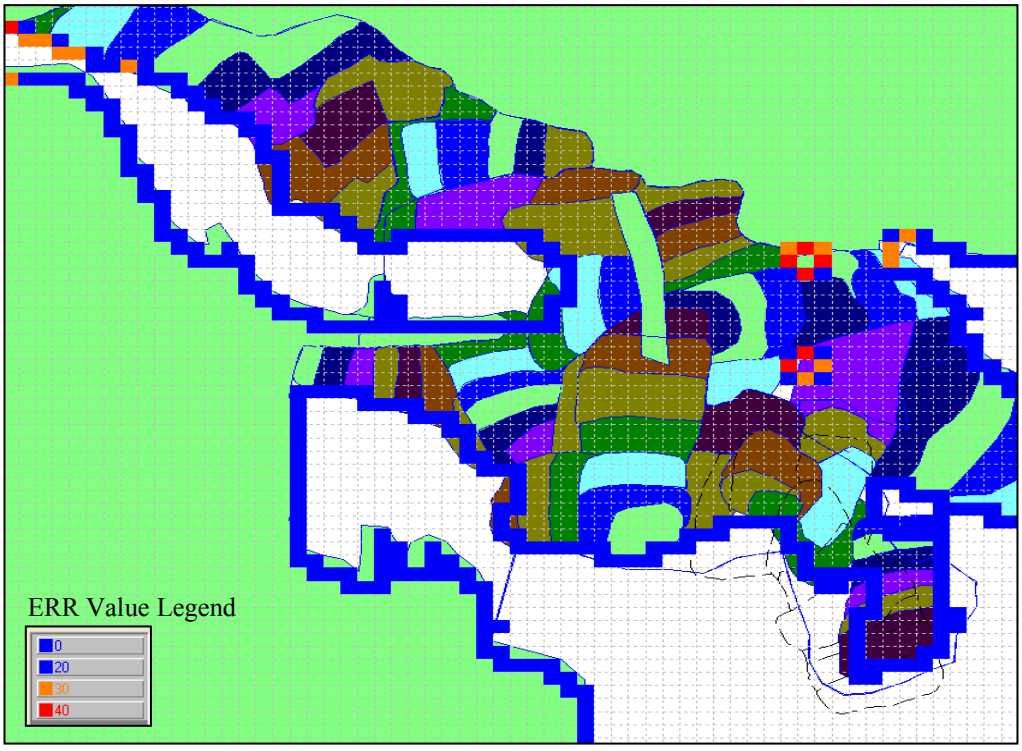


Figure 6.22 Sequenced layout for the modelling of VC22-30 area.

Figure 6.23 depicts some of the ERR values obtained from the numerical model. The particular step shown is during the period when VCR mining is conducted through the abutment of the de-stressed area. The middling of the area is less than 6 m. The ERR values are favorable in this area, although some areas have high peak values where unmined blocks of ground were left or if poor face shapes or layouts are present. The low ERR values, outside of the understoped area, can be attributed to the large amount of solid present in the area.

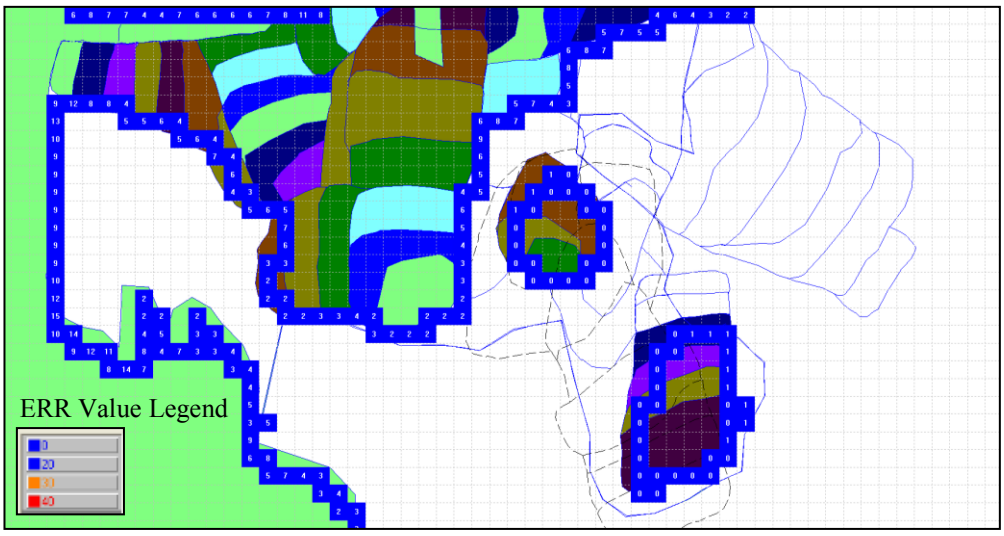


Figure 6.23 ERR results indicating the effect of the de-stressing at VC22-30.

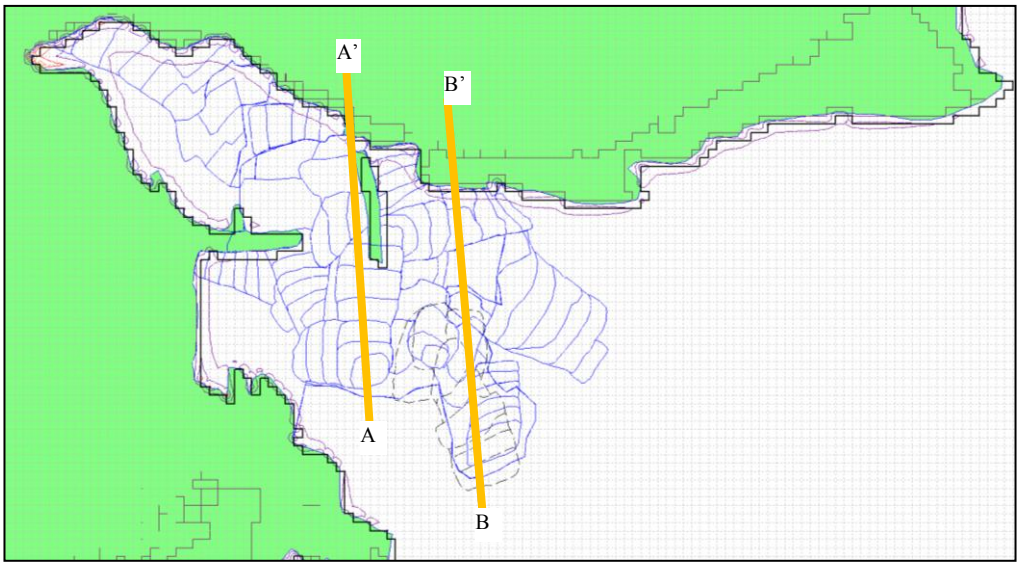


Figure 6.24 Location of on reef sections for a modelled layout.

Figure 6.24 indicates a stress contour plot of the major principal stress. The locations of two line plots of the stress is also indicated. Figures 6.25 and 6.26 depicts the two line plots. The stress indicated is well above the strength of the weak lava hangingwall and hence fracturing as indicated in Figures 6.19 and 6.20 is expected. The influence of the waste de stressing cut can be seen at a distance of 44 m in Figure 6.25.

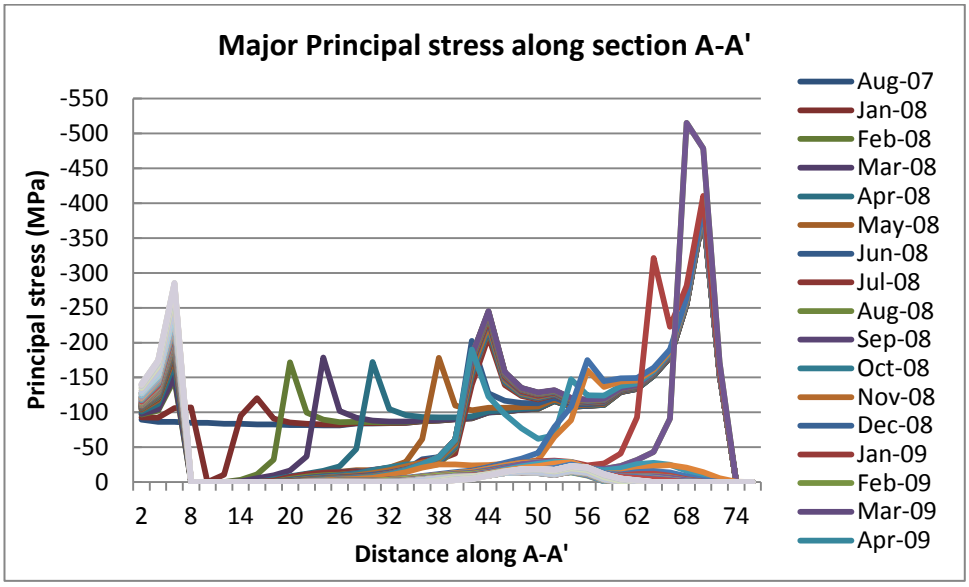


Figure 6.25 Plot of stress along section A-A'.

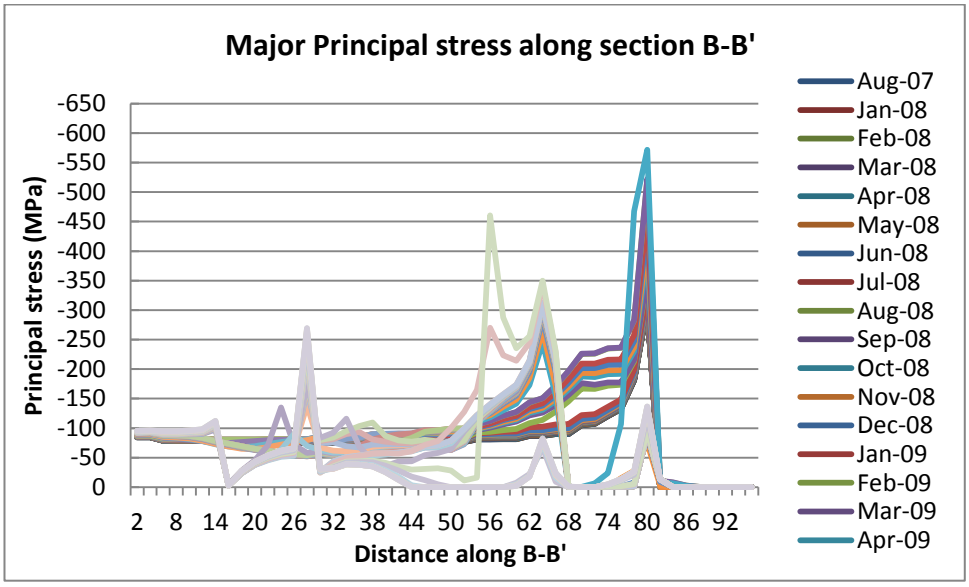


Figure 6.26 Plot of the stress along section B- B'.

Figure 6.27 depicts the conditions of the 20 m throw fault plane, as shown in Figure 6.1, on the up-dip siding of the stoping panel. Mining was conducted to the fault plane, stripping along the fault, the fault plane showed distinct movement as the mining progressed. The plane itself did not release any energy in a violent manner during the time that mining was conducted.



Figure 6.27 Slickensided movement along the 20 m fault.

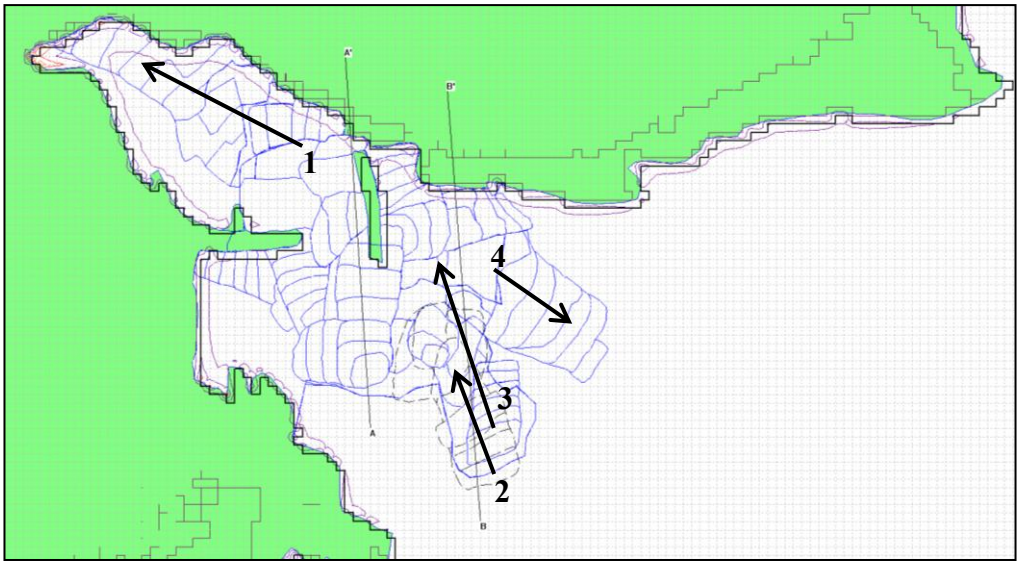


Figure 6.28 Mining sequence of VC22-30.

Figure 6.29 depicts the average face ERR values plotted against the cumulative production of the area. It is clear that there are 4 distinct mining periods. The annotations on Figure 6.28 depicts the mining location and direction of mining for these periods. The first period was towards the limit when mining occurred up to the final remnant to the South, hence the drastic increase in ERR. The second period is during the understoping (de-stressing) when the ERR values are lower than what was experienced on the reef elevation. The third period was during the overstoping of the understoped (de-stressed) area hence the zero values. Elevated values are also observable as the abutments were reached. Finally the fourth period was the mining towards the large solid, away from all the irregular layouts.

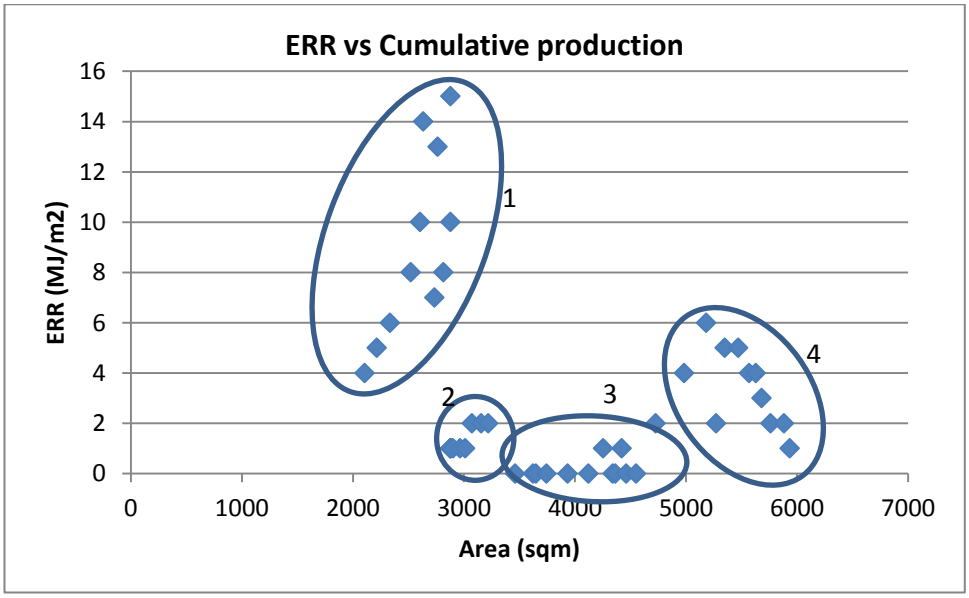


Figure 6.29 ERR and cumulative production comparison for VC22-30.

Figure 6.30 depicts the location where sections were drawn to determine the effect of de-stressing between the two mining horizons. Figure 6.31 to 6.35 depicts the results of the numerical modelling in terms of the major principal stress.

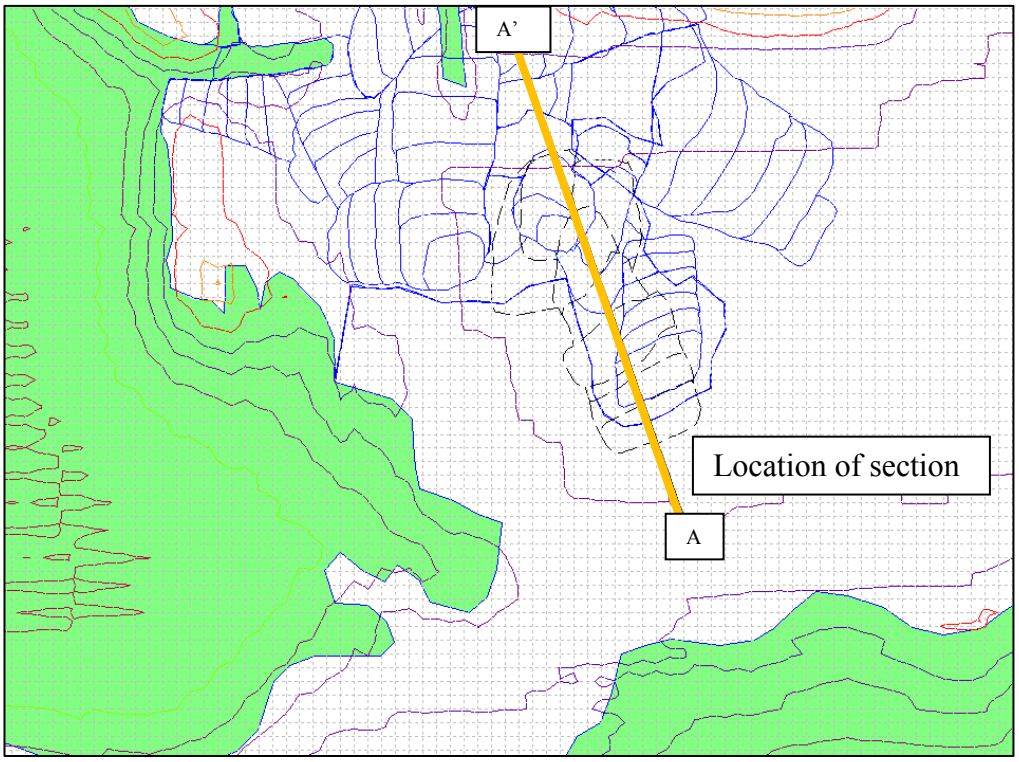


Figure 6.30 Position of an apparent dip section of the VC22-30 area.

Figure 6.31 shows a region of very high major principal stress on the edges of the stoped-out area. This concentration is confined to very localized areas. Figures 6.31 to 6.35 indicates the presence of stress concentrations on the abutments. The interaction between the two mining horizons is also visible. This interaction of the concentrations on the abutments will induce failure as well as shear as mentioned in Chapter 4. However one should take into consideration the other forms of energy dissipation as mentioned in Chapter 4.

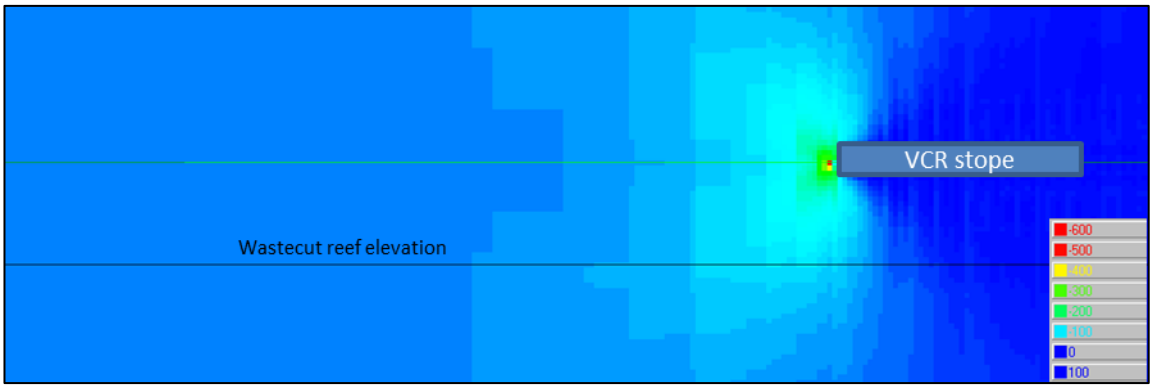


Figure 6.31 Contour plot of the principal stress prior to any mining on the de-stressing cut.

Figures 6.32 and 6.33 illustrates the introduction of the de-stressing cut. From the figures it is clear that the additional stope has a significant disruptive effect on the stresses and the interaction between the edges of the two stopes.

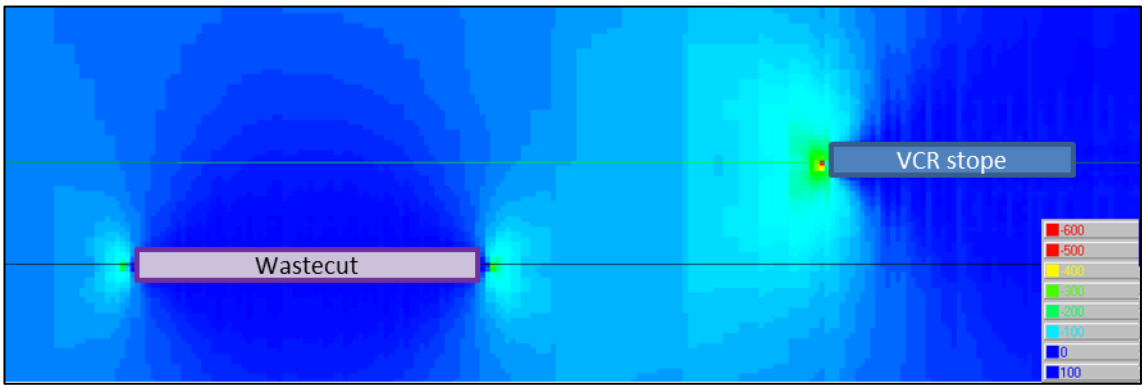


Figure 6.32 Contour plot of the principal stress during the understoping.

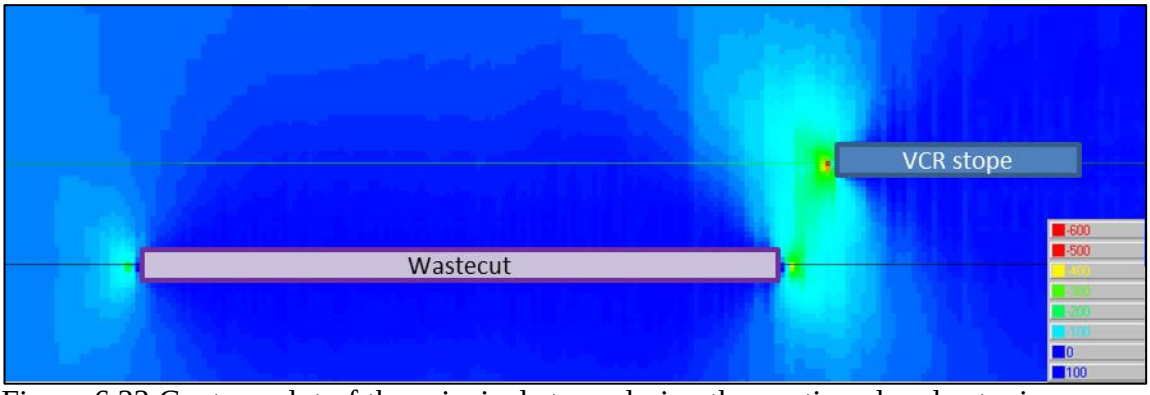


Figure 6.33 Contour plot of the principal stress during the continued understoping on the de-stressing cut.

Figure 6.34 indicates the partial de-stressing of both reef elevations as the VCR is mined in the under stoped area. Note the zone of high stress between the reef horizons.

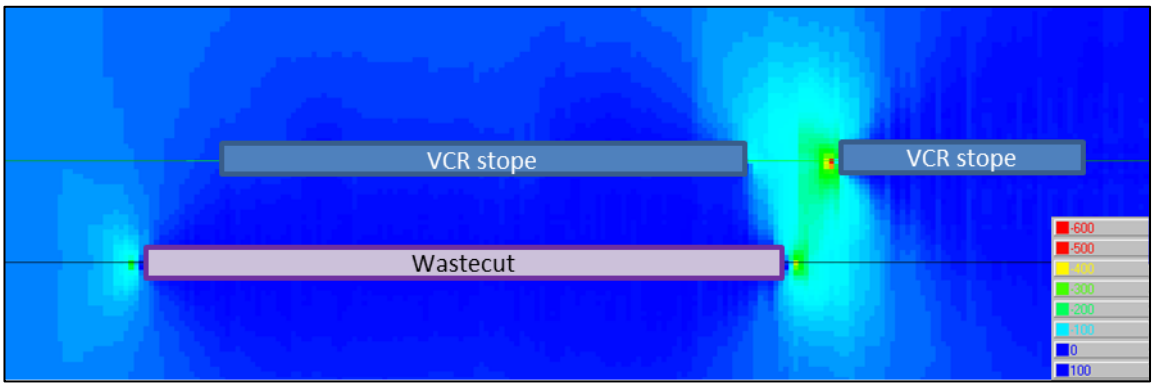


Figure 6.34 Contour plot of the principal stress during the mining of the VCR in the understoped area.

Figure 6.35 indicates the final de-stressing of both reef elevations as the VCR is completely mined out. The VCR breached the waste cut abutment and continued to hole into the down dip abutment of the old VCR stope without any significant problems. This concurs with the hypothesis of the weak layers assisting to stably dissipate the available energy.

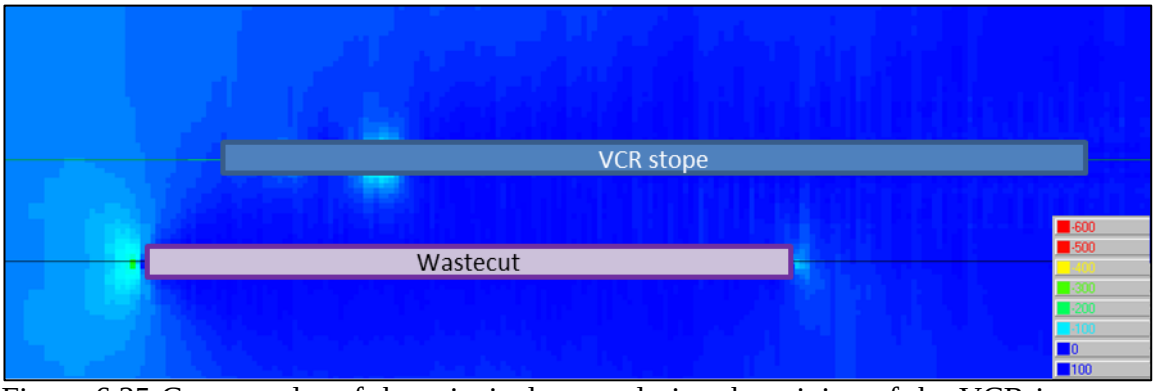


Figure 6.35 Contour plot of the principal stress during the mining of the VCR in the understoped area.

SUMMARY

In summary the analysis in this chapter indicated that VCR mining with a de-stressing waste cut in close proximity to reef resulted in a successful extraction. The lithology of the area included a weak shale in the footwall of the Libanon reef and a weak hangingwall lava above the VCR. Although no mining was conducted on the Libanon reef and the waste cut was only developed to provide access to the block of ground, the effects of the lithology and bedding planes may be contributing factors to the successful mining as it allowed for stable dissipation of some of the available energy. The high closure rates observed as well as the relatively small amount of energy that was released violently while mining in this area seem to support the hypothesis and predictions of an “extended” ERR in Chapter 4.

CHAPTER 7

CASE STUDY AND BACK ANALYSIS OF REMNANT C :VC20-31

The VC20-31 block of ground is located in close vicinity to Remnant B and to the North-East of the shaft. A 50 m throw fault is present in close vicinity to the block of ground. A number of offshoots with throws ranging from 10 m to 2 m are also present in the area. The parent fault is classified as high risk and has a M_{max} of 3.5. To the west of the block and on the other side of the fault a significant block of ground (19500 m^2) is also present. Below the block the mined span is in excess of 1000 m, while the only unmined ground is around the geological structures or losses caused by the geological structures.

During the initial planning it was noted that the 19 level hangingwall drive traverses the reef intersection in the target block. It can also be seen that a large portion of the drive is very shallow in the hangingwall and the layout of the drive is not ideal to ensure the stability of this excavation. The locality of the block of ground is shown in Figure 7.1 below.

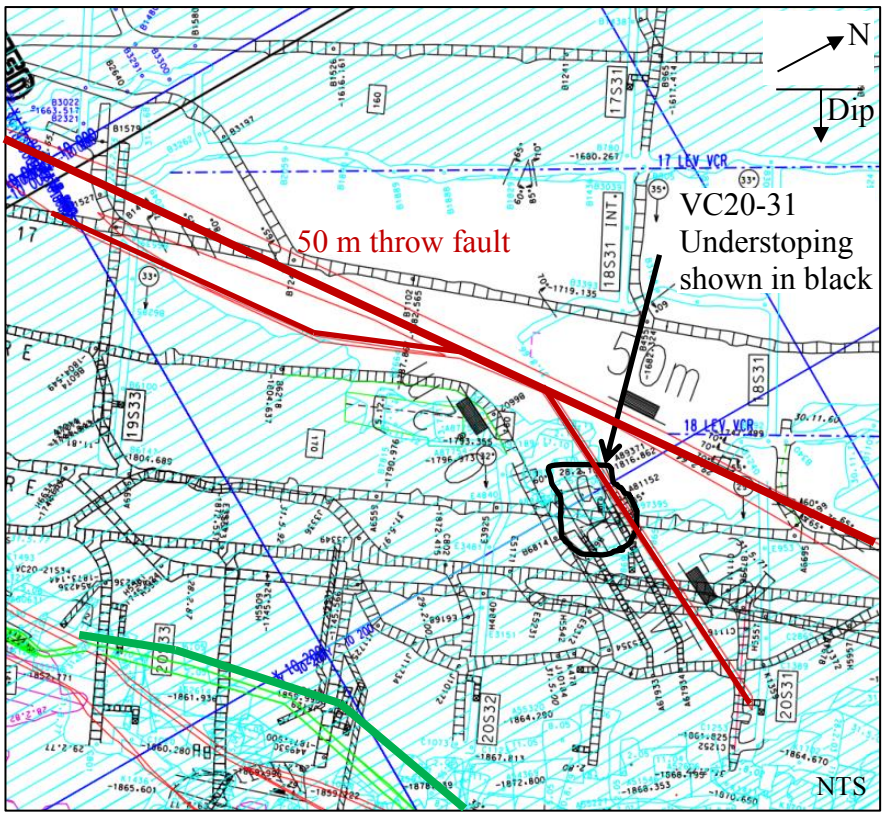


Figure 7.1 Locality plan view of the VC20-31 area.

The immediate hangingwall of the VCR is a weak lava and the footwall consists of quartzite down to the Libanon Reef elevation. Below the Libanon Reef the footwall consists of shale. No mining has been done on the Libanon Reef in this area, as a waste cut was developed from the bottom level to below the VCR reef in order to access the block of ground. The VCR target area was an isolated block of ground with mining on two boundaries and had an initial size of 3700 m^2. Figure 7.2 depicts the stope plan of the VC20-31.

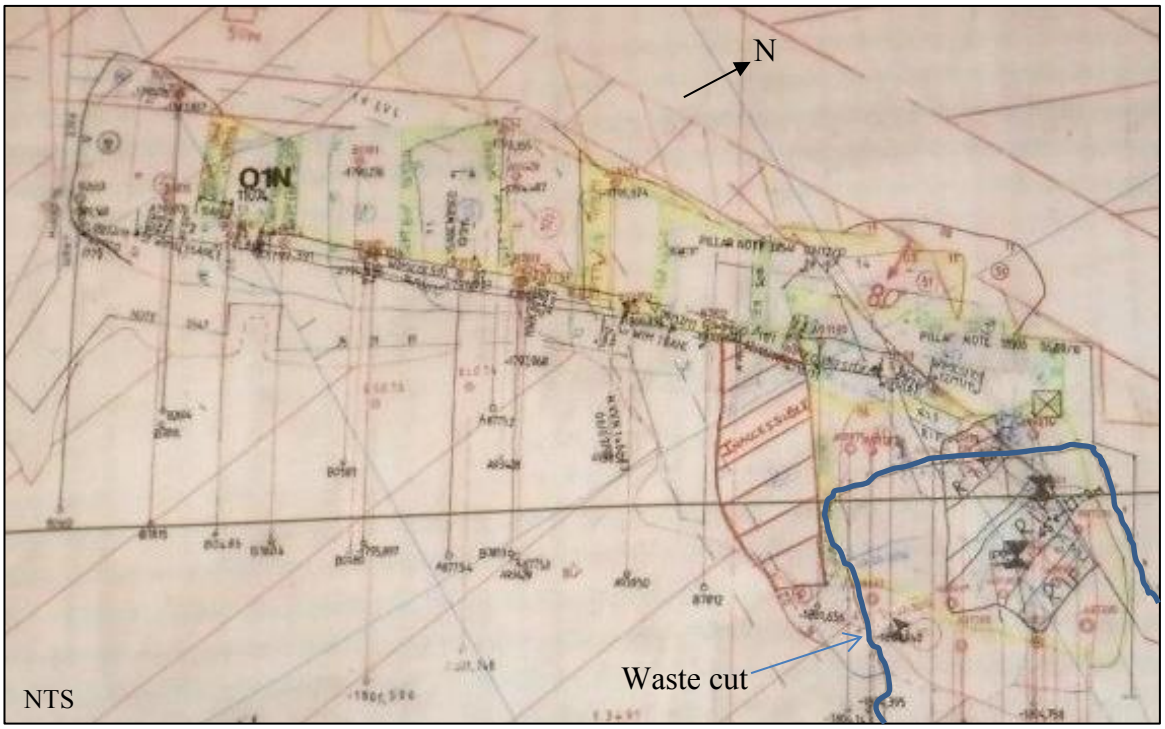


Figure 7.2 Plan view of the VC20-31 stope. The outline of a portion of the waste cut is indicated by the blue line.

Access development is situated deep in the footwall of the VCR and large portions had been extensively overstoped. The block was accessed by means of a waste cut that was mined from the footwall development situated almost 70 m below the block. This resulted in a extensive waste cut and travelling ways in the shale footwall. Figure 7.3 depicts a simplified section. From this position the understoped area was extracted first.

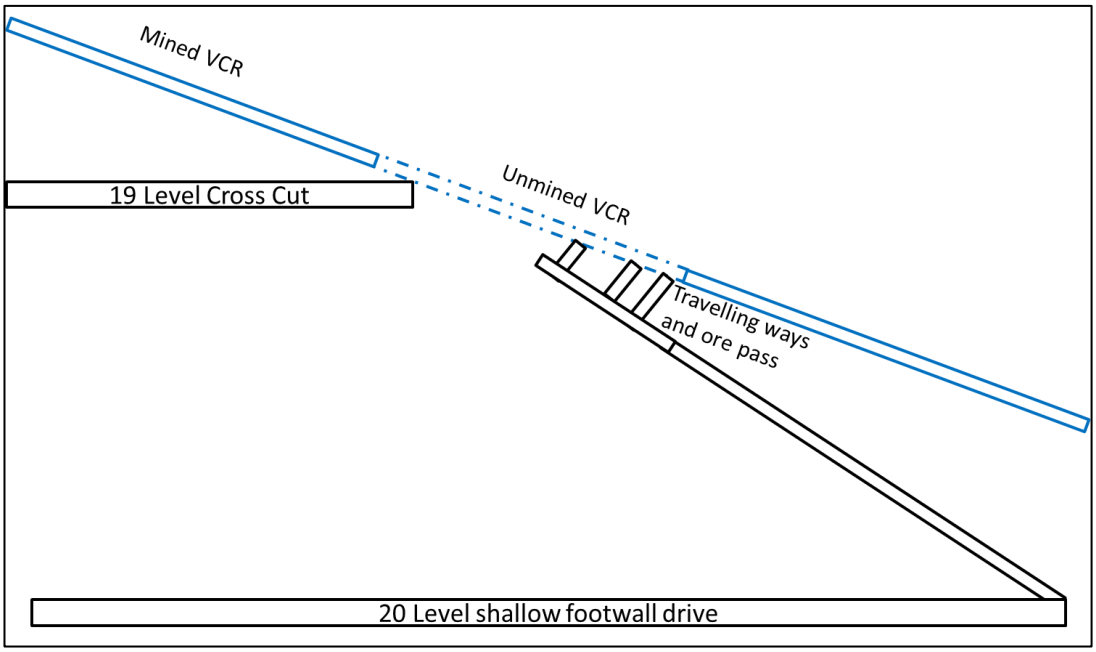


Figure 7.3: Simplified section through the VC20-31 depicting the waste cut access way.

The mining layout and sequence of the stoping operations on both reef and off-reef elevations was fairly well controlled, although it is evident that some difficulty was experienced to control the face shapes. There were no stabilising pillars or designed crush pillars left on either of the reef horizons during the extraction.

Figure 7.4 depicts a seismic plot of all events greater than a zero magnitude for the last 17 years within a 300 m radius of the stope. The event plots in this figure are coloured based on the date of occurrence, while the size of the plot is an indication of the magnitude. It appears that a few large seismic events occurred on the major geological structures in the vicinity of this block of ground, even when very little or no mining occurred. The largest observed seismic event was a M_L= 2.2, while the expected M_{max} is M_L 2.5.

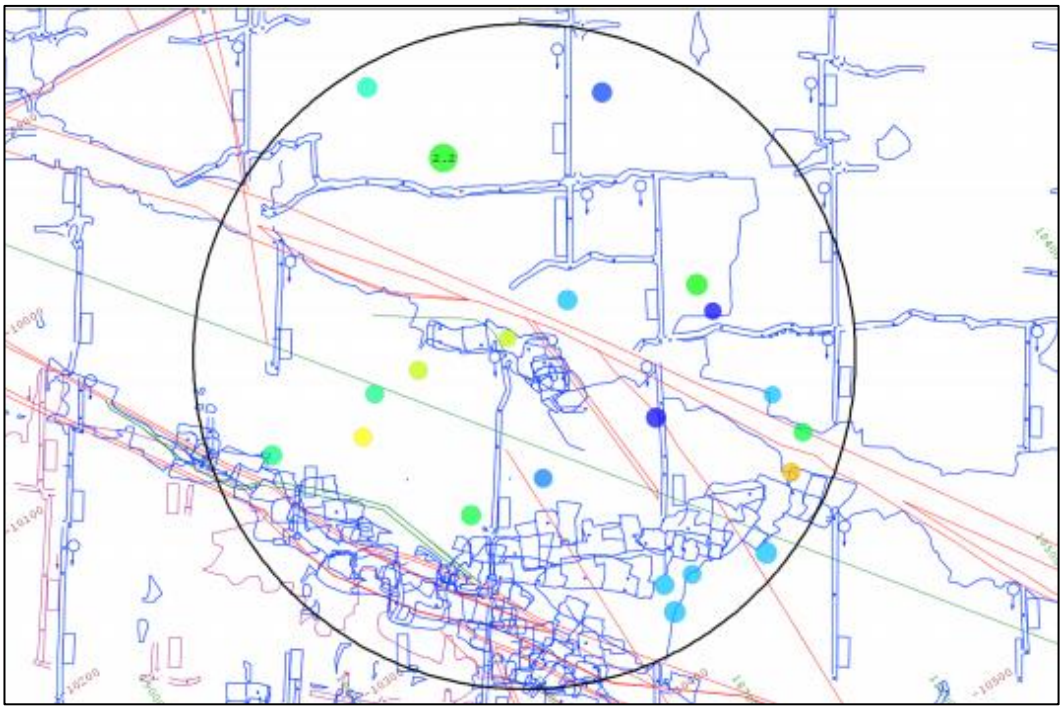


Figure 7.4 Plot of all events greater than M_L0.0 in a 300 m radius around VC20-31.

The activity rate shown in Figure 7.5 indicates that the seismic activity appears random and there was no pattern or influence of the mining on the M_L> 0.0 events.

Figure 7.6 shows the hourly distribution for the recorded events. This also has no clear trend. The shaft did not have a centralized blasting system until 2010 and operated without night shift in the VCR section.

In Figures 7.5 and 7.6, the magnitude ranges are represented by colours. Blue indicates events -1.0 to 0.0, green 0.0 to 1.0, orange 1.0 to 2.0 and red indicates events greater than M 2.0.

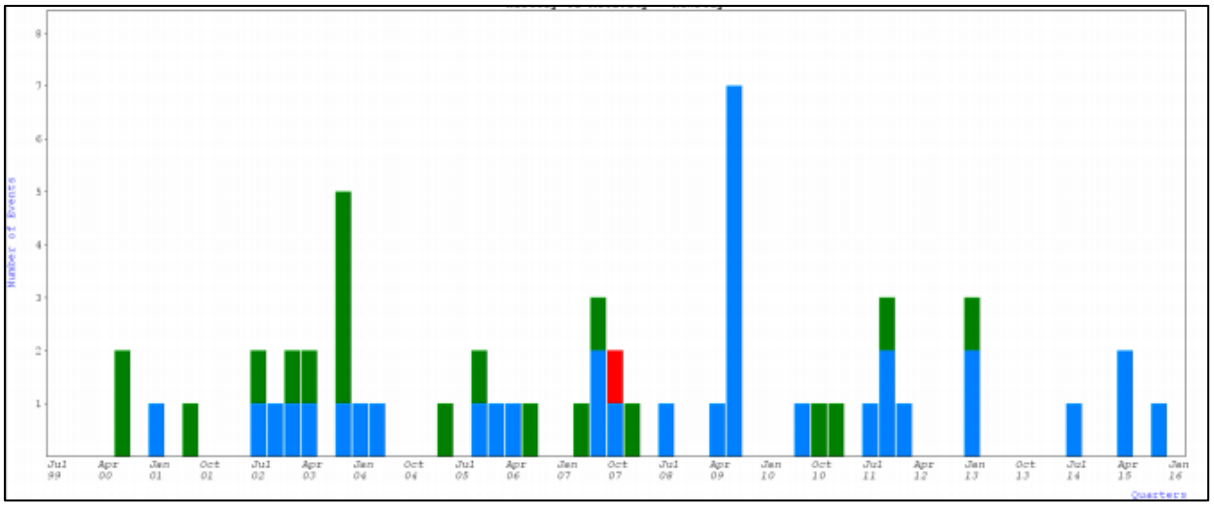


Figure 7.5 Activity rate of the VC20-31.

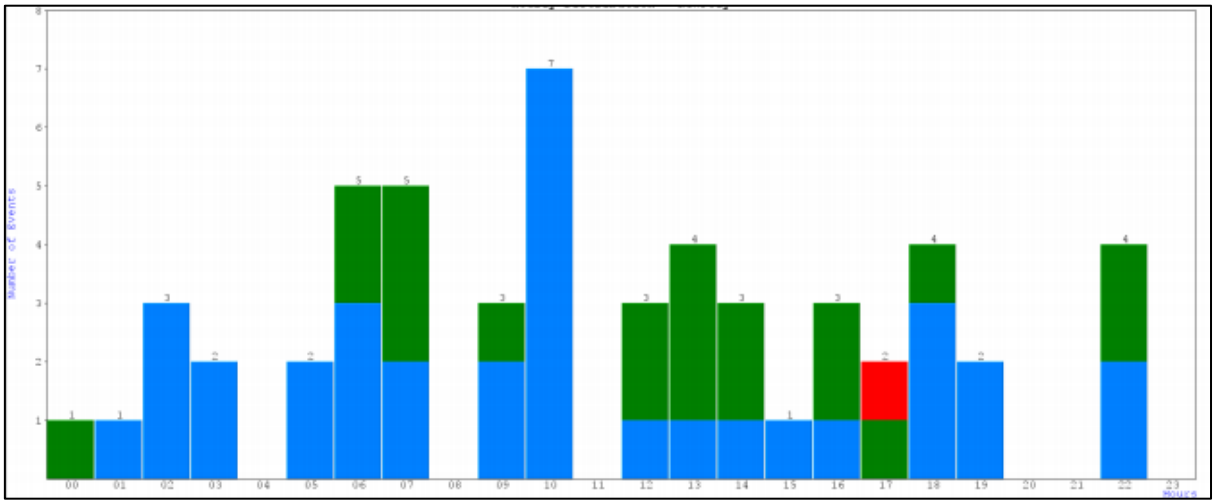


Figure 7.6 Hourly distribution of events at the VC20-31.

Figure 7.7 shows the energy released in MJ per annum for this area. Taking into consideration the time periods of mining, the peaks observed appears to be linked to the simultaneous extraction of multiple blocks of ground in the area.

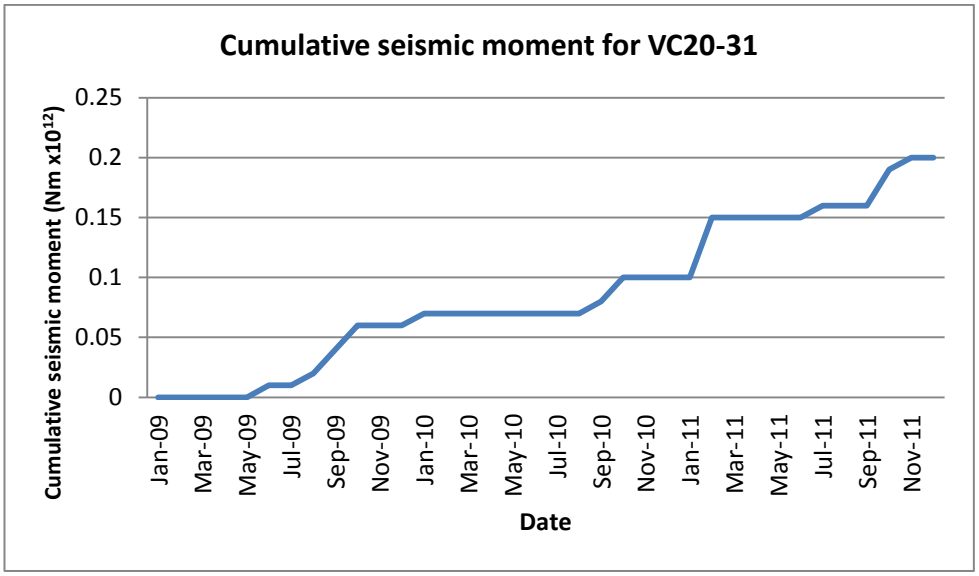


Figure 7.7 Cumulative seismic moment of the VC20-31 area for 2 years.

Year	Number of Events						Max. Mag.	Energy MJ	Moment 10^{12} Nm
	M<0	0≤M<1	1≤M<2	2≤M<3	3≤M	Total			
1999	0	0	0	0	0	0	-	0.00	0.00
2000	0	7	1	1	0	9	2.7	258.08	17.23
2001	0	1	0	0	0	1	0.0	0.02	0.02
2002	1	2	1	0	0	4	1.7	9.16	1.01
2003	9	5	0	1	0	15	2.9	926.61	18.44
2004	0	3	2	0	0	5	1.3	2.40	0.89
2005	4	1	3	1	0	9	2.1	24.31	5.22
2006	5	0	0	0	0	5	-0.7	0.00	0.01
2007	14	0	0	1	0	15	2.2	72.44	3.16
2008	6	2	1	0	0	9	1.1	0.65	0.37
2009	9	1	0	0	0	10	0.2	0.09	0.05
2010	9	1	1	0	0	11	1.1	1.04	0.30
2011	3	2	0	0	0	5	0.4	0.16	0.07
2012	0	2	1	0	0	3	1.0	0.63	0.26
2013	4	1	1	0	0	6	1.2	1.38	0.29
2014	0	1	0	0	0	1	0.7	0.35	0.06
2015	3	0	0	0	0	3	-0.1	0.01	0.02
2016	0	0	0	0	0	0	-	0.00	0.00
Total	67	29	11	4	0	**111**	**2.9**	**1297.35**	**47.39**

Figure 7.8 Summary of the seismic events in the VC20-31 area.

Figure 7.9 illustrates the cumulative production and the cumulative seismic moment and Figure 7.10 plots the number of events versus the production. Figure 7.9 can be described as the seismic response to production.

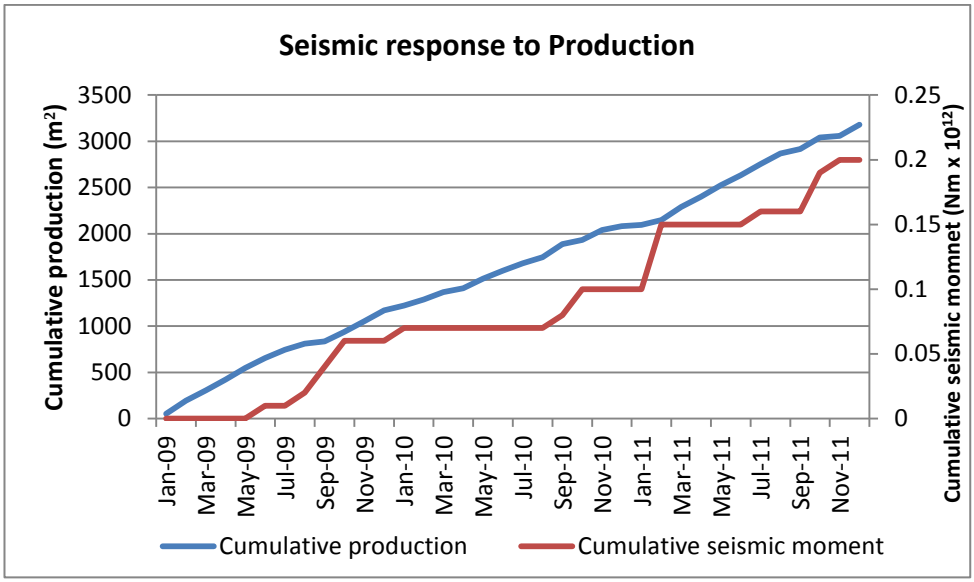


Figure 7.9 Seismic response to production of the VC20-31 area.

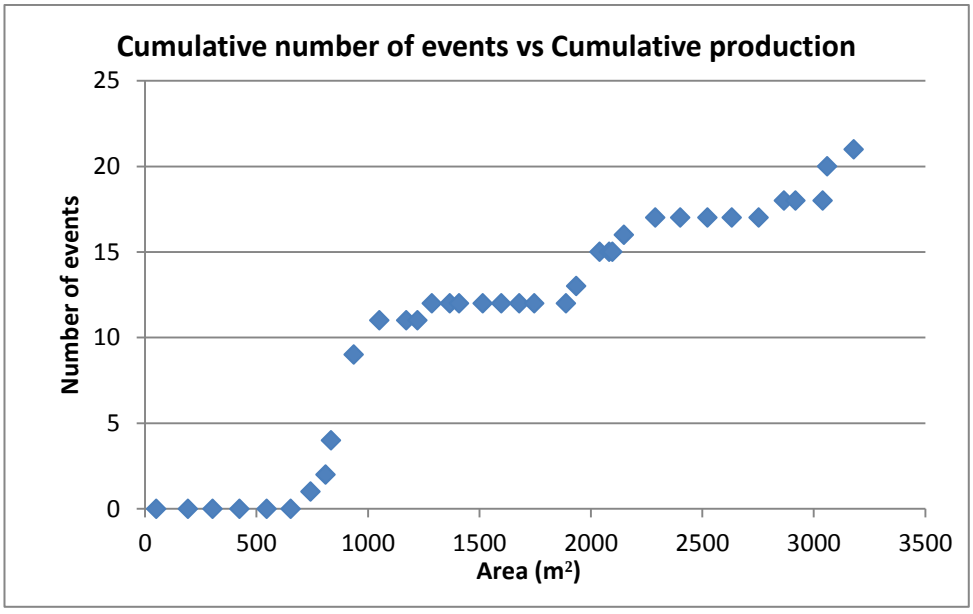


Figure 7.10 Cumulative number of seismic events compared to cumulative production of VC20-31.

The magnitude distribution of all events since 1999 is depicted in Figure 7.11. The incomplete nature of the data may be a result of the network characteristics. The green distribution indicates the given magnitude distribution while the cumulative distribution is indicated by the blue. The cumulative distribution add-up from the largest magnitude towards the vertical axis.

The recurrence period of the historic events was used to calculate the probability of various event magnitudes as summarised in Figure 7.12.

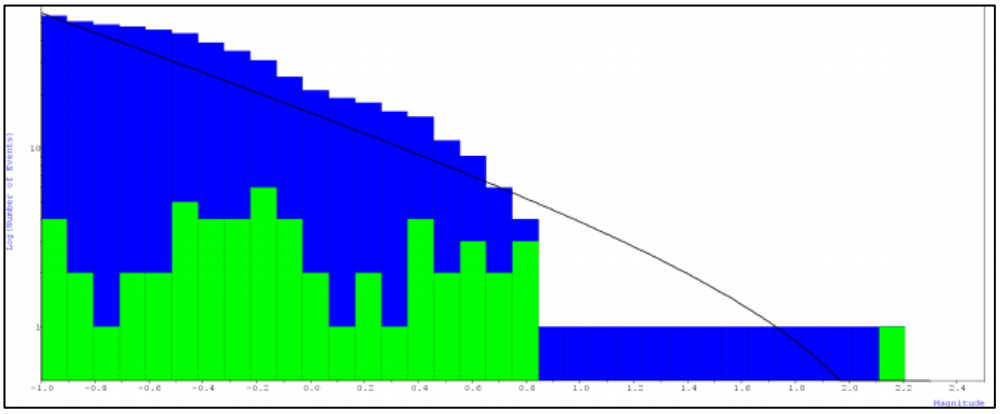


Figure 7.11 Magnitude distribution of seismicity in the VC20-31 area.

Probabilities of Seismic Event

Mag.	1 month	3 months	6 months	1 year	2 years	5 years
-1.0	24.9%	57.7%	82.1%	96.8%	99.9%	100.0%
-0.5	14.3%	37.0%	60.4%	84.3%	97.5%	100.0%
0.0	7.9%	21.8%	38.9%	62.6%	86.0%	99.3%
0.5	4.2%	12.0%	22.6%	40.0%	64.0%	92.2%
1.0	2.1%	6.1%	11.9%	22.4%	39.7%	71.8%
1.5	0.9%	2.8%	5.5%	10.6%	20.1%	43.0%
2.0	0.3%	0.9%	1.8%	3.5%	6.9%	16.3%

Figure 7.12 Seismic statistics of the VC20-31 area.

Figures 7.13 and 7.14 shows the production and number of seismic events as well as M_{max}. Figure 7.15 illustrates the seismic moment to the production.

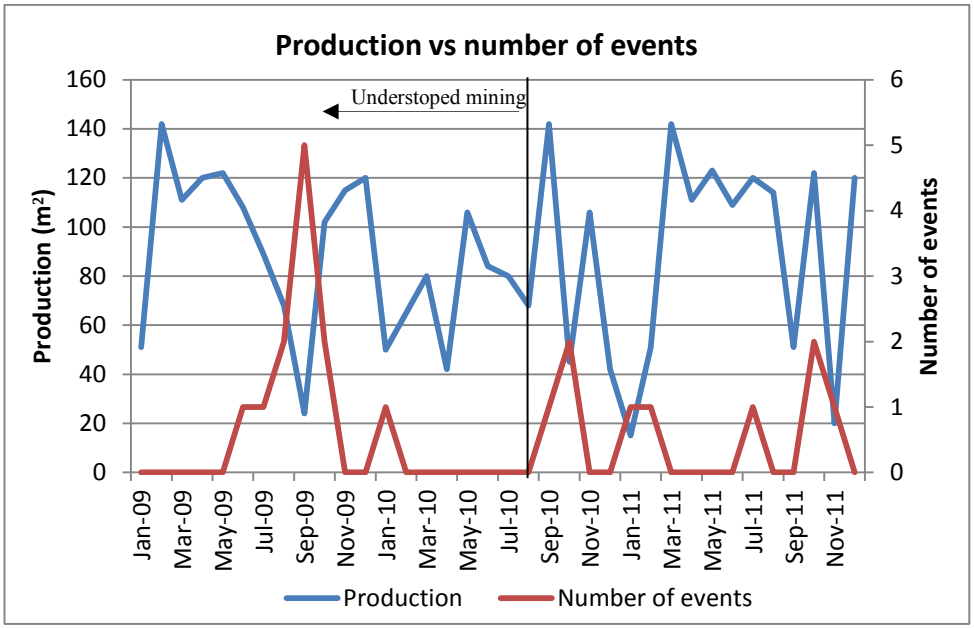


Figure 7.13 Production and the number of events of the VC20-31 area.

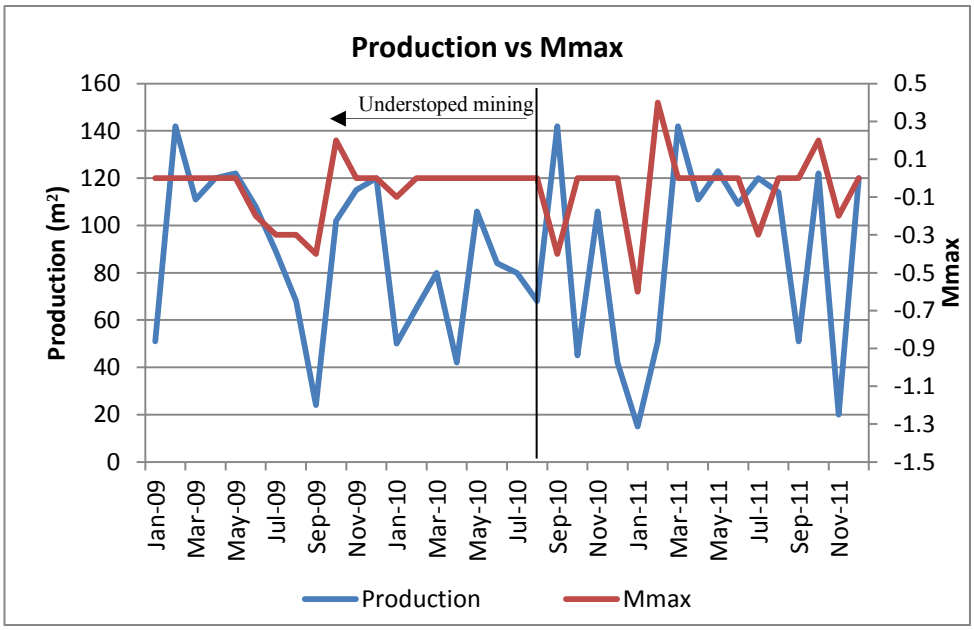


Figure 7.14 Production and the Mmax in the VC20-31 area.

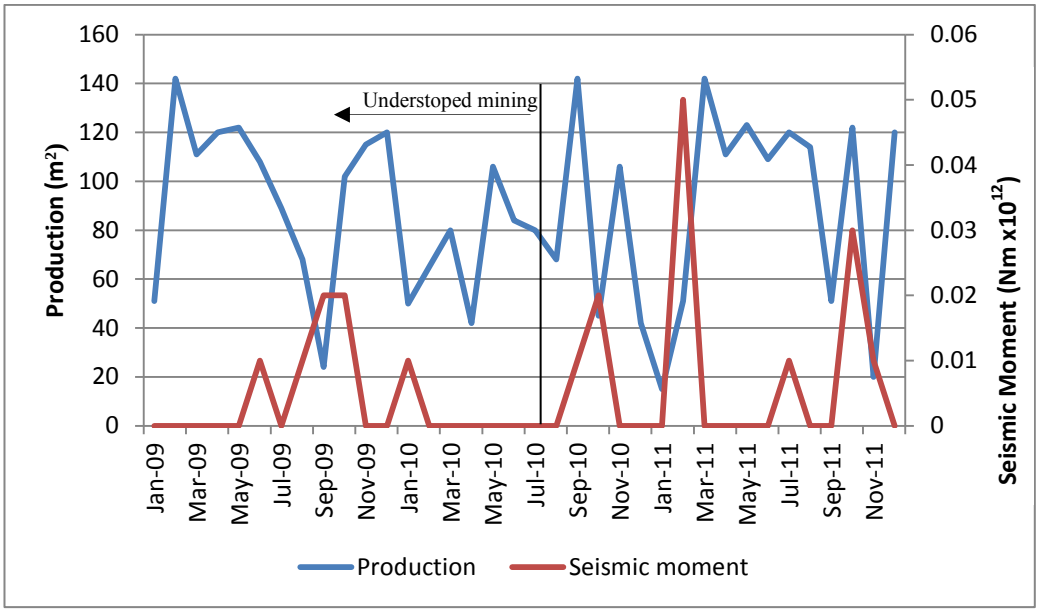


Figure 7.15 Number of events and production comparison for VC20-31.

From the seismic analysis can be seen that very few events larger than ML > 0.8 occurred. Analysis of the smaller events does not seem to show any meaningful trends.

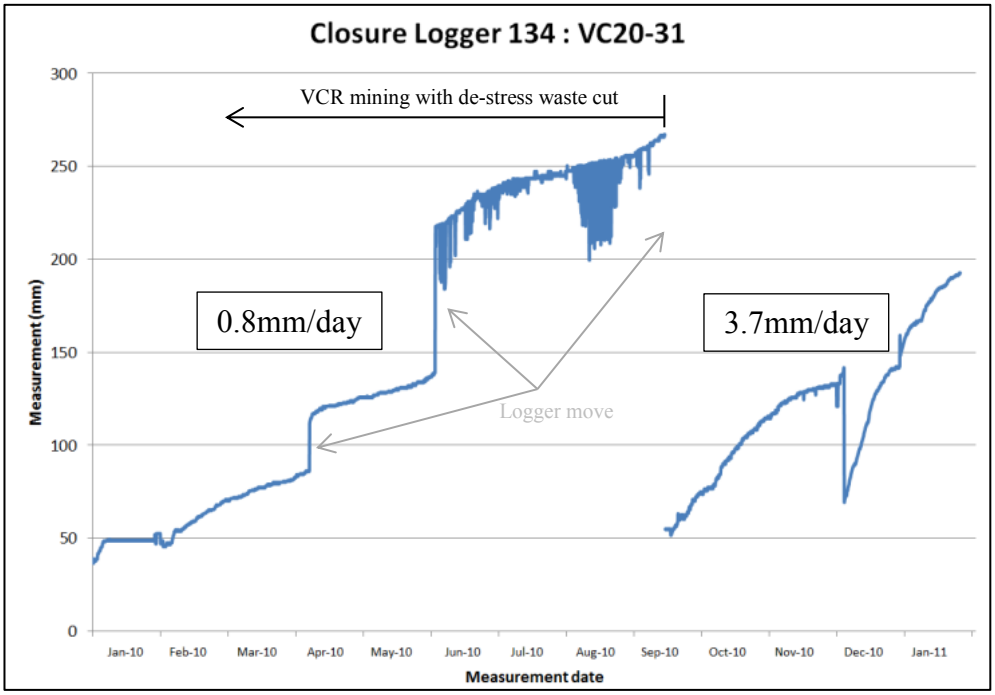


Figure 7.16 Closure measurements in the VC20-31 area.

Figure 7.16 is a closure measurement graph of the VC20-31 working place. Mining in the area occurred on the VCR horizon during the measurements. The measurements were taken electronically and recorded at a set interval. The station was re-installed a number of times during the mining operations due to various reasons such as accessibility. The graph also distinctly shows the difference between stoping in de-stressed ground and in normal conditions when comparing the indicated closure rates (the abutment of the de-stressed area was breached during September 2010).

Figures 7.17 to Figure 7.22 are visual records of the observed underground conditions. The underground conditions were fair but some areas were highly fractured with up to 3 joint sets present in the strata. The off-reef excavations were mined in the footwall shales through the strata layers in order to intersect the reef. These excavations were extremely fractured as the bedding planes were broken. It exposed multiple joint sets and other geological discontinuities as seen in Figures 7.17, 7.18 and 7.19. These 3 figures also depict the conditions within the inclined development between the waste cut and reef. The damage that is present in the inclined travelling way (Figure 7.19) is related to the absence of confining stresses as fallouts were bound by joint sets and bedding planes. No additional damage or shearing was observed in the excavation. Figure 7.20 depicts a fall of ground in another portion of the inclined development caused by the deterioration of installed support, and dilation and deterioration of the host rock (shale).



Figure 7.17 Ground conditions in an inclined travelling way into the VC20-31 area.



Figure 7.18 Ground conditions of an inclined travelling way to reef at VC20-31.

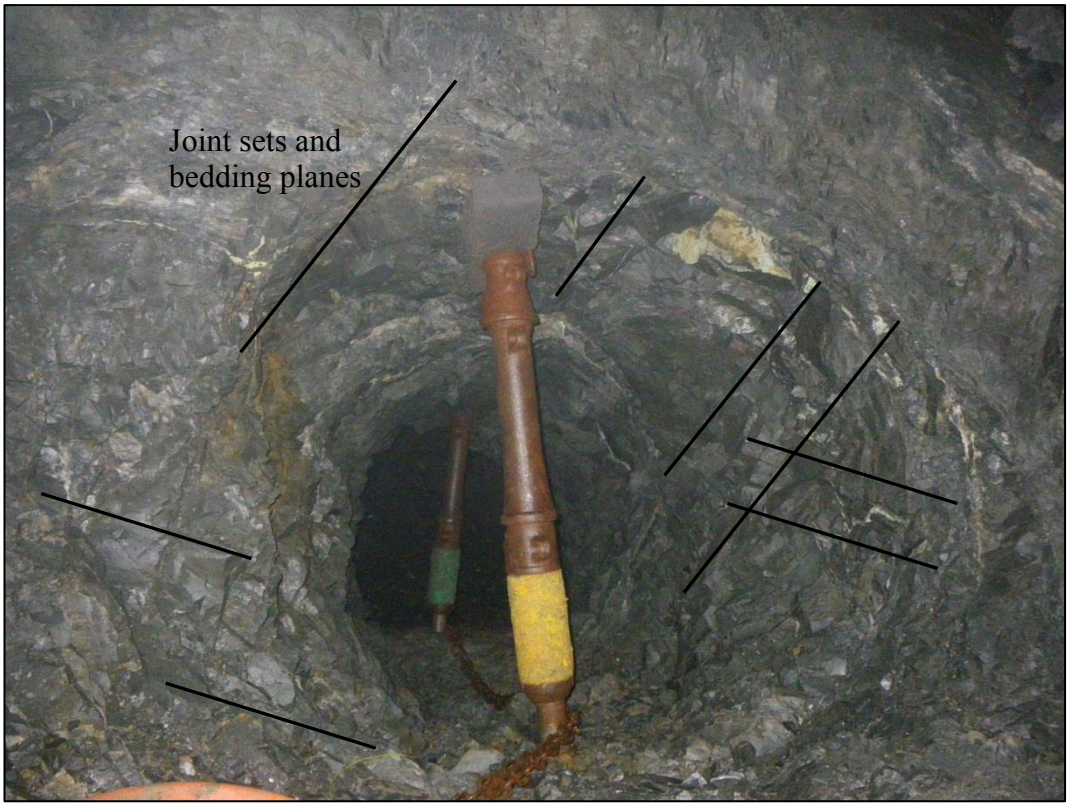


Figure 7.19 Inclined development to reef in the VC20-31 area.



Figure 7.20 Fall of ground in the inclined travelling way below the VC20-31 area.

Figure 7.21 depicts the ground conditions of the area not de-stressed whereas Figure 7.22 and 7.23 depicts the ground conditions of the stoping face in the de-stressed areas. Stress fracturing and joint sets are visible in the stoping excavations. A difference is however seen between the de-stressed and the areas

not de-stressed. This difference can be attributed to the lack of confinement in the host rock in the de-stressed area, similar to the expected for shallow mining conditions.



Figure 7.21 Hangingwall conditions of the ground not de-stressed in the VC20-31 area.



Figure 7.22 Ground conditions of the hangingwall and face of the de-stressed ground in the VC20-31 area.



Figure 7.23 On reef hangingwall conditions in the de-stressed area of VC20-31.

In Appendix C, simulated ERR values are presented for selected mining steps. The mining layout that was modelled is shown in Figures 7.24 and 7.25. In Figure 7.24 the solid green is the previously mined areas, blue lines indicates the on-reef VCR mining and the dotted black lines the off-reef understoping. The parameters used in the model is similar to that of Chapters 5 and 6.

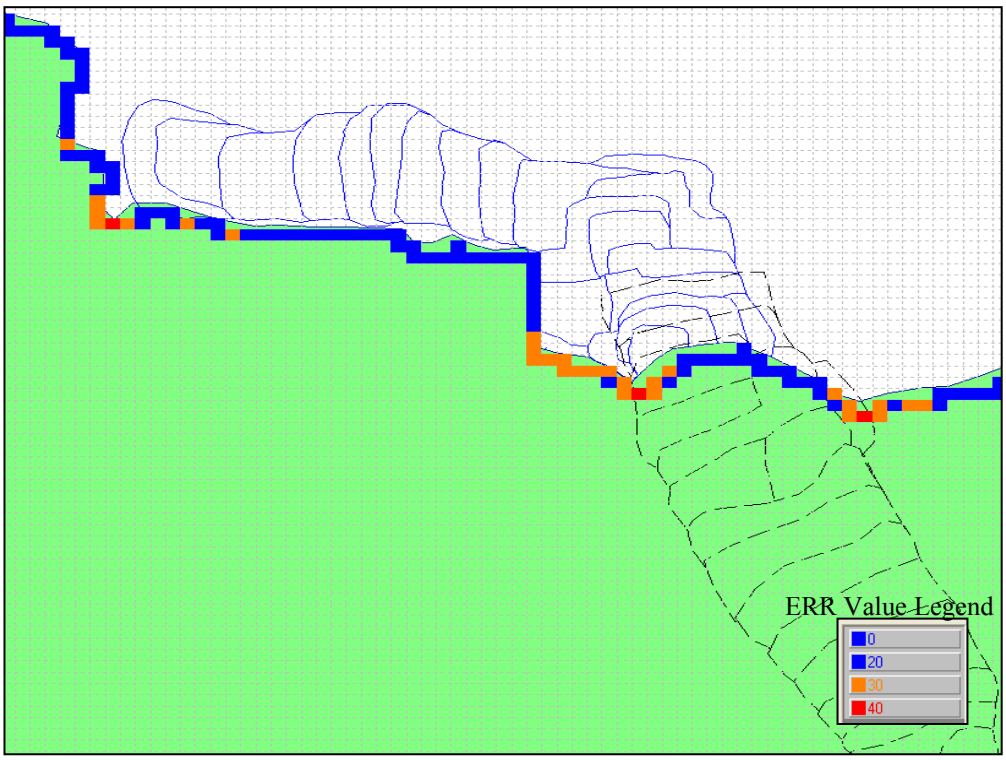


Figure 7.24 Outline of the modelled layout of the VC20-31.

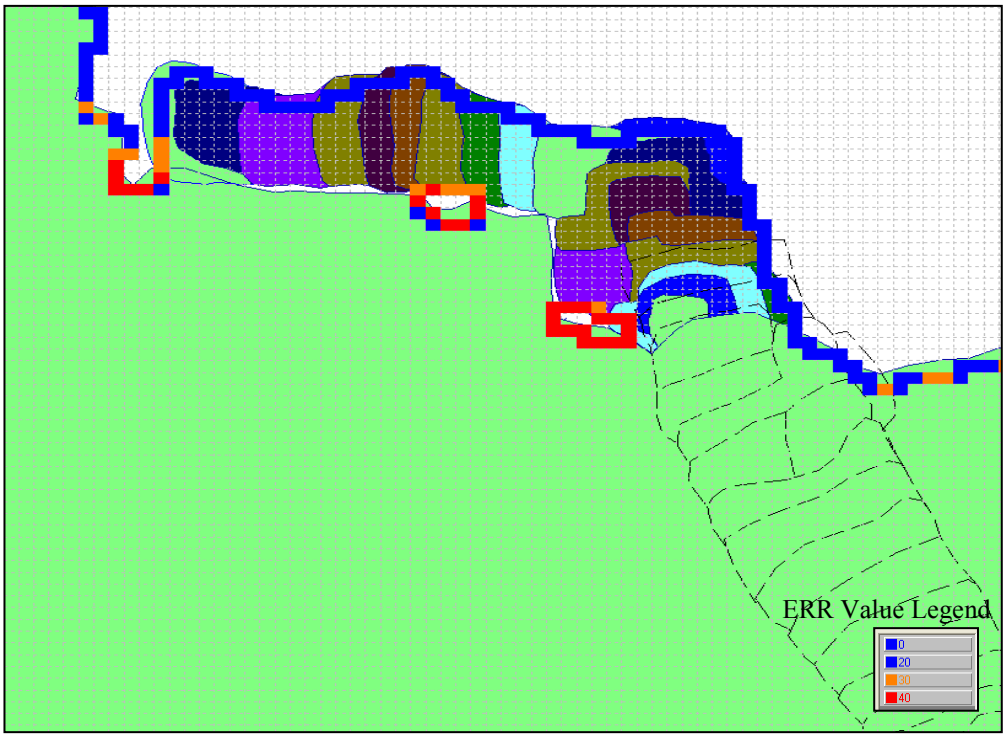


Figure 7.25 Sequenced layout for the modelling of VC20-31.

Figure 7.26 depicts some of the ERR values obtained from the numerical model. The particular step shown is during the period when mining occurs over the waste cut in a de-stressed area. The middling of the area is less than 6 m. The waste cut was mined primarily as an access way and hence it was mined below the entire block.

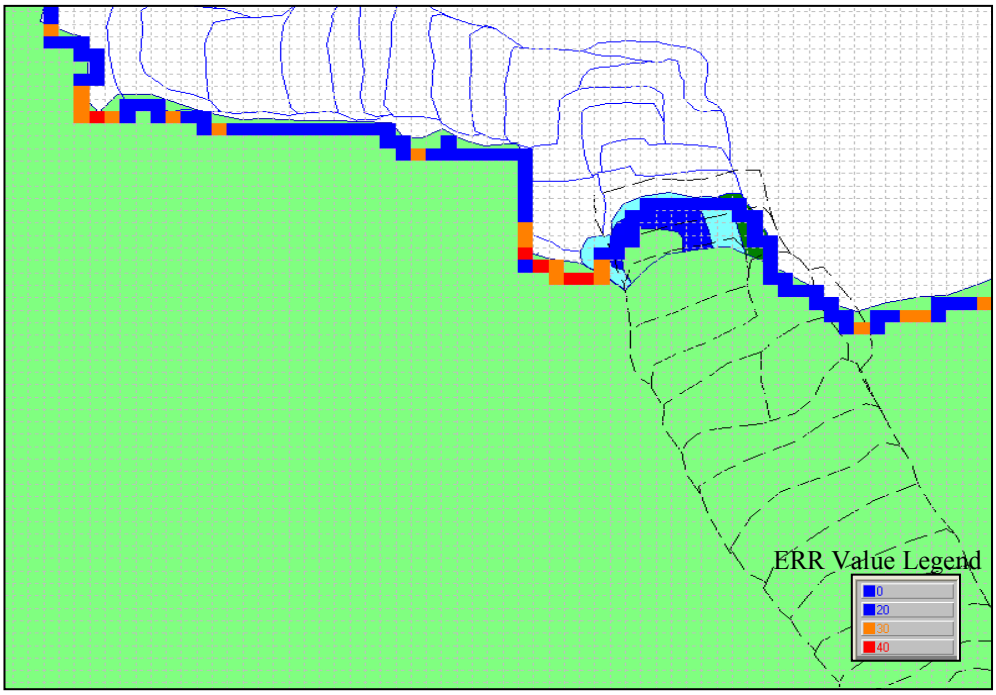


Figure 7.26 ERR results indicating the effect of the de-stressing at VC20-31.

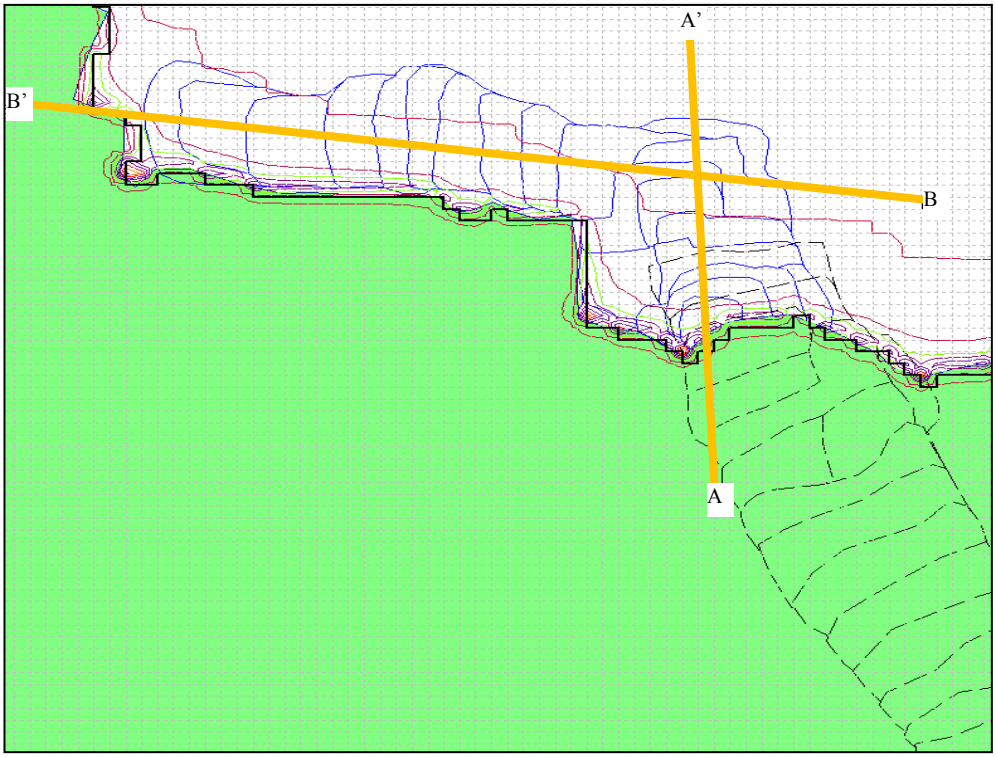


Figure 7.27 Positions of sections for the modelled layout.

Figure 7.27 indicates a stress contour plot of the major principal stress. The locations of sections for plots of the stress are also indicated.

Figures 7.28 and 7.29 depicts the two stress diagrams. The stress simulated is well above the strength of the weak lava hangingwall and hence fracturing as shown in Figures 7.21 and 7.23 is to be expected.

The influence of the waste cut can be seen at a distance of 19 m in Figure 7.28. In contrast breast mining in Figure 7.29 that is not de-stressed (section B-B'), indicates the increase in stress as the remnant size is reduced as well as the mining holes and forms part of the large mined span.

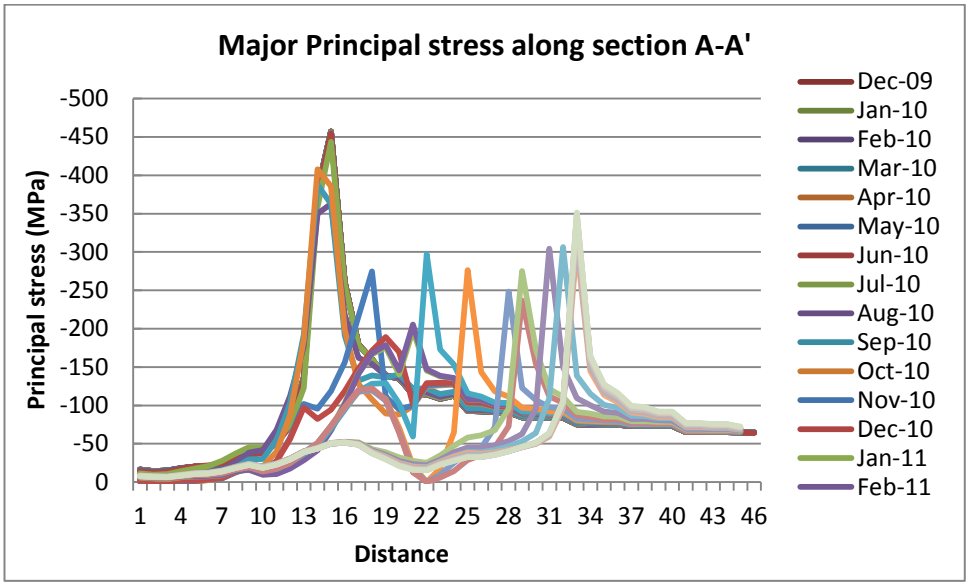


Figure 7.28 Plot of the stresses along section A- A'.

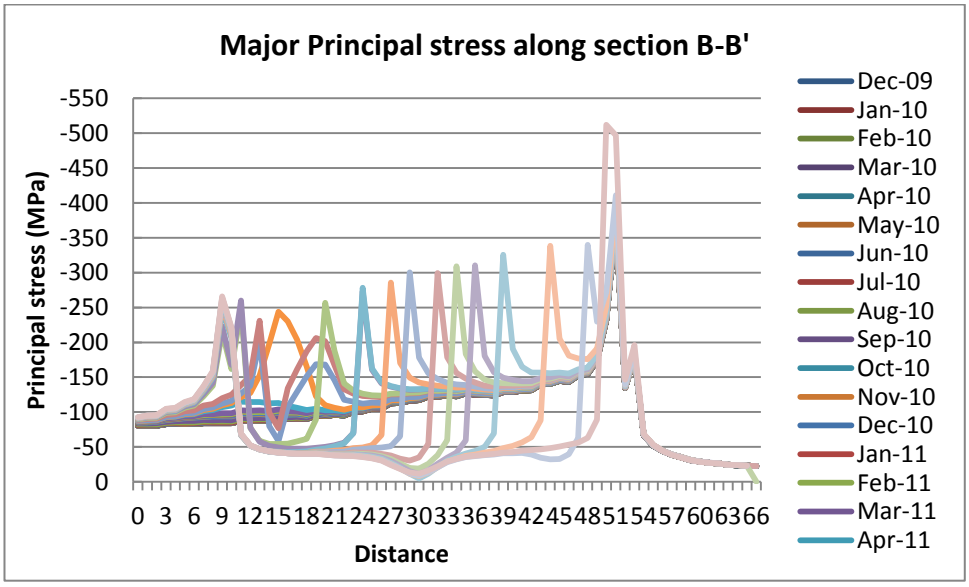


Figure 7.29 Plot of the stresses along section B- B'.

Figure 7.30 depicts the ERR values plotted against the cumulative production of the area. The values are considered to be small.

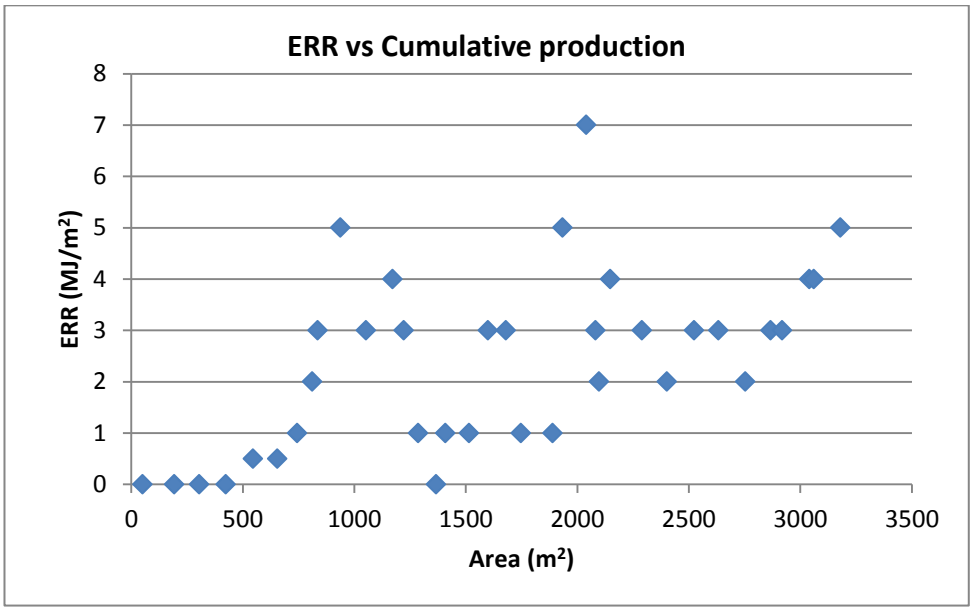


Figure 7.30 ERR and cumulative production plot for VC20-31.

Figure 7.31 indicates the location of a section that was further analysed. Figure 7.32 to 7.36 depicts the results of the numerical modelling in terms of the major principal stress on a plane between the two stoping excavations.

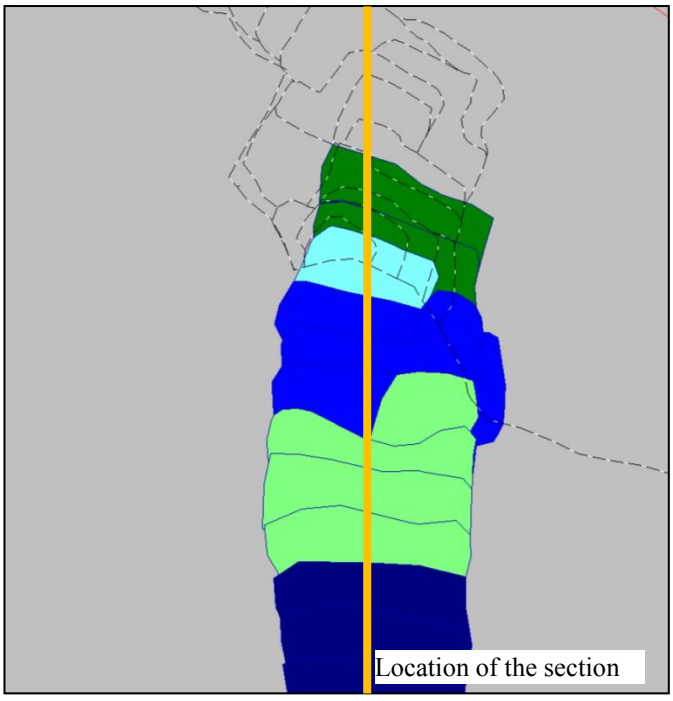


Figure 7.31 Location of a section on the waste cut at VC20-31.

Figure 7.32 illustrates a region of very high major principal stress on the edges of the stoped out area. The stress concentrations is confined to localized areas.

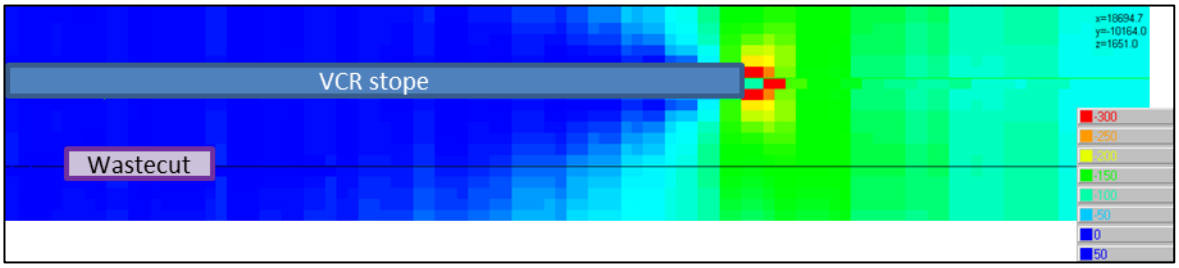


Figure 7.32 Contour plot of the major principal stress prior to any mining on the waste cut.

Figure 7.33 and 7.34 illustrates the introduction of the waste cut. From the figures it can be seen that the additional stope has a significant disruptive effect on the stresses and that there is interaction between the edges of the two stopes. Similar to the discussion in the previous chapters, this interaction may lead to violent shear failure. It was not observed for this case either which indicates that the available energy was dissipated, possibly through some movement on bedding planes.

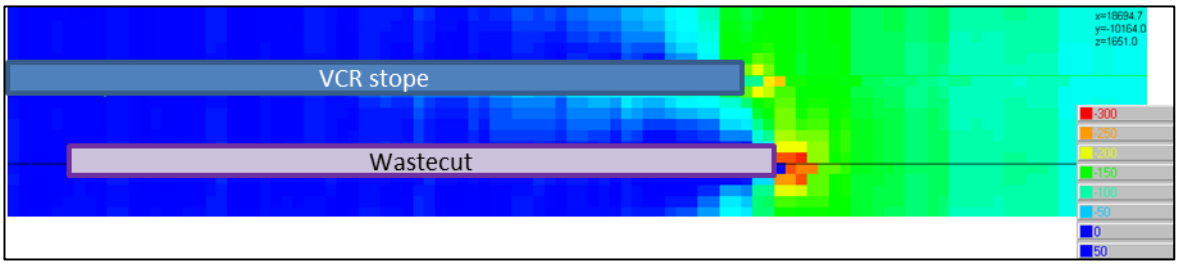


Figure 7.33 Contour plot of the major principal stress during the understoping.

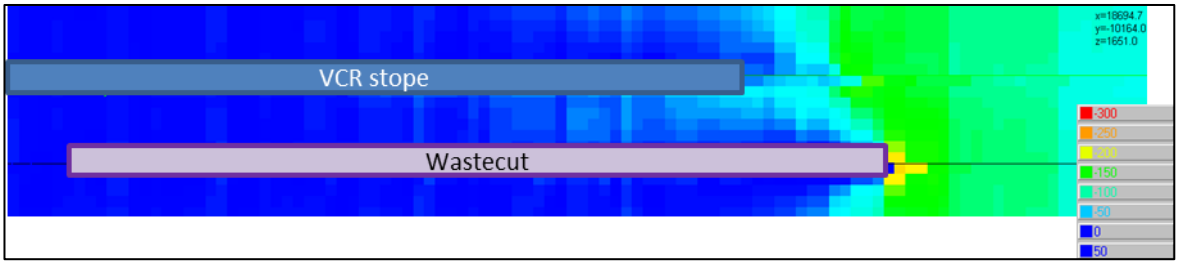


Figure 7.34 Contour plot of the major principal stress during the continued understoping on the waste cut.

Figure 7.35 illustrates the partial de-stressing of both mining elevations as the VCR is mined above the waste cut. This would mean that stoping occurred at a lower stress.

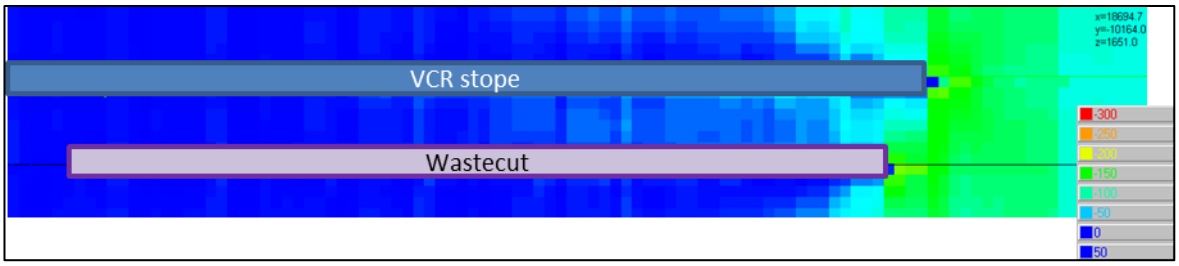


Figure 6.35 Contour plot of the major principal stress during the mining of the VCR through the abutment of the understoped area.

Figure 6.35 illustrates the VCR as mining continues past the abutment of the waste cut.

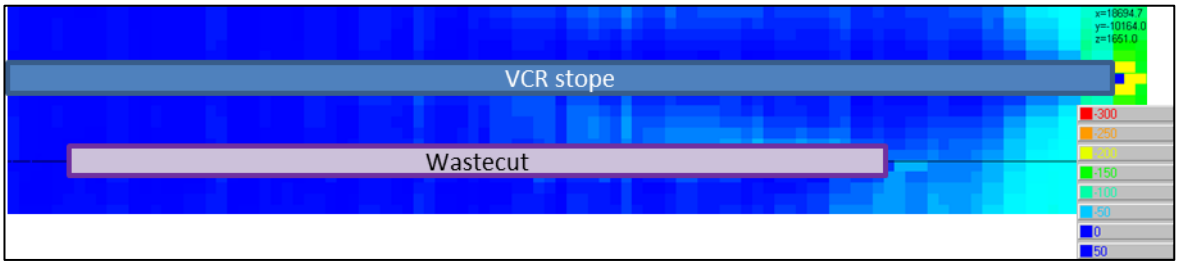


Figure 6.35 Contour plot of the major principal stress during the continued mining of the VCR past the abutment of the waste cut.

SUMMARY

In summary, the back analysis in Chapter 7 indicated that VCR mining of the area was successful, although VCR mining proceeded past the waste cut abutment. The lithology of the area included a weak shale in the footwall of the Libanon reef and a weak hangingwall lava above the VCR. Throughout the inclined excavations, joint sets and bedding planes were observed. The analysis also indicated high closure rates with low seismic emissions. The observed behaviour of the area can most probably be linked to and described by the hypothesis of energy dissipation and lower released energy as presented in Chapter 4.

CHAPTER 8

CASE STUDY AND BACK ANALYSIS OF REMNANTS D and E : KL23-48 and MB24-43

Not all the target blocks where multi-reef mining was conducted were successful. These case studies are valuable to compare with the successful extractions and to test the hypothesis of weak layers being important to enable multi-reef extractions. Two examples of this are the KL23-48 and the MB24-43 areas. Both the areas were partially extracted, but eventually the seismicity was so problematic that the areas were stopped. Although the KL23-48 is not far from Remnants A,B and C, both Remnants D and E have a lithology different to that of Remnants A, B and C.

KL23-48 mines a reef package situated between the two other reef packages located, above the Libanon and below the VCR. As described earlier, the VCR has a lava hangingwall and quarzitic footwall, and the Kloof reef thus has a quarzitic hangingwall. The reef package consists of a quartz conglomerate and also has a quarzitic footwall. The Middelvlei reef is also a quartzitic conglomerate with a quartzite hanging and footwall, situated below the Libanon reef.

The areas were mined with a normal scattered mining layout from where the crosscut intersected the reef elevation. The elevation difference between the two reef elevations is in excess of 100 m and 60 m for the KL23-48 and MB24-43, respectively. On plan, the KL23-48 area is not overstoped and the MB24-43 is overstoped. Figures 8.1 and 8.2 depicts a plan view of the areas.

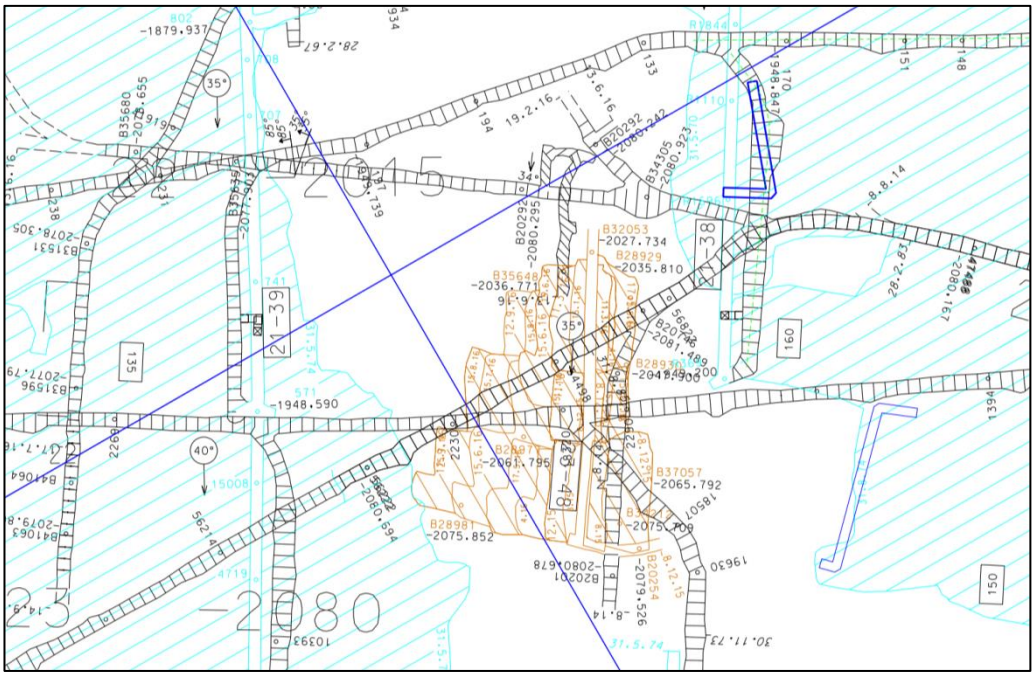


Figure 8.1 Locality plan of the KL23-48 stope.

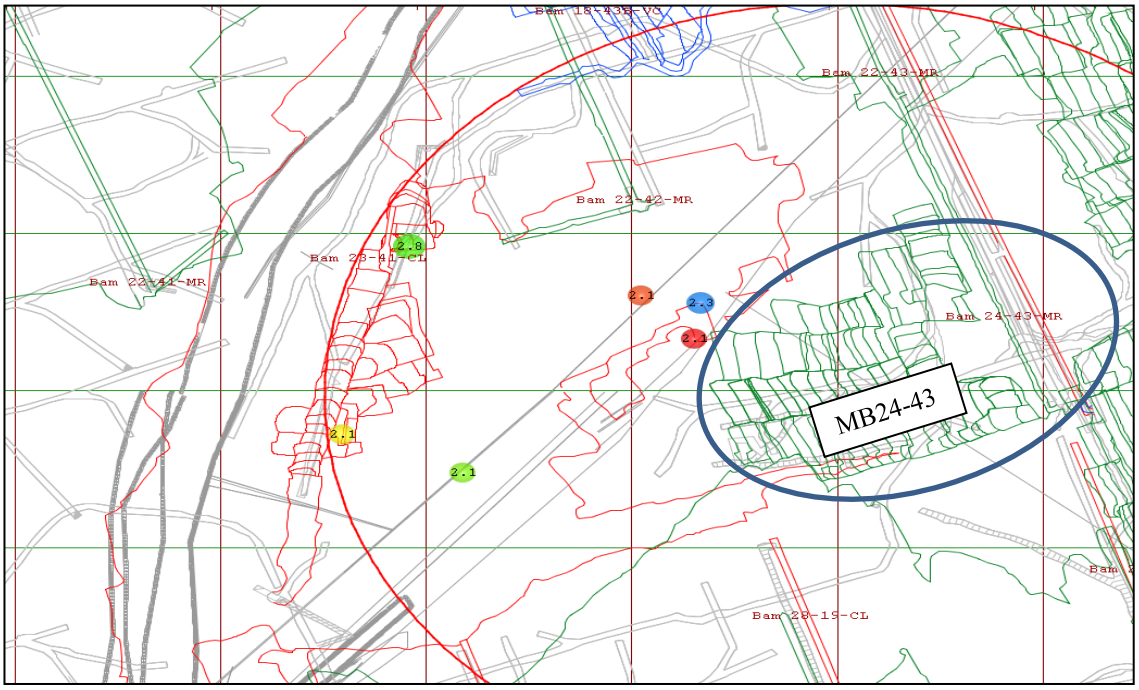


Figure 8.2 Locality plan of the MB 24-43 stope.

Figures 8.3 and 8.4 depicts the recorded seismicity in the areas. The colour of the plot is an indication of the date of occurrence, the red is the more recent, and the magnitude of the event is indicated by the size of the dot.

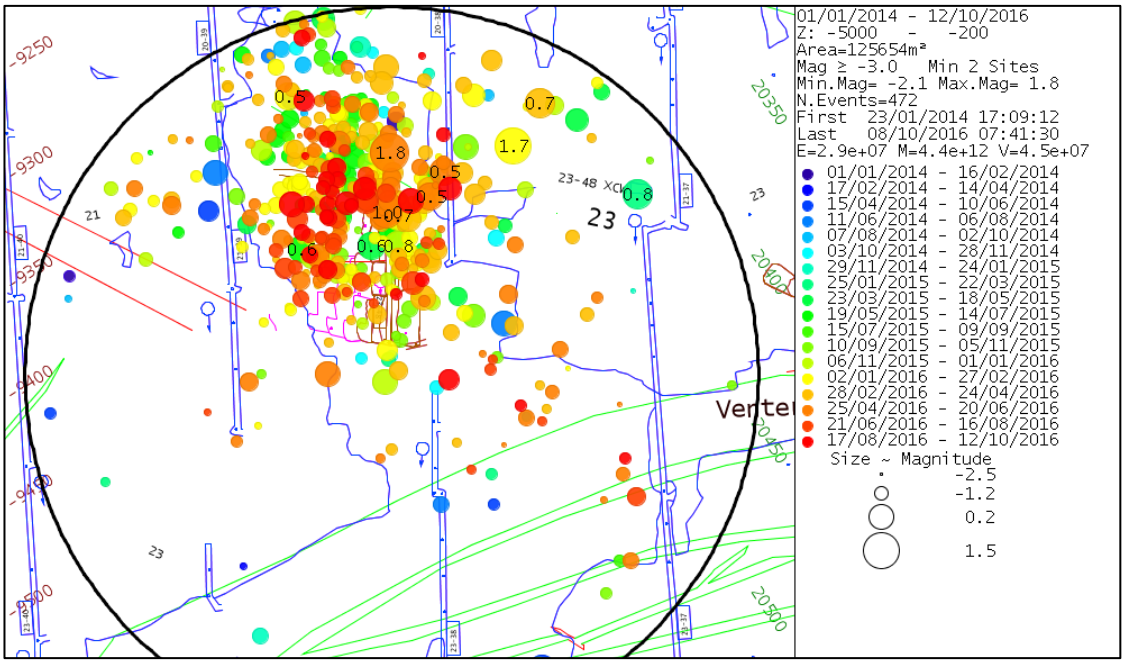


Figure 8.3 Plot of recorded seismic activity at KL23-48.

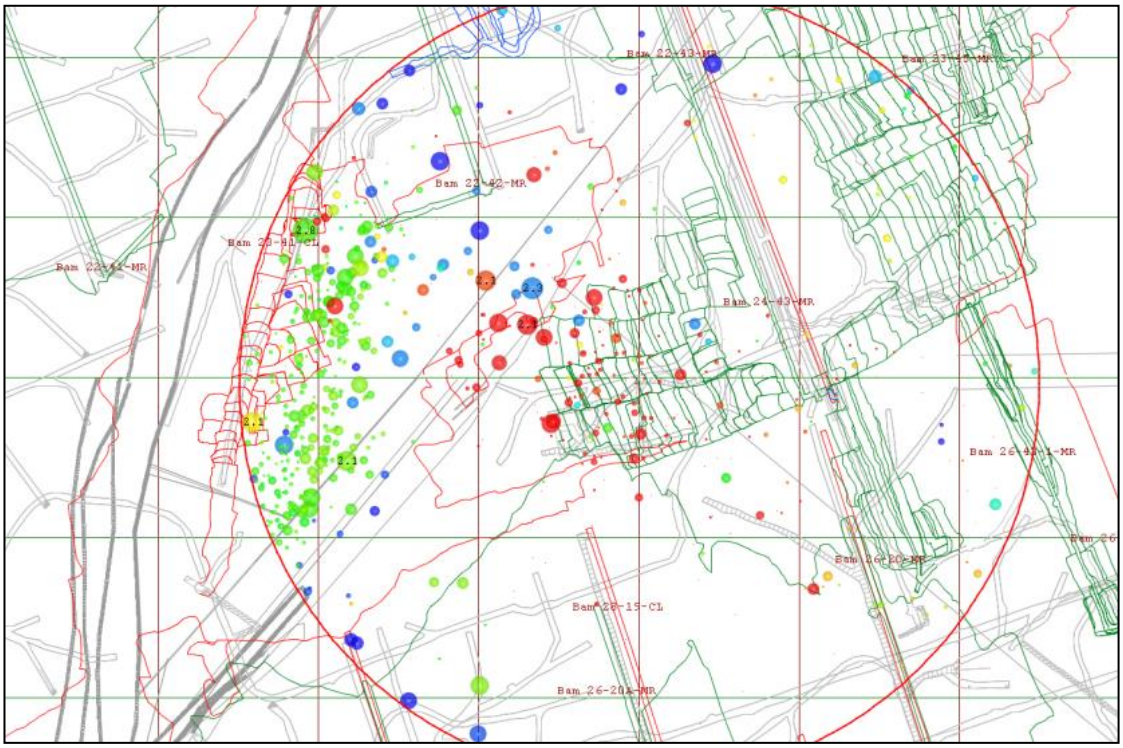


Figure 8.4 Plot of recorded seismic activity at MB24-43.

Figures 8.5 and 8.6 illustrates the seismic activity for the two areas. The magnitude of the events are indicated by the colour of the plots.

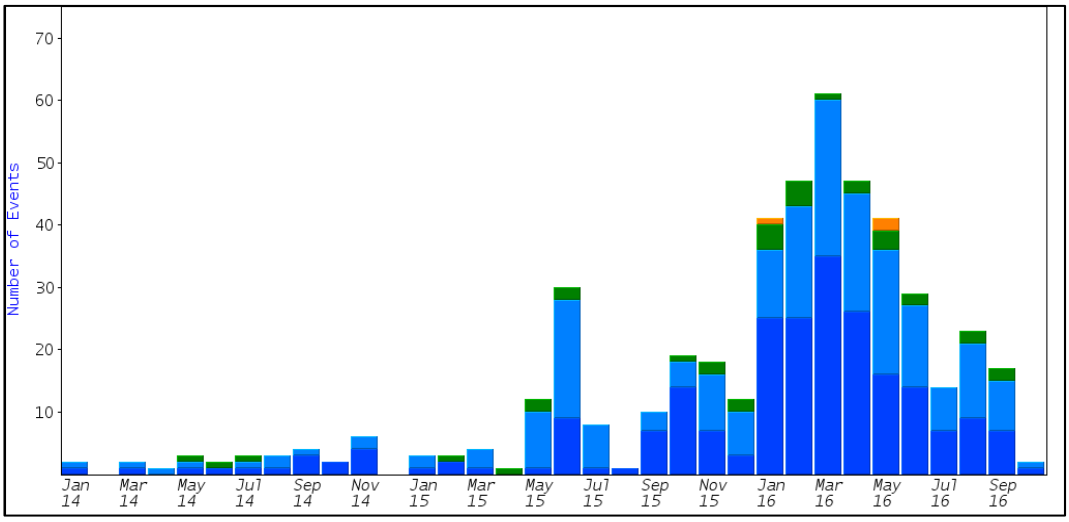


Figure 8.5 Indication of historic seismic activity at KL23-48.

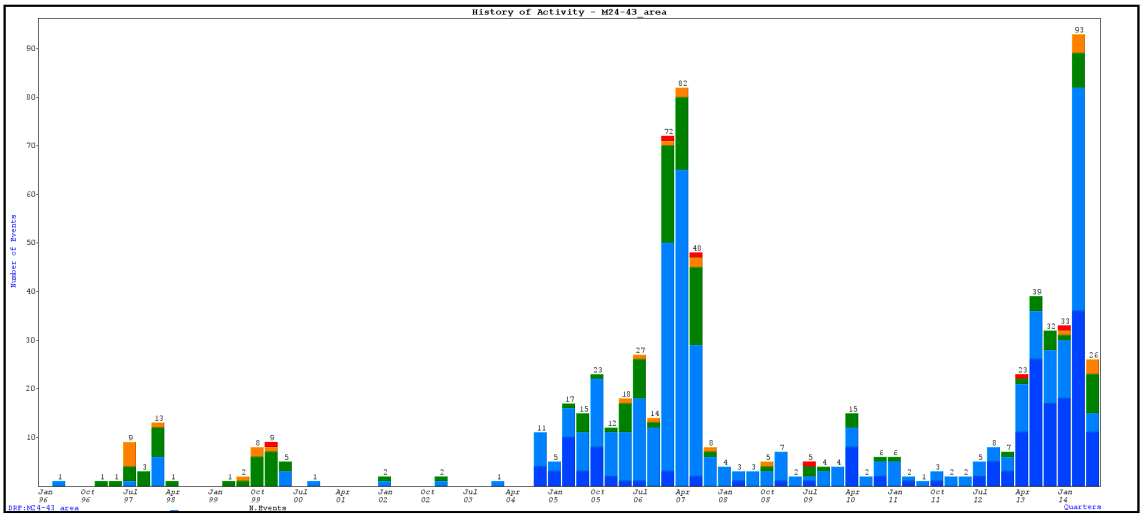


Figure 8.6 Indication of historic seismic activity at MB24-43.

Tables 8.1 and 8.2 is a summary of the recorded seismicity in the areas of interest. From these figures can be seen that some seismicity were occurring during the time before mining. The number of events as well as the Mmax for the areas increased as mining commenced.

Table 8.1 Summary of the seismic events in the KL23-48 area.

	Number of events					Maximum	Energy	Moment
Year	M<0	0<M<1	1<M<2	2<M<3	M>3	Magnitude	J	Nm
2014	28	3	0	0	0	0.4	7.40E+05	7.60E+10
2015	111	11	0	0	0	0.8	3.40E+06	6.50E+11
2016	299	20	3	0	0	1.8	2.50E+07	3.50E+07

Table 8.2 Summary of the seismic events in the MB24-43 area.

Year	Number of events					Maximum	Energy	Moment
	M<0	0<M<1	1<M<2	2<M<3	M>3	Magnitude	J	Nm
2012	9	0	0	0	0	-0.2	1.60E+06	3.80E+10
2013	81	8	0	1	0	2.1	1.10E+07	6.30E+12
2014	145	18	8	1	0	2.1	3.40E+07	1.30E+13
2015	102	7	1	1	0	2.3	4.70E+07	7.40E+12
2016	24	2	0	0	0	0.5	8.80E+04	3.10E+11

Figure 8.8 Summary of the seismic events in the MB24-43 area.

The seismic analysis of the KL23-48 area revealed that the largest event recorded was a M_L 1.8, while the M_{max} for the area is M_L 2.0. It was also determined that the majority of the events were slip-type events. The largest event observed at the MB24-43 was M_L 2.3, while the M_{max} for the area is M_L 2.5 and the majority of the recorded events were slip type events. From the historic data the probabilities and return periods of seismic events were also determined as shown in Figures 8.7 and Figure 8.8 for the KL23-48 and MB24-43 respectively.

Mean Return Periods

Mag.	Number of Events /Month	/Year	Return Period months	years
-1.0	6.74	80.9	0.148	0.01
-0.5	2.76	33.1	0.363	0.03
0.0	1.12	13.4	0.896	0.07
0.5	0.44	5.3	2.271	0.19
1.0	0.16	1.9	6.176	0.51
1.5	0.05	0.6	21.169	1.76

Probabilities of Seismic Event

Mag.	1 month	3 months	6 months	1 year	2 years	5 years
-1.0	99.9%	100.0%	100.0%	100.0%	100.0%	100.0%
-0.5	93.6%	100.0%	100.0%	100.0%	100.0%	100.0%
0.0	67.2%	96.5%	99.9%	100.0%	100.0%	100.0%
0.5	35.6%	73.3%	92.9%	99.5%	100.0%	100.0%
1.0	14.9%	38.5%	62.1%	85.7%	97.9%	100.0%
1.5	4.6%	13.2%	24.7%	43.3%	67.8%	94.1%

Maximum Expected Magnitude

In 1 year M = 1.29
In 2 years M = 1.54
In 5 years M = 1.77

Seismic Events Distribution

Magn >	-1.0	-0.5	0.0	0.5	1.0	1.5
Theor.	225	92	37	15	5	1.6
Observed	244	88	37	12	3	2

Figure 8.7 Seismic statistics of the KL23-48 area.

Mean Return Periods

Mag.	Number of Events /Month	/Year	Return Period months	years
-1.0	1.45	17.4	0.690	0.06
-0.5	0.81	9.8	1.228	0.10
0.0	0.45	5.4	2.214	0.18
0.5	0.25	2.9	4.081	0.34
1.0	0.13	1.5	7.859	0.65
1.5	0.06	0.7	16.640	1.39
2.0	0.02	0.3	45.831	3.82

Probabilities of Seismic Event

Mag.	1 month	3 months	6 months	1 year	2 years	5 years
-1.0	76.5%	98.7%	100.0%	100.0%	100.0%	100.0%
-0.5	55.7%	91.3%	99.2%	100.0%	100.0%	100.0%
0.0	36.3%	74.2%	93.3%	99.6%	100.0%	100.0%
0.5	21.7%	52.1%	77.0%	94.7%	99.7%	100.0%
1.0	11.9%	31.7%	53.4%	78.3%	95.3%	100.0%
1.5	5.8%	16.5%	30.3%	51.4%	76.4%	97.3%
2.0	2.2%	6.3%	12.3%	23.0%	40.8%	73.0%

Maximum Expected Magnitude

In 1 year M = 1.29
In 2 years M = 1.71
In 5 years M = 2.10

Seismic Events Distribution

Magn >	-1.0	-0.5	0.0	0.5	1.0	1.5	2.0
Theor.	357	200	111	60	31	15	5
Observed	362	218	121	54	23	14	5

Figure 8.8 Seismic statistics of the MB24-43 area.

Figures 8.9, 8.10 and 8.11 indicates the modelled ERR of the two working areas.

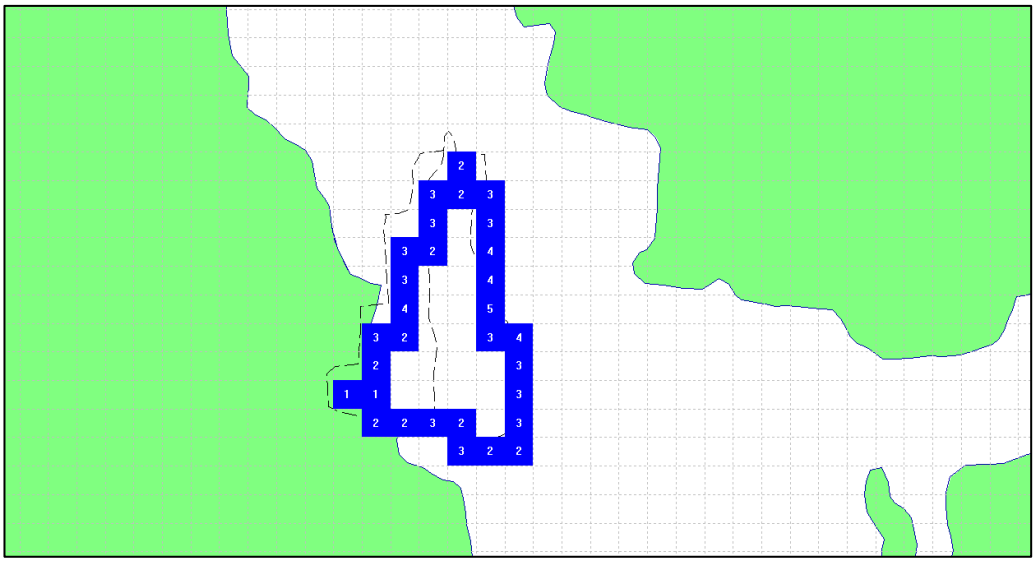


Figure 8.9 ERR plot of Kl23-48 area on the Kloof reef elevation.

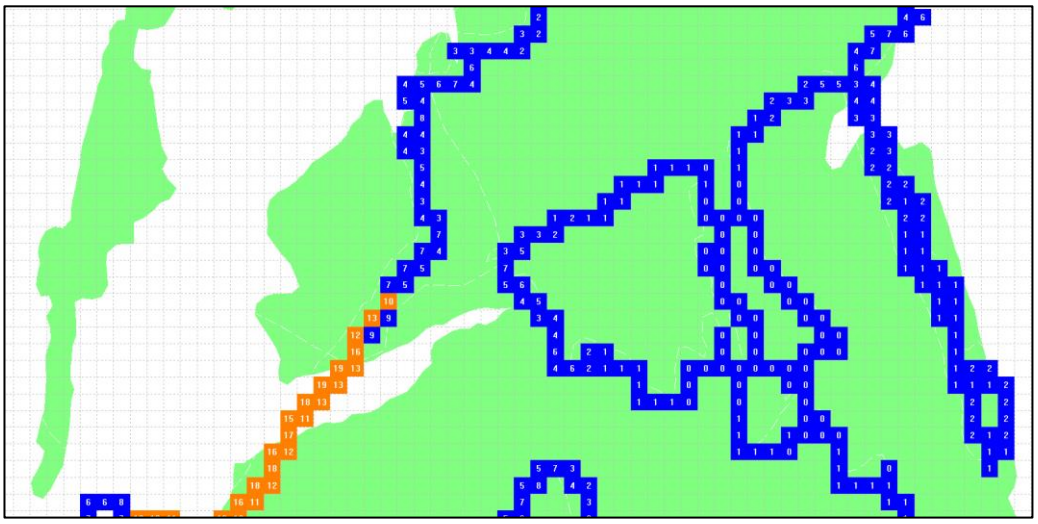


Figure 8.10 ERR plot of the Main reef elevation at MB24-43 area.

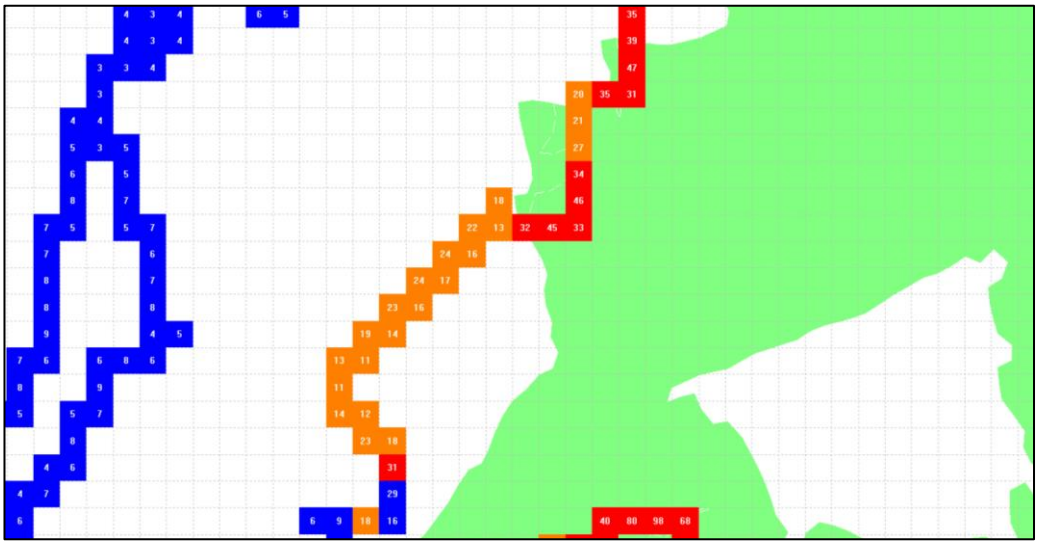


Figure 8.11 ERR plot of the MB24-43 area on the Carbon leader elevation.

SUMMARY

A comparison between the closure rates of remnants A, B, C, D and E would have been valuable. Unfortunately that detail is not available for the areas, the comparison of closure rates is therefore included as future work. It should be noted that even if the closure data was available it should not be compared directly. Closure readings are very sensitive to the position of installation, type of station, mining layout as well as the stope geometry.

Comparing the information presented in this Chapter to that of Chapter 6 and 7, a clear difference in the seismicity is noted. The recorded seismicity presented in Chapters 6 and 7 is small in comparison to what was recorded in the areas presented in Chapter 8, although the seismic parameters are the same and it was recorded by the same seismic system.

Another factor that will affect the seismic response is the rock properties. The properties of the host rocks found in the areas of concern is noted below. Table 8.3 is a summary of the rock strengths as found in the Code Of Practice (Anon, 2016) of Mine A. Similar information was also presented by Schweitzer and Johnson (1997) as depicted in Figure 8.12.

Table 8.3 Rock strengths at Mine A.

Rock Type	**Rock strength (MPa)**
Alberton Lava	220 MPa
WAF	80 MPa
VCR Quartzite	200 MPa
Elsburg Quartzite	180 MPa
Booysens Shale	140 MPa
Middelvlei Reef Quartzite	220 MPa
Carbon Leader	260 MPa
KR Quartzite	180 MPa
Argillaceous Quartzite	140 MPa

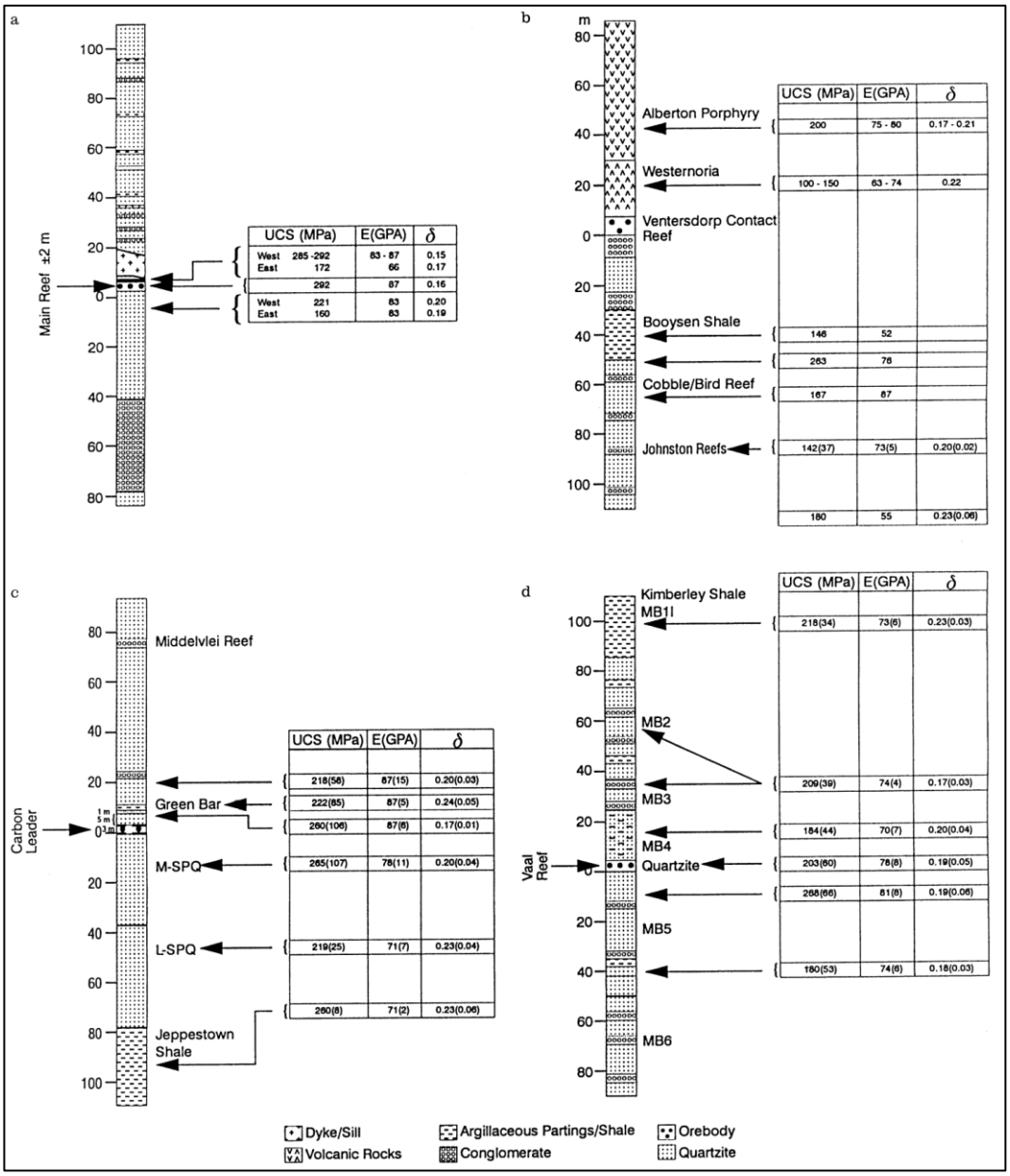


Figure 8.12 Rock properties of Stratigraphic profiles found in the Carletonville area. a- Main Reef, b- MVR and Carbon leader, c- VCR and d- Vaal Reef (after Schweitzer and Johnson, 1997).

In these two areas, the quarzitic rock mass between the reefs usually consists of multiple packages, separated by bedding planes. The strength of the quartzite is 200MPa in this area and no shales are present. It appears that stable energy release is not as effective as in the areas where shale is present, but this needs to be investigated further in future studies.

CHAPTER 9

CONCLUSIONS AND RECOMMENDATIONS

9.1 CONCLUSIONS

Even after years of mining, a vast gold resource remains in the Carletonville area of the Witwatersrand basin. Mining in this area nevertheless predates 1934 and the accessible ore-reserves on the primary reefs are being depleted. Mining of secondary reefs and remnants has therefore become important in recent years. Of particular interest is multi-reef mining as it will become much more prevalent in this part of the gold mining industry. Very little rock engineering research on multi-reef mining scenarios at great depth is available in the literature. Owing to the lack of proper understanding and guidelines for remnant selection and extraction in a multi-reef environment, a study was conducted by the author.

The key references of earlier work are discussed in the literature survey. From this study it is clear that the behaviour of the rock mass surrounding multi-reef tabular layouts is not well understood. This is especially true when the middling is small. Most of the knowledge on multi-reef mining is based on empirical data and past experience. According to Jager and Ryder (1999), designing layouts or support for multi-reef mining is best done by approaching every design as a unique problem. These designs typically require the consideration of additional parameters, such as mining depth, middling, effect of pillars and remnants, as well as the influence of surrounding rock types. There are two sub categories of multi-reef mining: simultaneous and subsequent extraction. Each category would involve a different set of considerations that should be met to successfully extract the planned area. Even at shallow depths, these multi-reef layouts can exacerbate the problem of pillar failures, as well as lead to the creation of large shear stresses and higher than expected energy releases. Multi-reef mining also creates the potential for large closure and has a greater potential for hangingwall collapse in weak strata (Napier and Malan, 2008). Du Plessis and Talu (1997) described pillar mining in a

multi-reef scenario on a deep level gold mine in the West Wits region. The authors mention that problems were encountered when the middling was too small and this can cause the middling to collapse. In contrast, if no waste cut was carried, the closure rates within the stope were very high, the hangingwall of the VCR deteriorated and even mined itself ahead of the reef face. Hustrulid (2001) mentioned that a significant reduction in the vertical stress component is achieved in the deep mines without significantly affecting the horizontal clamping component if an area is de-stressed. The change in the stress field will affect the rock mass and the fracturing patterns, thereby increasing the support requirements. Other associated problems include bed-separation when understoping or complete closure and stress-regeneration when overstoping. Singh et al. (2005) indicated the significant influence of middling and the presence of tensile horizontal skin stresses. The study concluded that mining conditions of a shallow operation may be similar to that of deep level mining when mining below remnants. Maritz et al. (2012) indicated that reef dip and multi-reef mining has a profound influence on the stress and loading regime of pillars. This complex stress interaction is due to the introduction of a shear stress component, even if the pillars are perfectly superimposed and the reef has no dip. In summary from these various literature studies, it can be concluded that only limited empirical guidelines are available when considering multi-reef mining. Local knowledge and know-how is passed on to Rock Engineering practitioners on the operations and unfortunately few of these experiences were published.

As a first step in the current study, the author compared two displacement discontinuity boundary element codes, MINSIM and TEXAN, to simulate multi-reef environments. The study found that there is no significant difference between the results obtained from these two codes. Only a slight difference in simulated values was noted and this can be ascribed to MINSIM using a “quarter grid” correction scheme to improve the accuracy of simulated convergence values when using constant strength elements. This correction is not implemented in TEXAN. The agreement between the codes allowed for both to be used in the study. MINSIM was used for the actual case studies as digitizing of the problem was

easy using this code. TEXAN was used for the studies where specialized parameters, such as the "extended ERR", had to be calculated.

The initial geometry simulated with TEXAN consisted of two remnant pillars as a base model. One of these pillars was then understoped. This preliminary analysis proved to be valuable and indicated that a small middling with a large overlap of mining is required to achieve a significant reduction of ERR and average pillar stress on the remnant pillar.

Simulation of ERR values proved to be useful to indicate the value of a de-stressing cut. The ERR values of the small de-stress cut were significantly lower when compared to the values for the on-reef mining prior to de-stressing. This lower value is caused by the small span of the de-stress cut, even though it is crossing below the highly stressed abutments of the remnant on the primary reef horizon. Once completed, this de-stress cut has a significant effect in reducing the ERR values on the primary reef.

To better understand the process of understoping, the simplified geometry of a pillar being understoped was investigated in greater detail. An analysis of the incremental stress evolution in the middling between two reef horizons, as the pillar was being incrementally understoped, revealed valuable information. A zone of very high major principal stress and low minor principal stress develops between the two reefs. This indicates a high risk of violent shear failure between the two reefs. The reason for successful historic extractions of actual multi-reef remnants was therefore not clear and explored in more detail in the rest of the study.

As part of this analysis, an "extended" ERR concept introduced by Napier (1991) was utilized. According to Ryder and Jager (2002), ERR should be considered as a measure of stress concentration and underground conditions at mining faces. The ERR concept has some shortcomings as a measure of rockburst hazard as no allowance is made for dissipation of energy due to face crushing or failure on

bedding planes or discontinuities. The “extended” ERR concept was introduced to address these shortcomings by including an energy dissipation term (ΔW_D). This allows for energy that is stably dissipated on discontinuities to be subtracted from the released energy. This “extended” ERR is described in this dissertation. The “extended” ERR calculations was built into the TEXAN framework and the models were therefore simulated with this code.

A number of simulations were run to investigate the influence of a bedding plane on the released energy. The bedding plane parameters as well as the influence of middling between the reefs were also investigated in this study. A key finding of this study was that if an appropriate mechanism exists to dissipate energy in a stable manner, the understoping process will be less hazardous than predicted by the simple elastic model. A correctly positioned bedding plane reduces the potential for violent energy release.

By comparing the closure and the cumulative work done (total energy available), it can be seen that these parameters are related. For a weak bedding plane between the reefs, the closure is substantially higher and this results in the largest cumulative work done. The energy dissipated stably by the bedding plane is also the highest, but it cannot compensate for the greater cumulative work done. This therefore results in a higher released energy and greater risk. In contrast, bedding planes in other positions reduced the released energy and risk. In summary, the study indicated that the stope convergence and the various energy components are affected by the presence, position and properties of a bedding plane. The energy solutions are very complex and sometimes counterintuitive. Care should therefore be exercised when modelling specific cases.

As a further step, actual multi-reef remnants were selected and back analysed to verify the hypothesis of weak layers being useful to make multi-reef mining less hazardous. Aspects such as seismic history, numerical modelling and photographic records were studied. Five case studies are included in the dissertation. It was illustrated that VCR mining with a destressing waste cut in

close proximity to the reef resulted in successful extractions. This was found for 3 of the case studies. The lithology of these successful mining areas included weak shale in the footwall of the Libanon reef and a weak hangingwall lava above the VCR. In contrast, for the two other case studies where destressing was not successful, the quarzitic rock mass between the reefs is typically hard and brittle and stable energy release appears not to be as effective as in the other areas. In summary, from the analysis it was found that multi-reef extraction was successful in cases where a weak rock type was present in the immediate stratigraphy or where pertinent bedding planes were found. This supports the hypothesis as presented above.

An important practical outcome of this study is that much greater emphasis needs to be placed on studying the rock mass surrounding multi-reef environments at depth to determine the risk of extraction in these conditions. This should be added to the list of remnant selection criteria.

9.2 RECOMMENDATIONS

As a recommendation from this study, when selecting or attempting multi-reef remnant mining, the following points should be addressed:

- A thorough geological survey should be conducted to identify the stratigraphy. This should be supplemented by laboratory testing to determine the rock mass properties of the different rock types.
- Detailed modelling of every multi-reef mining scenario is required to determine the extent of de-stress mining required and to give an initial prediction of the expected conditions. A key question to be addressed is whether the rock mass will be able to dissipate the energy in a stable manner during the process of destressing. This should be addressed by careful consideration of the modelling, geological study and laboratory testing.
- When mining in de-stressed conditions, the support system should be as stiff as possible to account for poor ground conditions formed by the tensile zones.

- Closure measurements, visual monitoring of excavations and recording of seismicity should be conducted to determine if the rock mass behaves as expected.

9.3 FUTURE WORK

Bedding planes seem to reduce the energy available for release, and this mechanism is revealed by the extended ERR concept. The study, however, indicated that the various energy components have complex relationships with the particular geometry and number and position of discontinuities included in the model. The energy consumed during the formation of new face fractures is not explicitly simulated in the current model. Hence the following work is required to establish the usefulness of the extended ERR concept:

- This numerical modelling study was done using boundary element codes. This limited the simulation of inelastic rock behaviour to slip on bedding planes. Future work should be conducted using codes that can simulate large scale rock failure of weak zones in conjunction with slip along contact planes. The FLAC or UDEC codes should be investigated in this regard. FLAC and UDEC have an embedded coding language allowing the user some control over parameters calculated. It is however, not clear if the energy components can be easily calculated.
- The "extended ERR" calculations in this study was valuable to investigate the stated hypothesis. Further study of the concept and calibration of the models need to be done before it can be used as a practical tool. A limiting factor is that the amount of energy dissipated will probably be dependent on the number of discontinuities that can be included in the boundary element models. This needs to be studied in detail. In this regards other papers that already investigated the inclusion of bedding planes such as Katsaga and Potyondy (2012) need to be considered.

- A larger number of multi-reef case studies need to be investigated. Examples from other reef types and mining areas will be valuable in this regard.

REFERENCES

Albu Bart, G. (1935). Letter from Head of the General Mining and Finance Corporation regarding the Jubilee year of the Rand of Johannesburg.

Anon, (2012), Code of Practice Gold mine A.

Bienwaski, Z. T. (1991). In search of a design methodology for rock mechanics, Rock Mechanics as a Multidisciplinary Science, *Procedings 32nd U S Symposium on Rock Mech.*, Roegiers Balkema, (eds.), p. 1027–1036.

Brady, B. H. G. and Brown, E. T. (2005). Rock Mechanics for Underground Mining, New York: Lower Academic Publishers.

Brink, A. Z., Robers, M. K. C., Spottiswoode, S. M. (2002). Further assessment of seismic hazard/risk in the Bushveld complex platinum mines and the implication for regional and local support design, GAP821.

Brown, E. T. (2011). Fifty years of the ISRM and associated progress in rock mechanics, in Harmonising Rock Engineering and the Environment, *Proceedings 12th Congress International Society for Rock Mechanics*, p. 29–45.

Brown, E. T. (2012). Progress and challenges in some areas of deep mining, *Deep Mining 2012,* p177-191.

COMRO. (1988). An industry guide to methods of ameliorating the hazards of rockfalls and rockbursts, Johannesburg: Chamber of Mines of South Africa, Vol. 144, p. 12-33.

Cook , N. G. W. and Salamon, M. D. G. (1966). The use of pillars for stope support, Chamber of Mines of South Africa, unpublished report.

Cook, N. G. W., Hoek, E., Pretorius, J. P. G., Ortlepp, W. D., Salamon, M. D. G. (1966). Rock mechanics applied to the study of rockbursts, *J. S.Afr. Inst. Min. Metall.*, p. 435–528.

Deist, F. H., Georgiadis, E. and Moris, J. P. E. (1972). Computer applications in rock mechanics, *J. S.Afr. Inst. Min. Metall.*, Vol. 72, p. 265-272.

Du Plessis, A. P. and Talu, M. S. (1997). Ventersdorp Contact Reef pillar extraction at Libanon - a division of Kloof Gold Mining Company Limited, *First Southern African Rock Engineering Symposium 1997*, p. 459-466.

Durrheim, R. J. (1997). Site response to rockbursts. Proceedings of SIMRAC seminar, Welkom, GAP 201.

Durrheim, R. J., Spottiswoode S. M., Roberts M. K. C. and Brink A. van Z. (2005). Comparative seismology of the Witwatersrand Basin, *J. S.Afr. Inst. Min. Metall.*, Vol 105, p. 40-416.

Hackett, P. (1959). An elastic analysis of rock movements caused by mining, Transactions Institution of Mining Engineers., Vol. 118, p. 421-433.

Hill, F. G. (1944), A system of longwall stoping in a deep level mine, with special reference to its bearing on pressure burst and ventilation problems, Association of mine managers of the Transvaal, Papers and discussions 1942-1945, Vol. 1, p. 257-270.

Hoover, H. C., (1909). Principals of Mining: Valuation, Organization and Administration, McGraw Hill, 1909, p. 64.

Hustrulid, W. A. (2001). Underground mining methods: Engineering fundimentals and international case studies, SME 2001.

Jager, A. J. and Ryder, J. A. (1999). A Handbook on Rock Engineering Practice for Tabular Hard Rock Mines, The Safety in Mines Research Advisory Committee (SIMRAC), Johannesburg.

Johnson, R. (1994). Literature review on mining at ultradepth and in highly stressed areas, GAP 033.

Katsaga, T. and Potyondy, D.O.A. (2012). Generic Stope Model for Investigation of Fracturing Mechanisms in Deep Gold Mines. *46th US Rock Mechanics / Geomechanics Symposium*, Chicago, USA.

Legge, N. and Spottiswoode S. M. (1987). Fracturing and micro-seismicity ahead of a deep gold mine stope in the pre-remnant and remnant stages of mining, *6th Congress of the International Society of Rock Mechanics*, Herget G. and Vongpaisal S., (eds), Rotterdam Netherlands, p. 1071-1077.

Letcher, O. (June 1936). The Gold Mines of Southern Africa Vol no1.

Malan, D. F. (1999). Time-dependent Behaviour of Deep Level Tabular Excavations in Hard Rock, *Rock Mechanics and Rock Engineering*, Vol. 32 (2), p123-155

Maritz, J. A. (2014). The presence of shear stresses in pillars and the effect on factor of safety in a room-and pillar layout, *J. S.Afr. Inst. Min. Metall.*, p. 1049 -1055.

Maritz, J. A., Malan, D. F., and Piper, P. S. (2012). Estimating pillar stresses in complex multi-reef layouts, *Southern Hemisphere International Rock Engineering Symposium*, 2012, p. 125-143.

Minney, D. S. and Naismith W. A. (1993). Quantitative analysis of seismic activity associated with the extraction of a remnant pillar in a moderately deep level gold mine' Rockbursts and Seismicity in Mines, Young (ed.), Balkema, p. 95–100.

Napier, J. A. L. (1983). Unpublished material.

Napier, J. A. L. (1991). Energy changes in a rockmass containing multiple discontinuities, *J. S. Afr. Inst. Min. Metall.*, p. 91, 145 -157.

Napier, J. A. L. and Malan D. F. (2007). The computational analysis of shallow depth tabular mining problems, *J. S.Afr. Inst. Min. Metall.*, vol. 107, 2007, p. 725-742.

Napier, J. A. L. and Malan, D. F. (2008). Numerical simulation of a multi-reef tabular mining layout in a South African platinum mine - Austrailian centre for geocience, *Southern Hemisphere International Rock Engineering Symposium*, 2008, p. 367-378.

Napier, J. A. L. and Malan, D. F. (2011). The design of stable pillars in the Bushveld Complex mines: a problem solved?, *J. S.Afr. Inst. Min. Metall.*, vol. 111, no. 12, p. 821-836.

Napier, J. A. L. and Malan, D. F. (2011). Numerical computation of average pillar stress and implications for pillar design, *The South African Institute of Mining and Metallurgy*, p. 837-846.

Napier, J. A. L. and Malan, D. F. (2014). A simplified model of local fracture processes to investigate the structural stability and design of large-scale tabular mine layouts, *48th US Rock Mechanics / Geomechanics Symposium*, Minneapolis, USA.

Plewman, R. P., Deist, F. H. and Ortlepp, W. D. (1969). The development and application of a digital computer method for the solution of strata control problems, *J. S. Afr. Inst. Min. Metall.*, p. 70, 33 -44.

Rangasamy, T. and Jager, A. J. (2002). A Selective Review of Remnant Definitions and Creation in the South African Gold Mining Industry, *Re-Defining The Boundaries*, SANIRE Symposium.

Rangasamy, T., Oelofse, J., Sellers, E. and Linzer, L. (2003). An integrated, simplistic approach for determining the viability of extracting three associated remnants in a scattered, deep level gold mine. – Technology roadmap for rock mechanics, South African Institute of Mining and Metallurgy.

Riemer, K. L. and Durrheim, R. J. (2011). Mining Seismicity in the Witwatersrand Basin: Monitoring, Mechanisms and mitigation strategies in perspective, *Journal of Rock Mechanics and Geotechnical Engineering 2011*.

Ryder, J. A. and Jager, A. J. (2002). A textbook on rock mechanics for tabular hard rock mines, SIMRAC, Johannesburg: SIMRAC.

Ryder, J. A. and Napier, J. A. L. (1985). Error analysis and design of a large-scale tabular mining stress analyser, *5th International Conference on Numerical Methods in Geomechanics*, Japan., p. 1549 -1555.

Salamon, M. D. G. (1968). Two-dimensional treatment of problems arising from mining tabular deposits in isotropic transversely isotropic ground, *Int. J. rock Mech. Min Sci*, v. 5, p. 159 -185.

Salamon, M. D. G. (1964). Elastic analysis of displacements and stresses induced by mining of seam or reef deposits. *J. S. Afr. Inst. Min. Metall.*, v. 65, p. 319 -338.

Salamon, M. D. G. (1984). Energy considerations in rock mechanics: fundamental results, *J. S. Afr. Inst. Min. Metall.*, p. 84, 233 -246.

Salamon, M. D. G., Ryder, J. A. and Ortlepp, W. D. (1964). An analogue solution for determining the elastic response of strata surrounding tabular mining excavations, *J. S.Afr. Inst. Min. Metall.*, vol. 64, p. 115 -137.

SAPA., (2012). SA minerals wealth worth R30 trillion: http://www.iol.co.za/business/business-news/sa-minerals-wealth-worth-r30-trillion. Cited 2012.

Schweitzer, J. K., Johnson, R.A. (1997). Geotechnical classification of deep and ultra-deep Witwatersrand mining areas, South Africa. *Mineralium Deposita*, vol. 32, issue 4, p. 335-348.

Singh, N., Urcan, H., Naidoo, K., Ryder, J., Watson, B. P., Milev, A. M. and Roberts, M. K. C. (2005). The influence of pillars on the Merensky Reef horizon on stoping operations on the underlying UG2 Reef horizon, *J. S.Afr. Inst. Min. Metall.*, vol. 105, 2005.

Stacey, T. R., Terbrugge, P. J. and Wesseloo, J. (2006). Risk as a rock engineering design criterion, in Proceedings Third International Seminar on Deep and High Stress Mining.

Starfield, A. M. and Cundall, P. A. (1988). Towards a methodology for rock mechanics modelling, *International Journal of Rock Mechanics and Mining Sciences*, vol. 25, No. 3, p. 99 -106.

This is Gold (2015): South African Gold, Today and Tomorrow Fact Sheet Page 1: http://www.thisisgold.co.za/downloads/finish/4-fact-sheets/59-south-african-gold-today-and-tomorrow.pdf, Cited 2015.

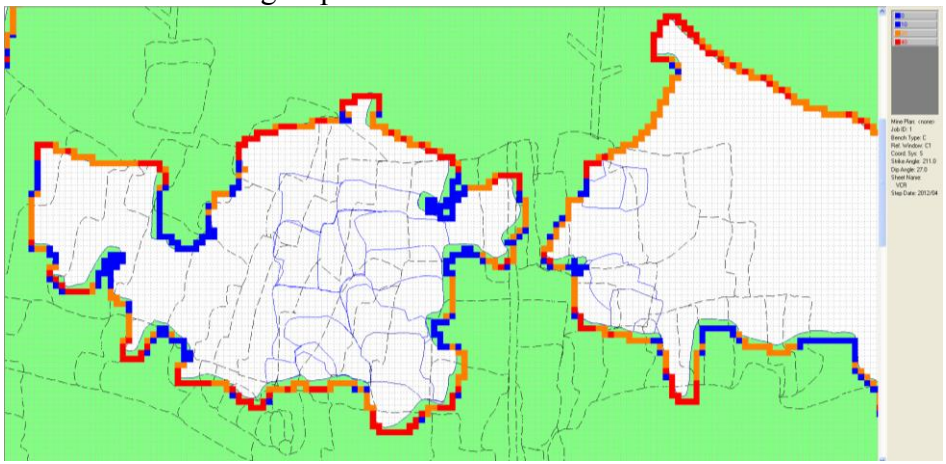
Viljoen, M. (2009). The life, death and revival of the central Rand Goldfield, *2009 World Gold Conference*, p132 -p138.

Wilson, M. G. C. and Anhaeusser (1998).The Mineral resources of South Africa, p. 294 -p346.

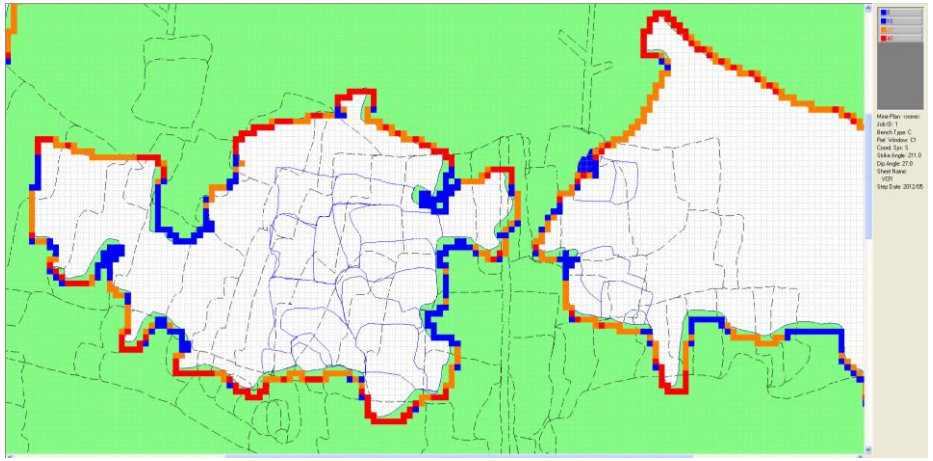
Appendix A : Numerical Modelling of VC25-23

Model Setup:
Grid size: 2 m
Youngs modulus: 60 GPa
Friction angle: 30 degrees
Poissons ratio: 0.27
VRS: ZZ -0.03 / m
XX;YY : ZZ 0.5

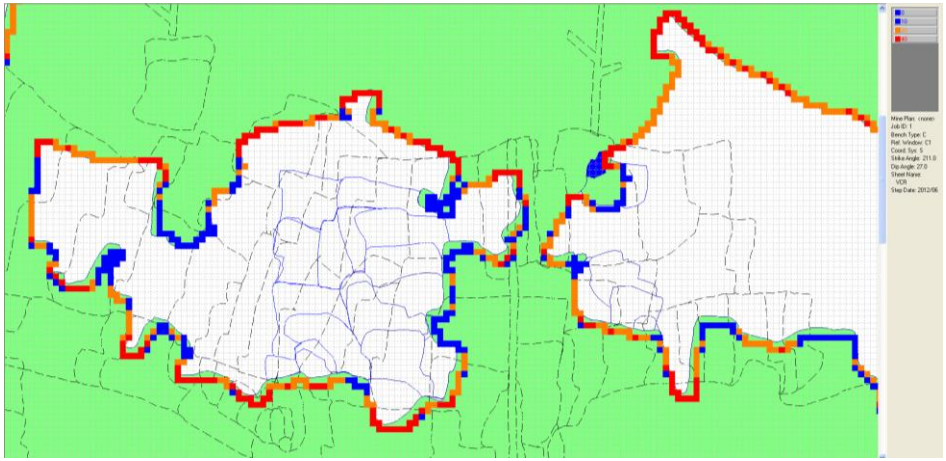
On reef VCR Mining steps:



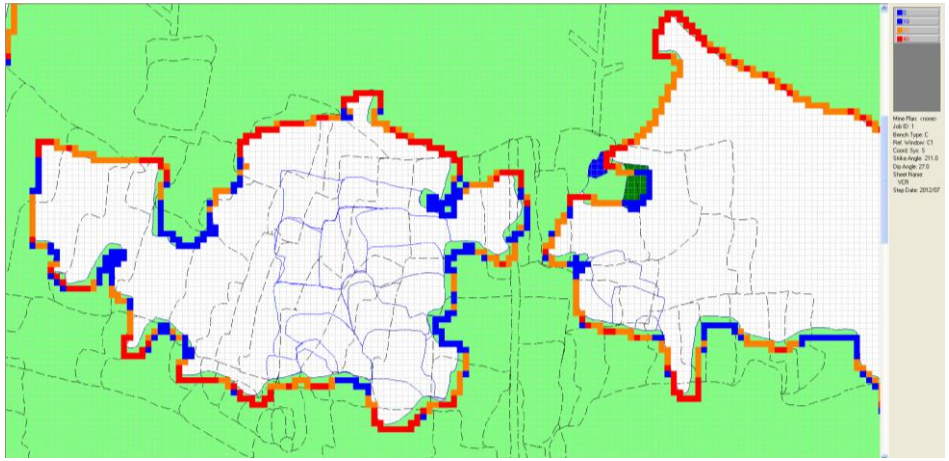
Step 4



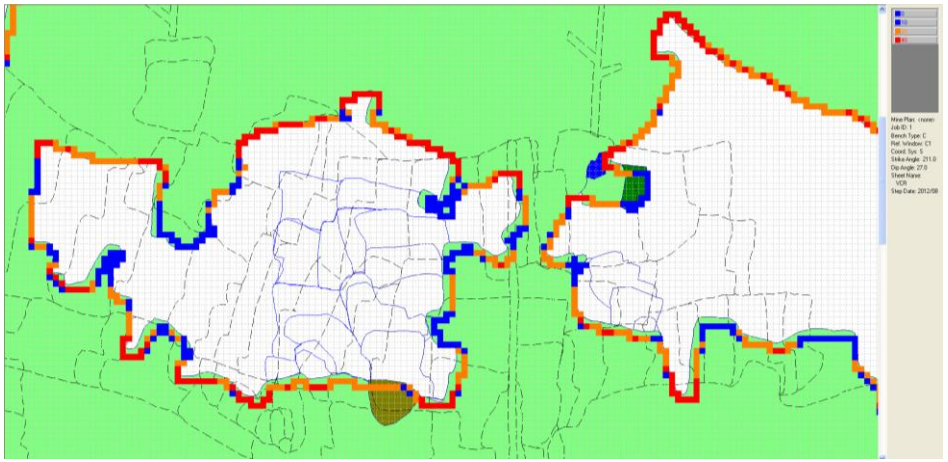
Step 5



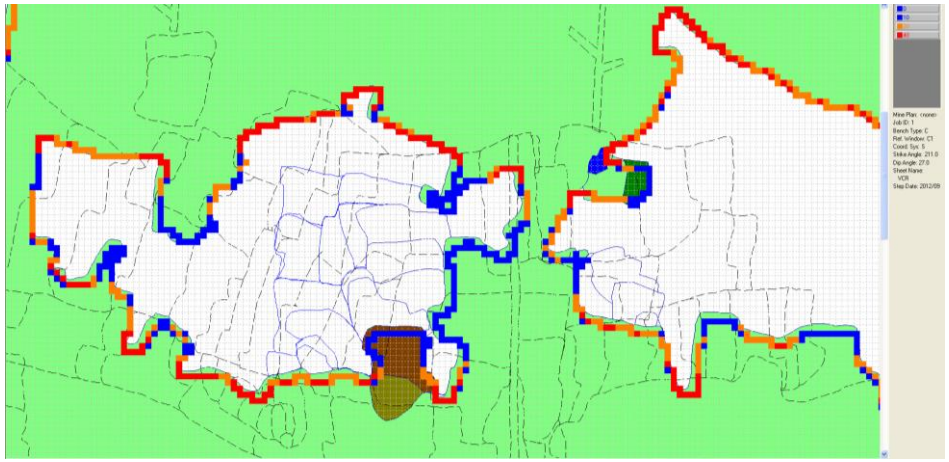
Step 6



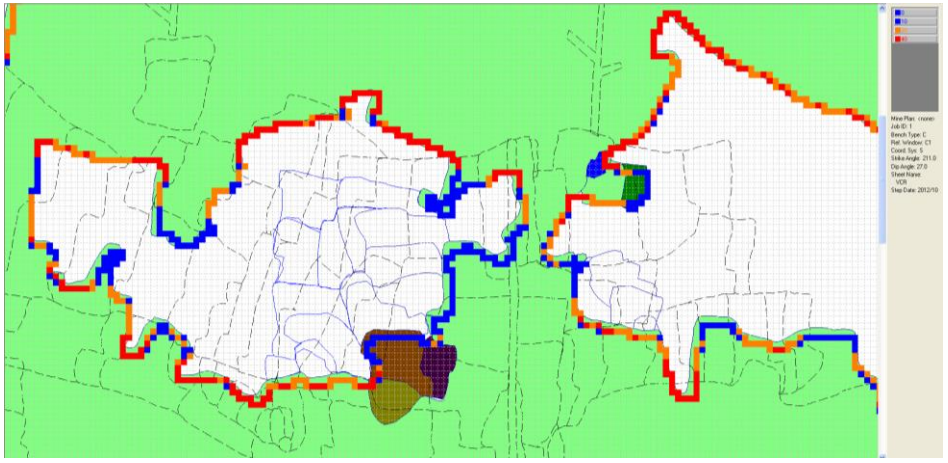
Step 7



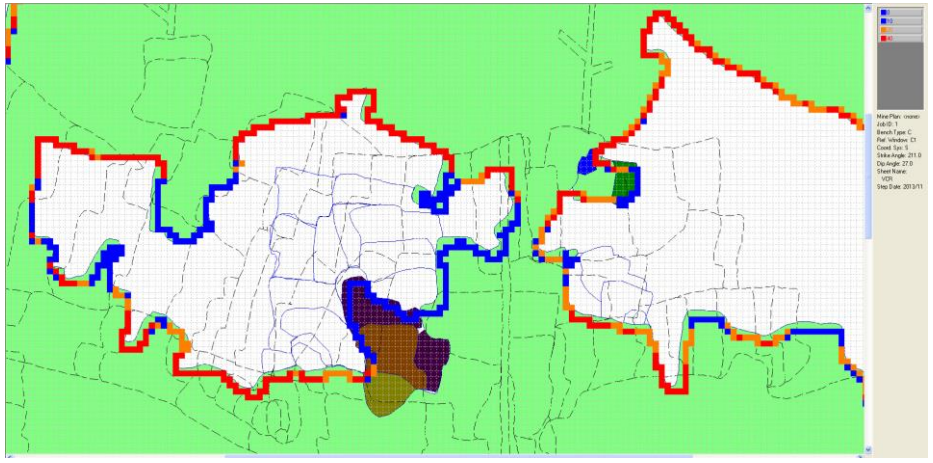
Step 8



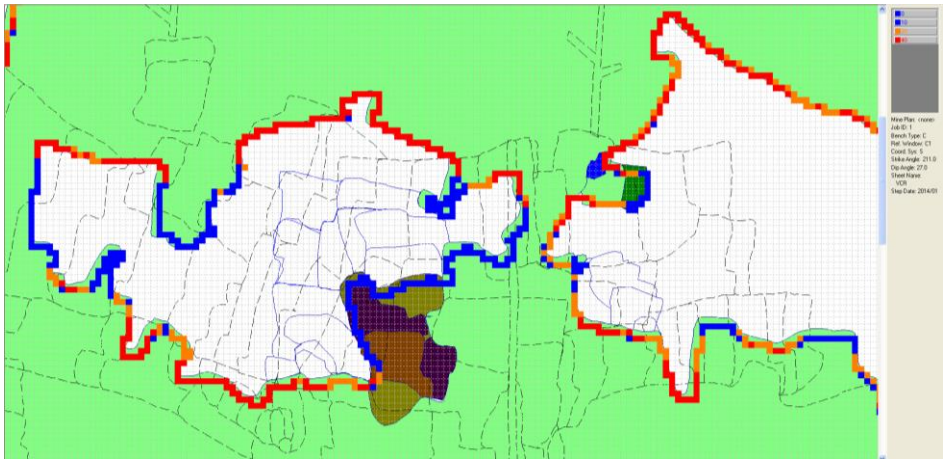
Step 9



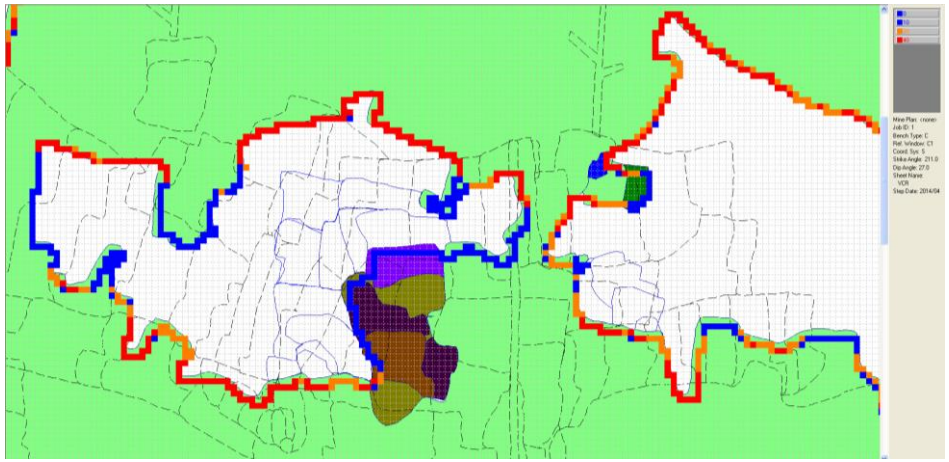
Step 10



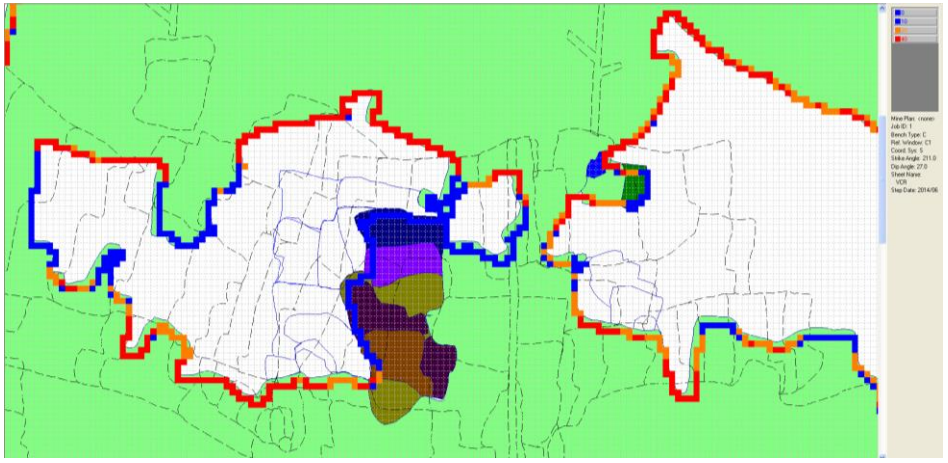
Step 20



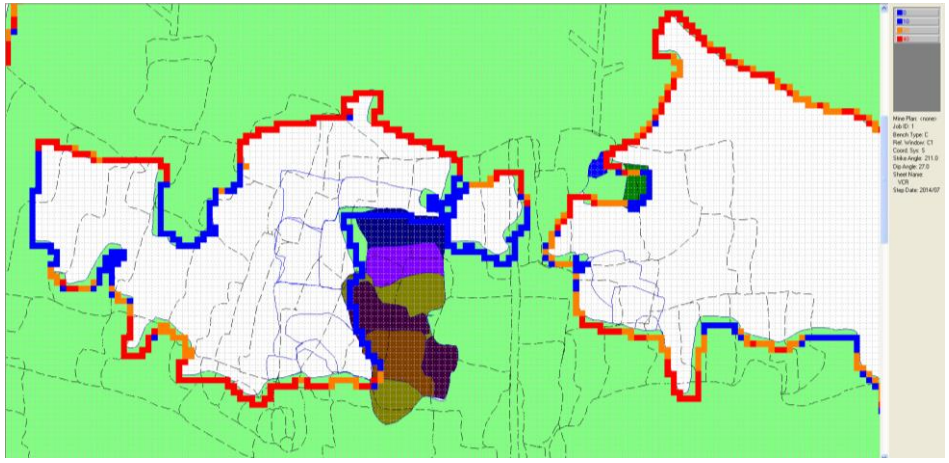
Step 21



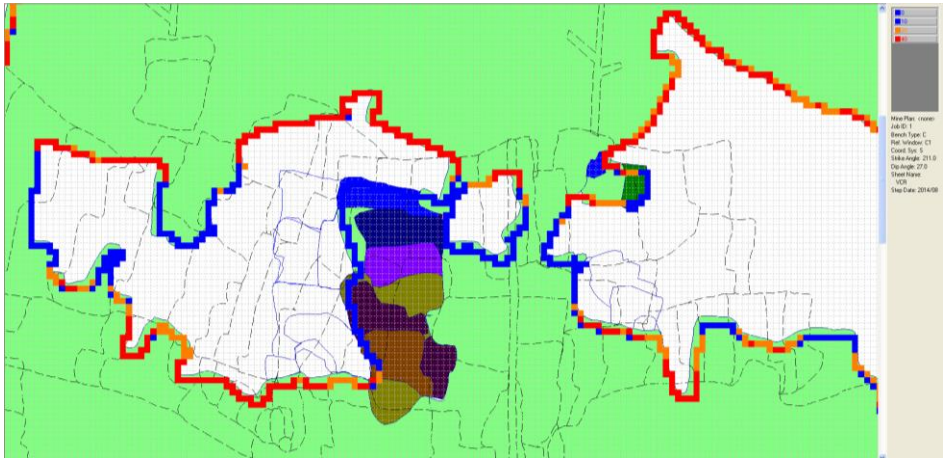
Step 22



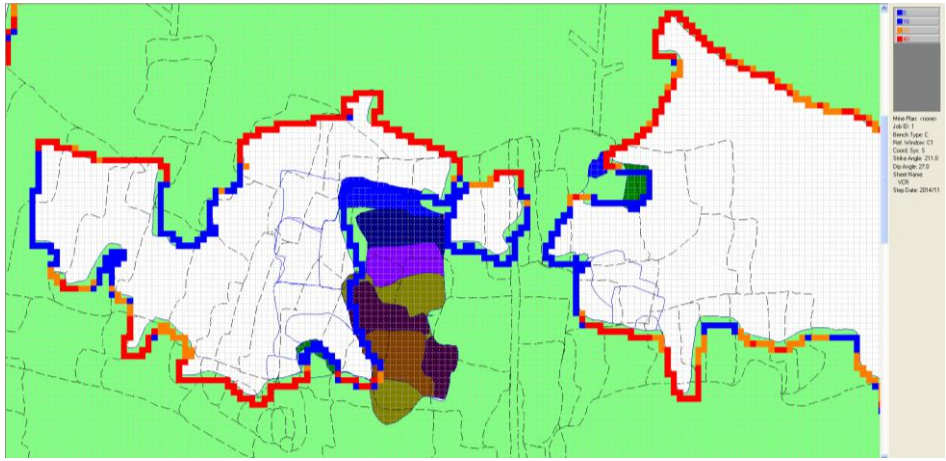
Step 23



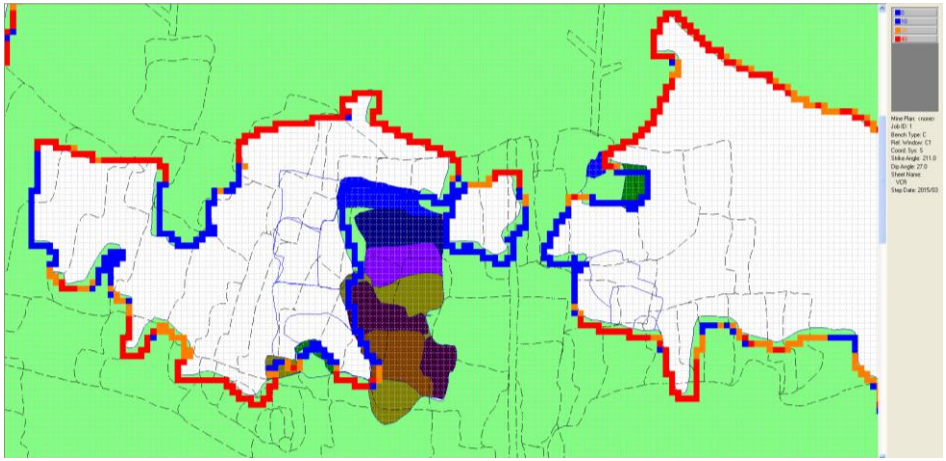
Step 24



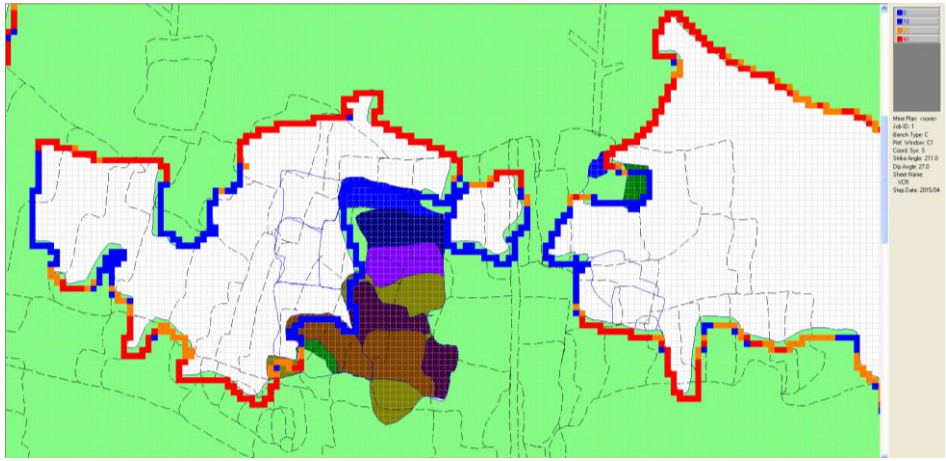
Step 25



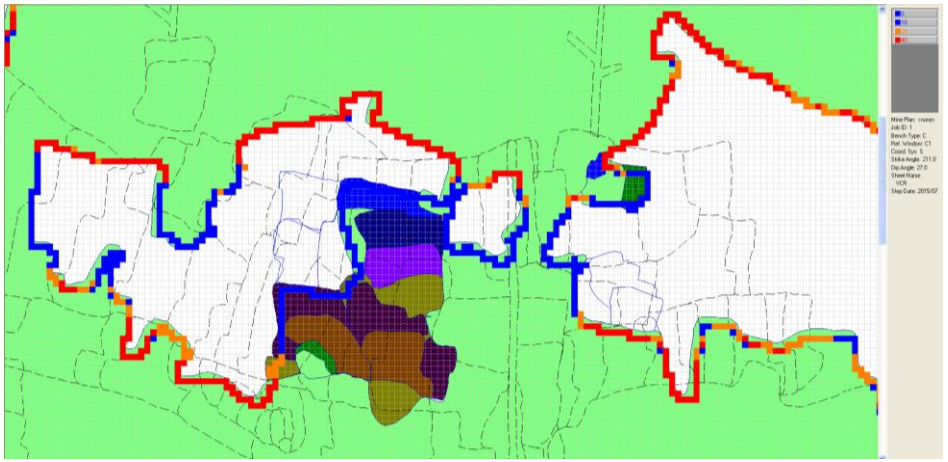
Step 26



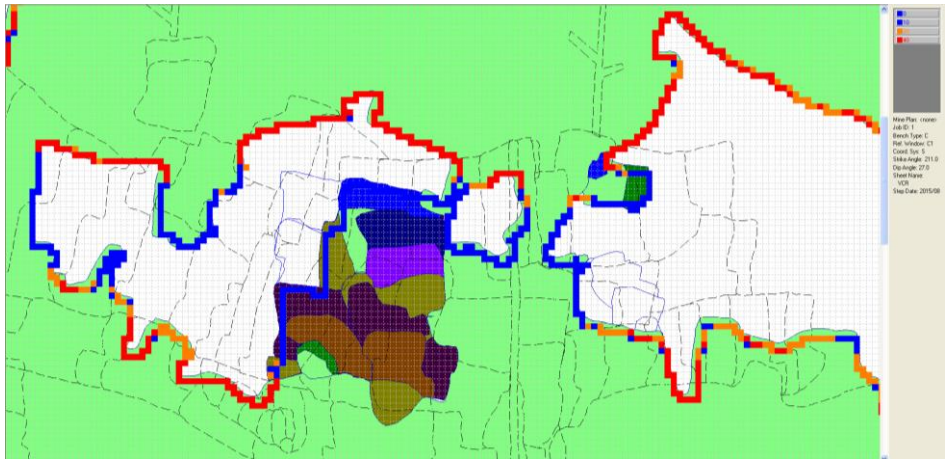
Step 27



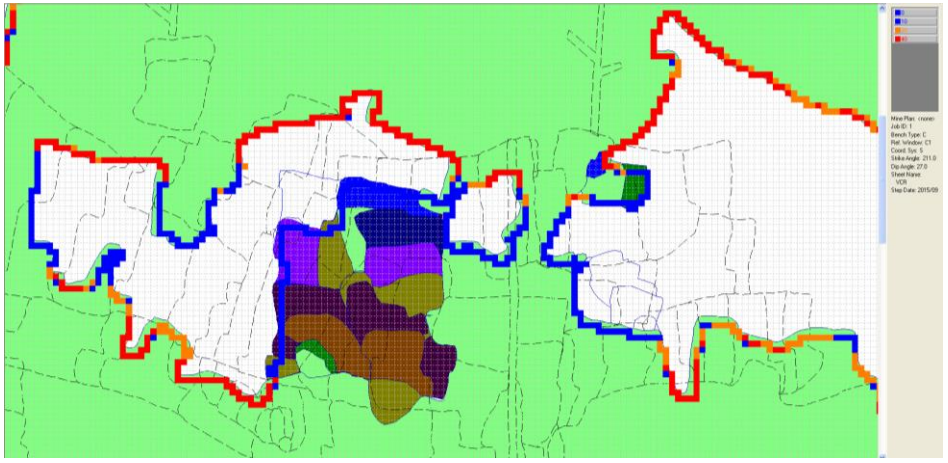
Step 28



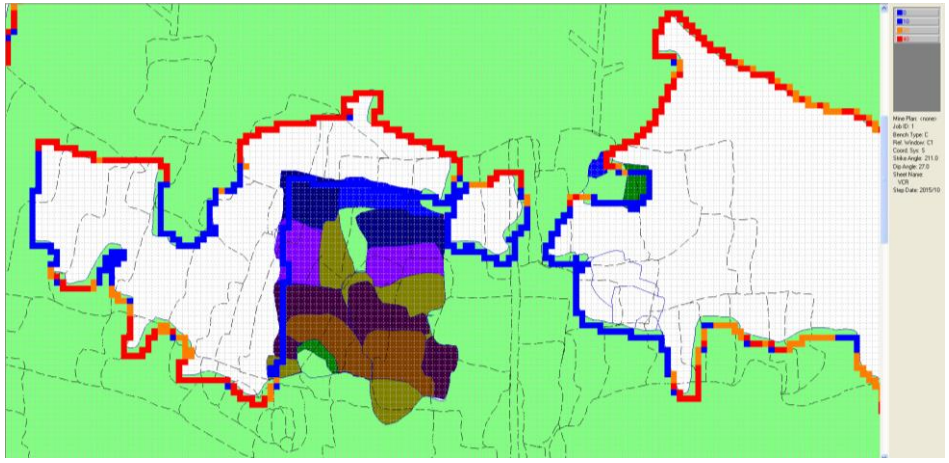
Step 29



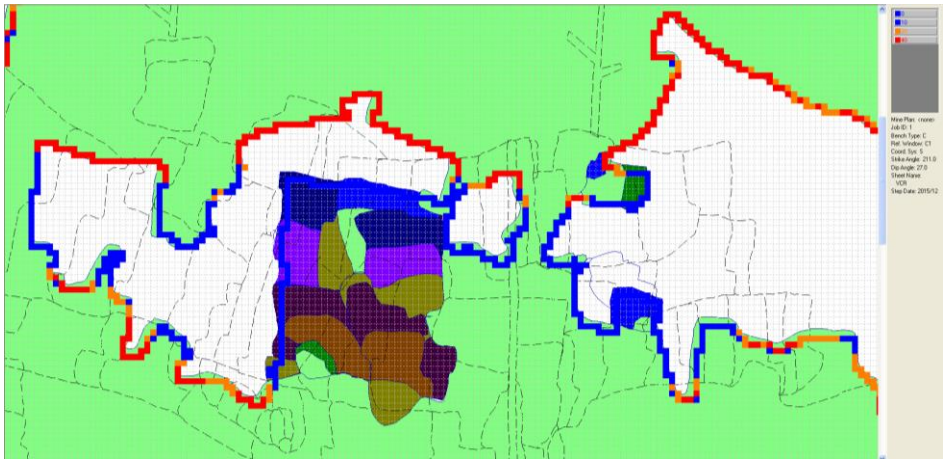
Step 30



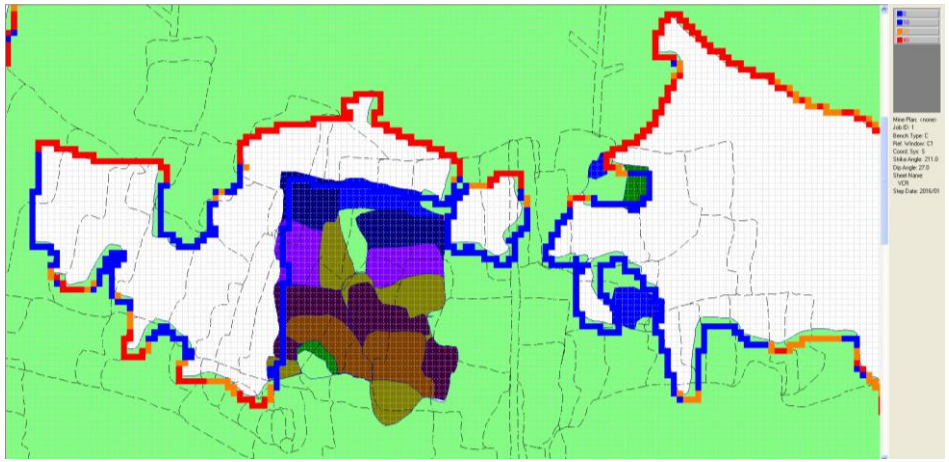
Step 31



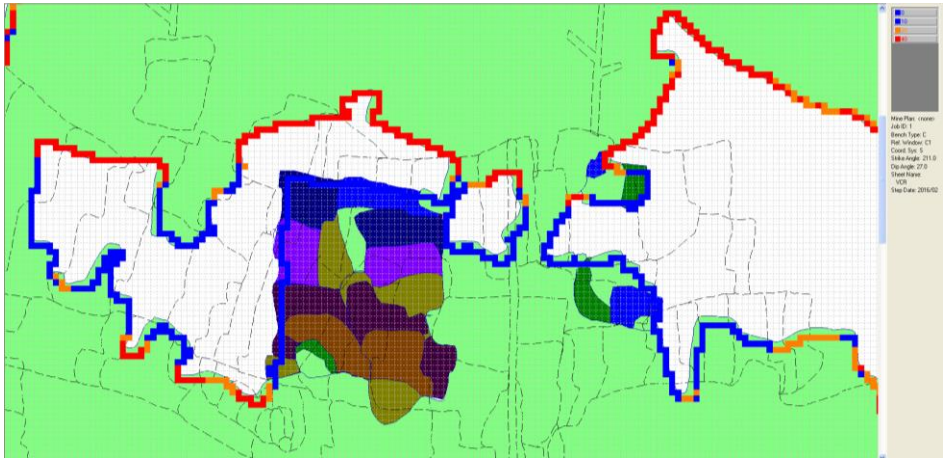
Step 32



Step 34

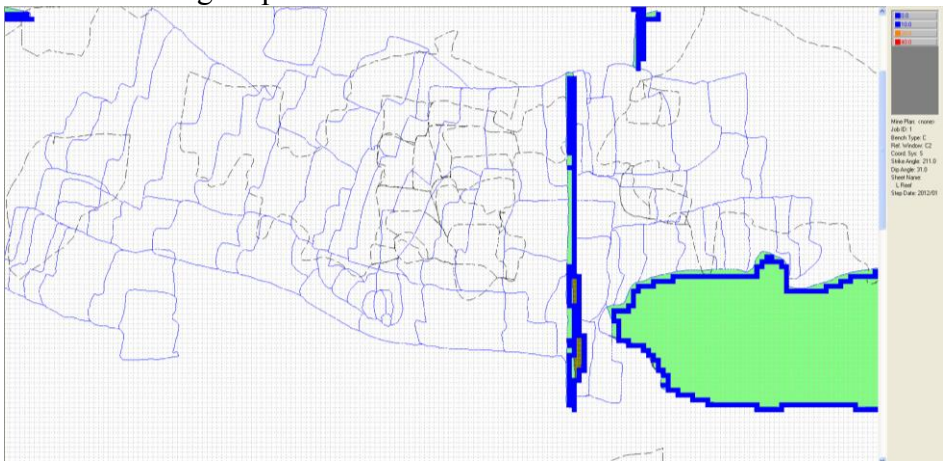


Step 35

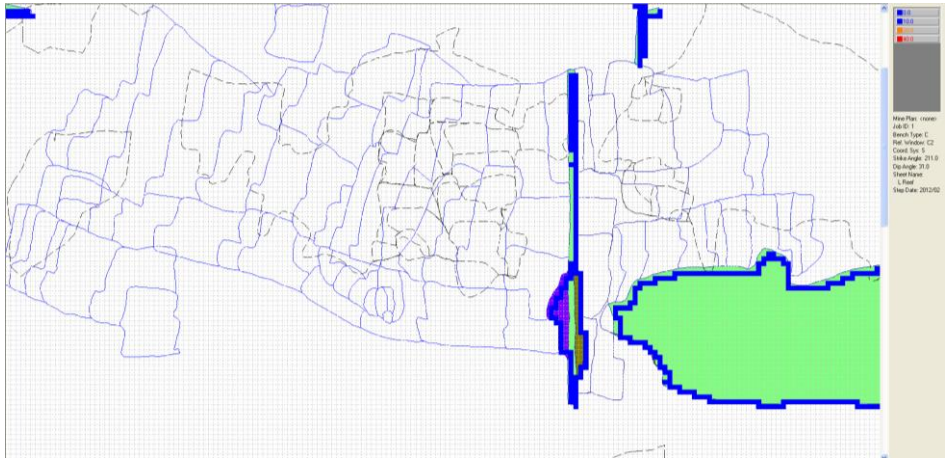


Step 36

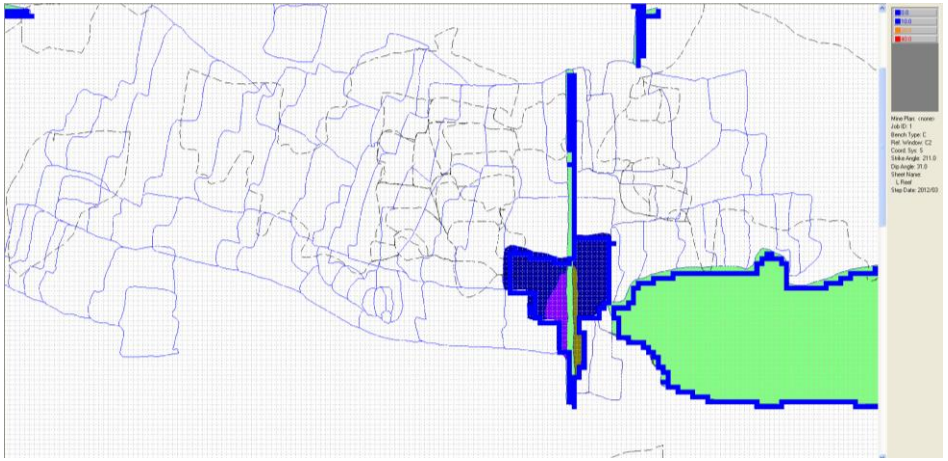
Libanon Mining Steps:



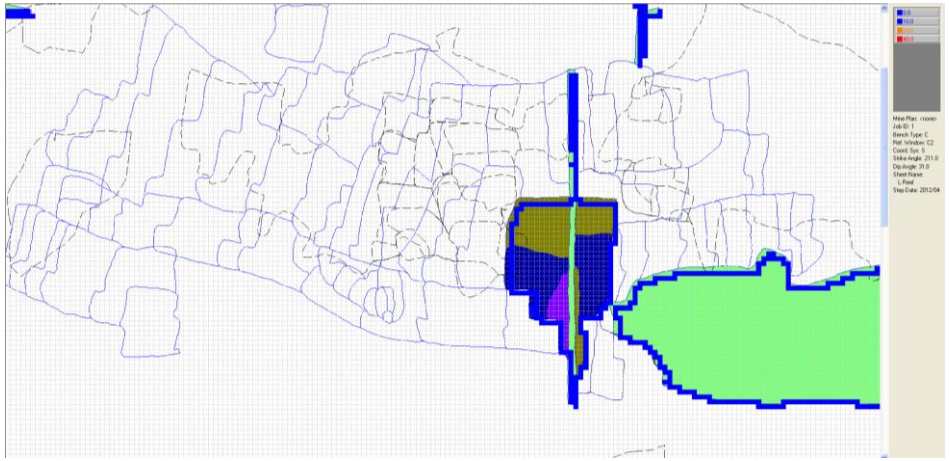
Step 1



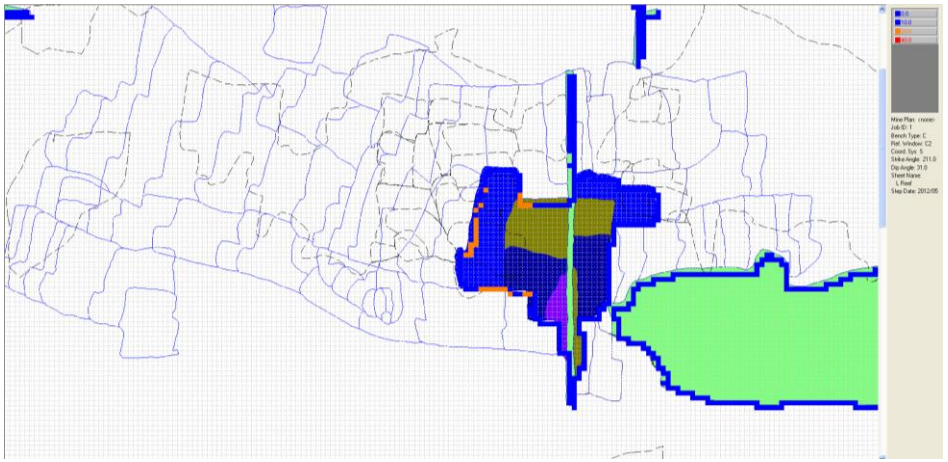
Step 2



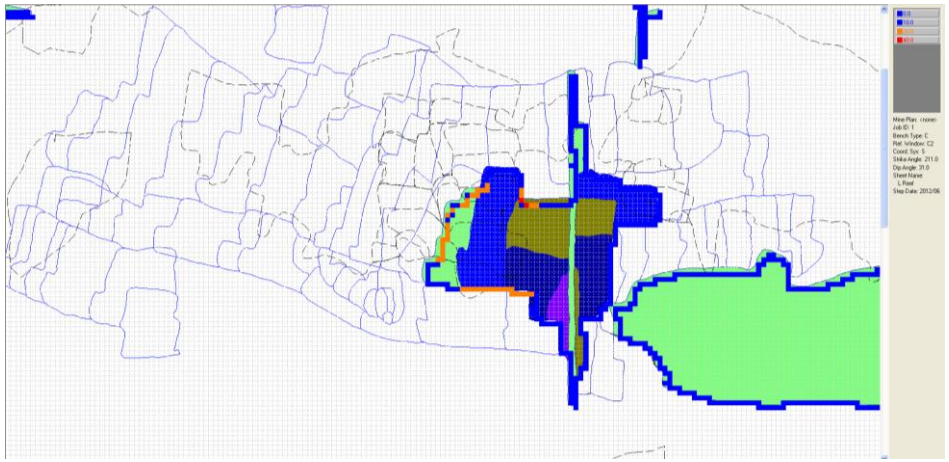
Step 3



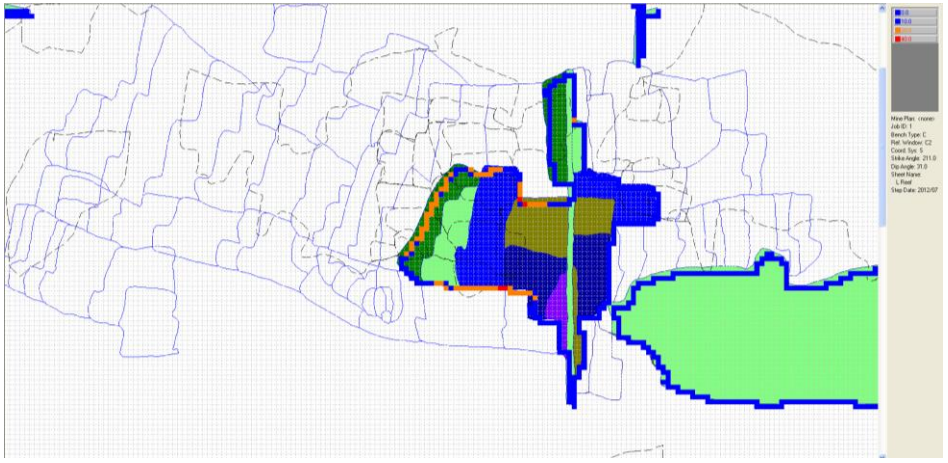
Step 4



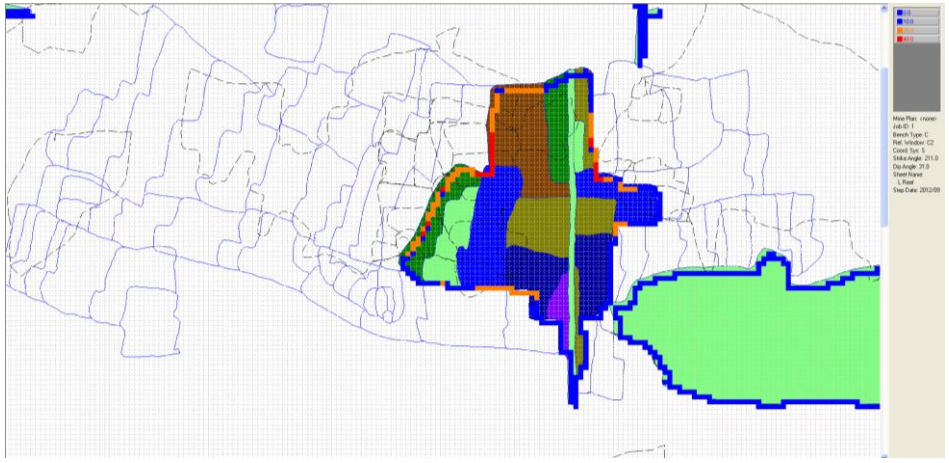
Step 5



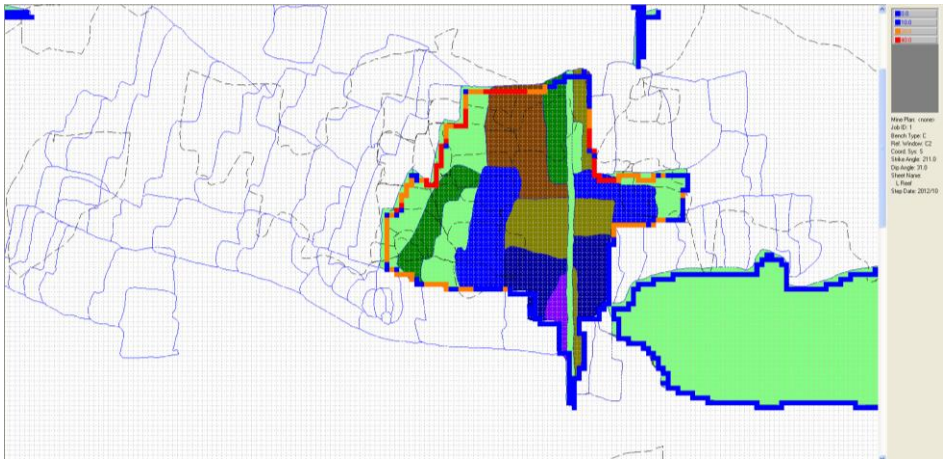
Step 6



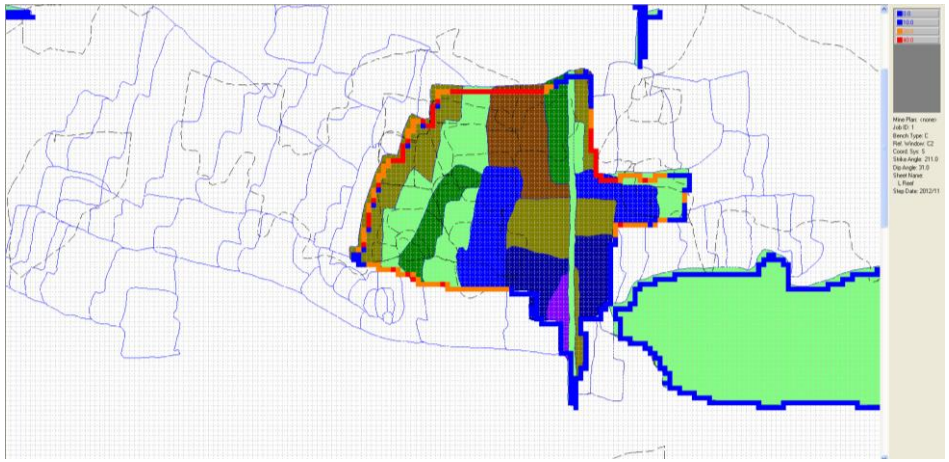
Step 7



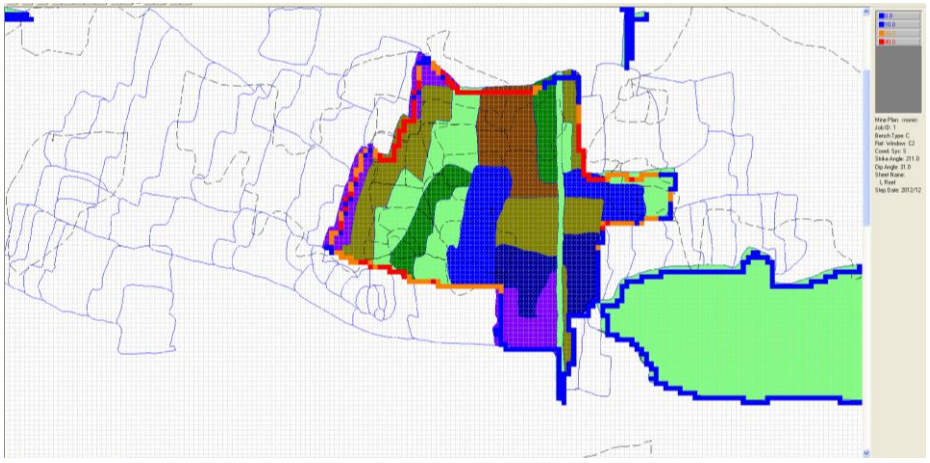
Step 9



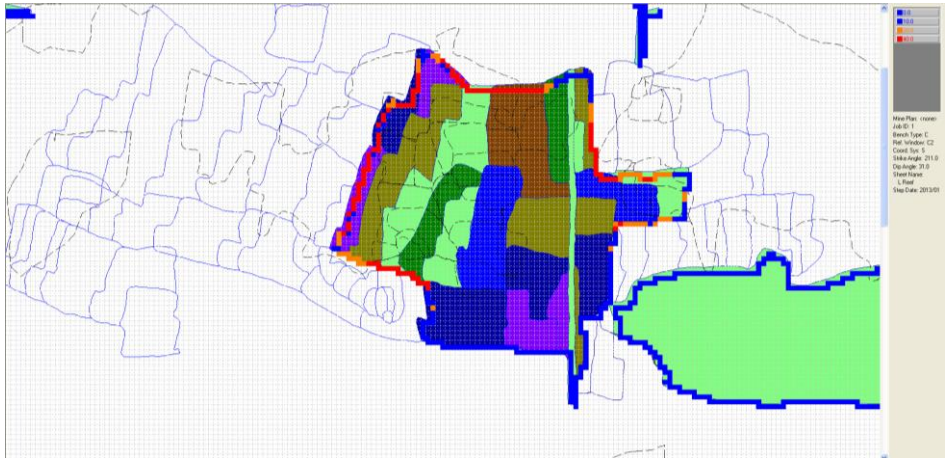
Step 10



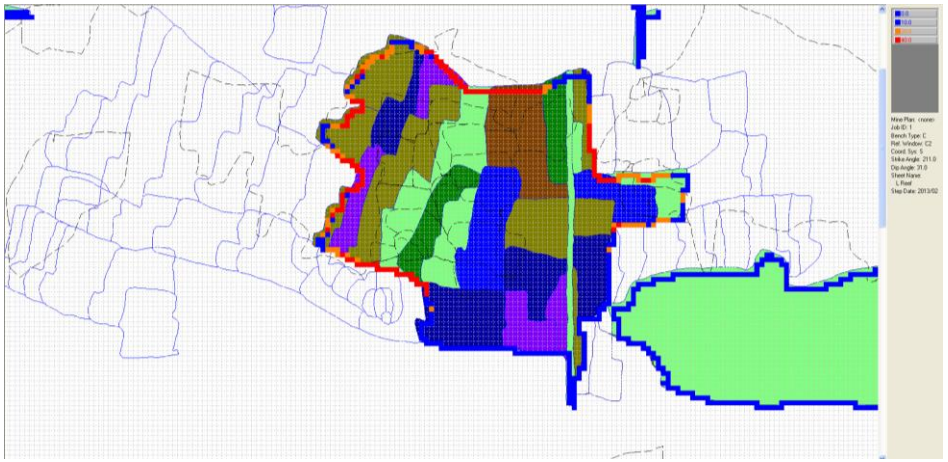
Step11



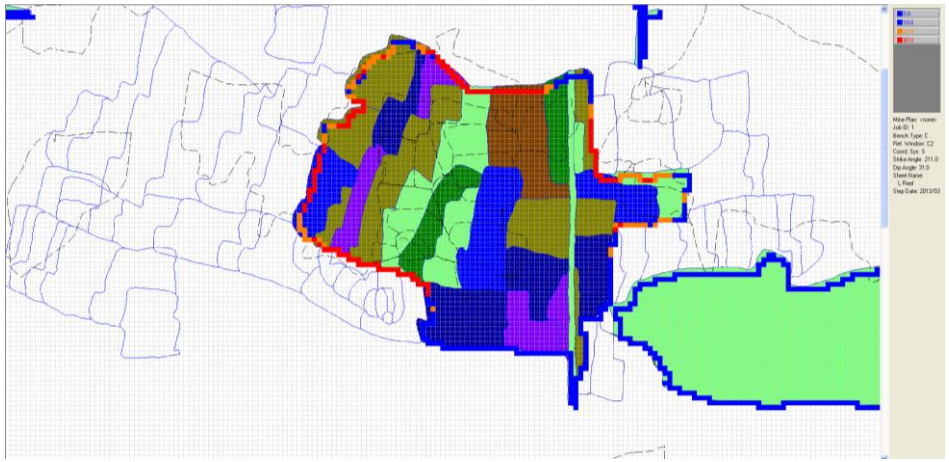
Step 12



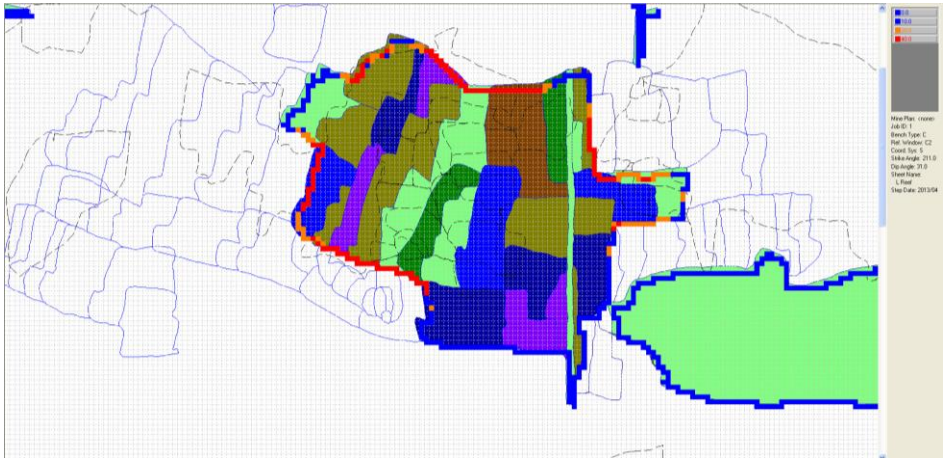
Step 13



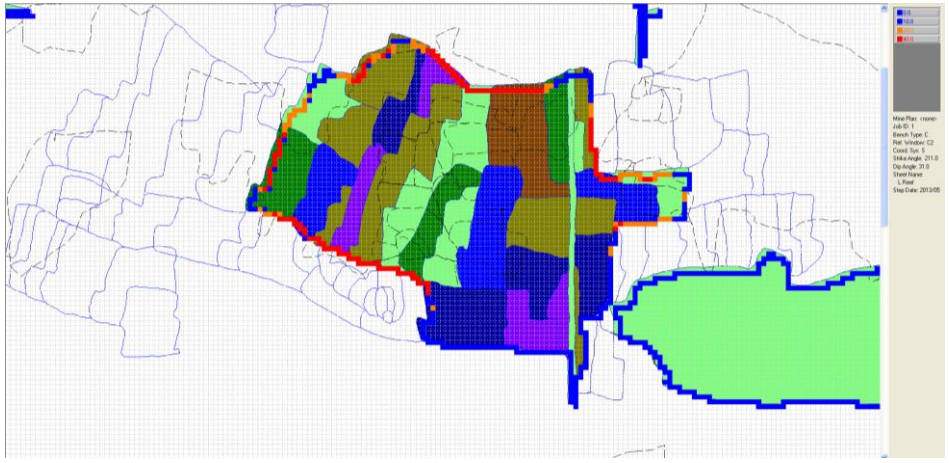
Step 14



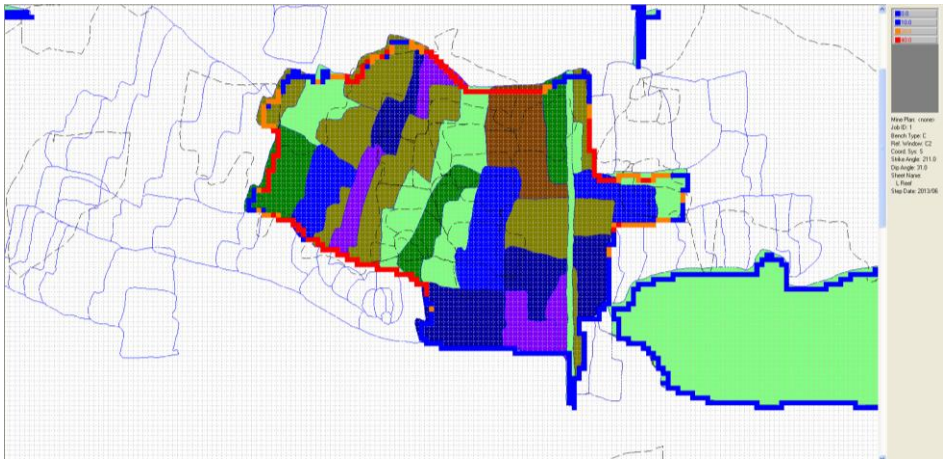
Step 15



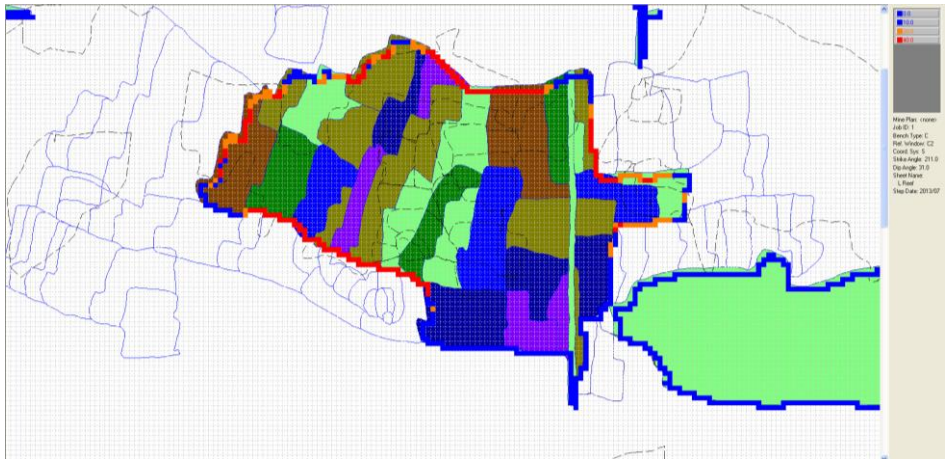
Step 16



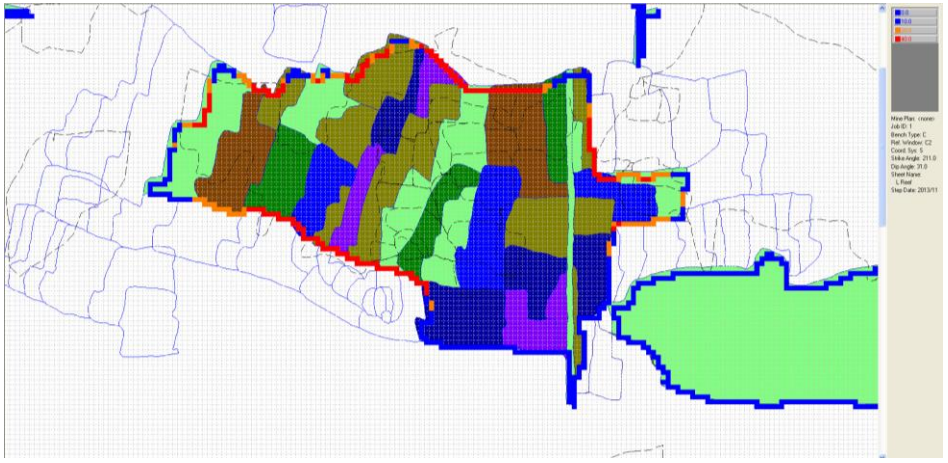
Step 17



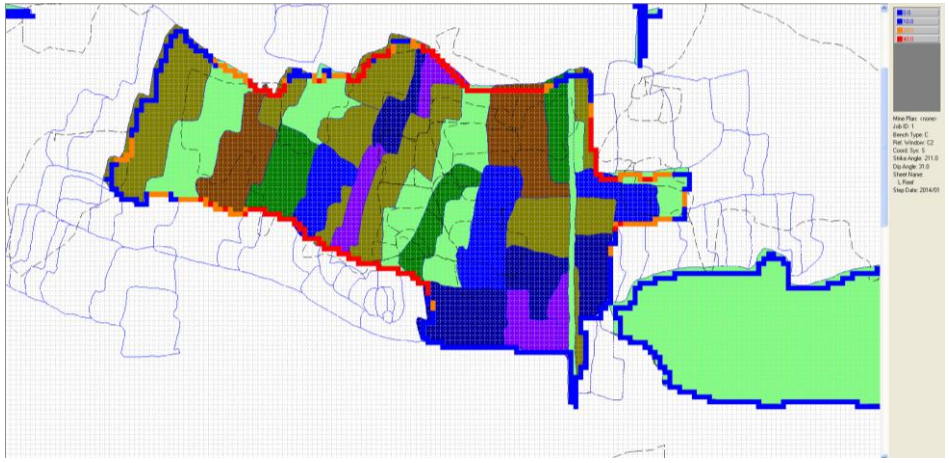
Step 18



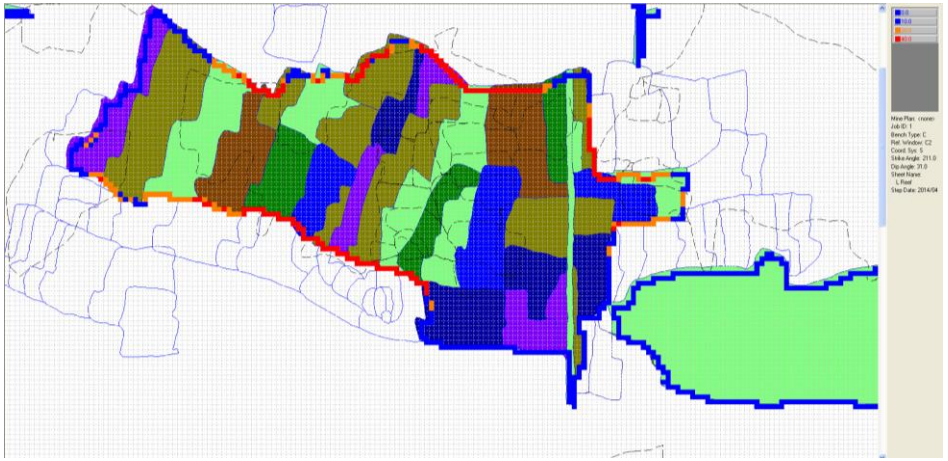
Step 19



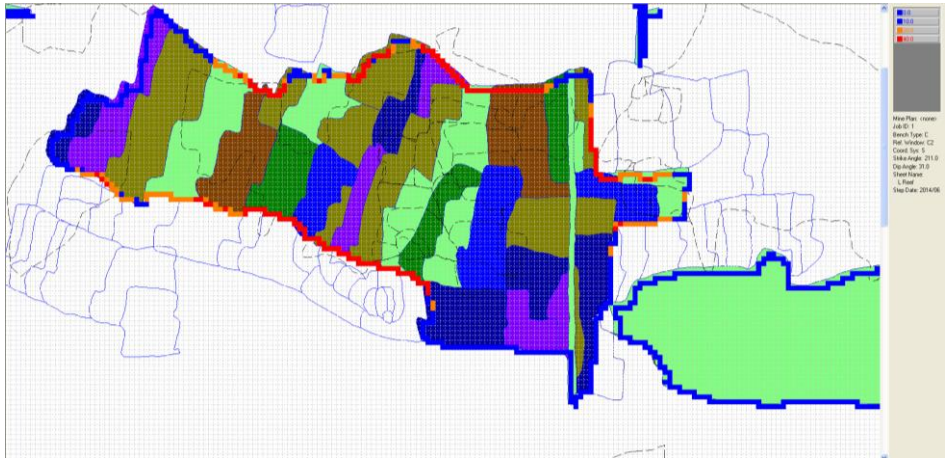
Step 20



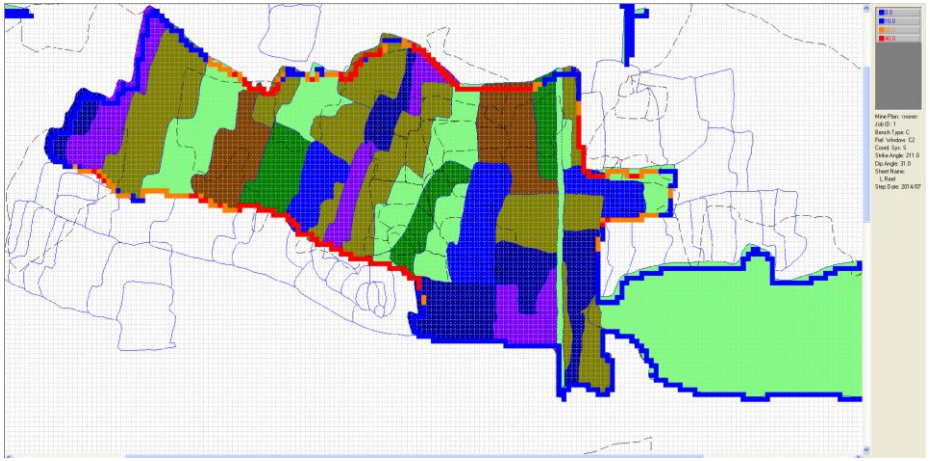
Step21



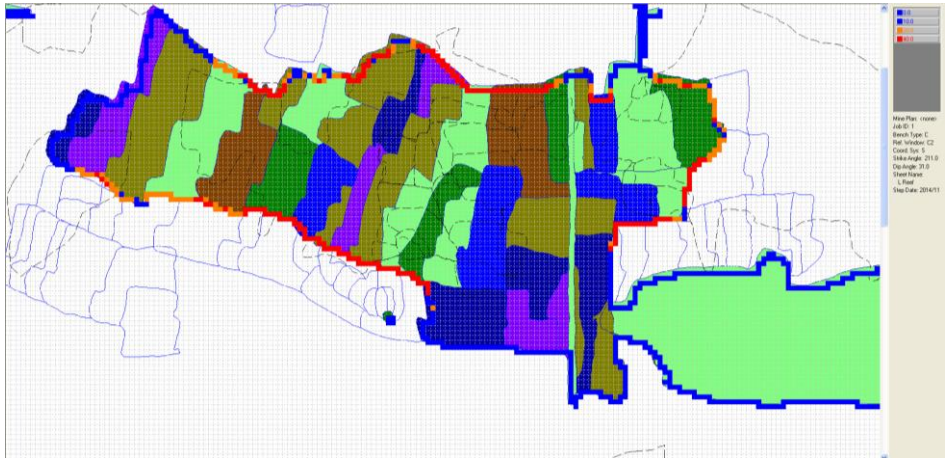
Step 22



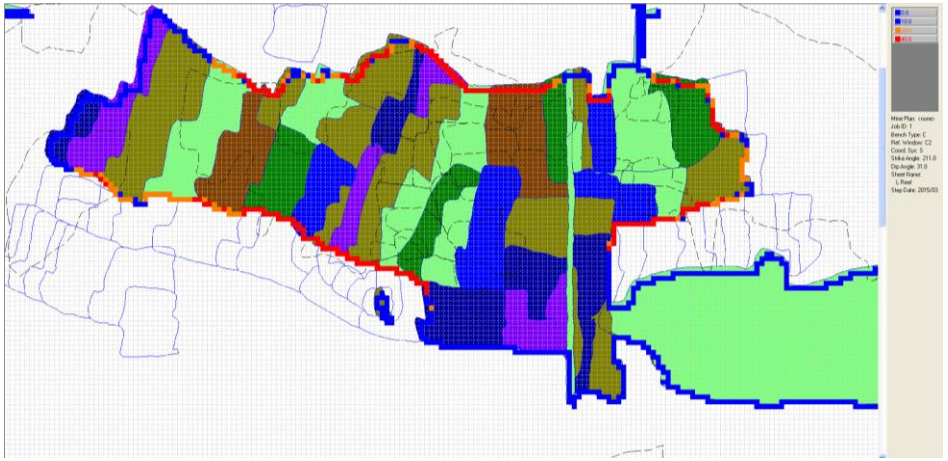
Step23



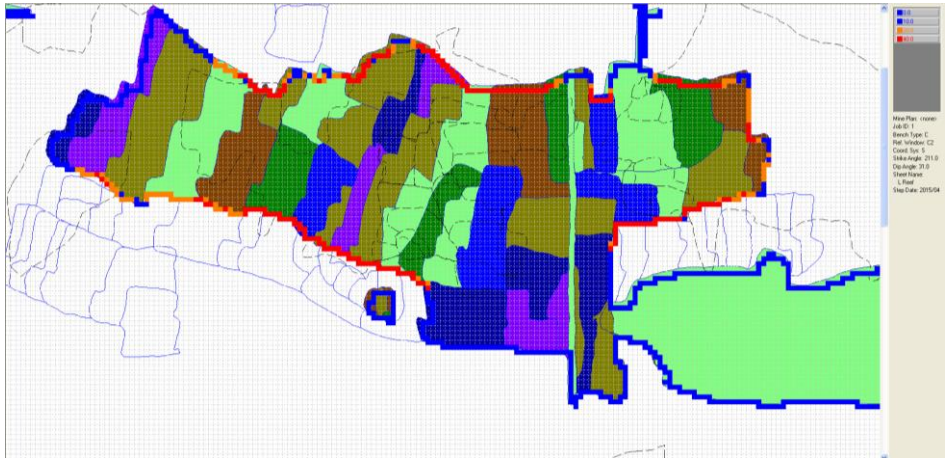
Step 24



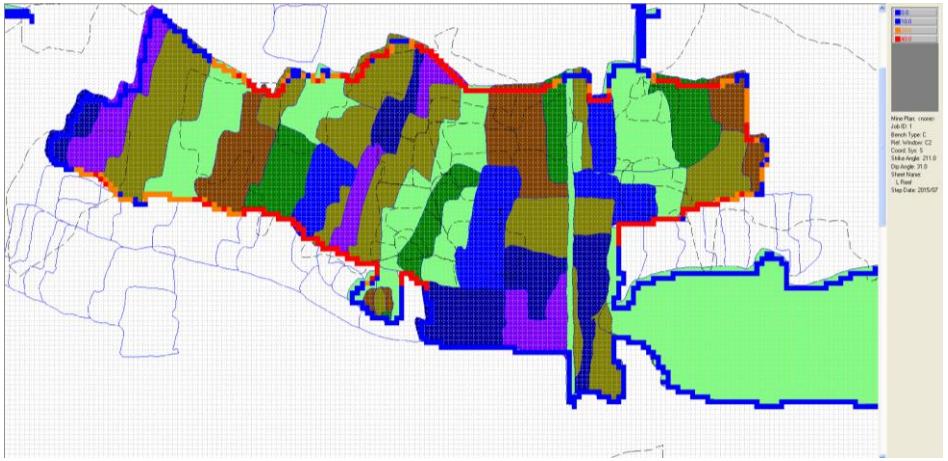
Step26



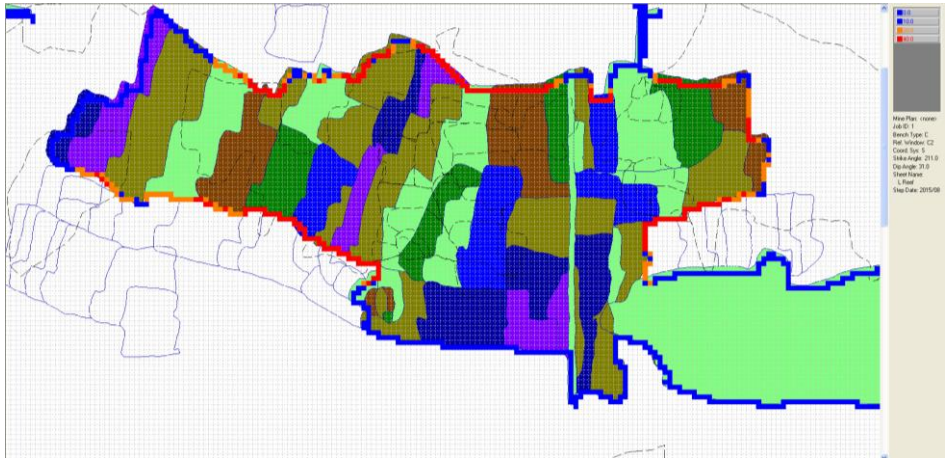
Step 27



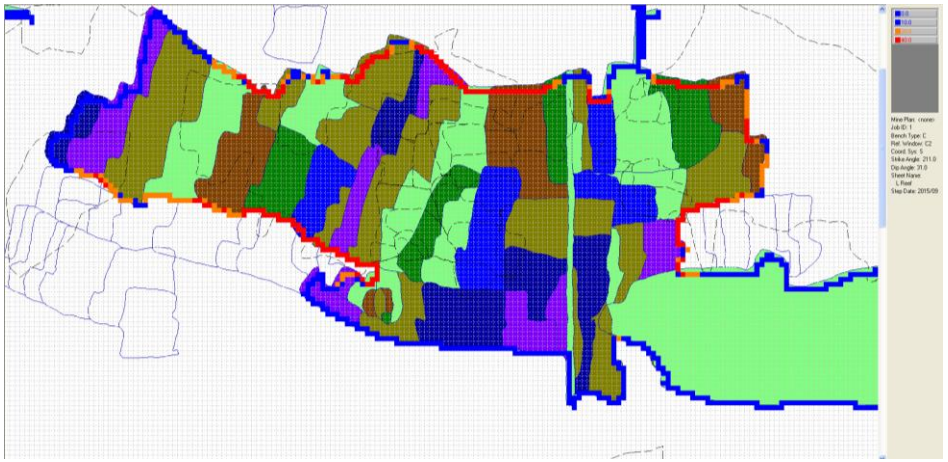
Step28



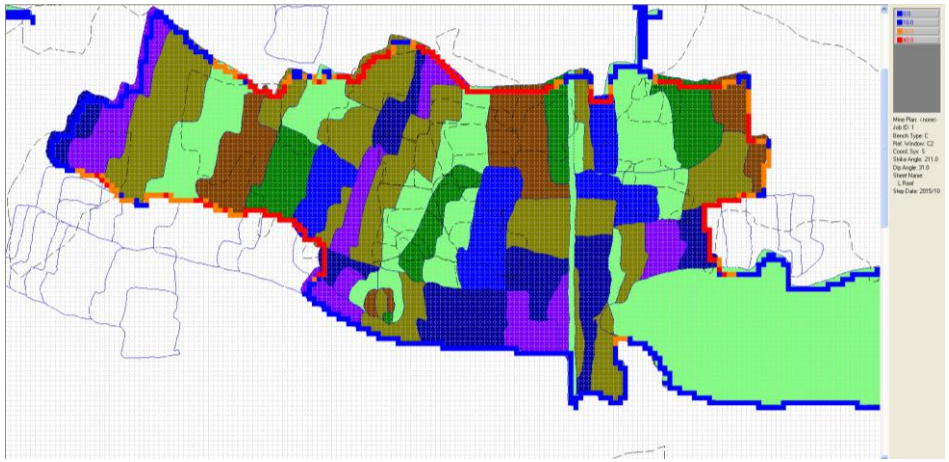
Step 29



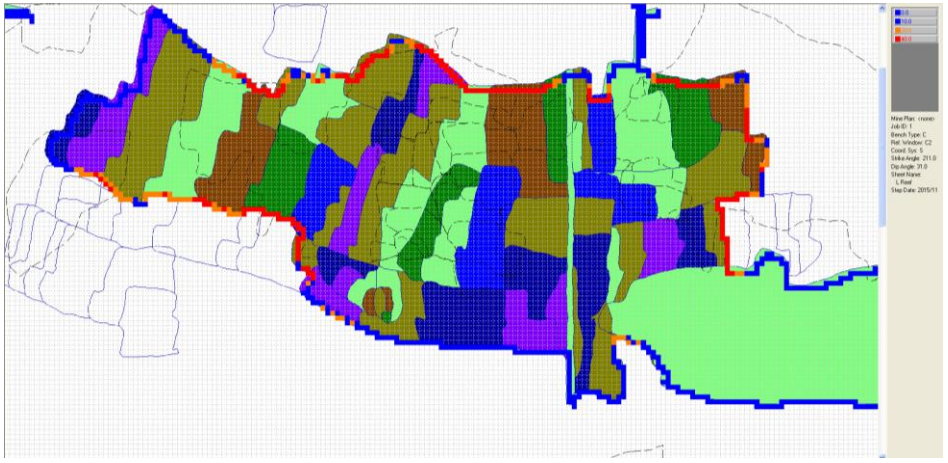
Step 30



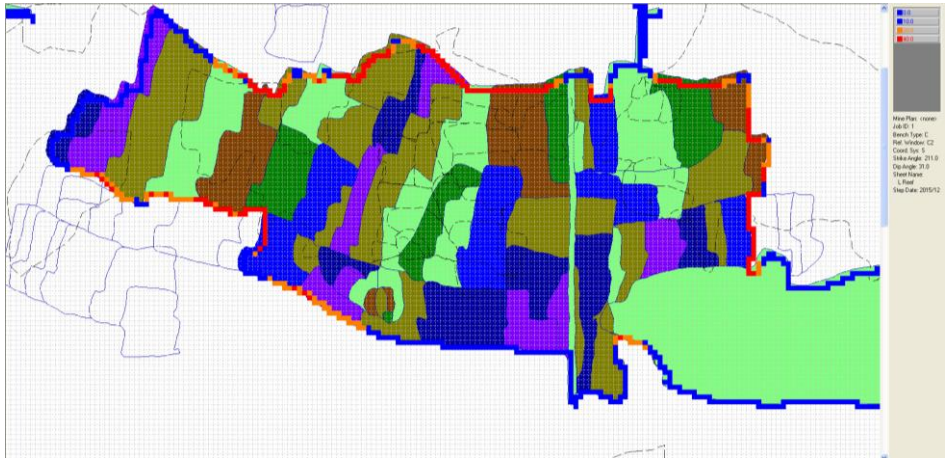
Step 31



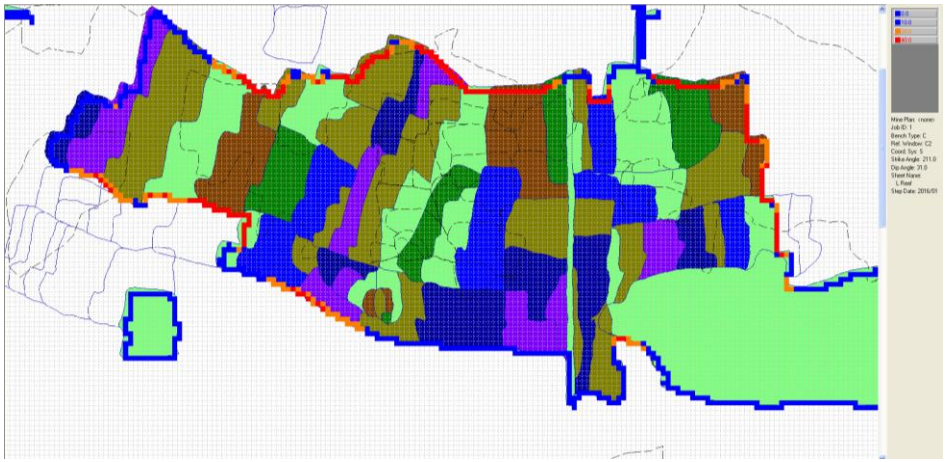
Step32



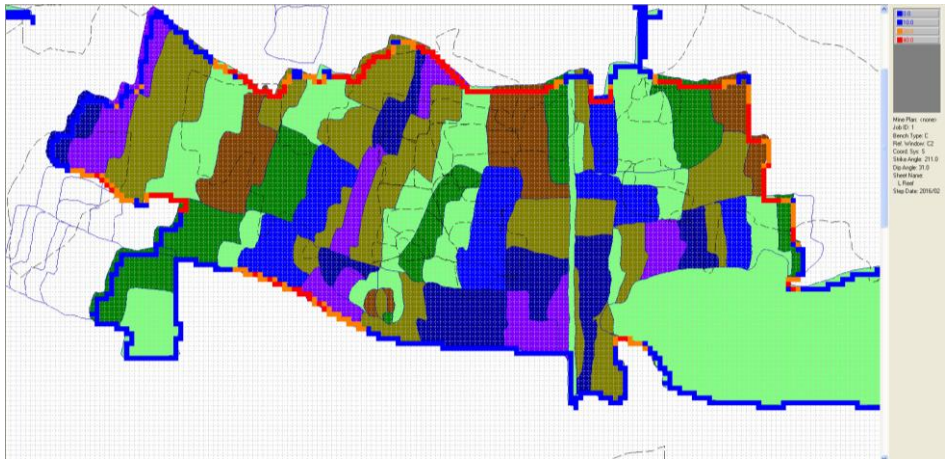
Step 33



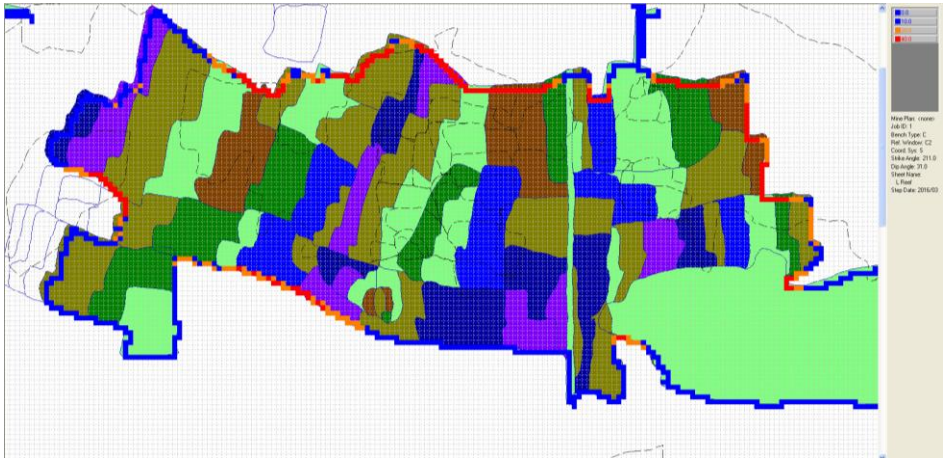
Step34



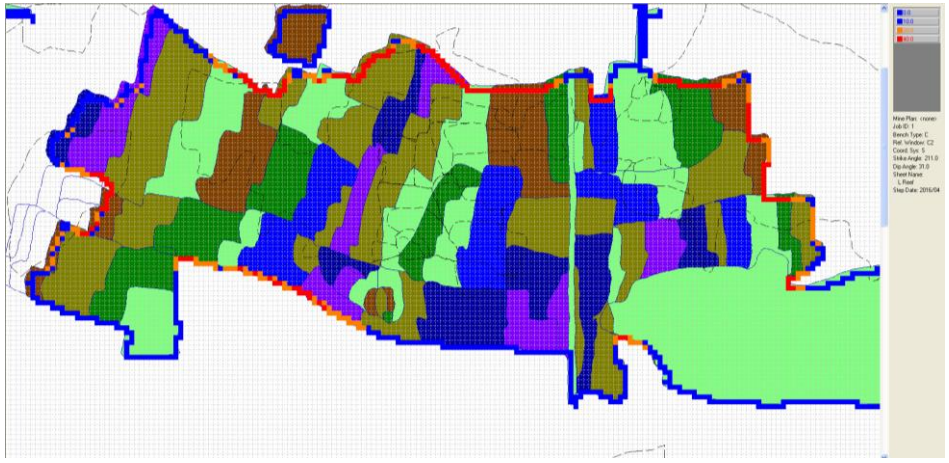
Step 35



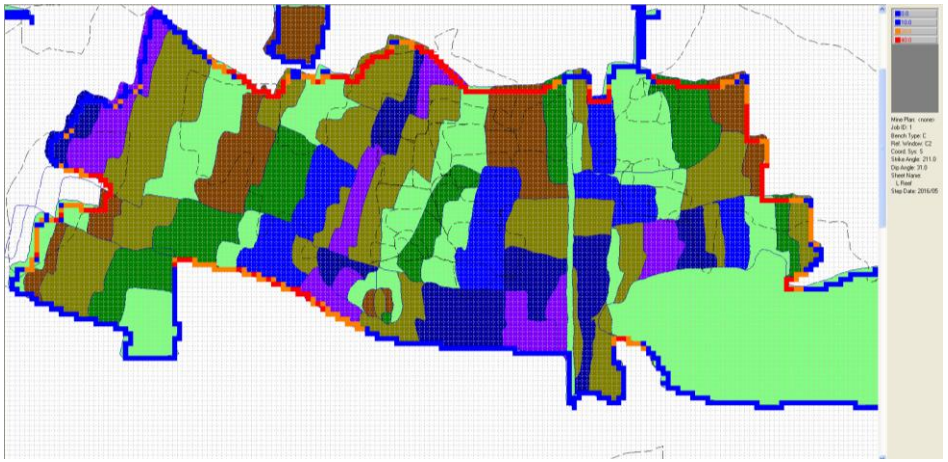
Step 36



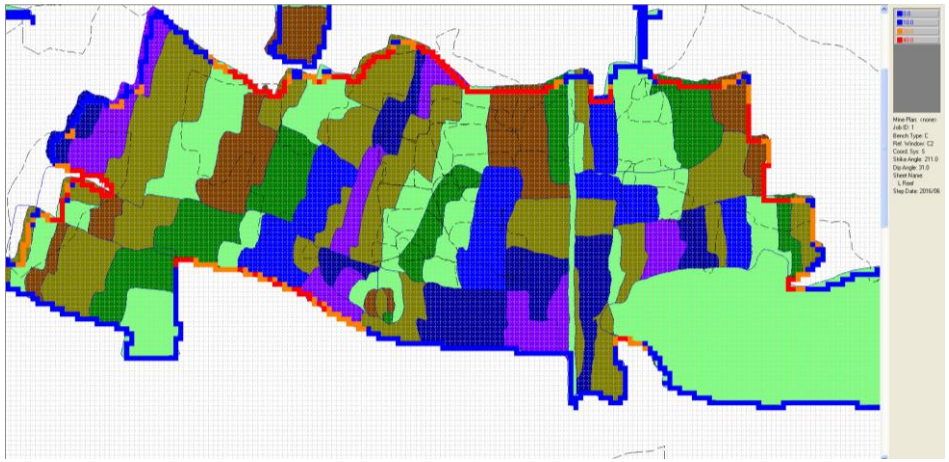
Step 37



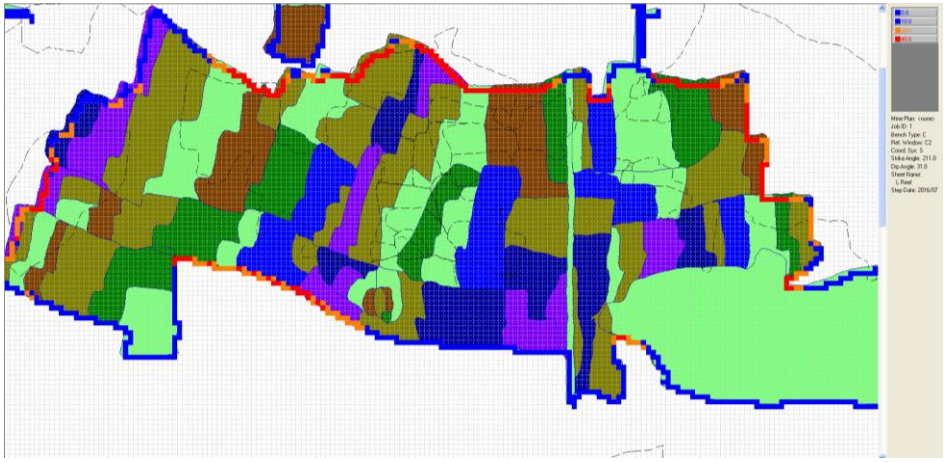
Step38



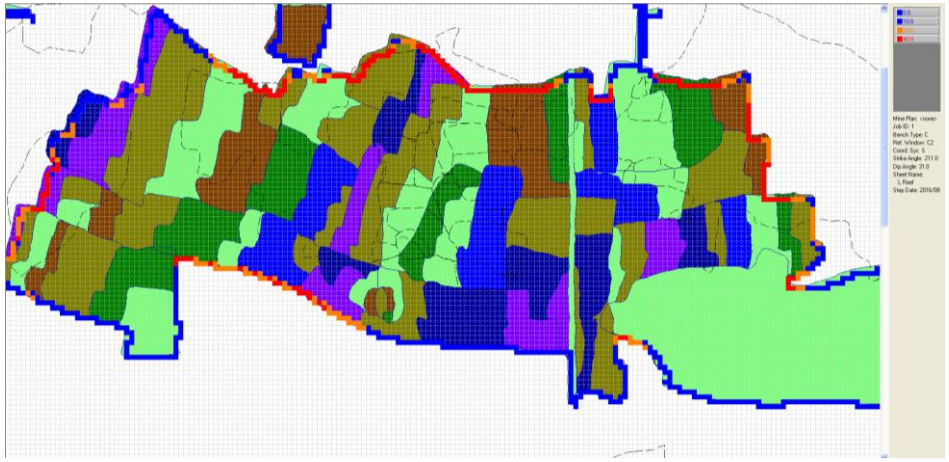
Step 39



Step 40



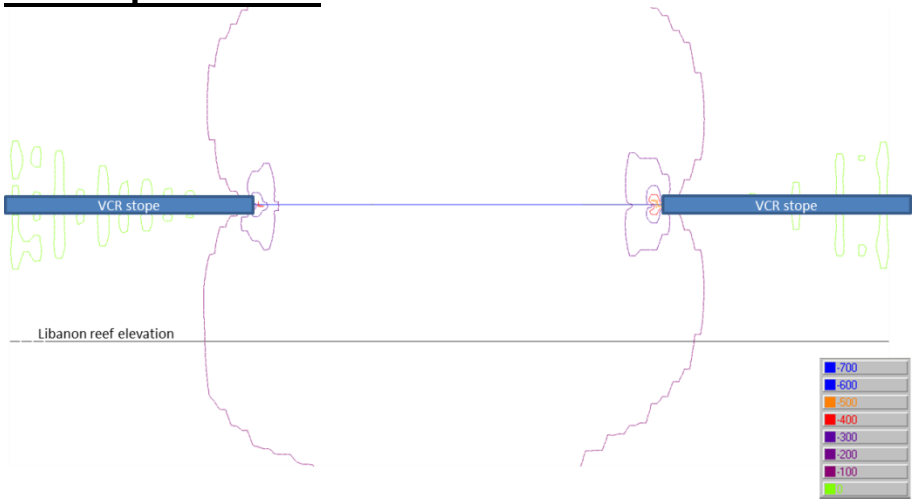
Step 41



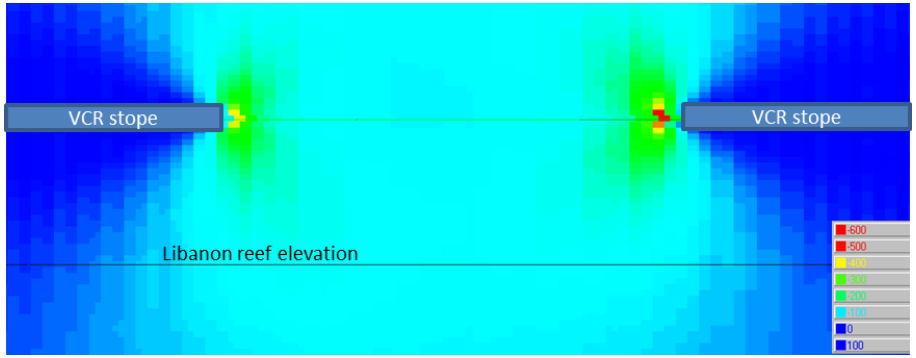
Step 42

Location of Section A-A’ on Libonon reef elevation
Location of Section B-B’ on VCR elevation

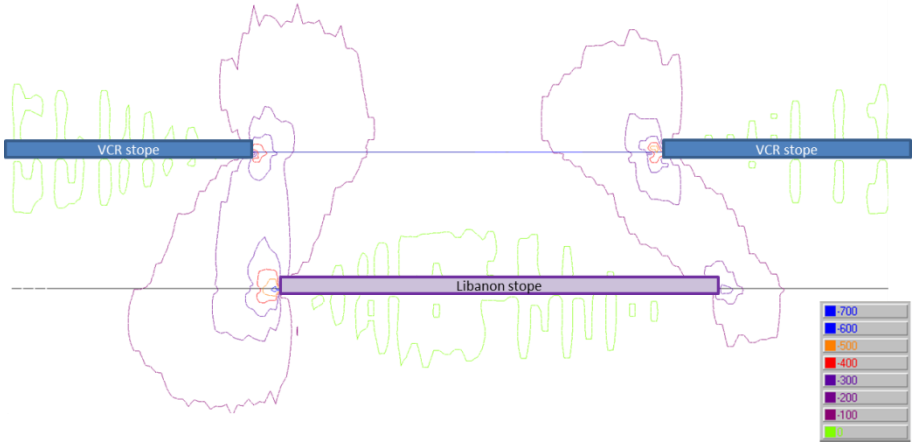
Section plot of A-A'



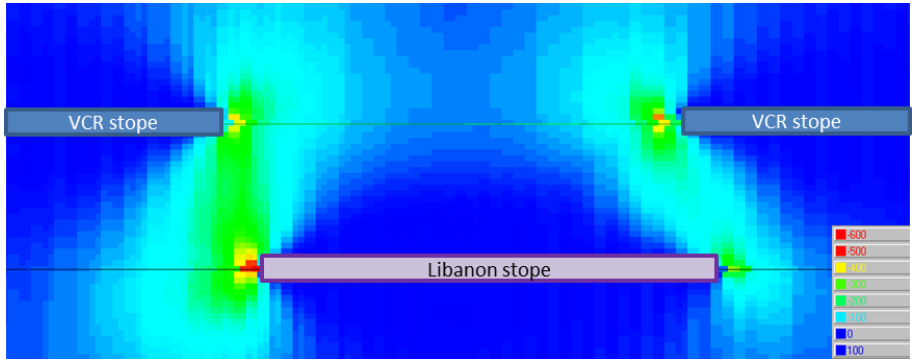
Contour plot of Step 6



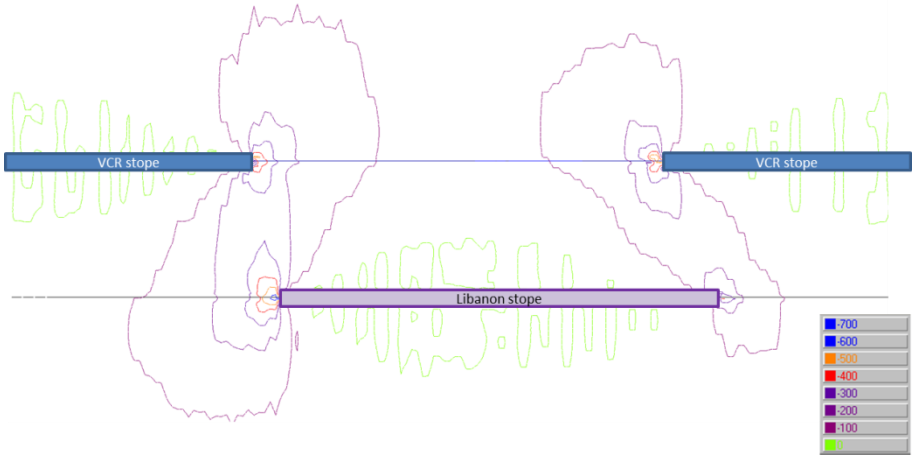
Contour map of Step 6



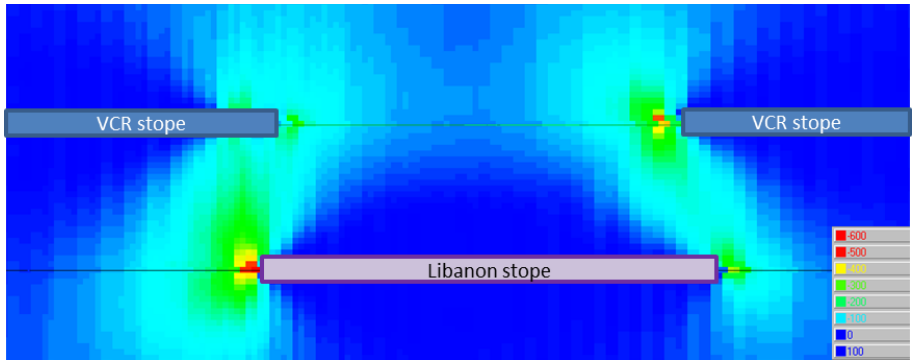
Contour plot of Step 19



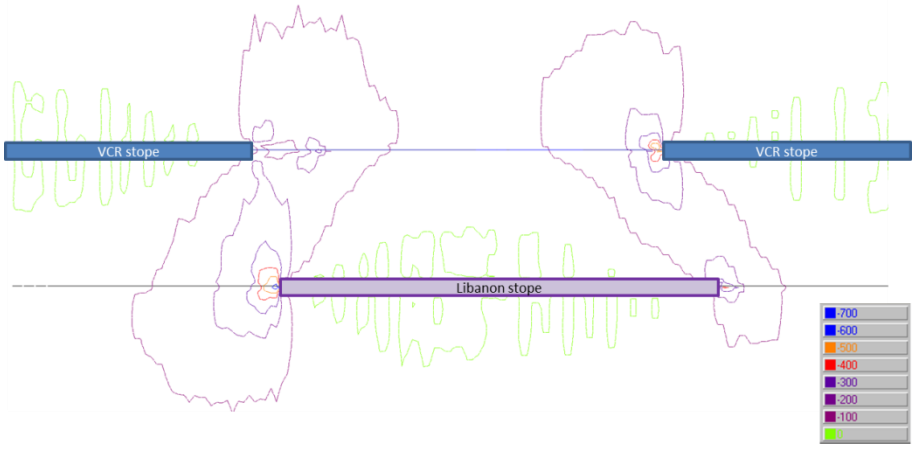
Contour map of Step 19



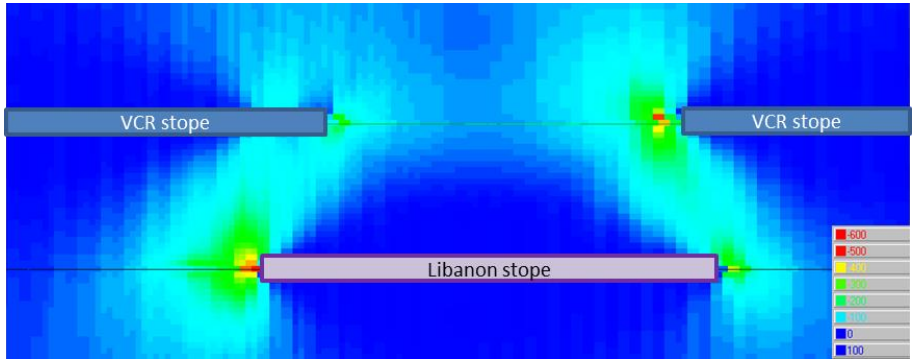
Contour plot of Step 26



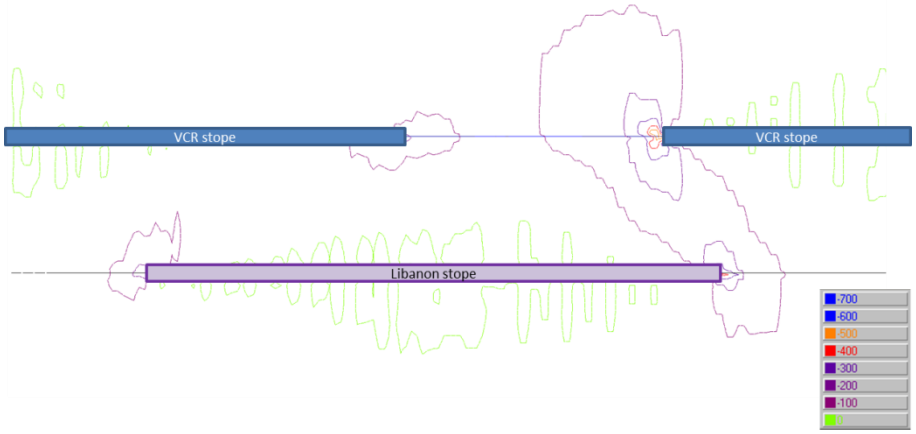
Contour map of Step 26



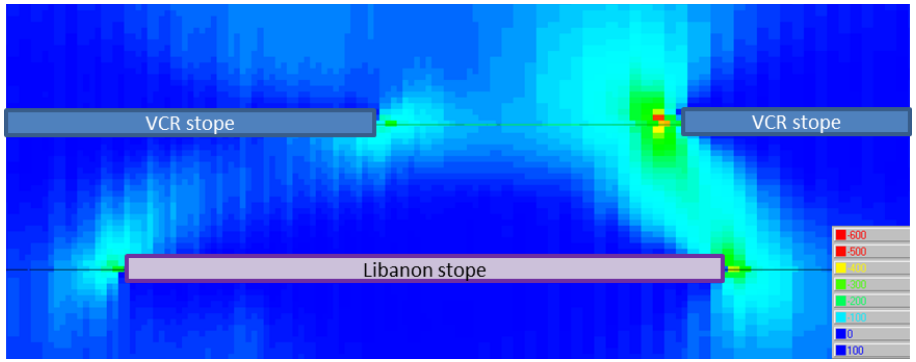
Contour plot of Step 28



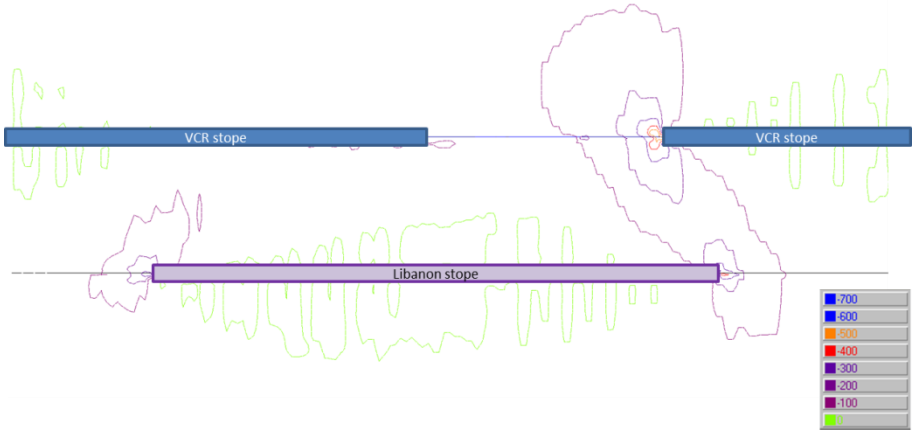
Contour map of Step 28



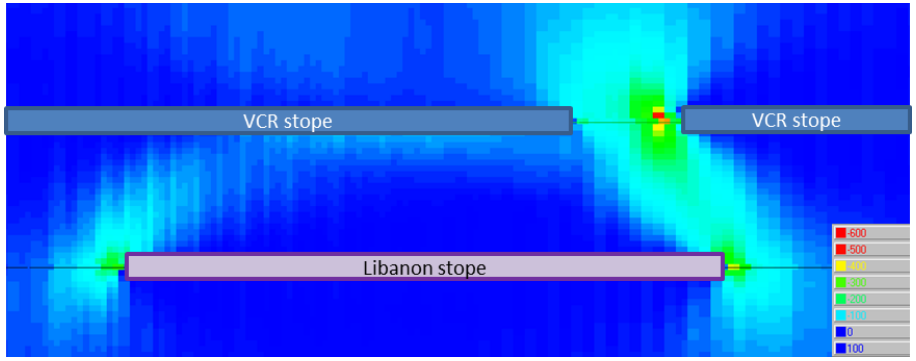
Contour plot of Step 30



Contour map of Step 30

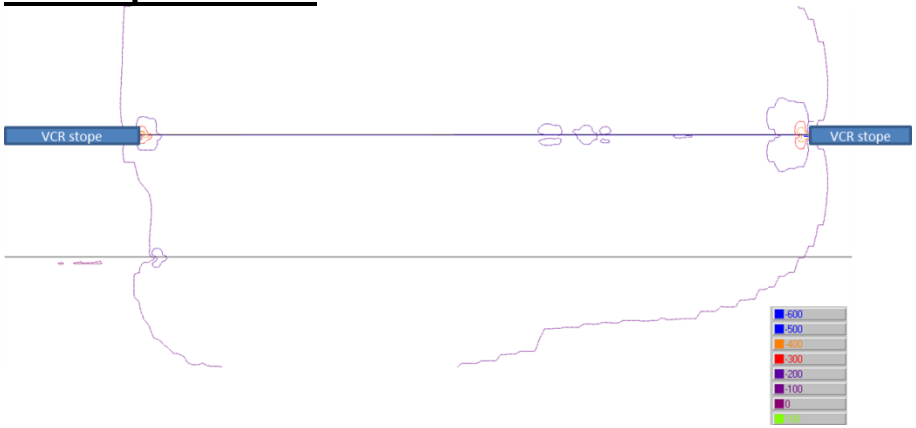


Contour plot of Step 32

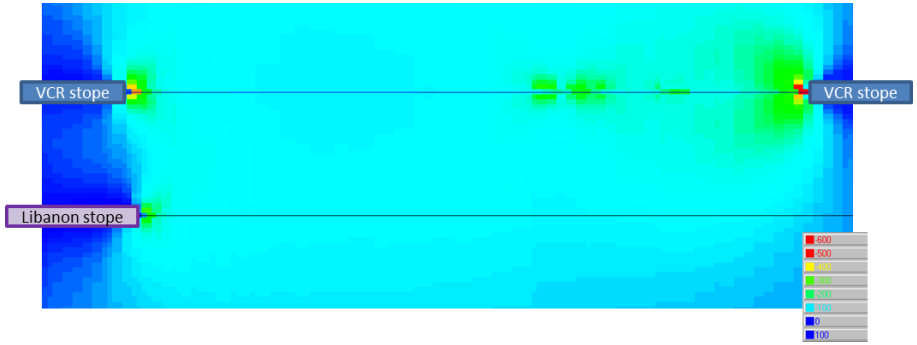


Contour map of Step 32

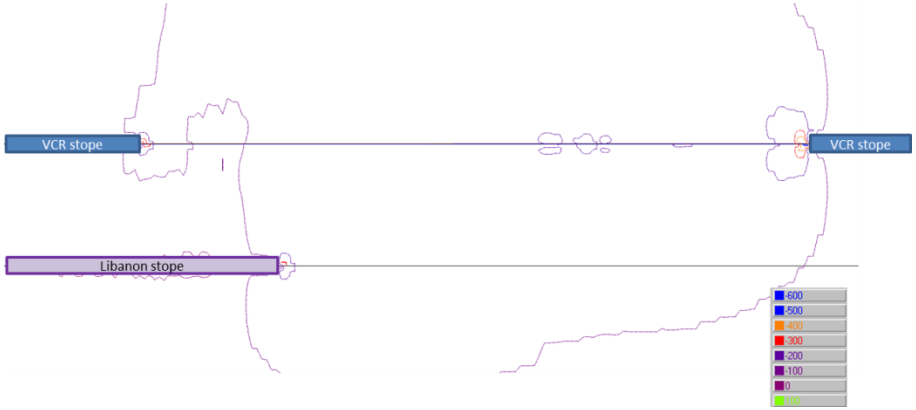
Section plot of B-B’



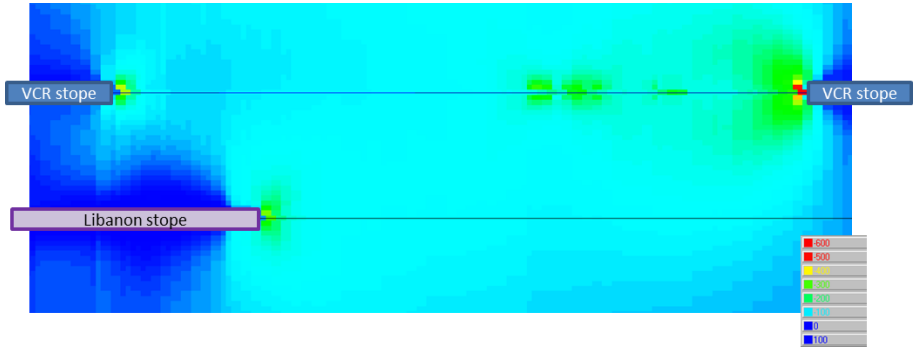
Contour plot of Step 4



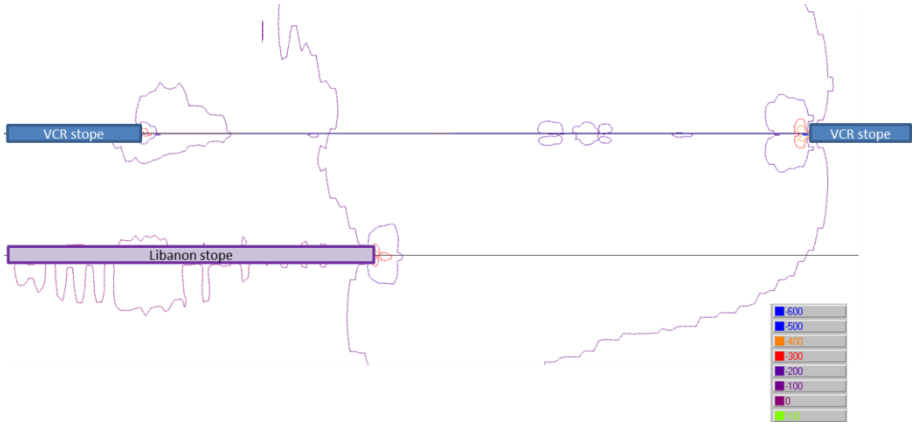
Contour map of Step 4



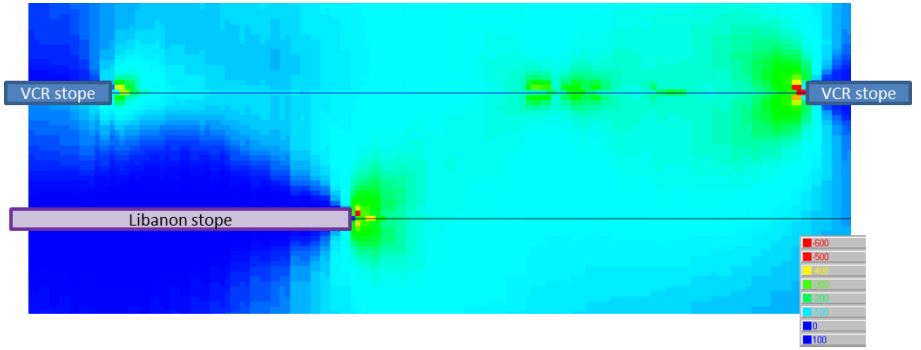
Contour plot of Step 6



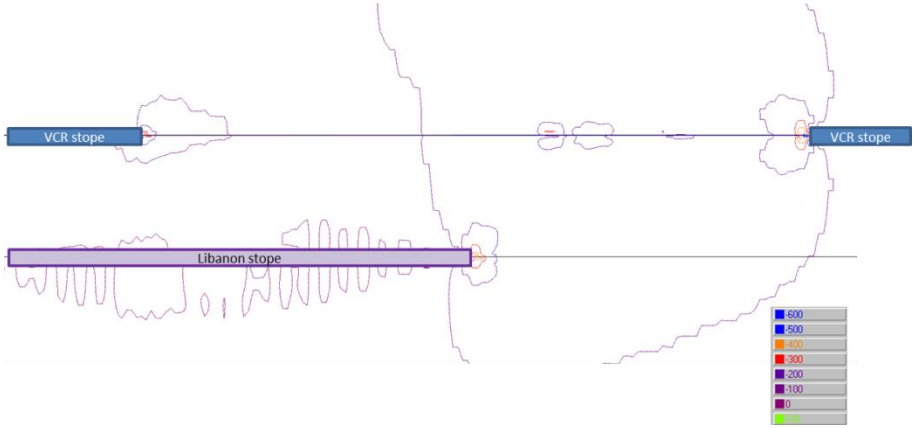
Contour map of Step 6



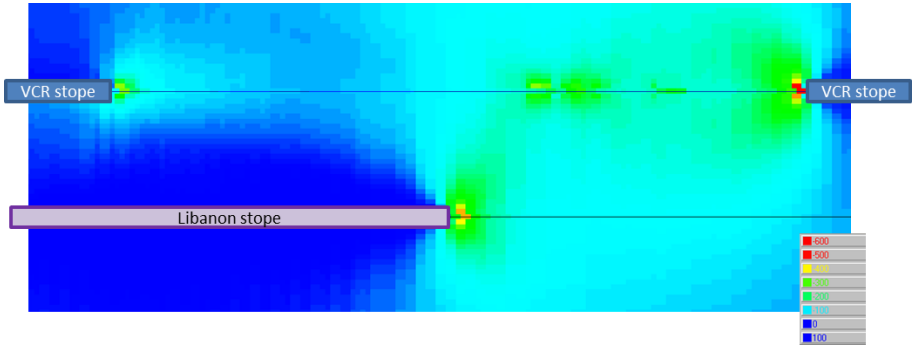
Contour plot of Step 10



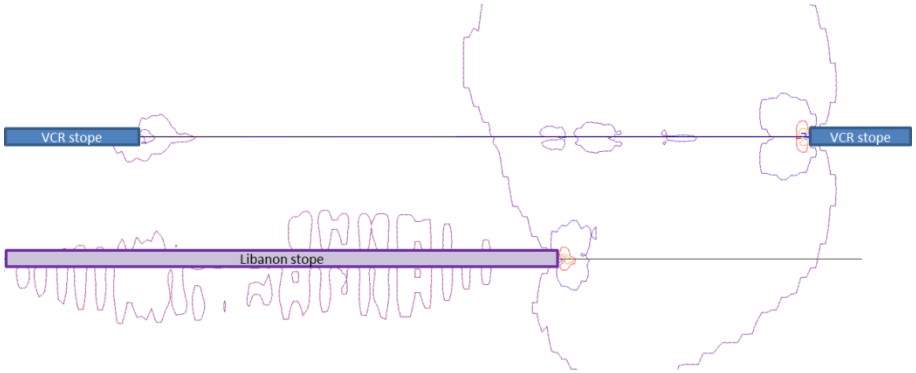
Contour map of Step 10



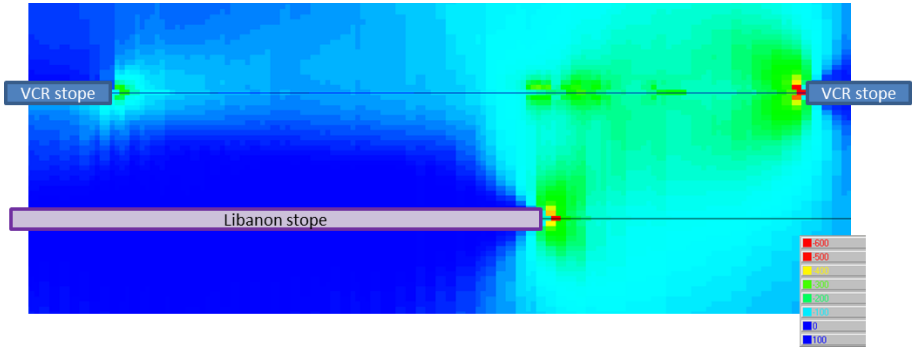
Contour plot of Step 12



Contour map of Step 12



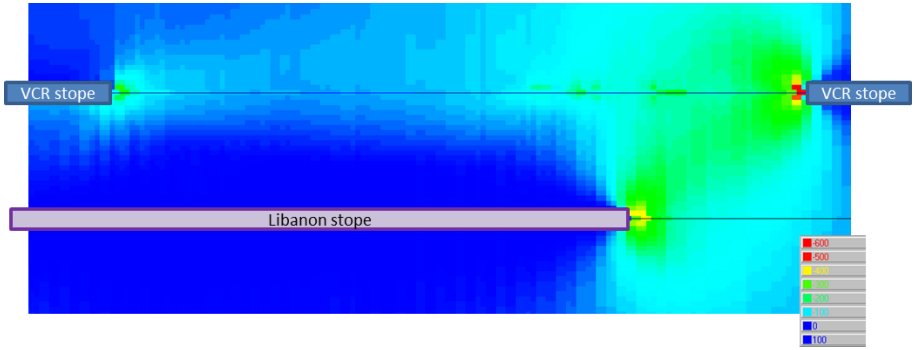
Contour plot of Step 15



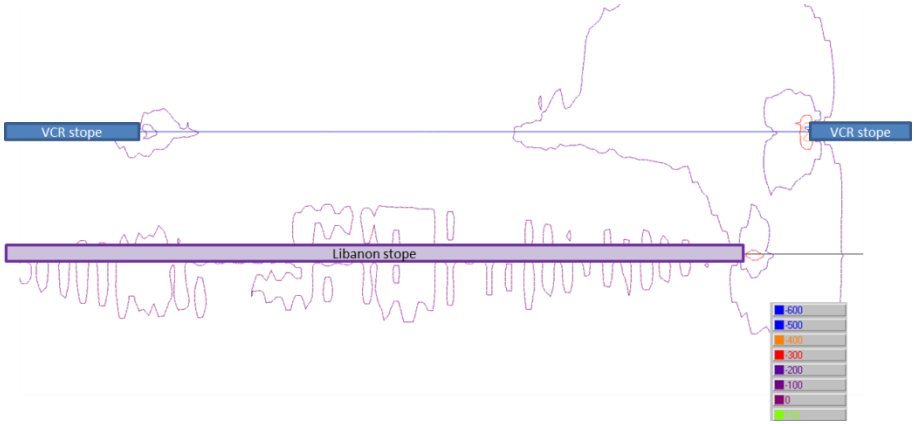
Contour map of Step 15



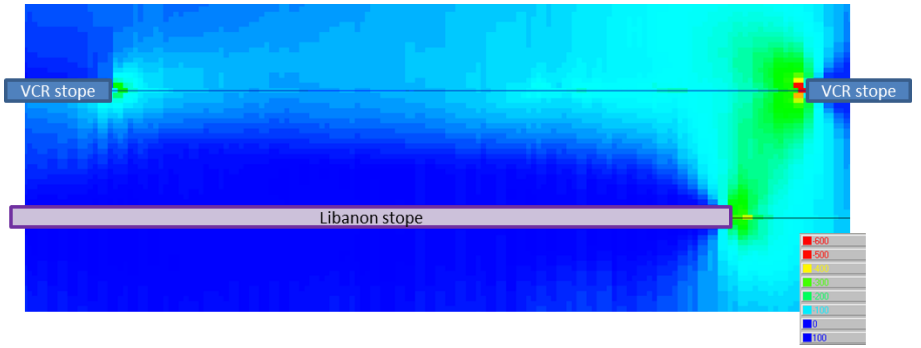
Contour plot of Step 18



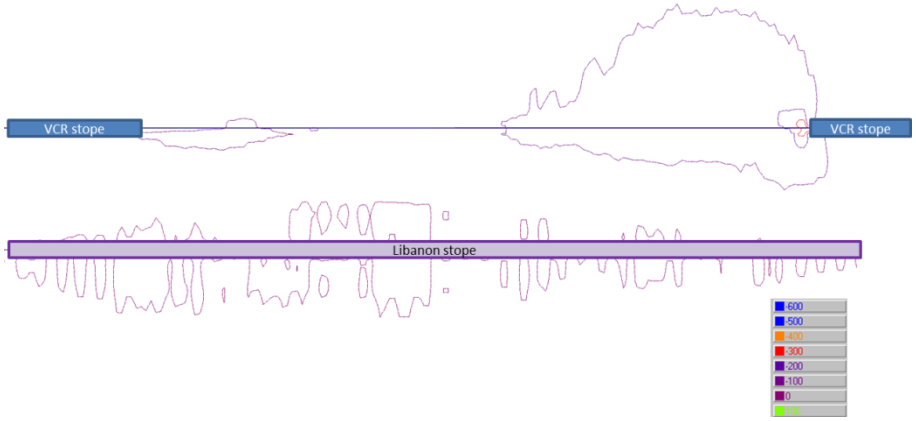
Contour map of Step 18



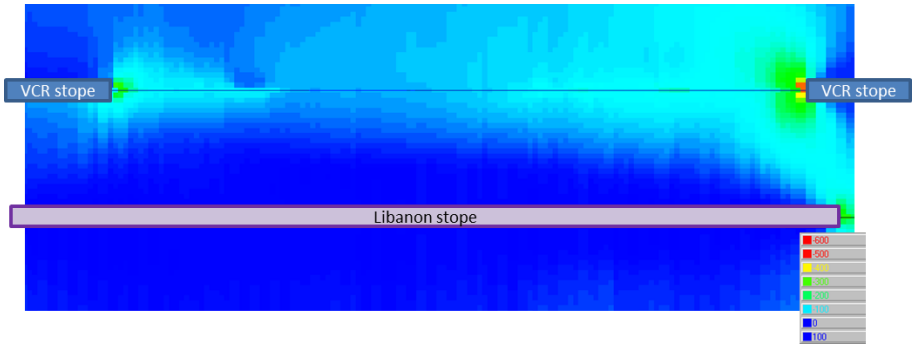
Contour plot of Step 19



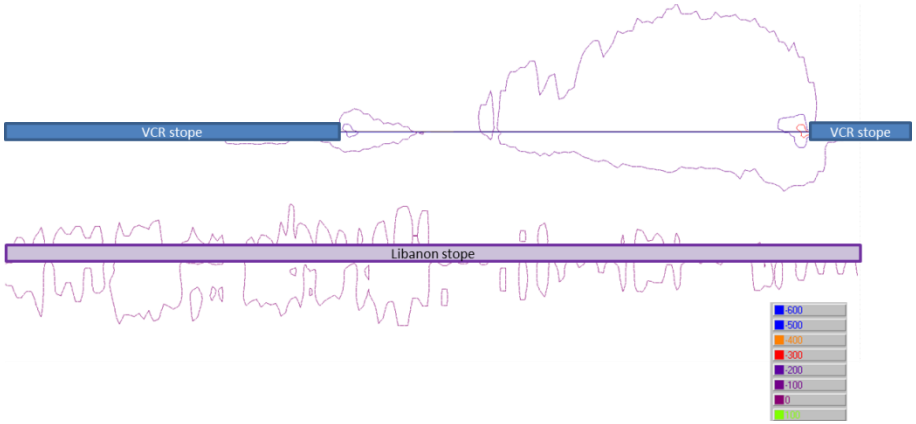
Contour map of Step 19



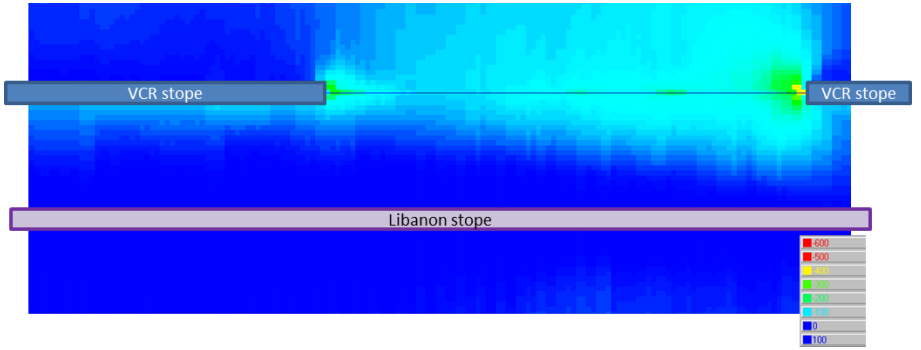
Contour plot of Step 20



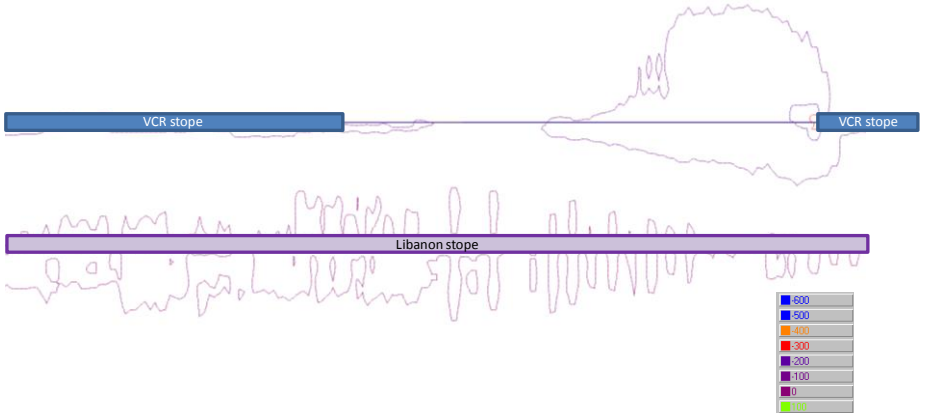
Contour map of Step 20



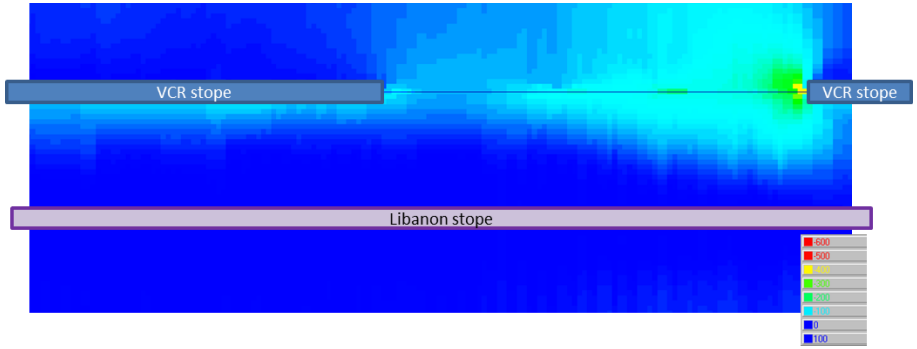
Contour plot of Step 30



Contour map of Step 30



Contour plot of Step 34



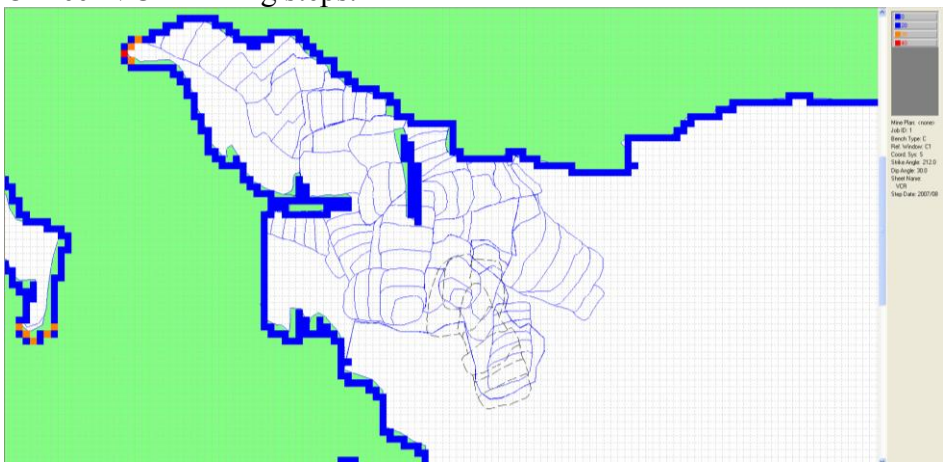
Contour map of Step 34

Appendix B : Numerical Modelling of VC22-30

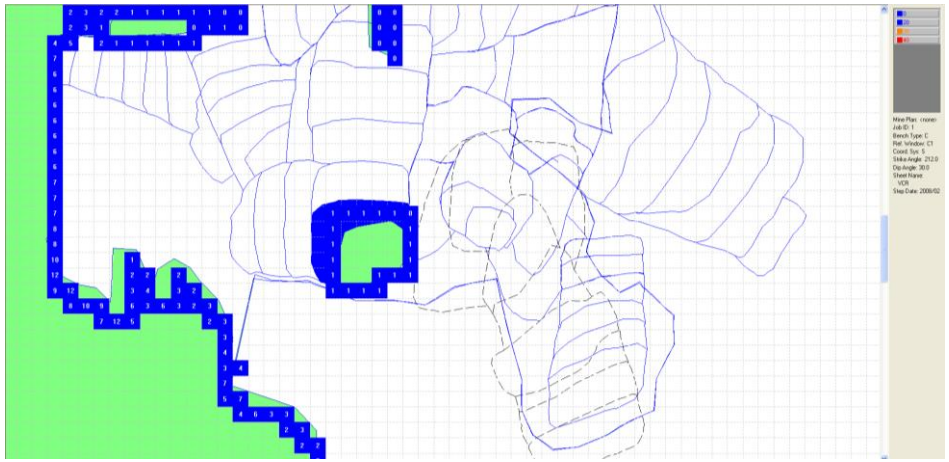
Model Setup:

Grid size: 2 m
Youngs modulus: 60 GPa
Friction angle: 30 degrees
Poissons ratio: 0.27
VRS: ZZ -0.03 / m
XX;YY : ZZ 0.5

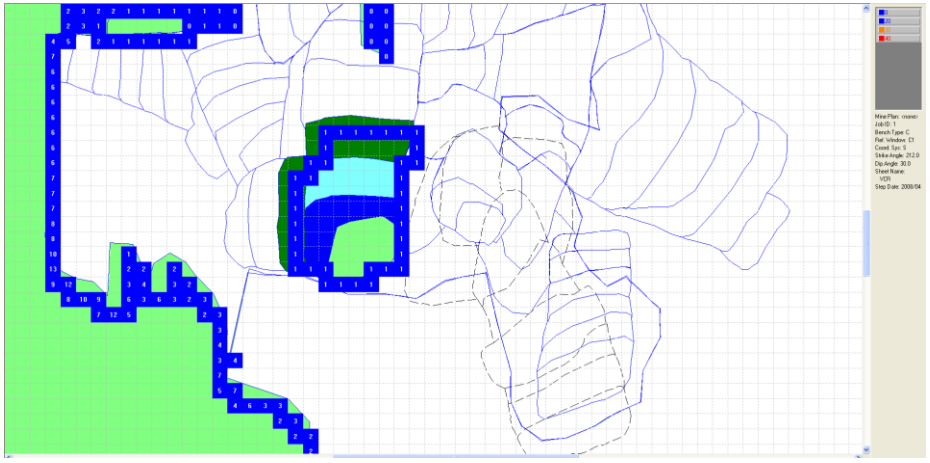
On reef VCR Mining steps:



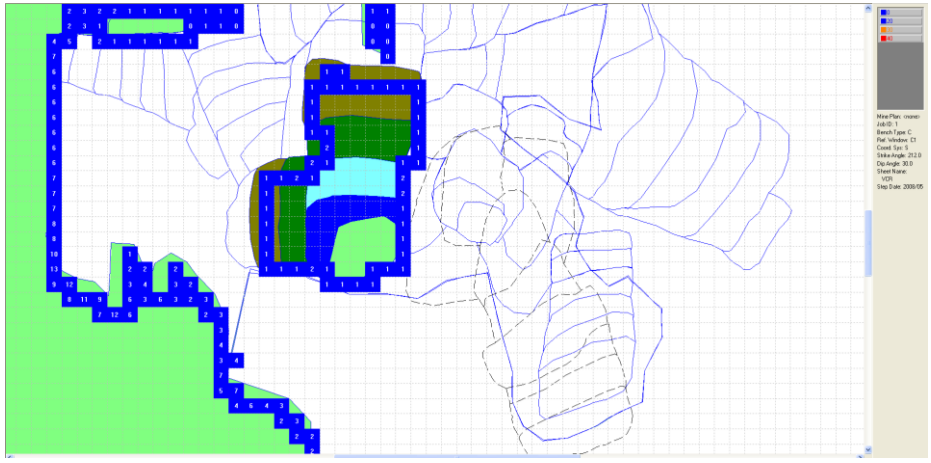
Step 1



Step 2



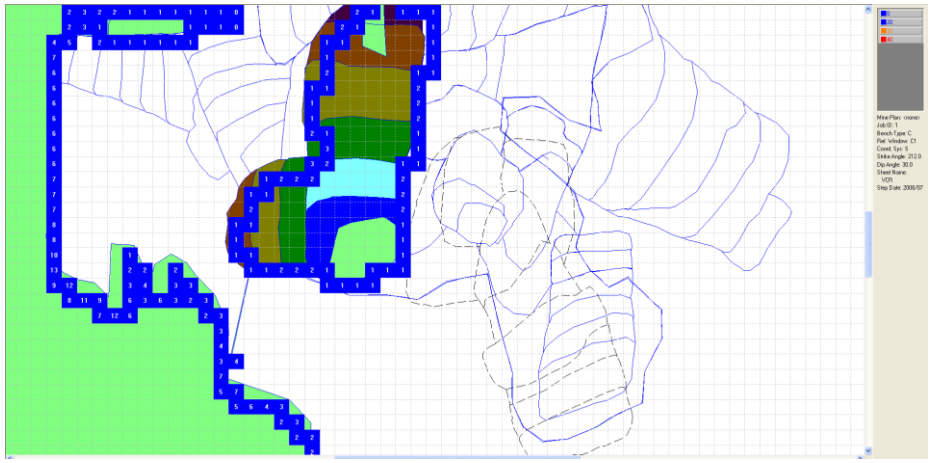
Step 3



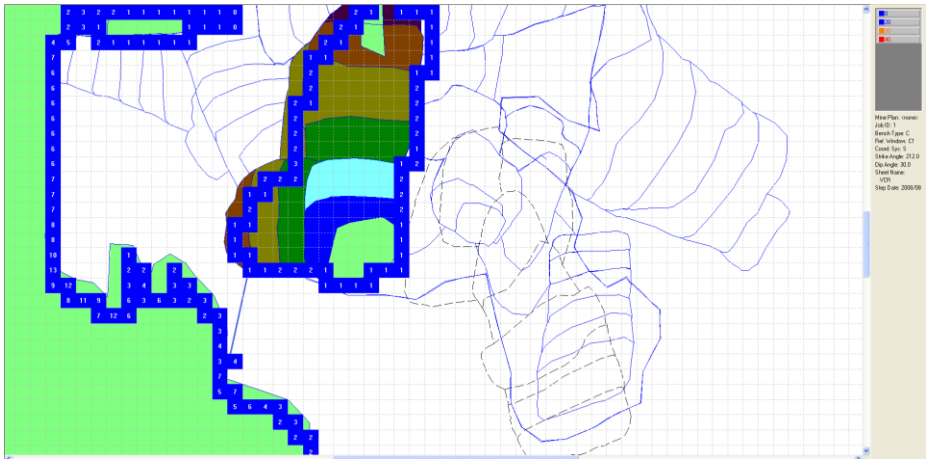
Step 4



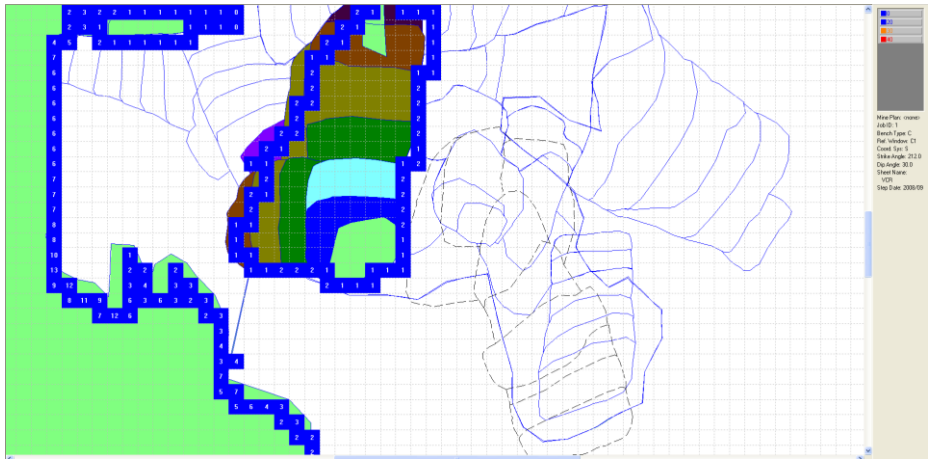
Step 5



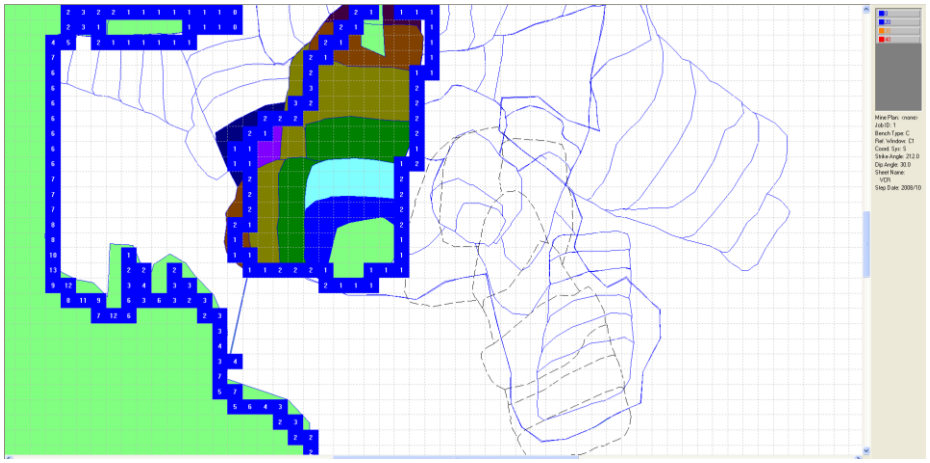
Step 6



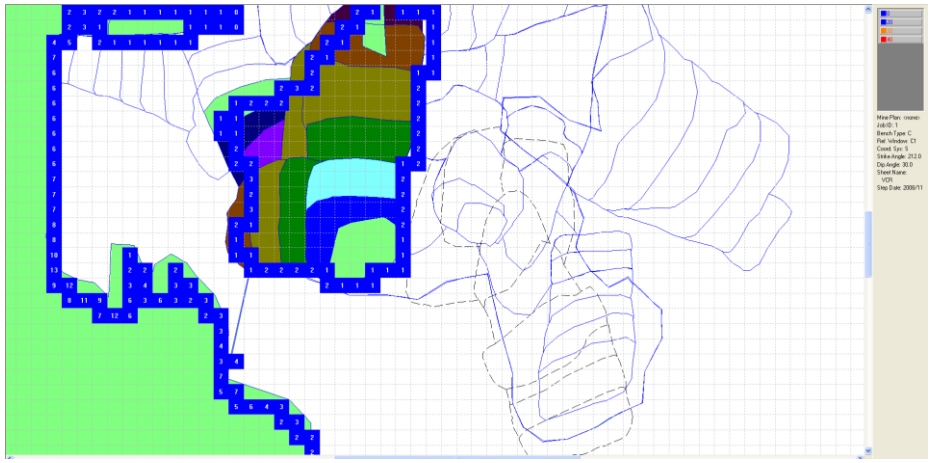
Step 7



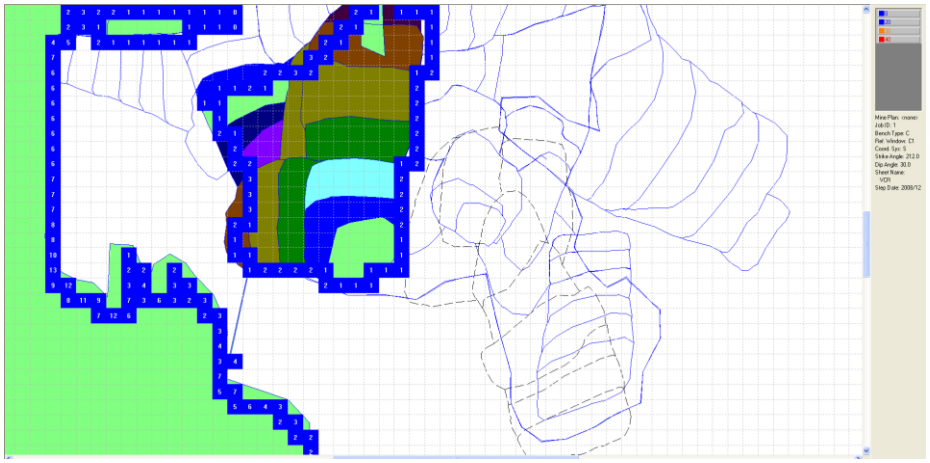
Step 8



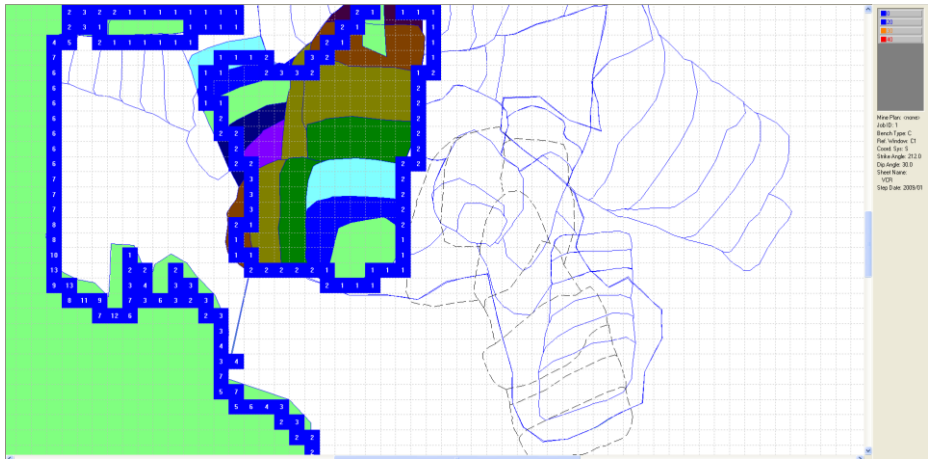
Step 9



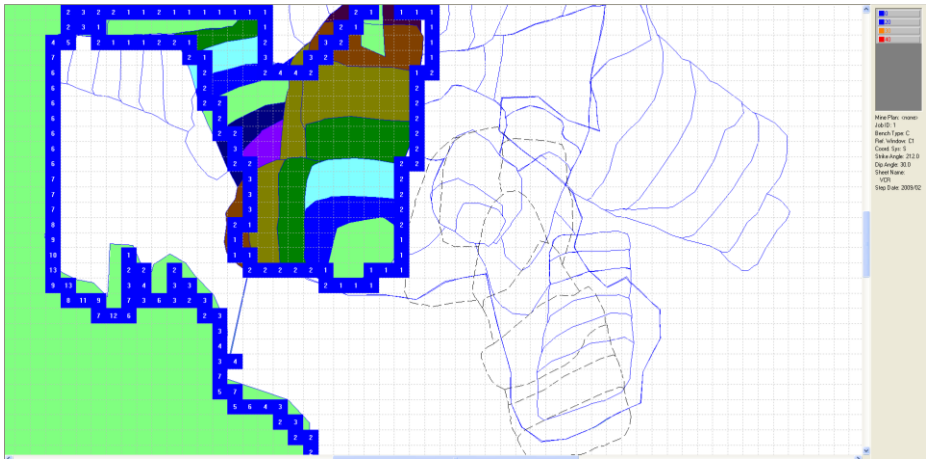
Step 10



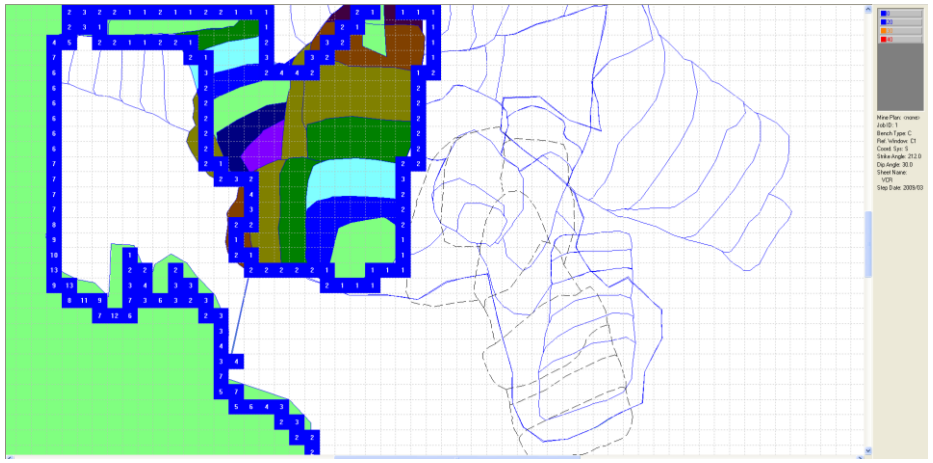
Step 11



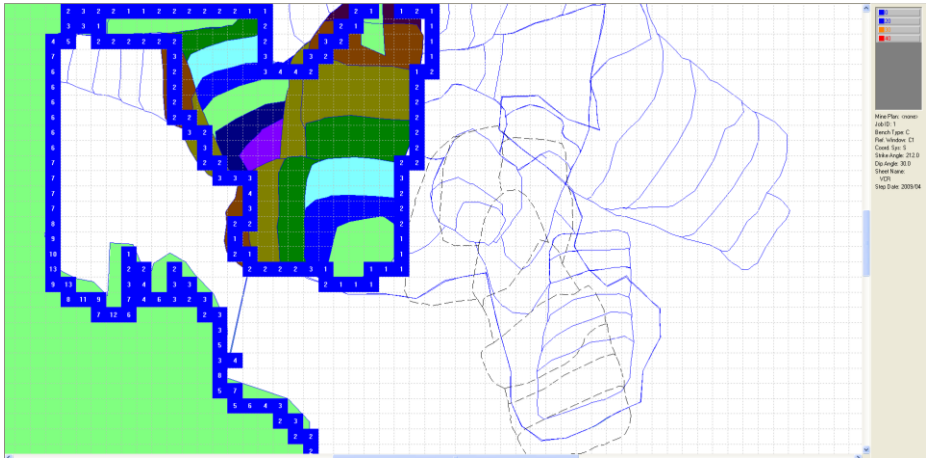
Step 12



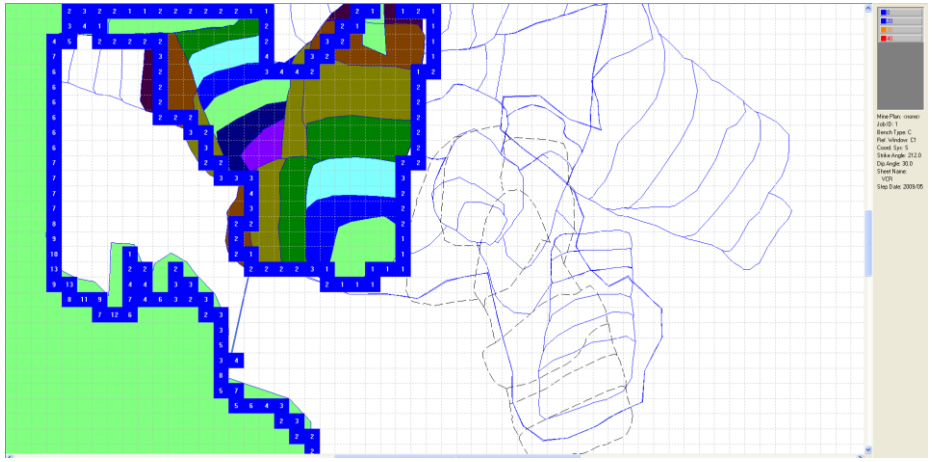
Step 13



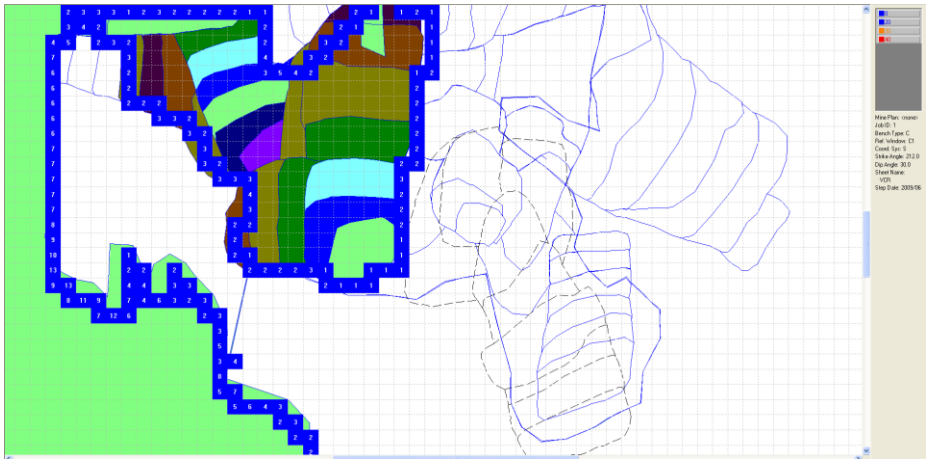
Step 14



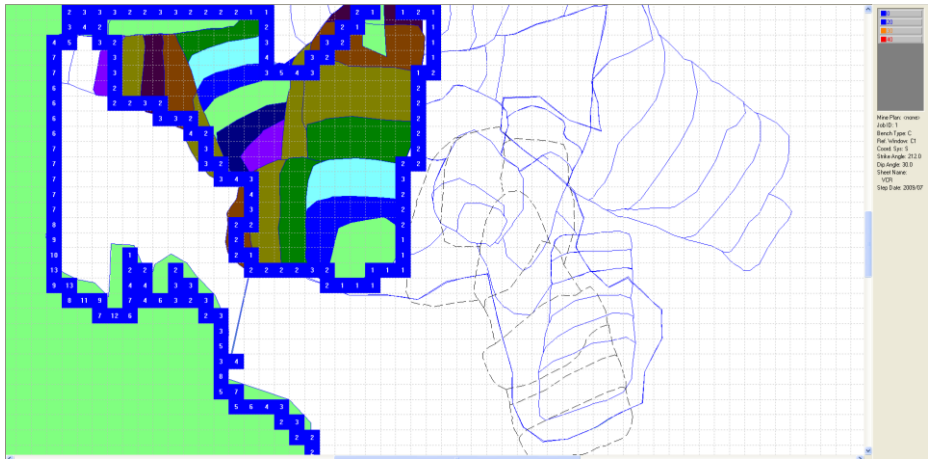
Step 15



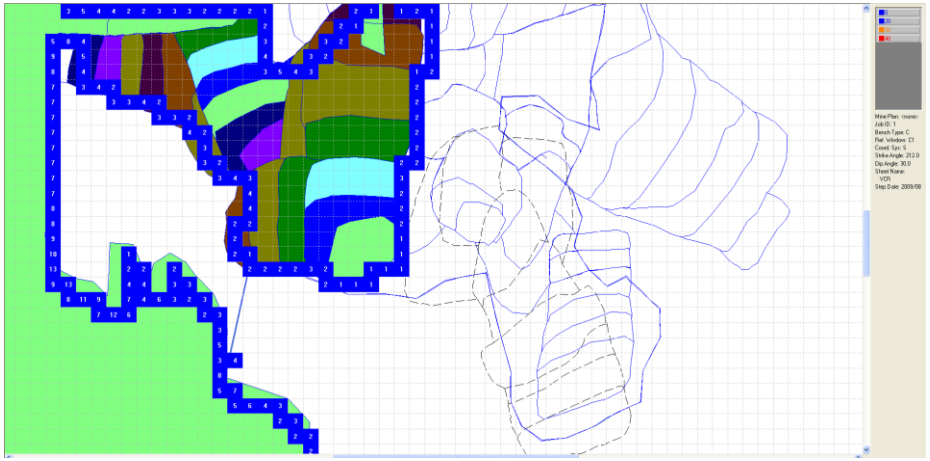
Step 16



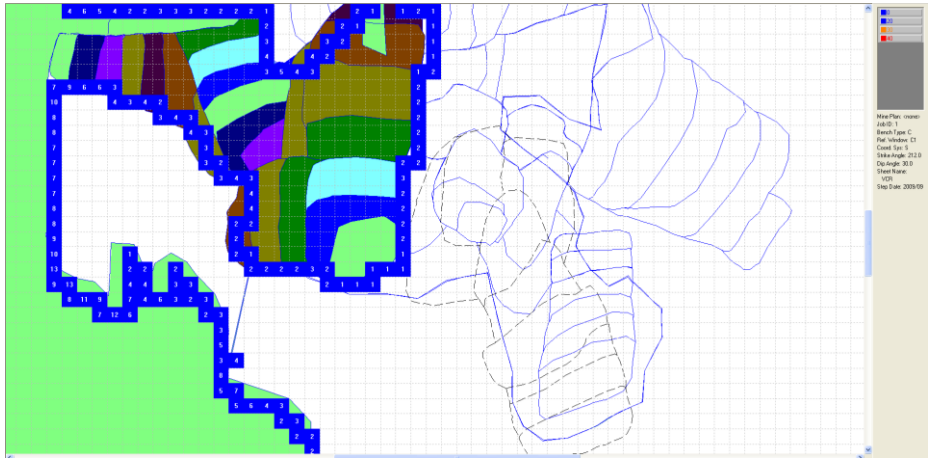
Step 17



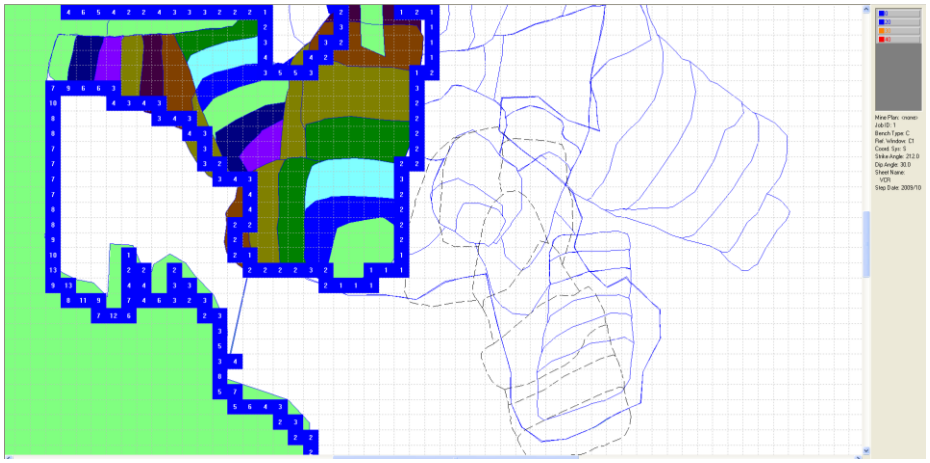
Step 18



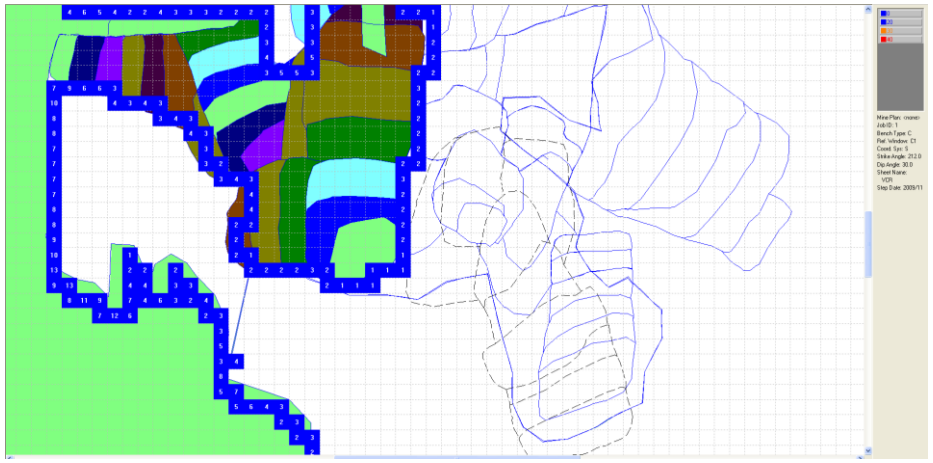
Step 19



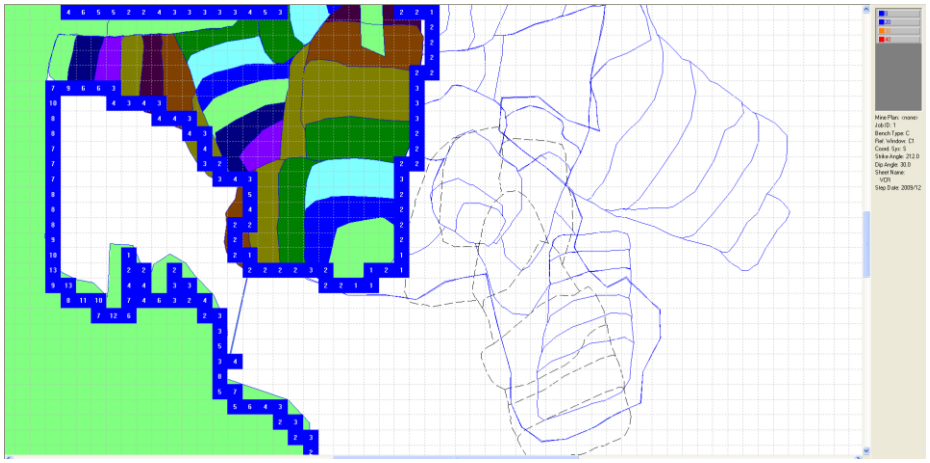
Step 20



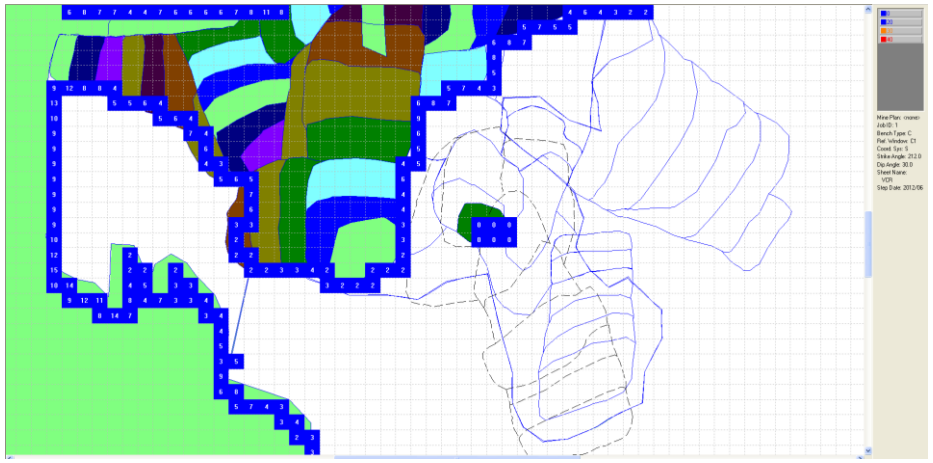
Step 21



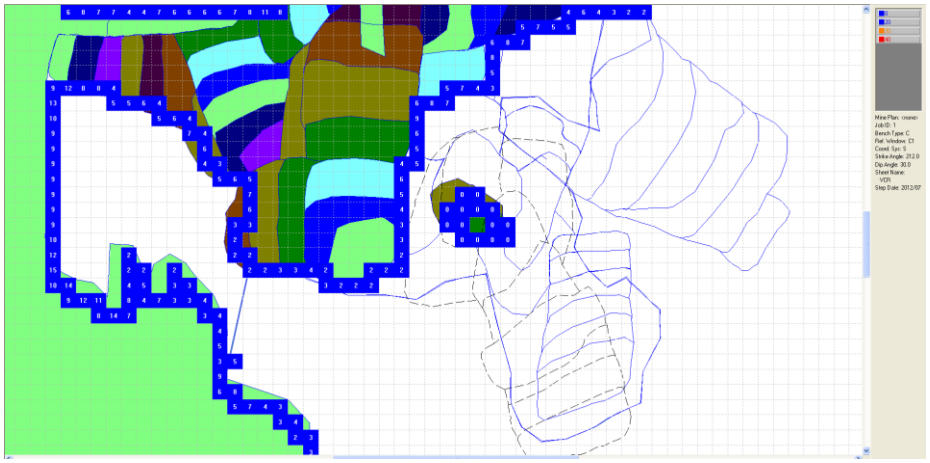
Step 22



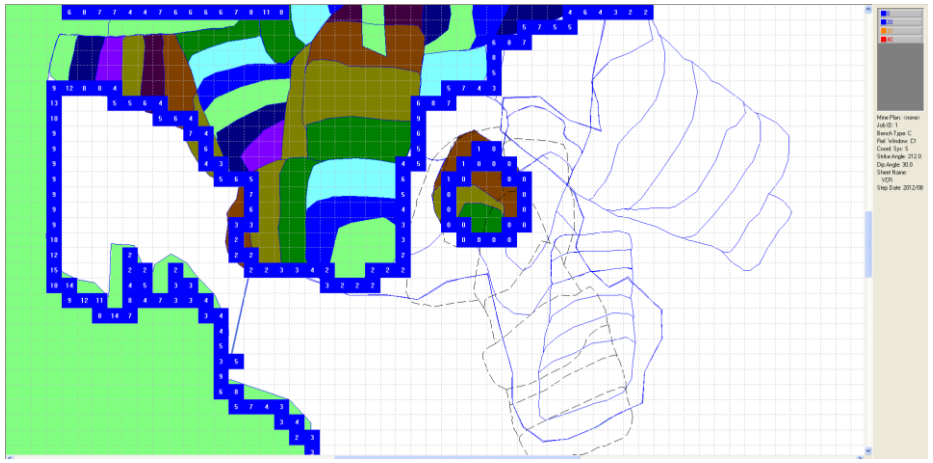
Step 23



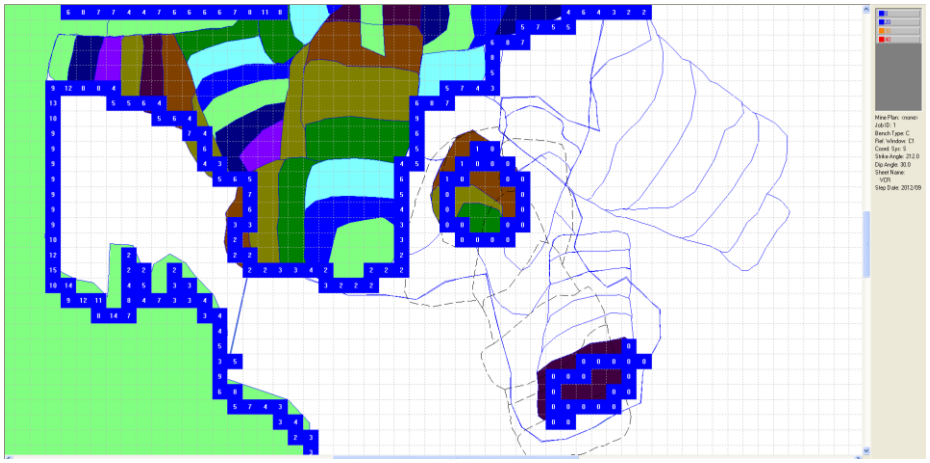
Step 33



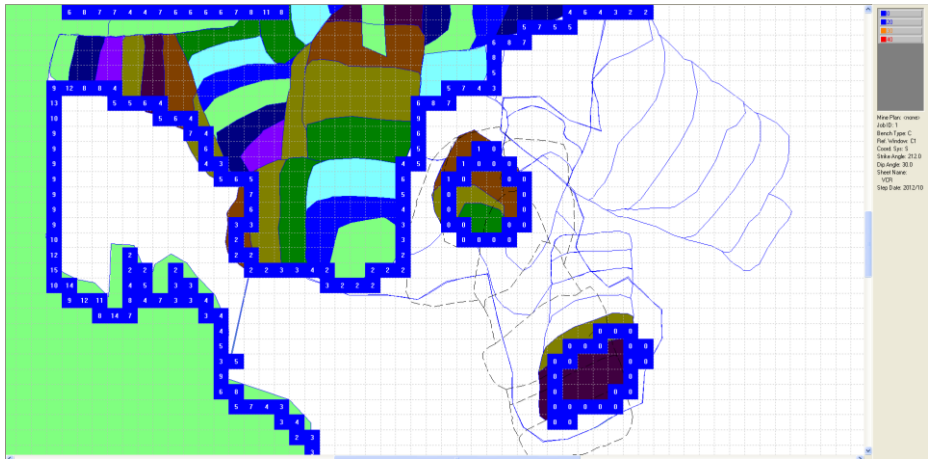
Step 34



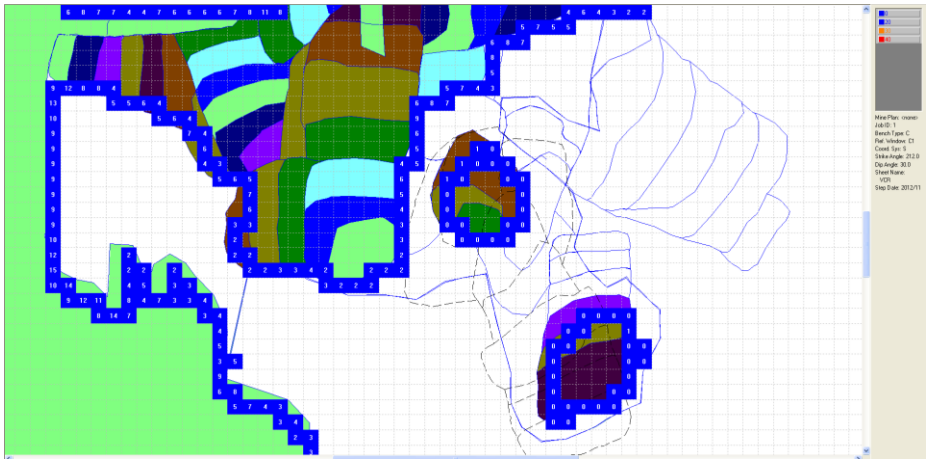
Step 35



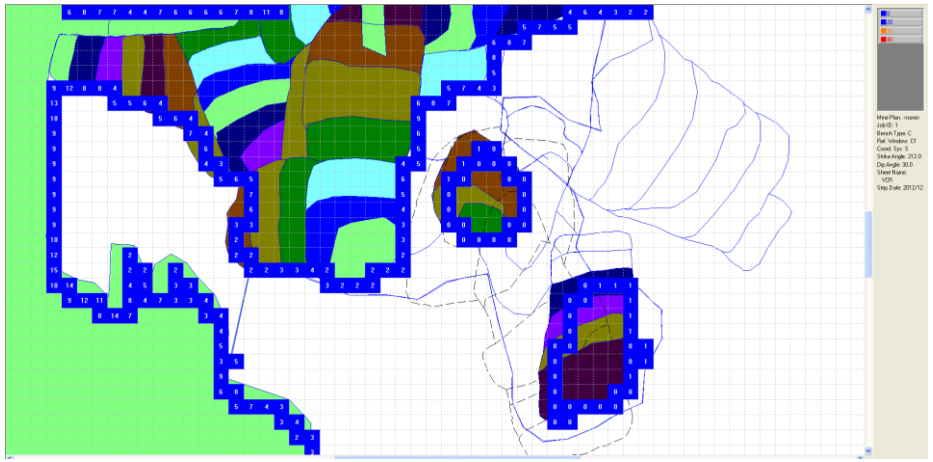
Step 36



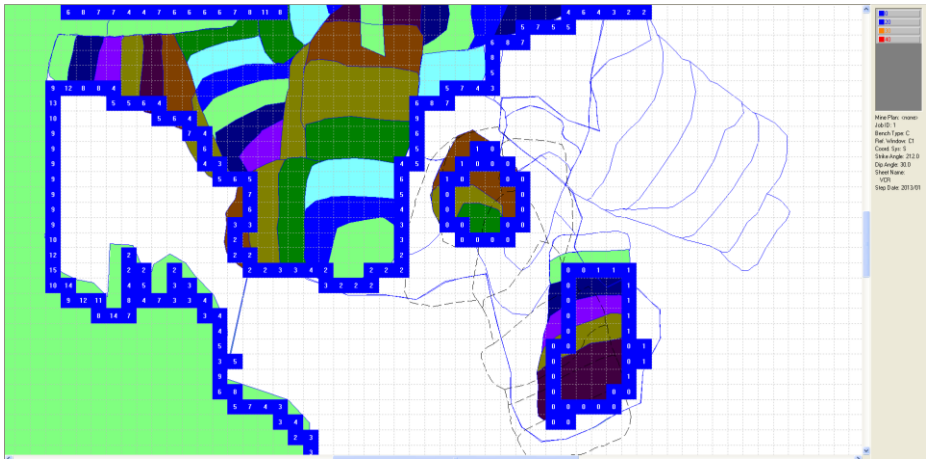
Step 37



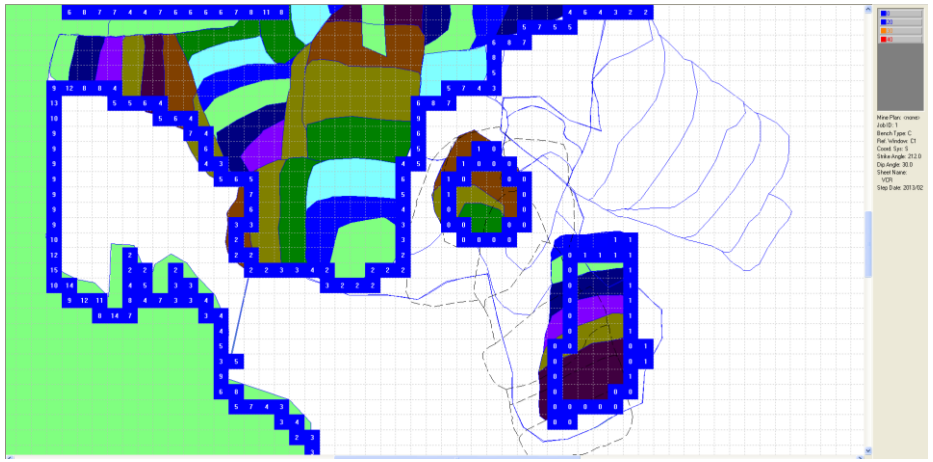
Step 38



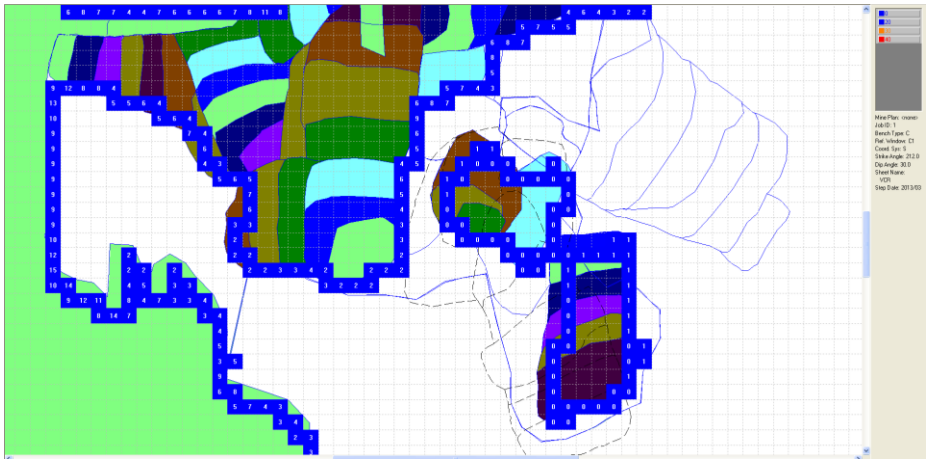
Step 39



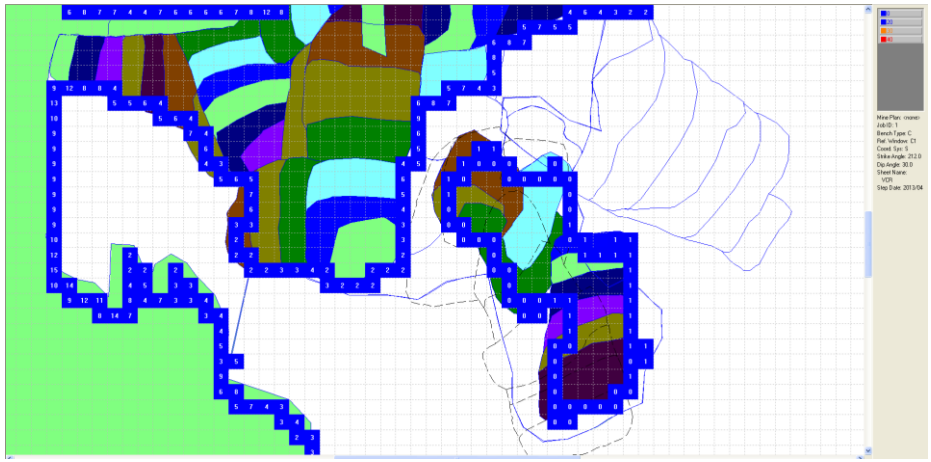
Step 40



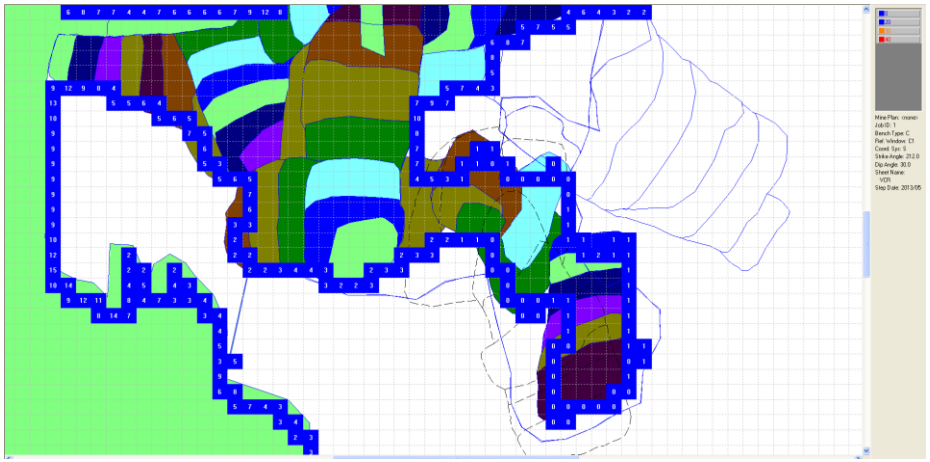
Step 41



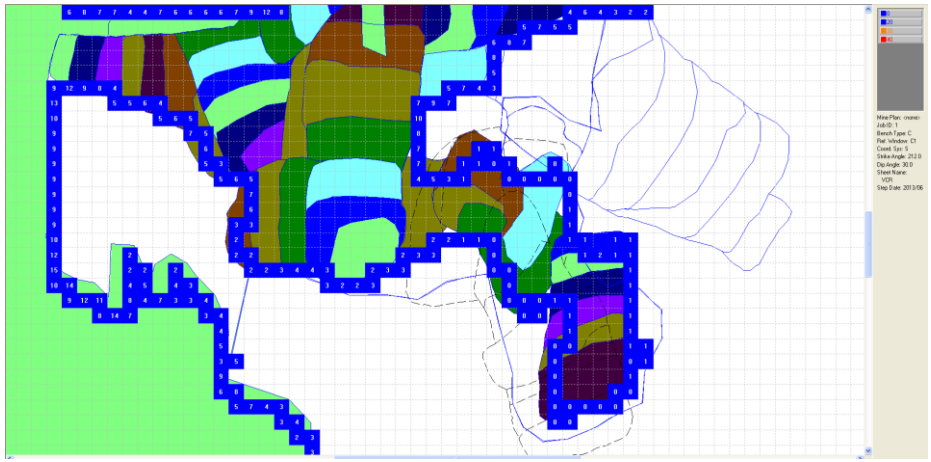
Step 42



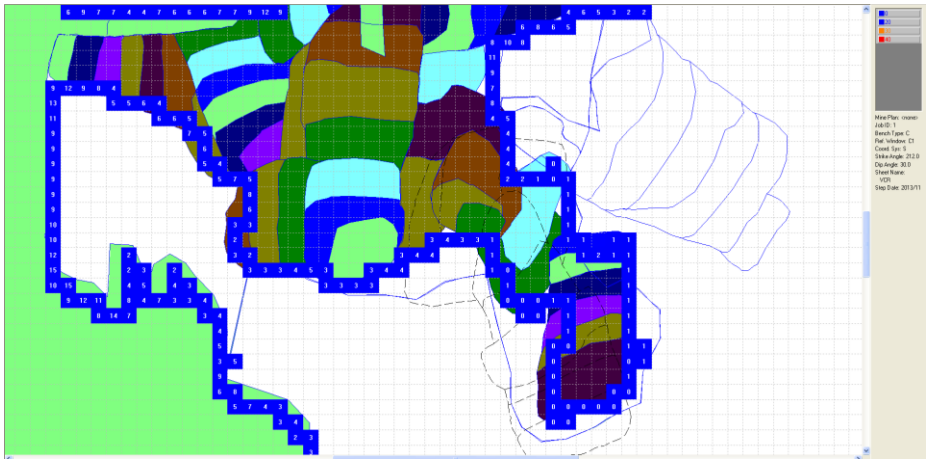
Step 43



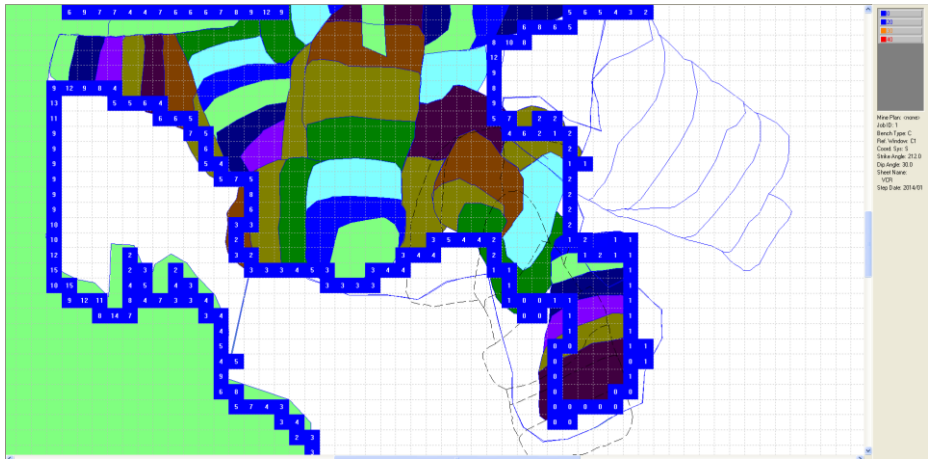
Step 44



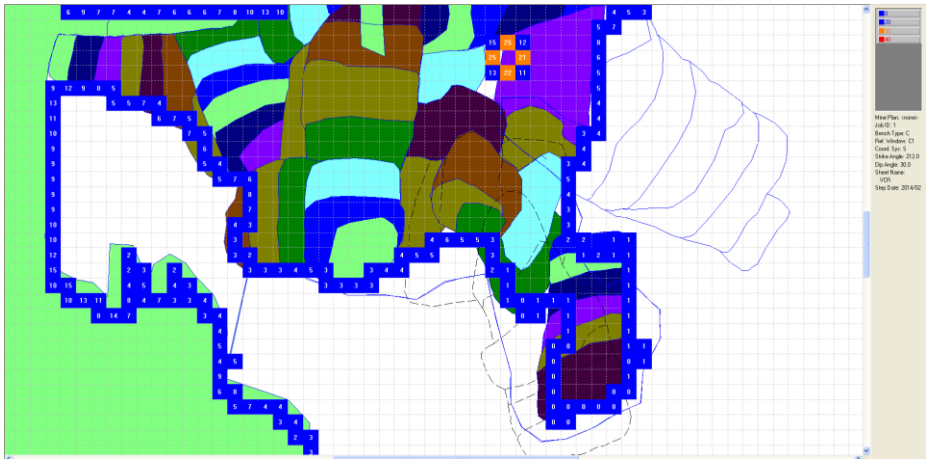
Step 45



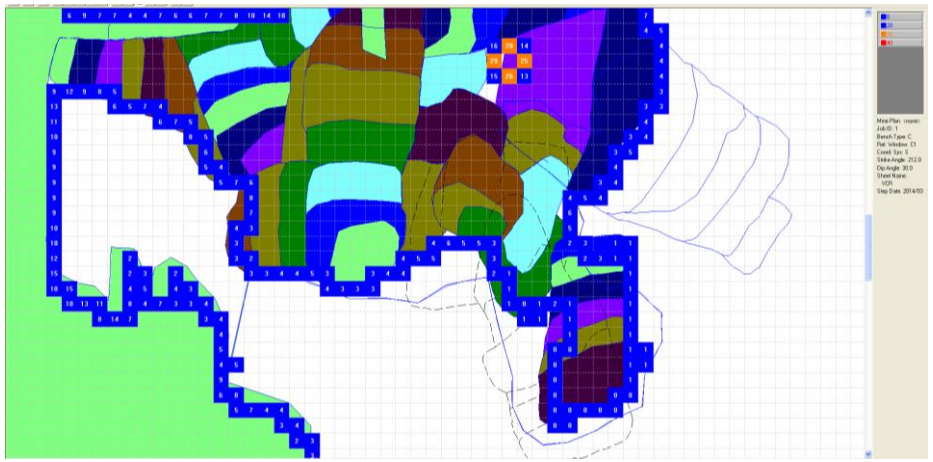
Step 46



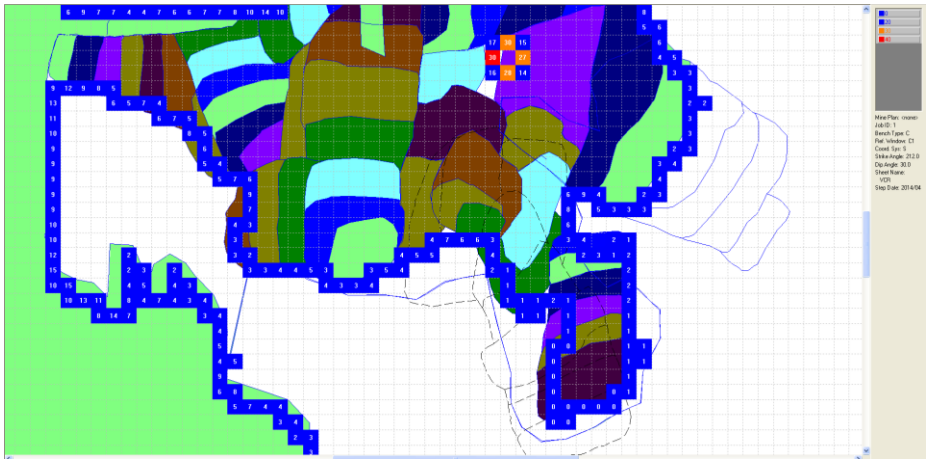
Step 47



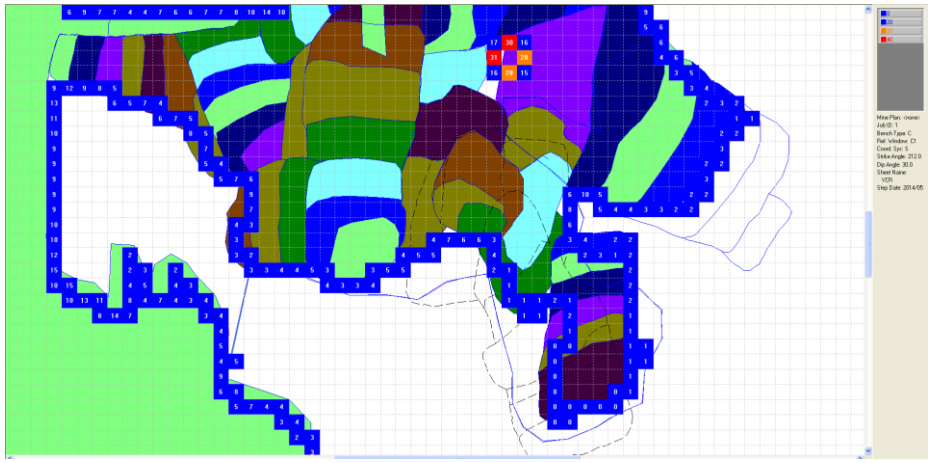
Step 48



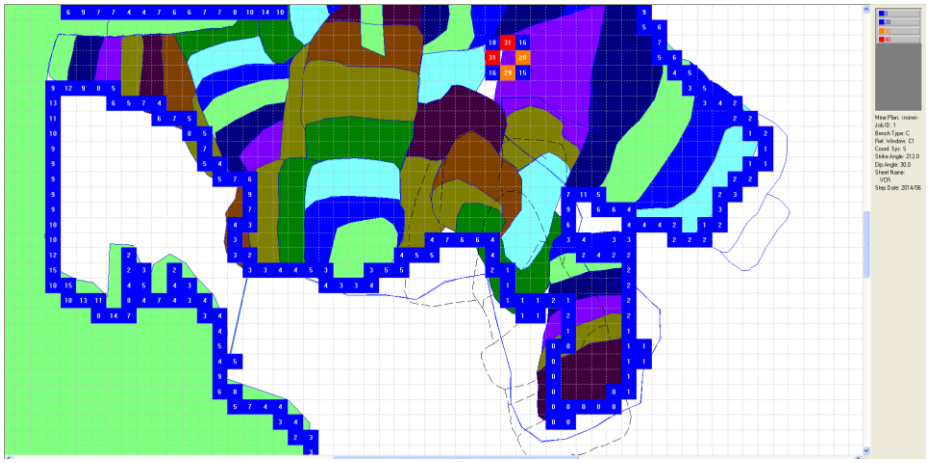
Step 49



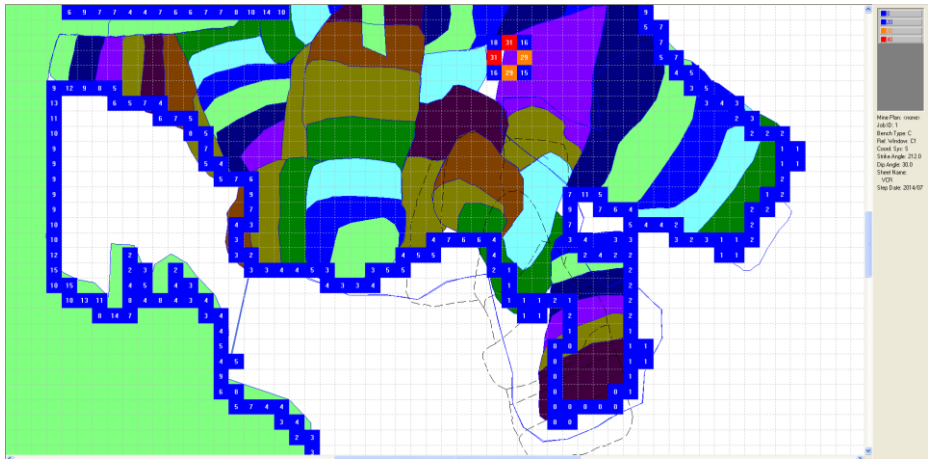
Step 50



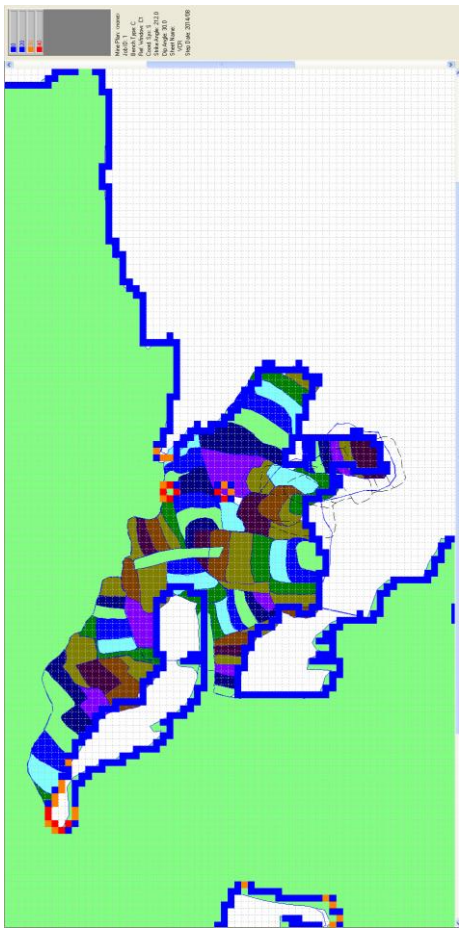
Step 51



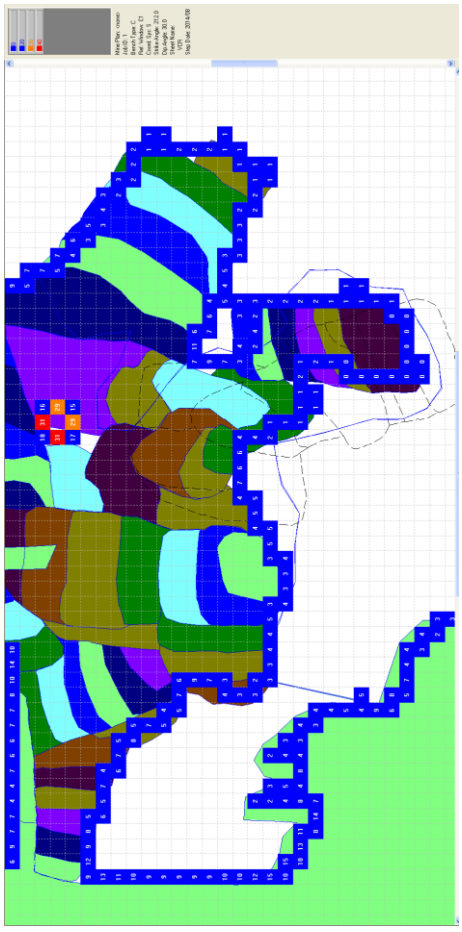
Step 52



Step 53

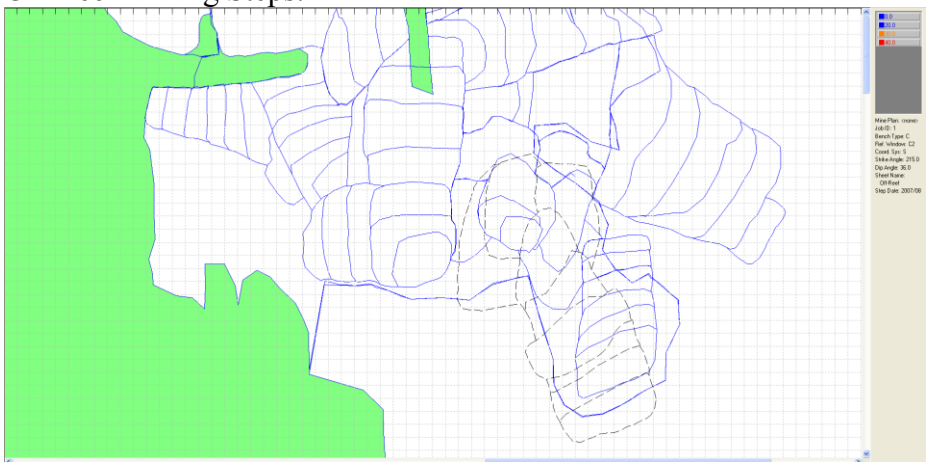


Step 54

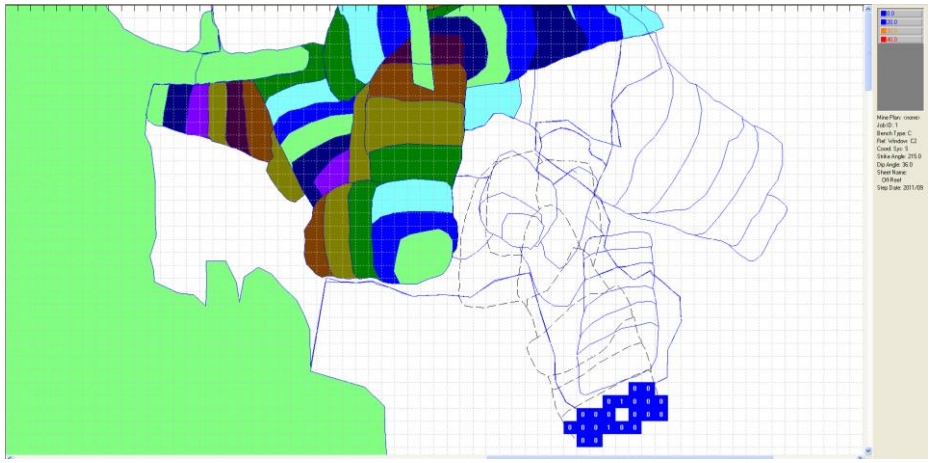


Step 54

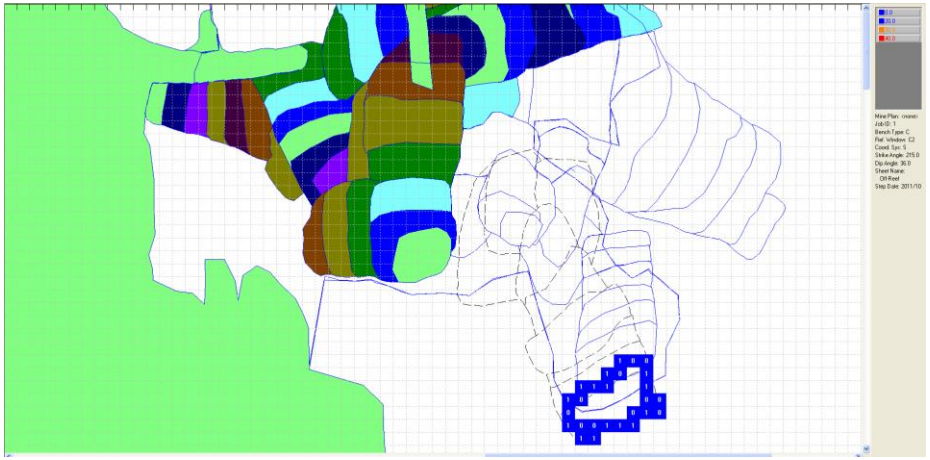
Off Reef Mining Steps:



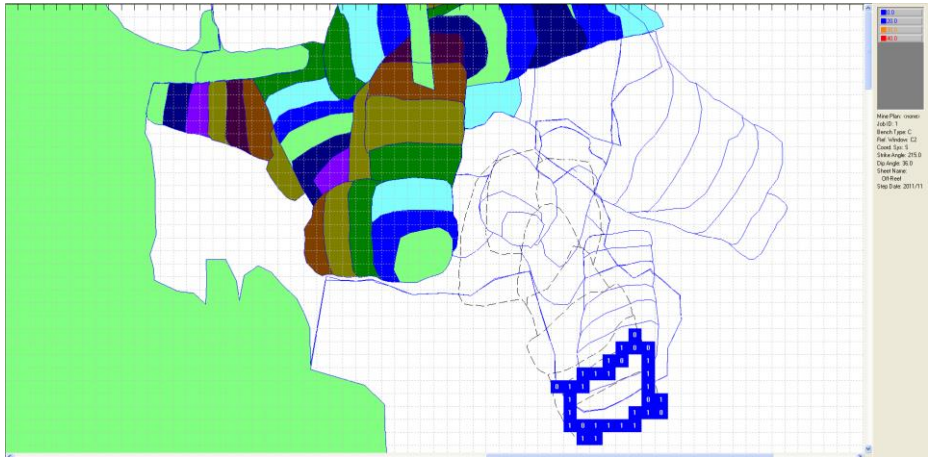
Step 1



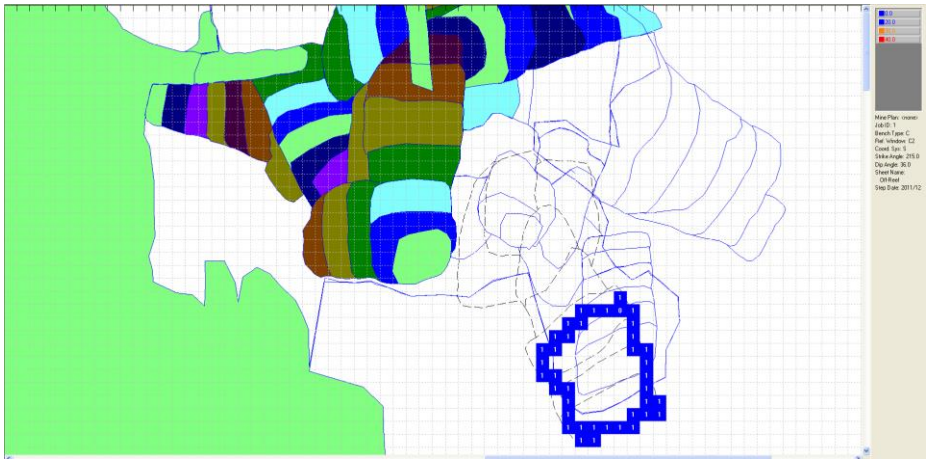
Step 24



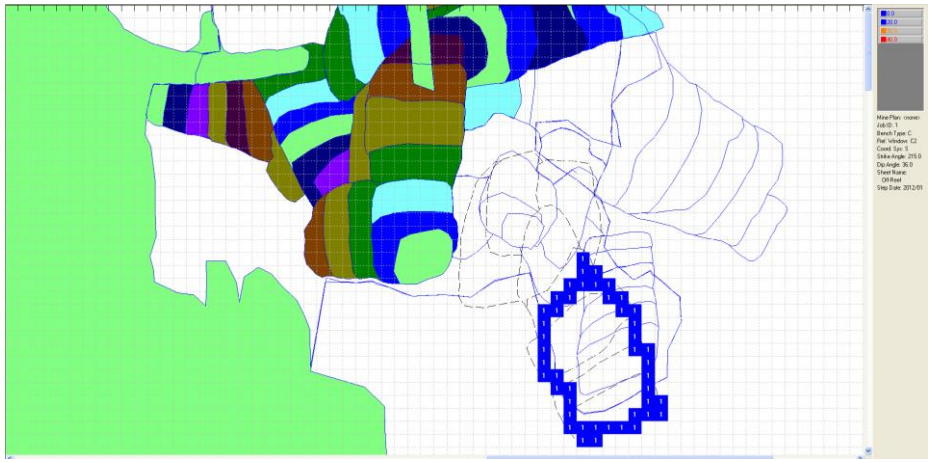
Step 25



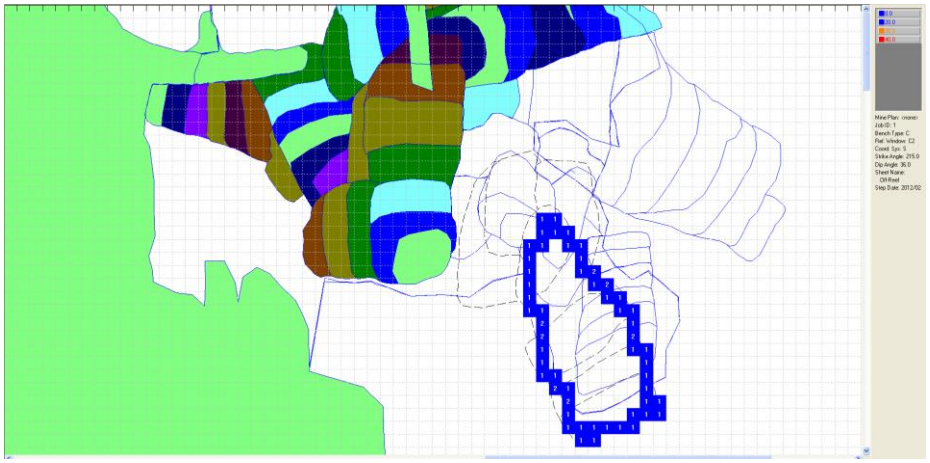
Step 26



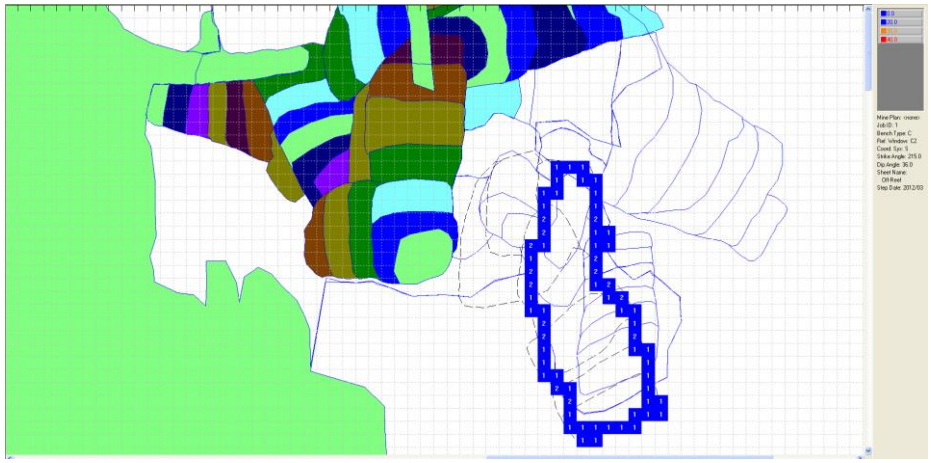
Step 27



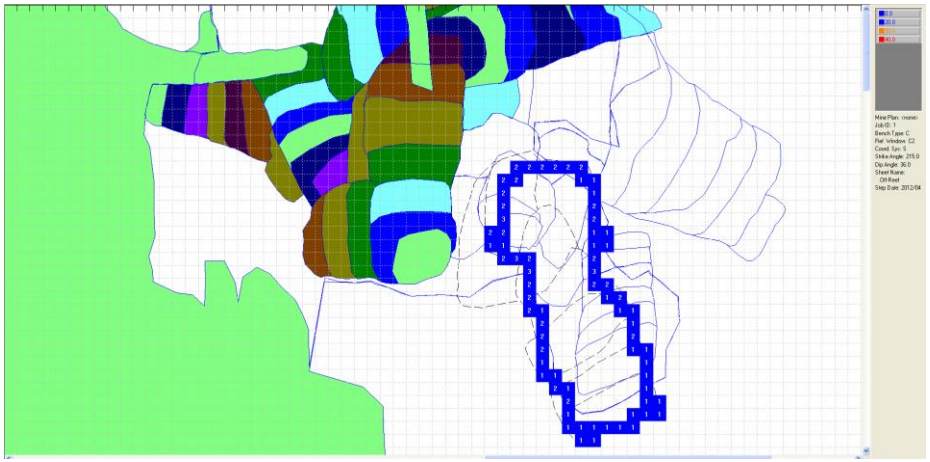
Step 28



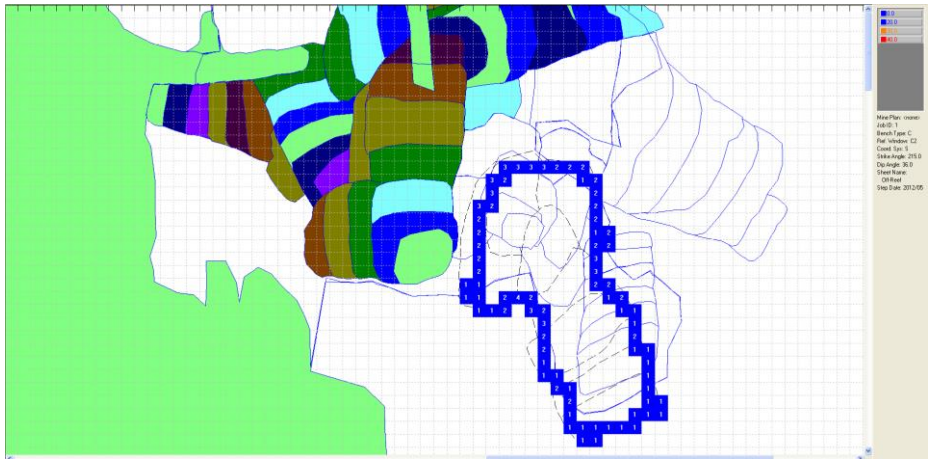
Step 29



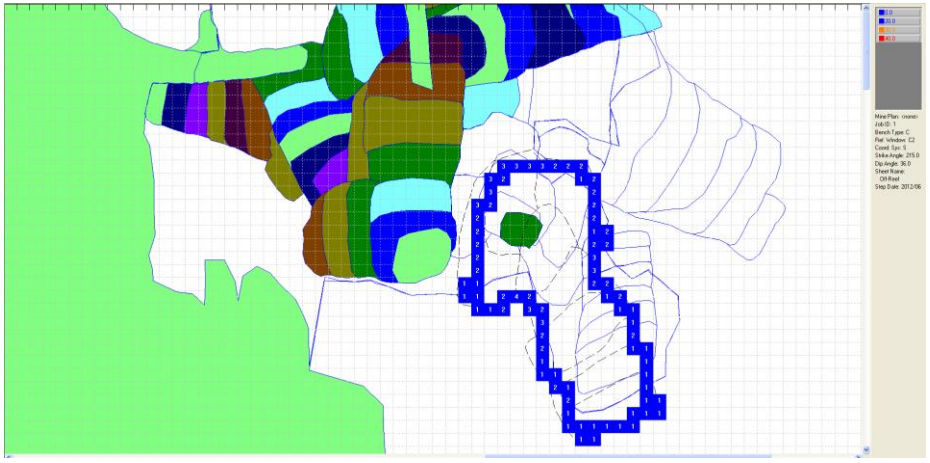
Step 30



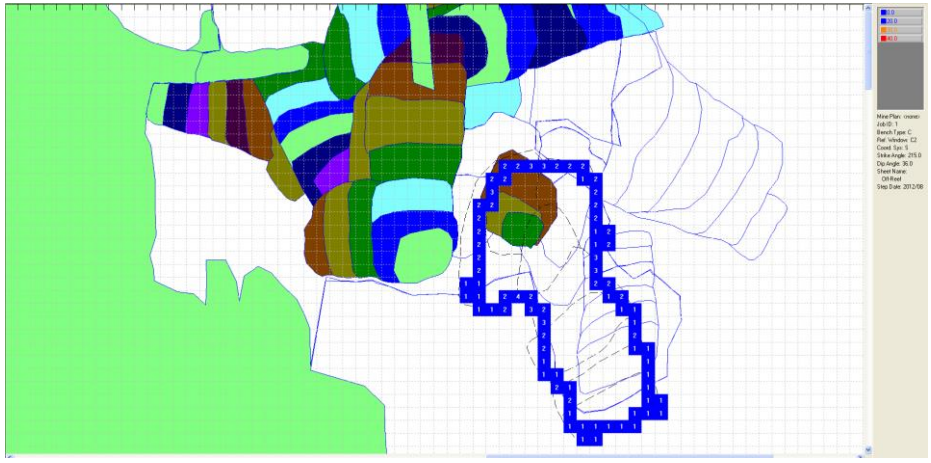
Step 31



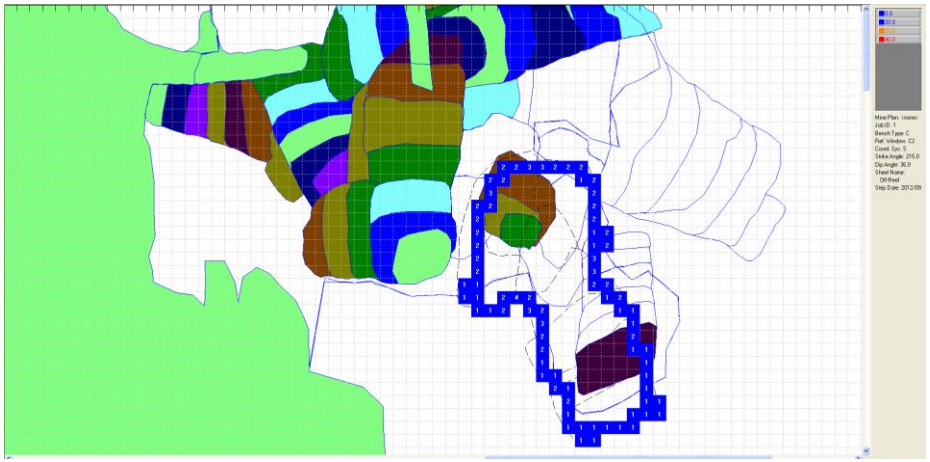
Step 32



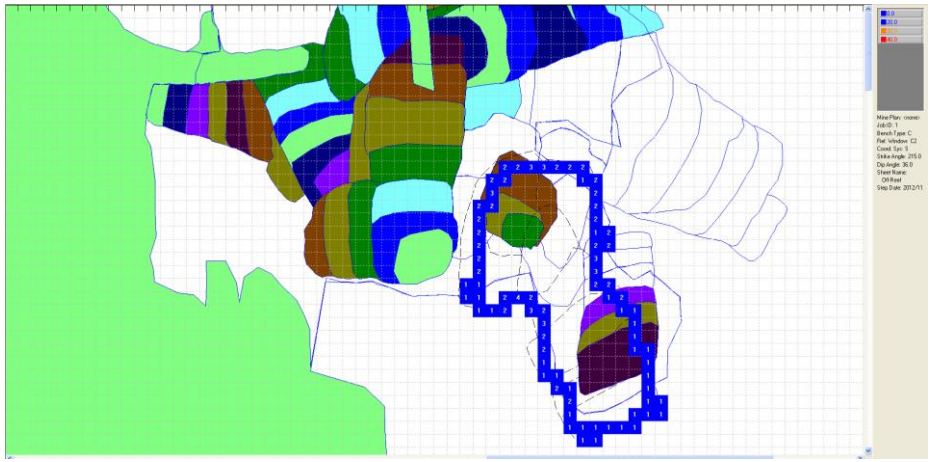
Step 33



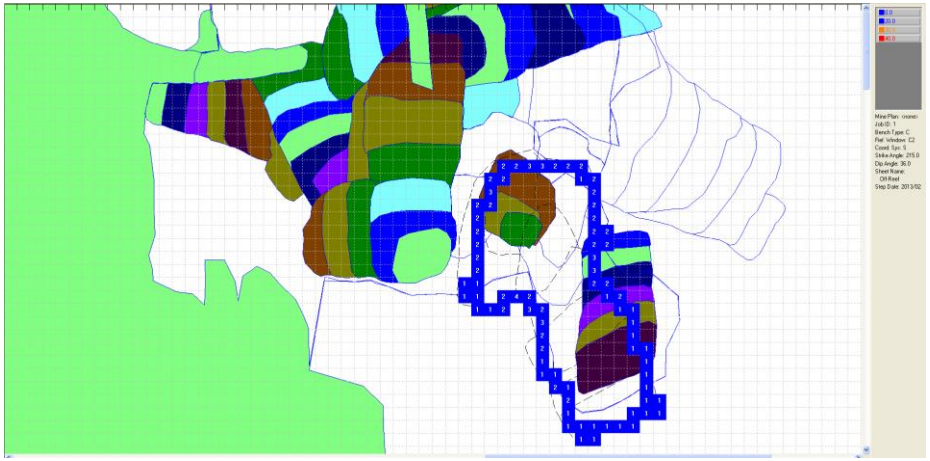
Step 35



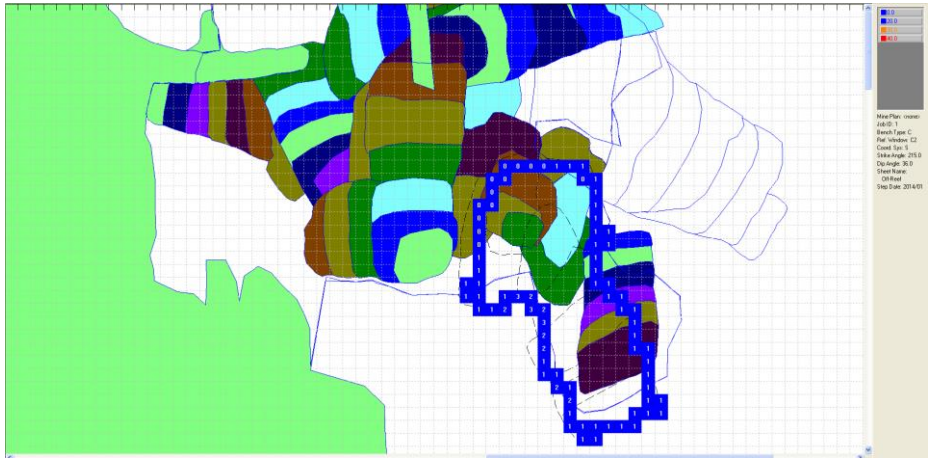
Step 36



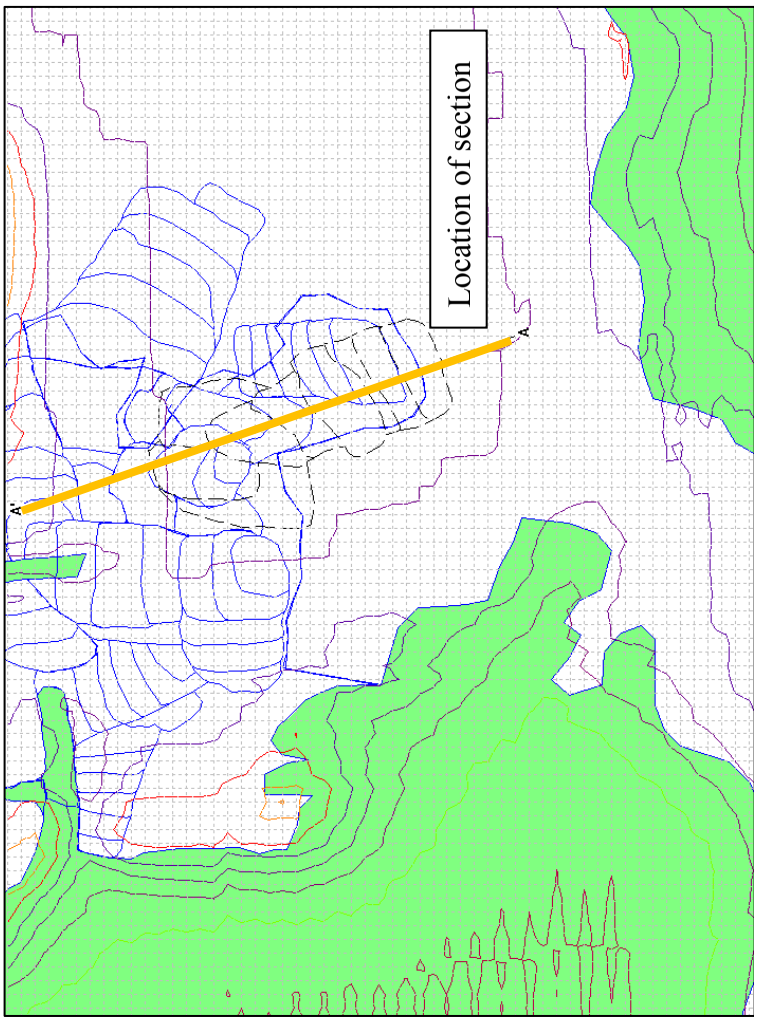
Step 38



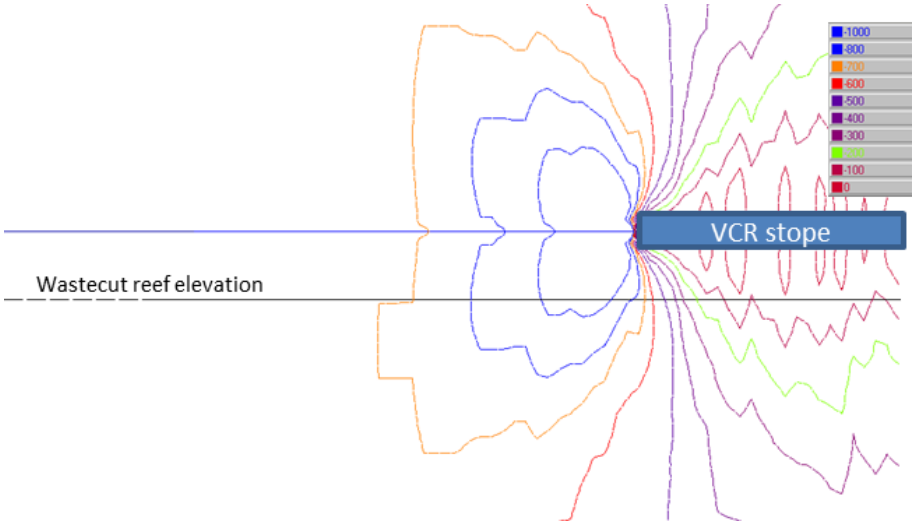
Step 41



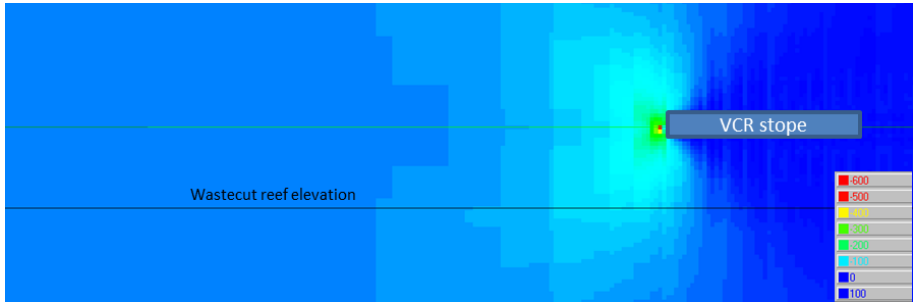
Step 47



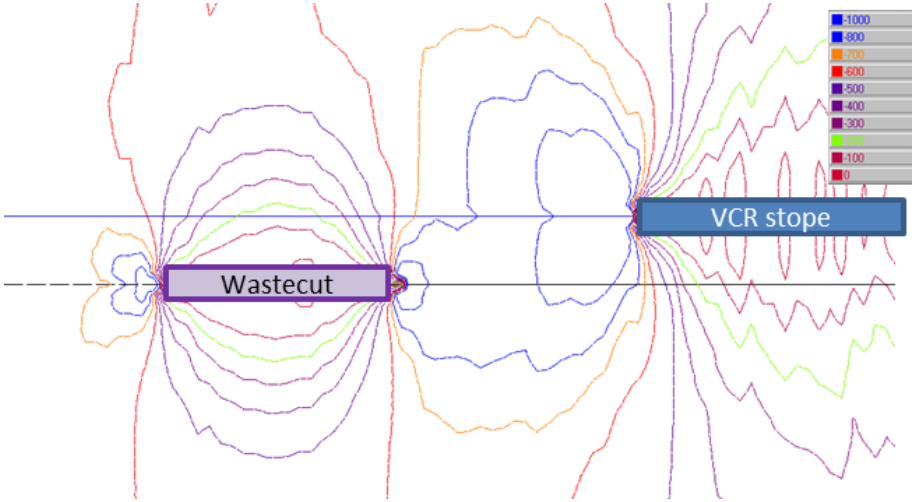
Location of section on waste cut elevation



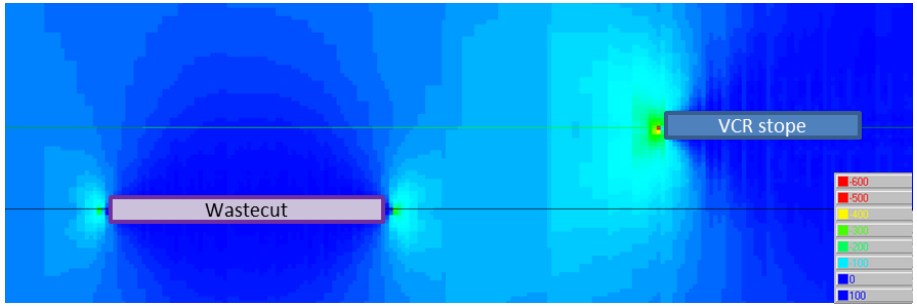
Contour plot of Step 23



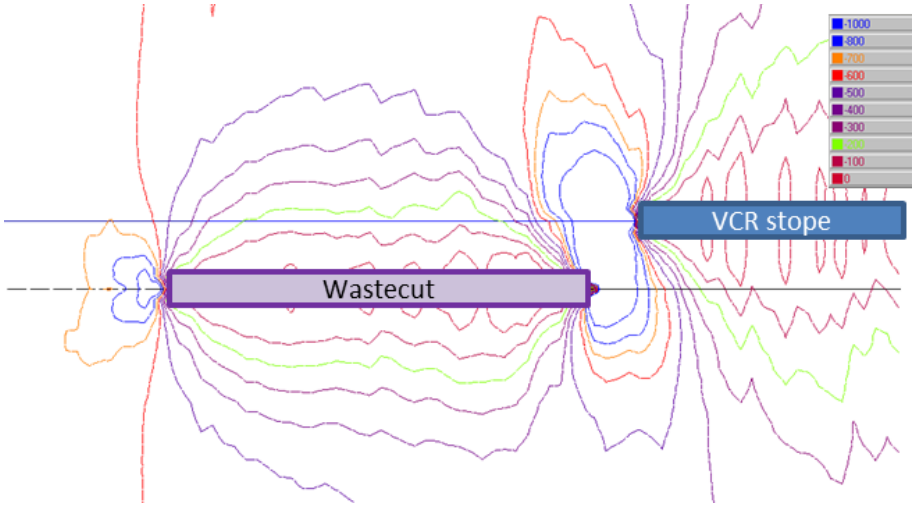
Contour map of Step 23



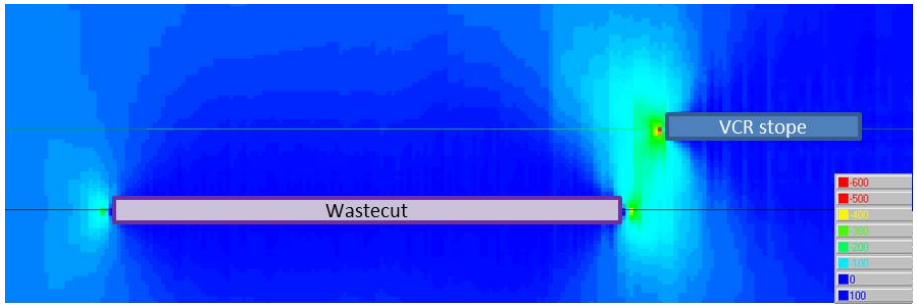
Contour plot of Step 28



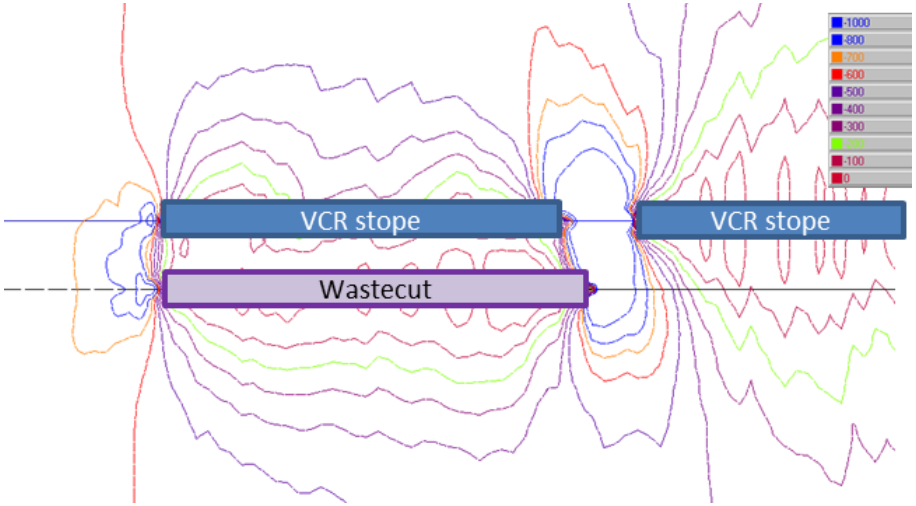
Contour map of Step 28



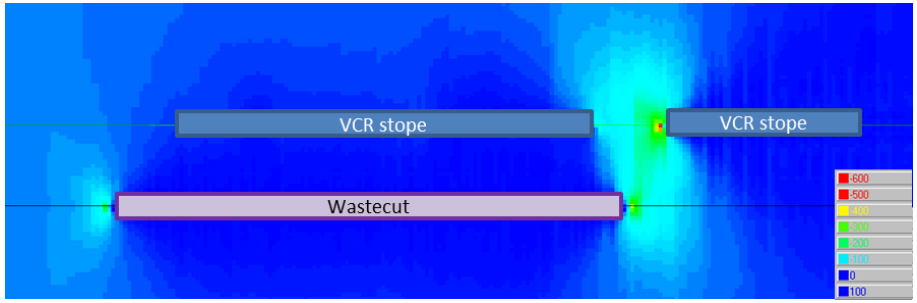
Contour plot of Step 32



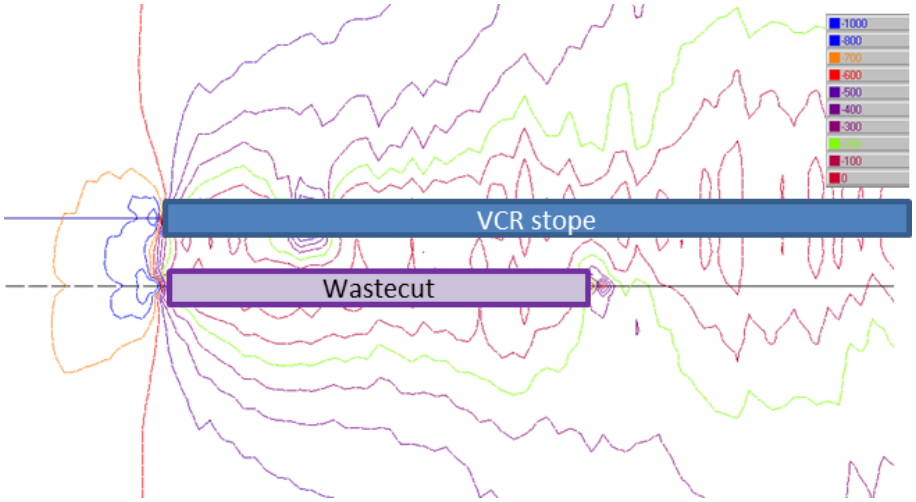
Contour map of Step 32



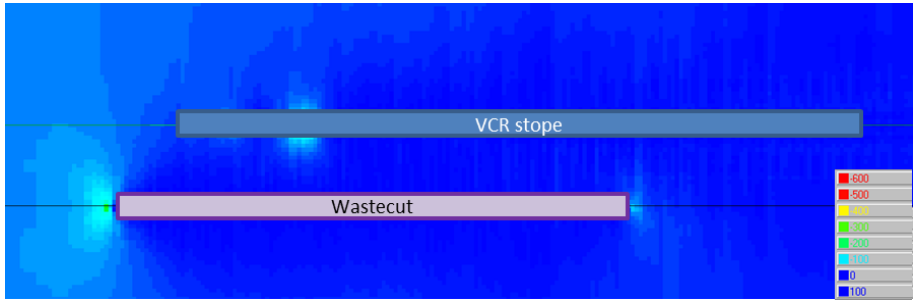
Contour plot of Step 38



Contour map of Step 38



Contour plot of Step 48

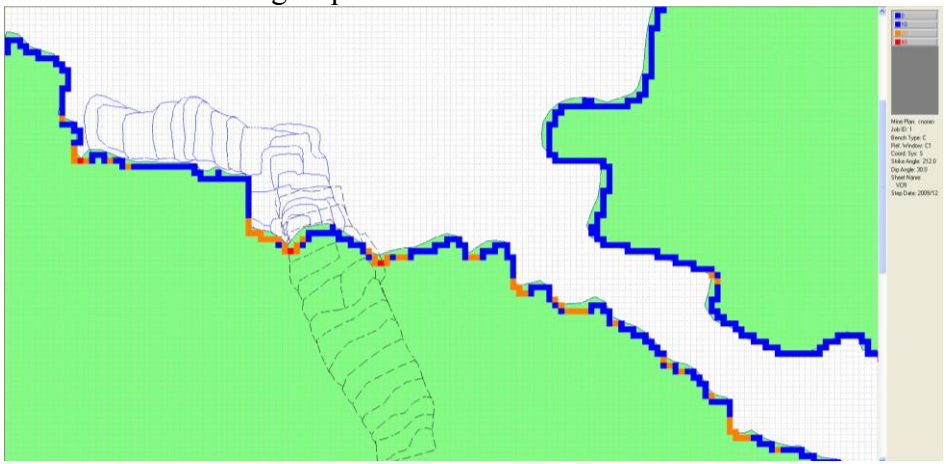


Contour map of Step 48

Appendix C : Numerical Modelling of VC20-31

Model Setup:
Grid size: 2 m
Youngs modulus: 60 GPa
Friction angle: 30 degrees
Poissons ratio: 0.27
VRS: ZZ -0.03 / m
XX;YY : ZZ 0.5

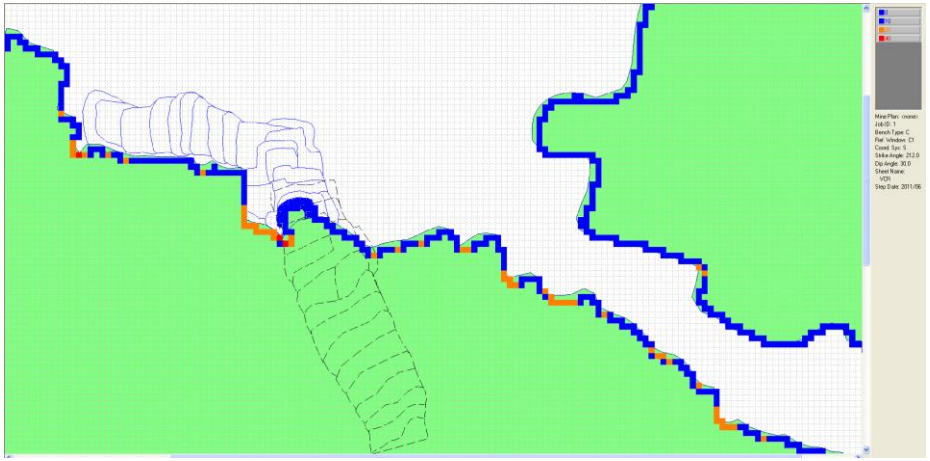
On Reef VCR Mining steps:



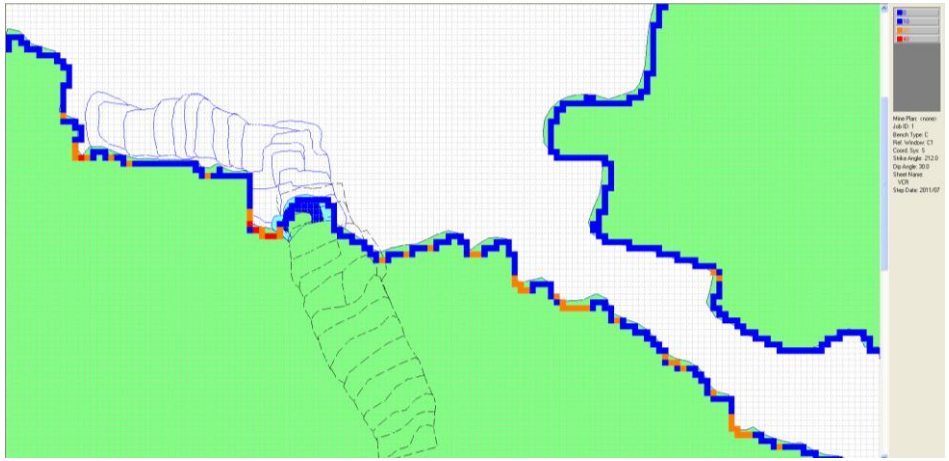
Step 1



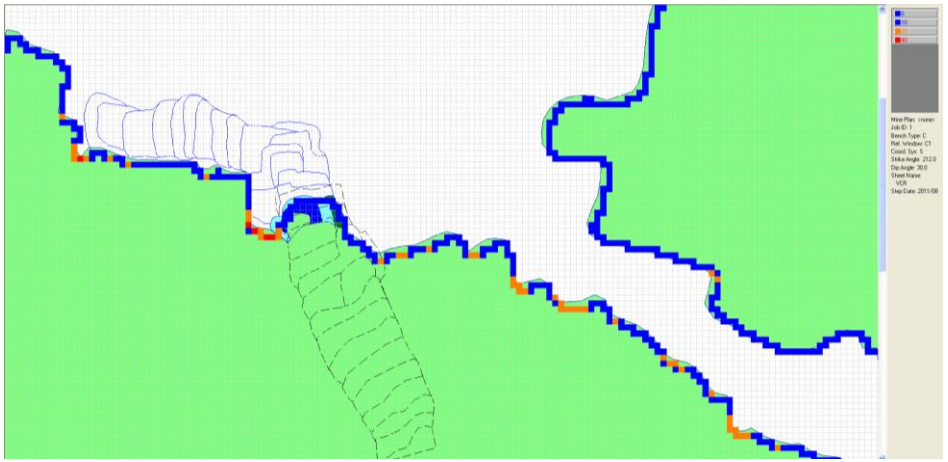
Step 18



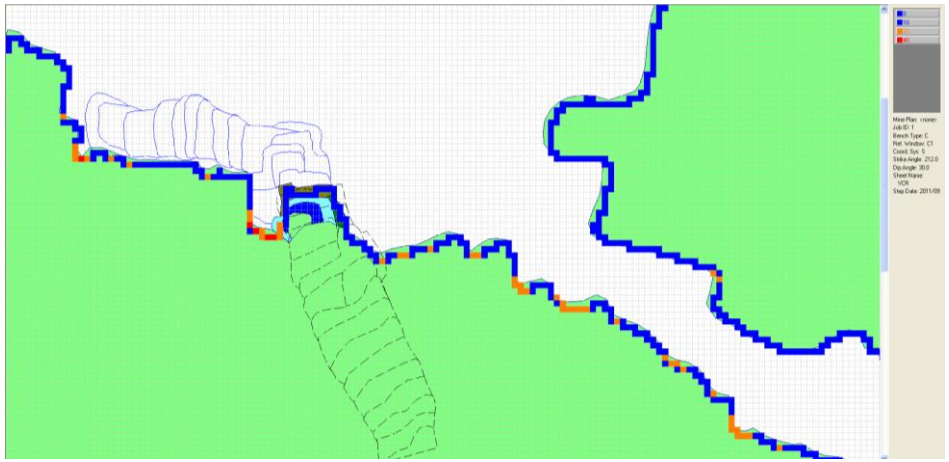
Step 19



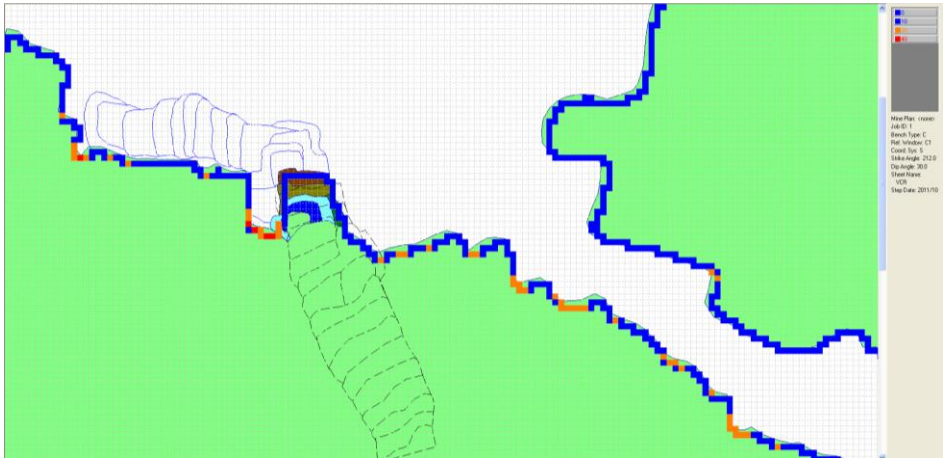
Step 20



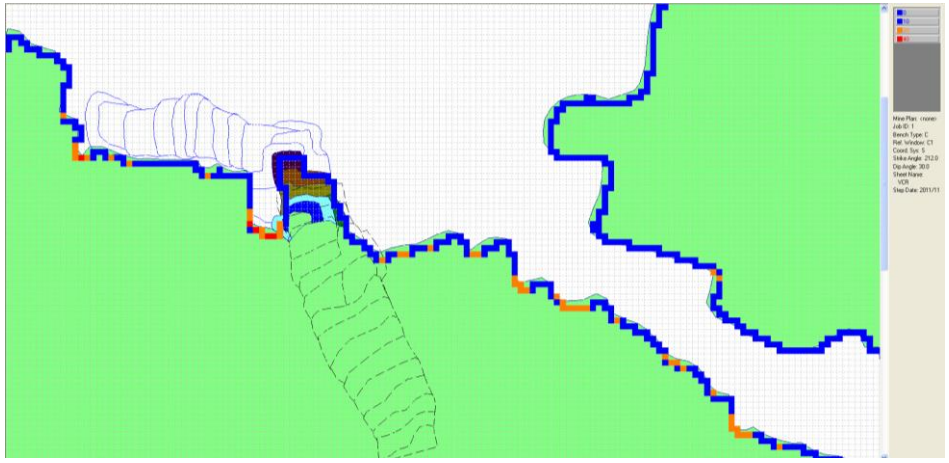
Step 21



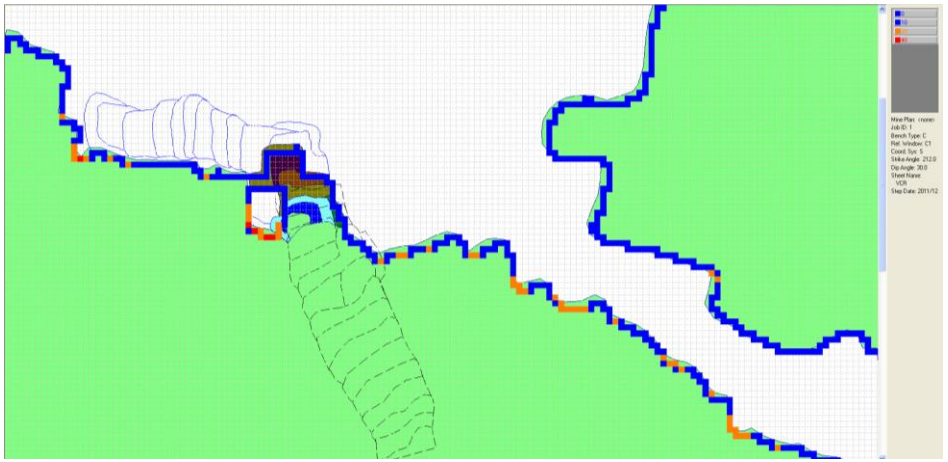
Step 22



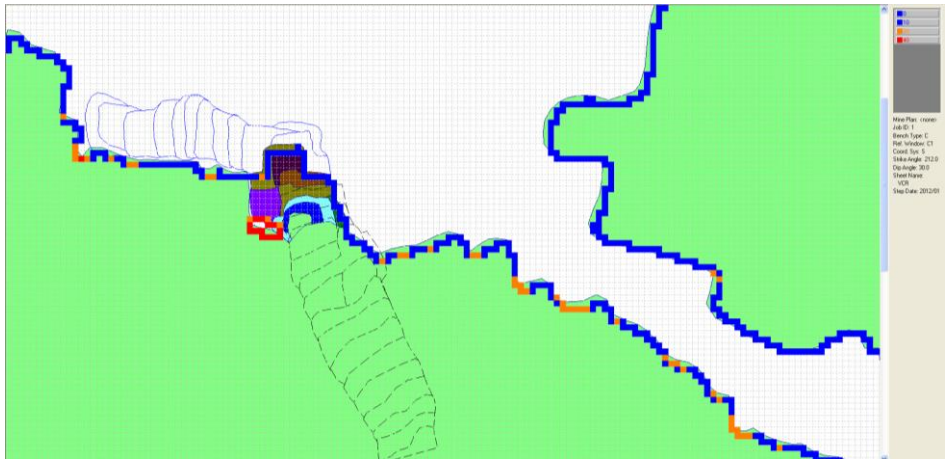
Step 23



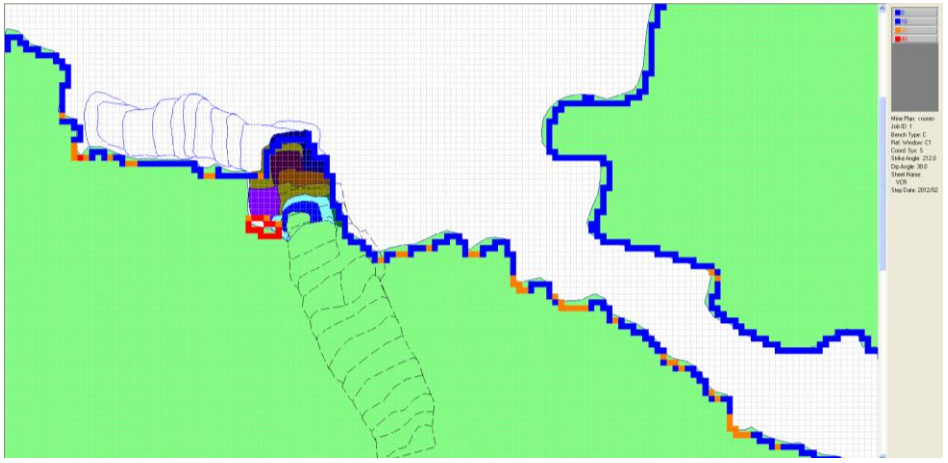
Step 24



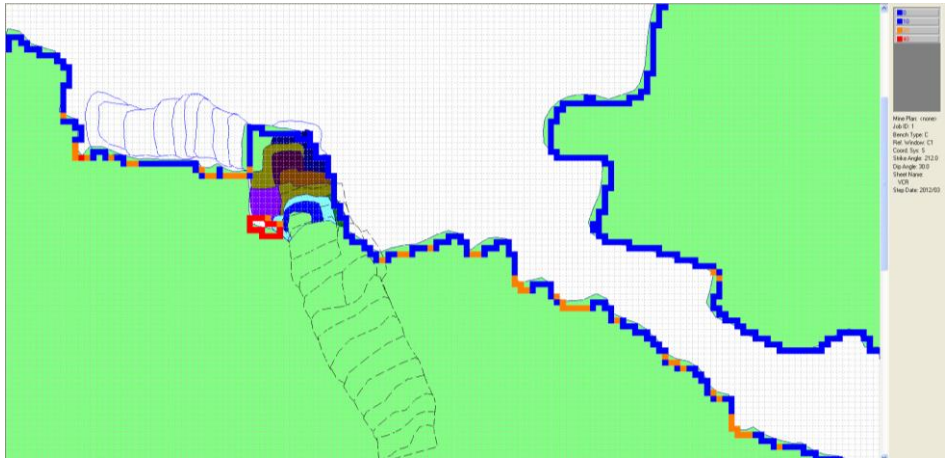
Step 25



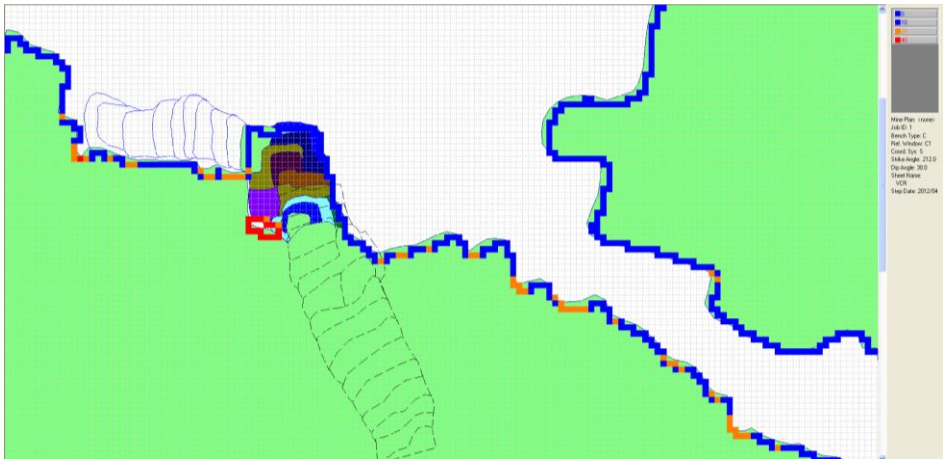
Step 26



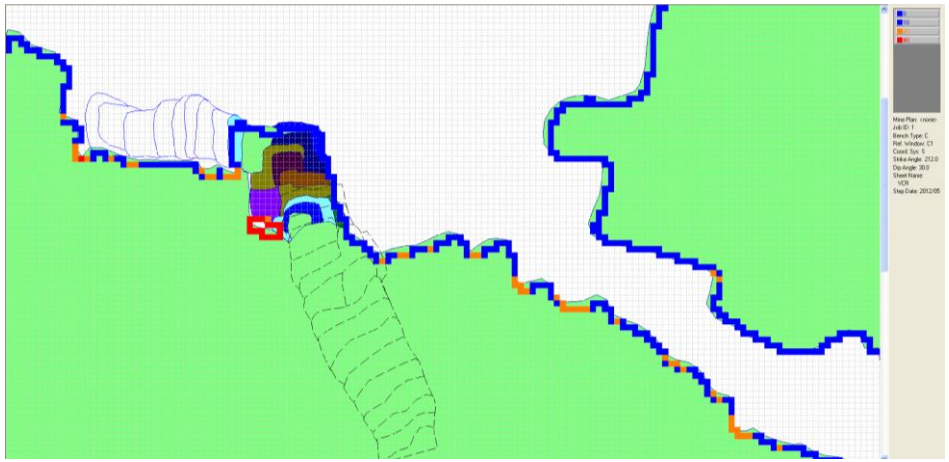
Step 27



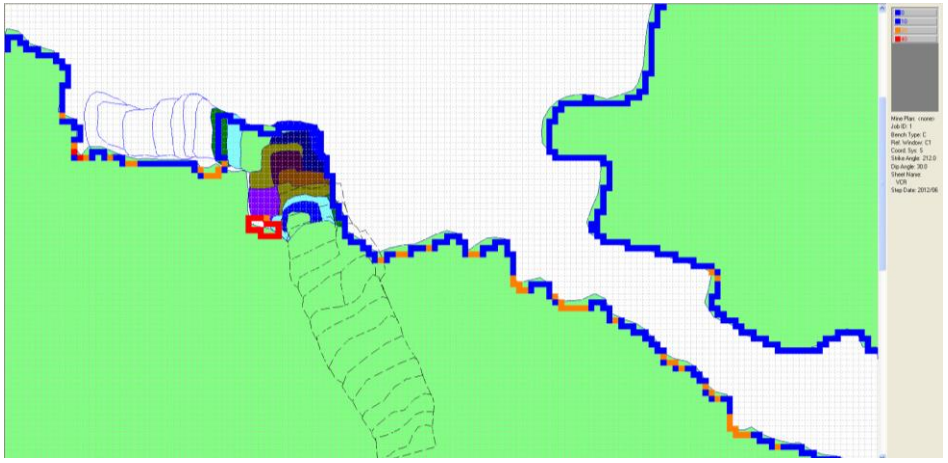
Step 28



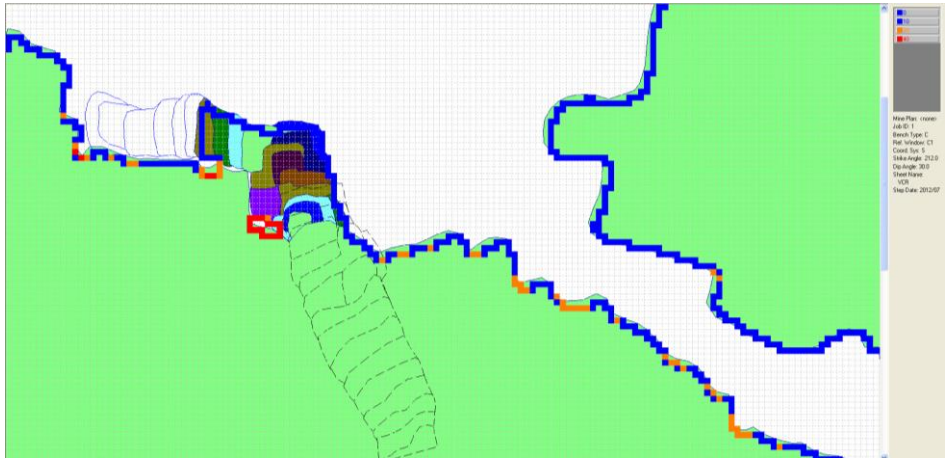
Step 29



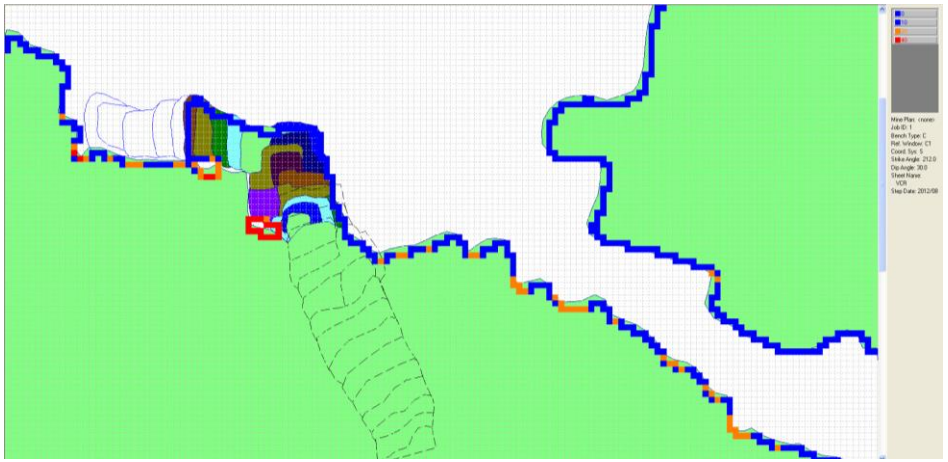
Step 30



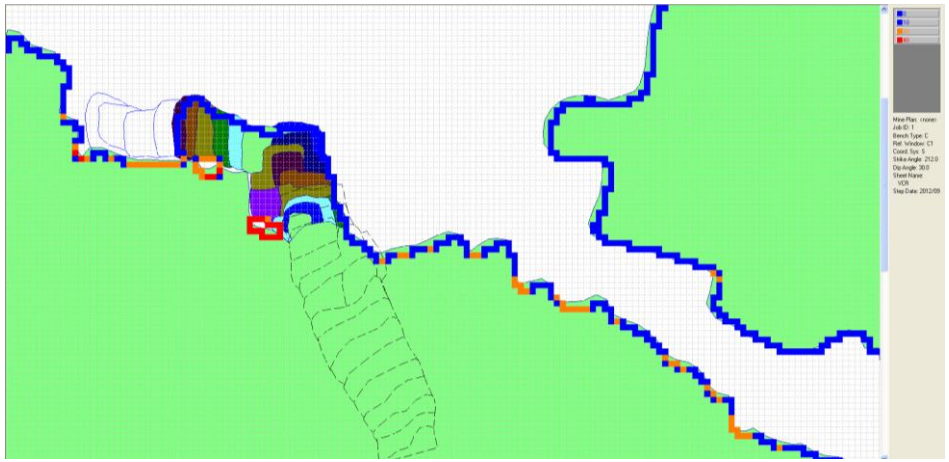
Step 31



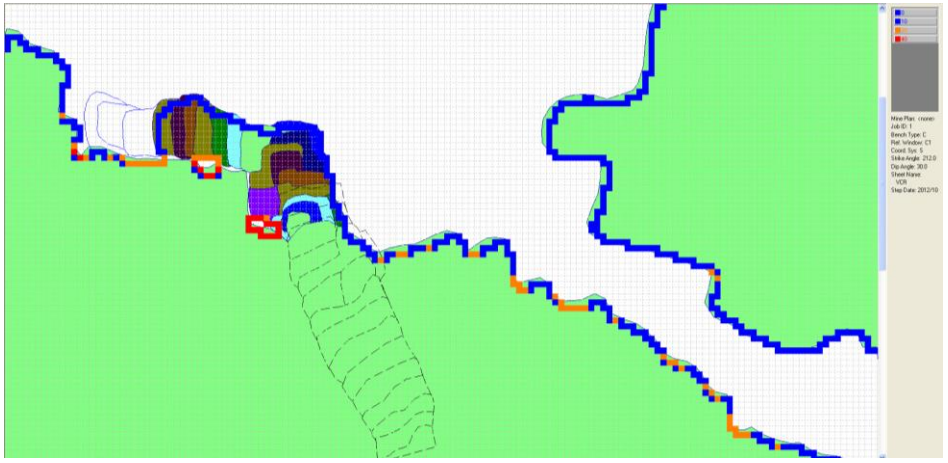
Step 32



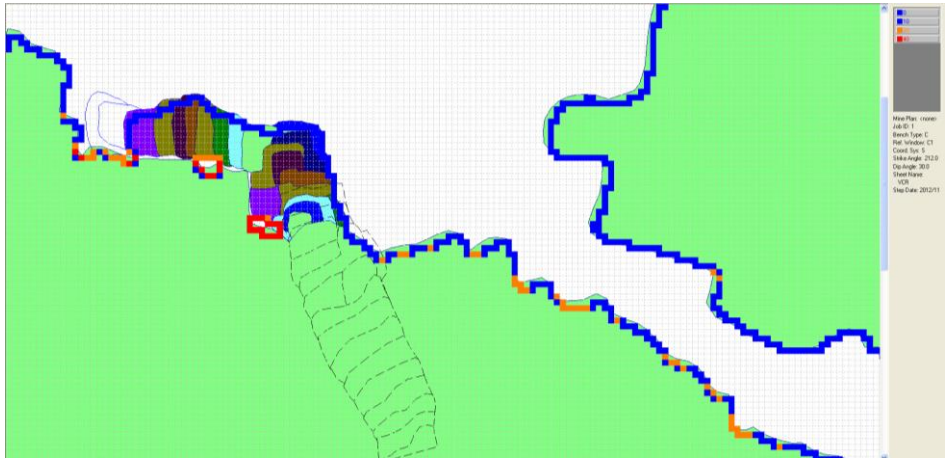
Step 33



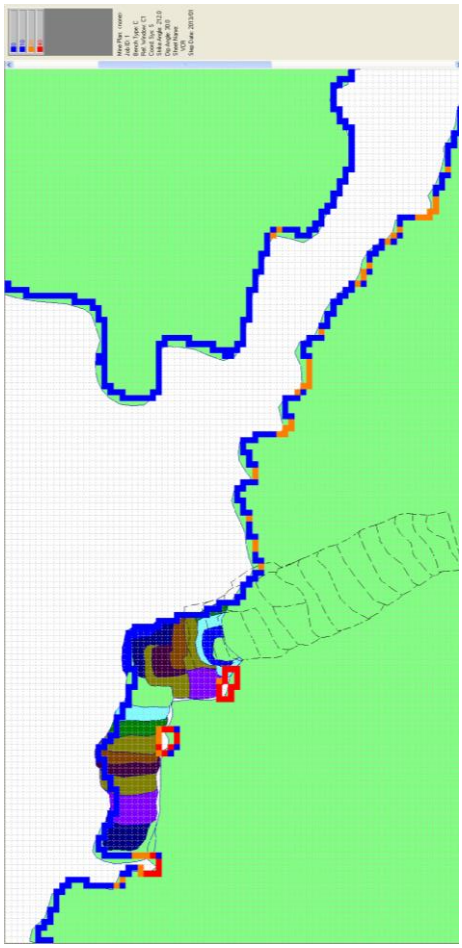
Step 34



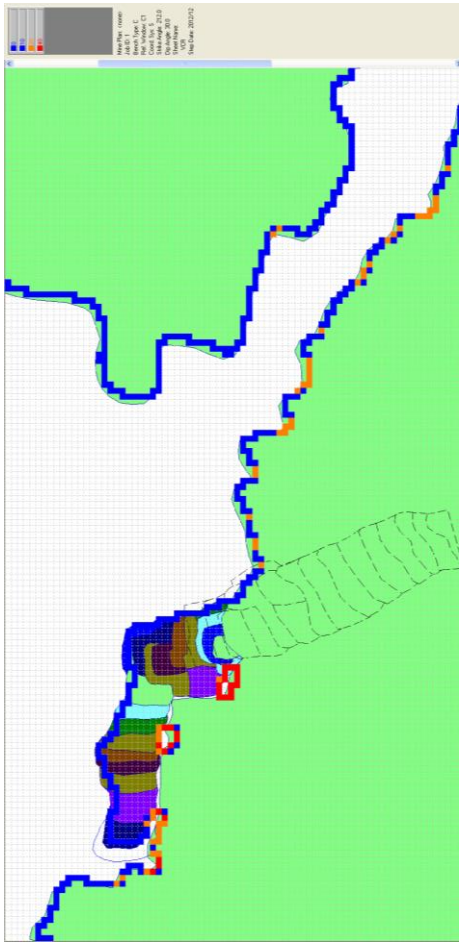
Step 35



Step 36

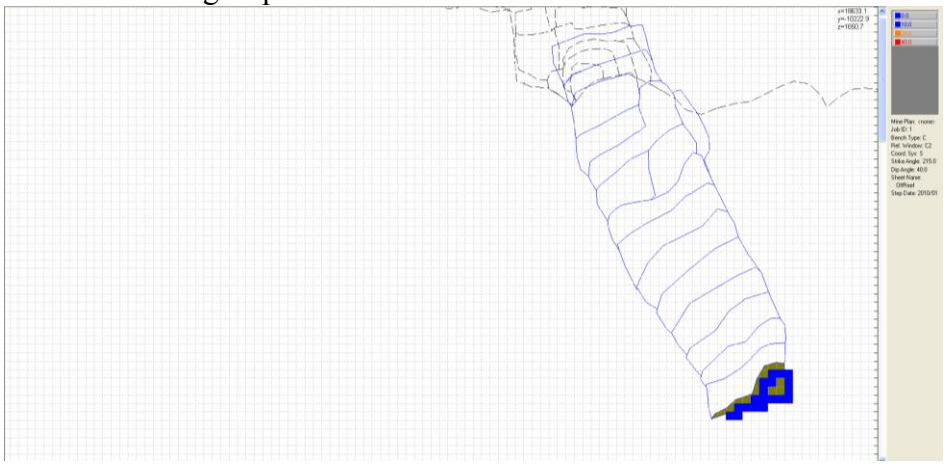


Step 38



Step 37

Off Reef Mining steps:



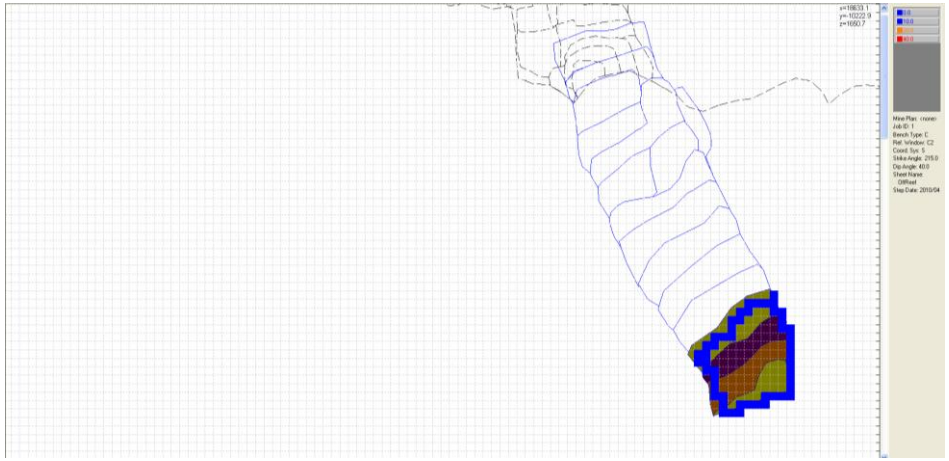
Step 2



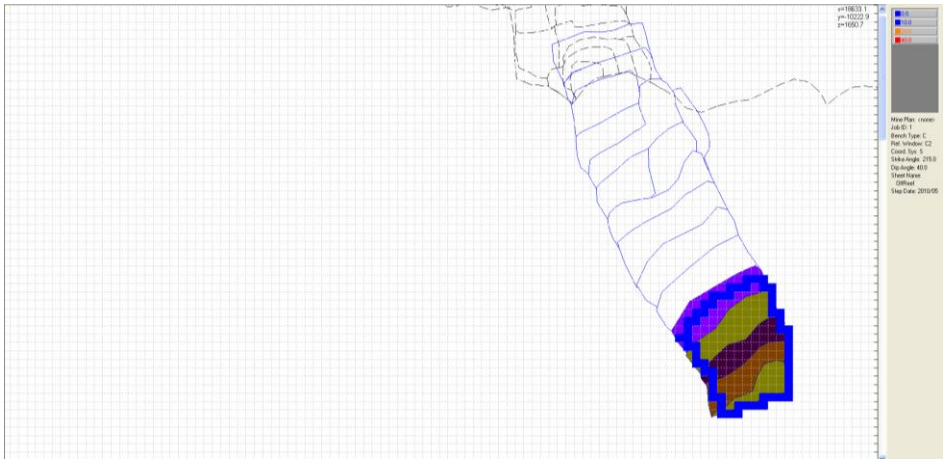
Step 3



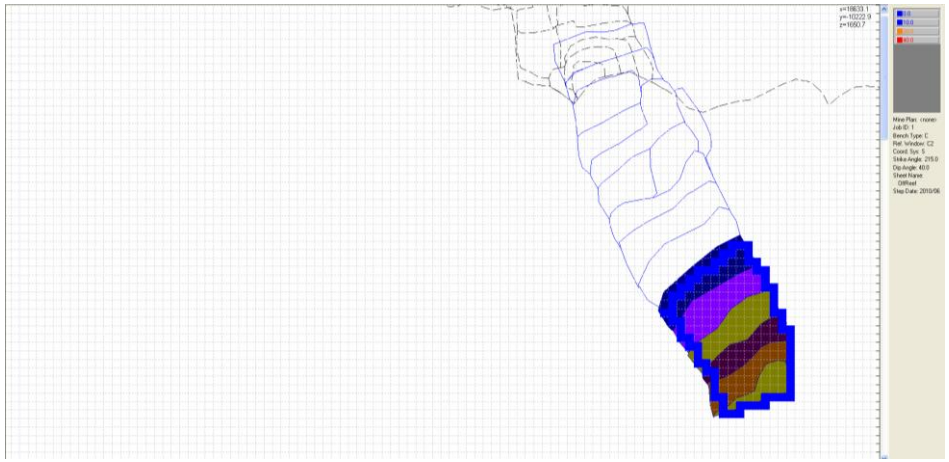
Step 4



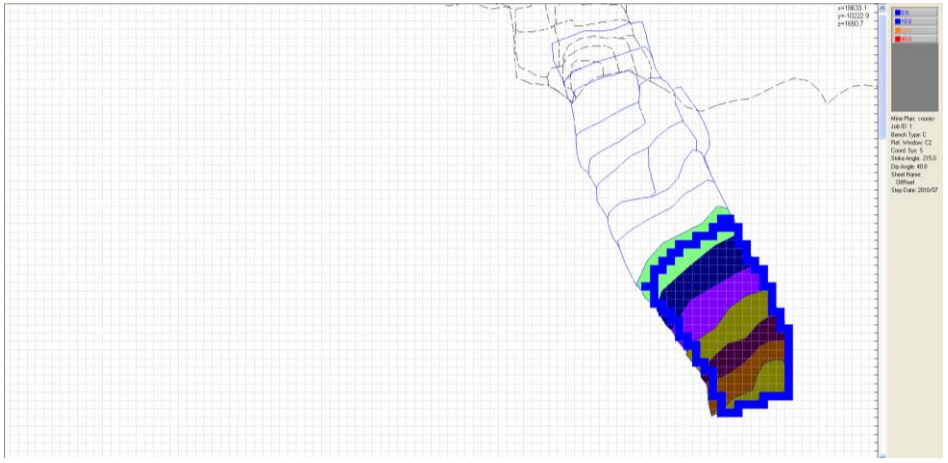
Step 5



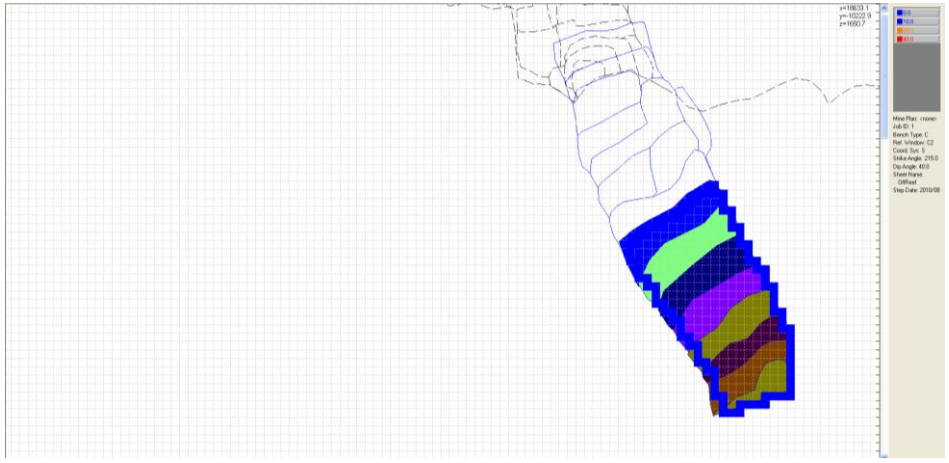
Step 6



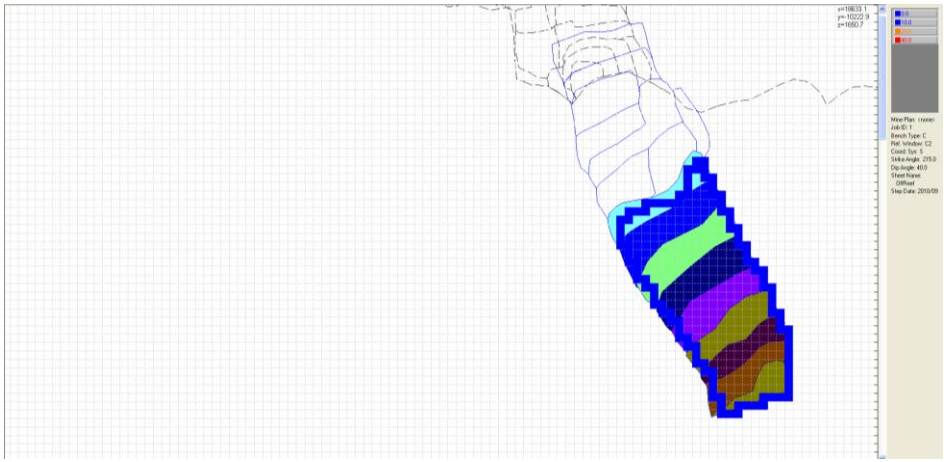
Step 7



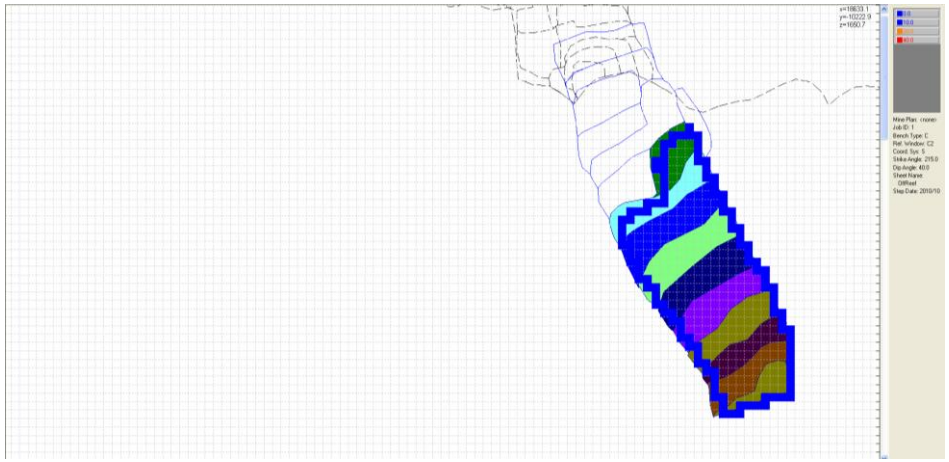
Step 8



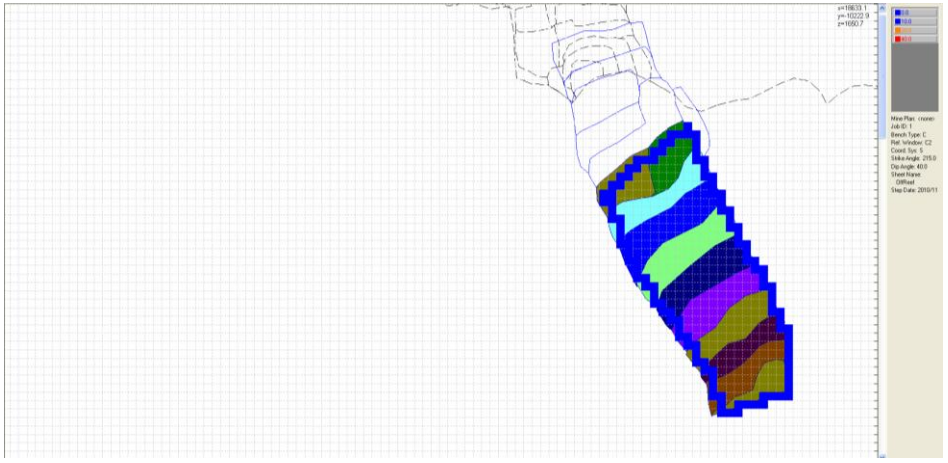
Step 9



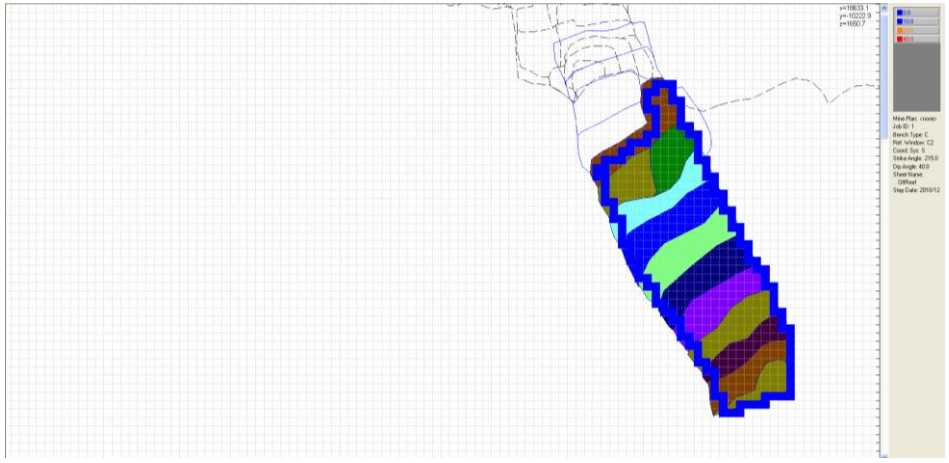
Step 10



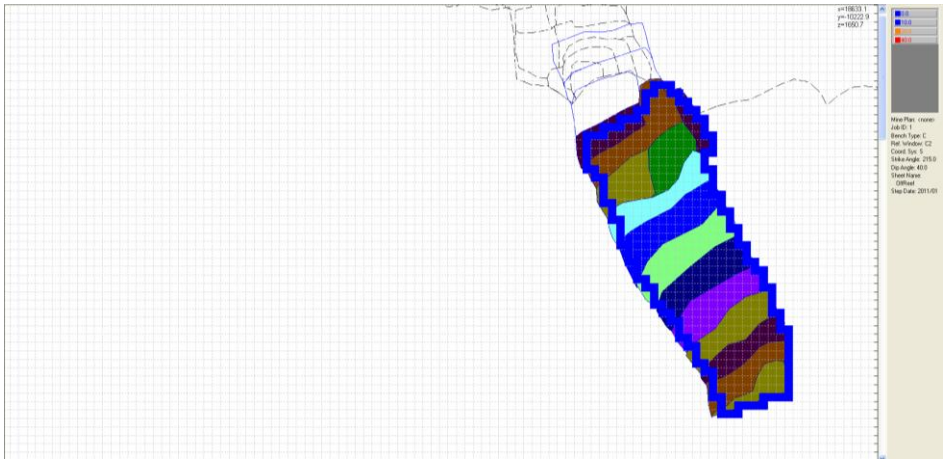
Step 11



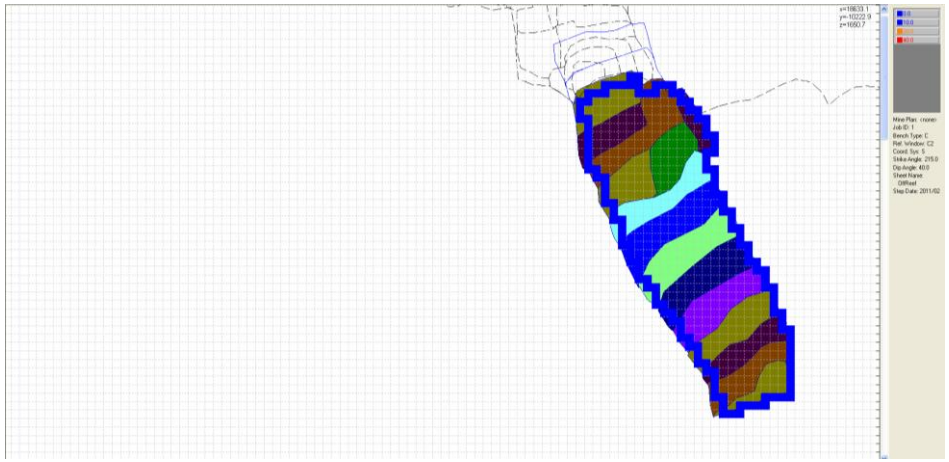
Step 12



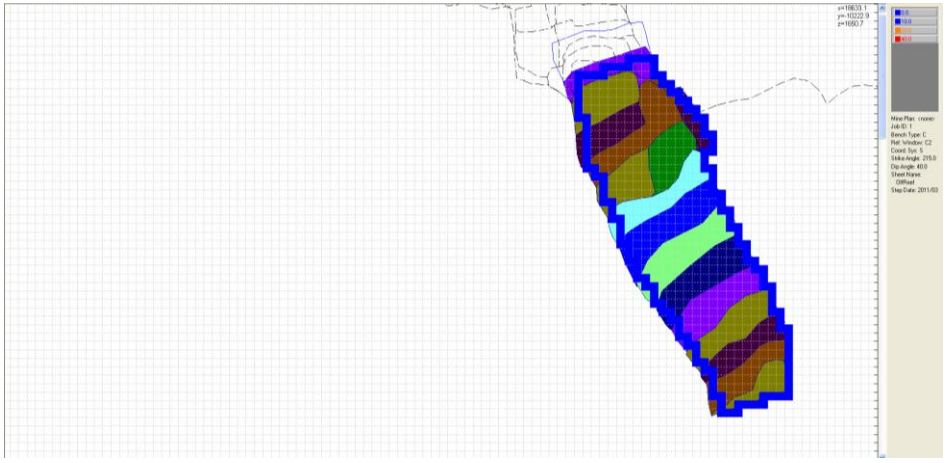
Step 13



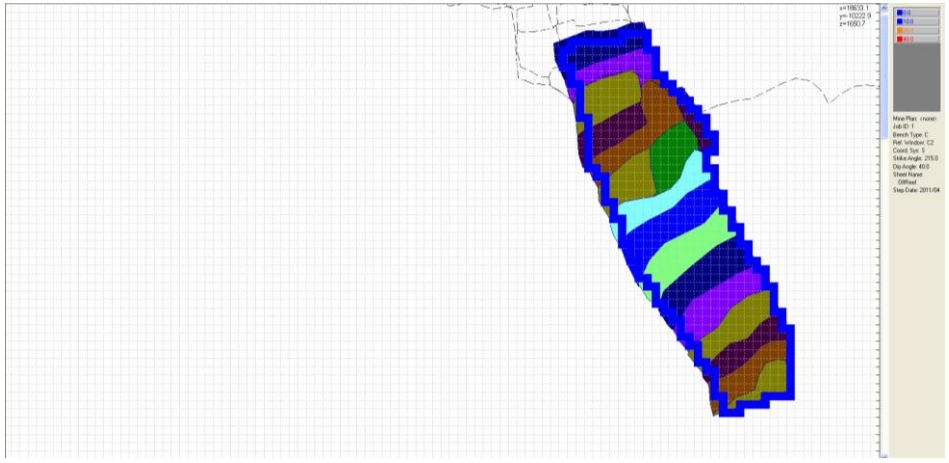
Step 14



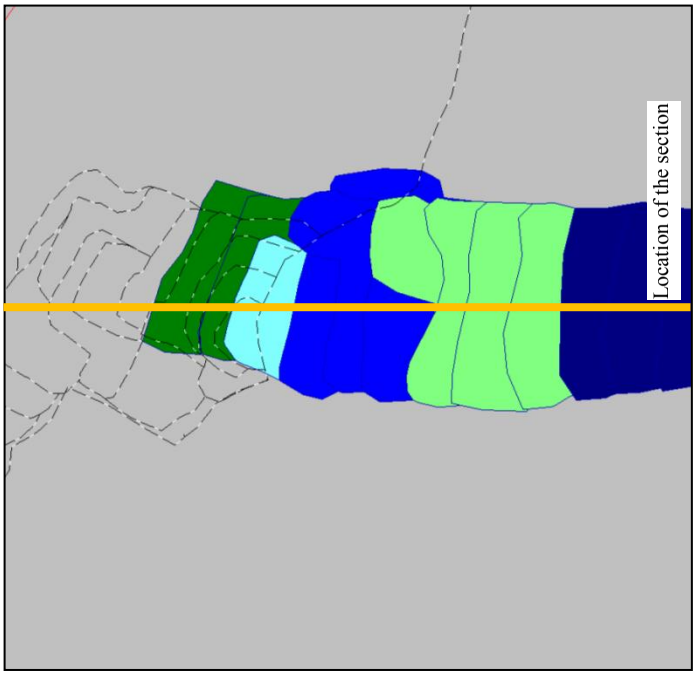
Step 15



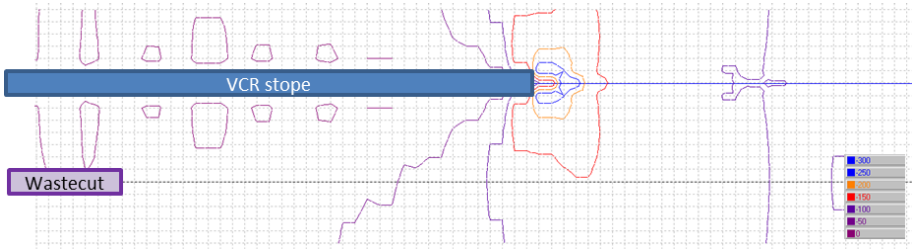
Step 16



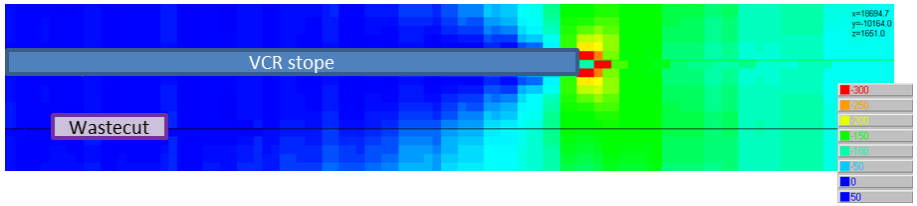
Step 17



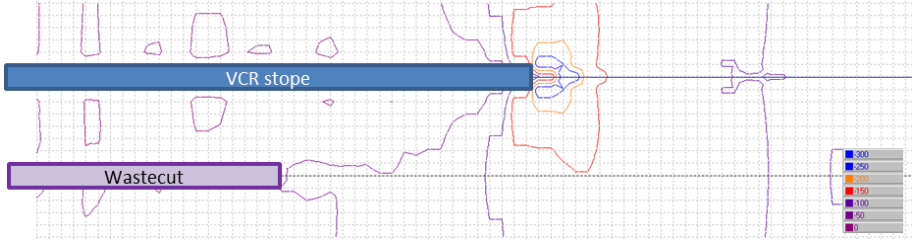
Location of the section on the wastecut elevation



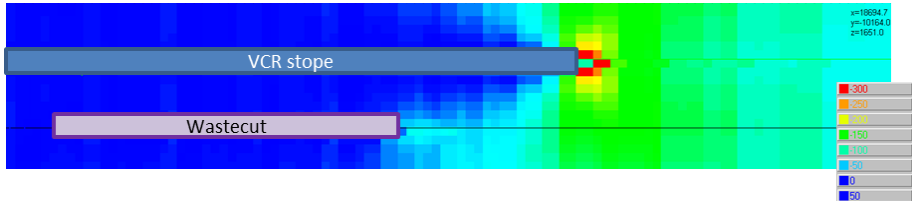
Contour plot of Step 7



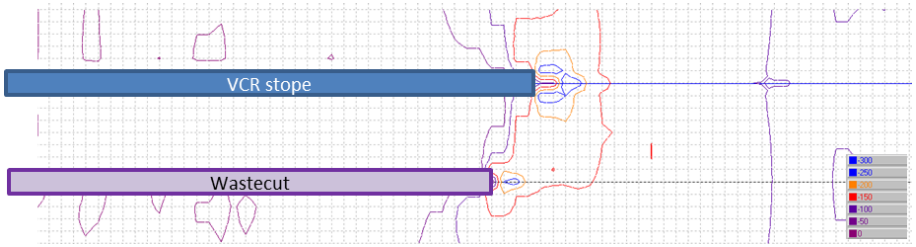
Contour map of Step 7



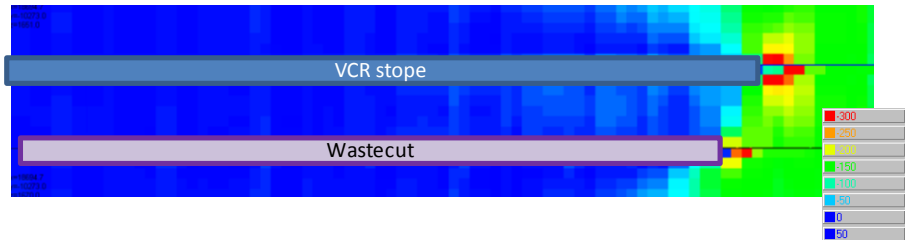
Contour plot of Step 11



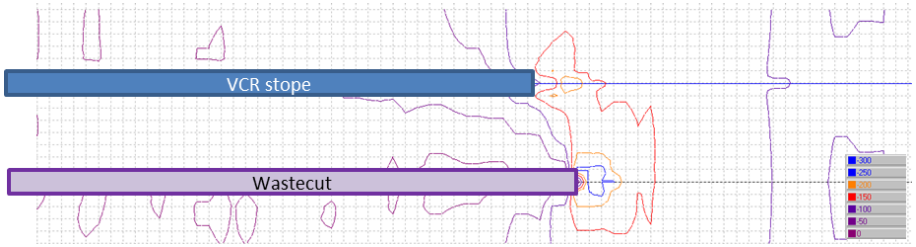
Contour map of Step 11



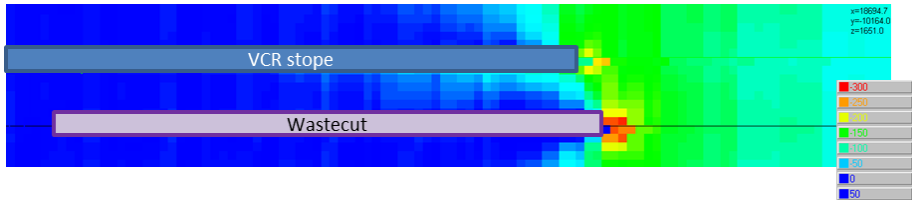
Contour plot of Step 14



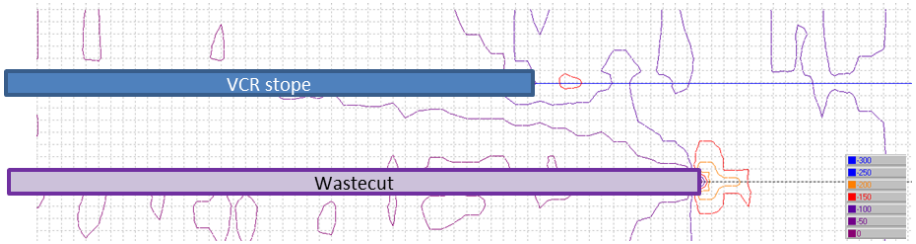
Contour map of Step 14



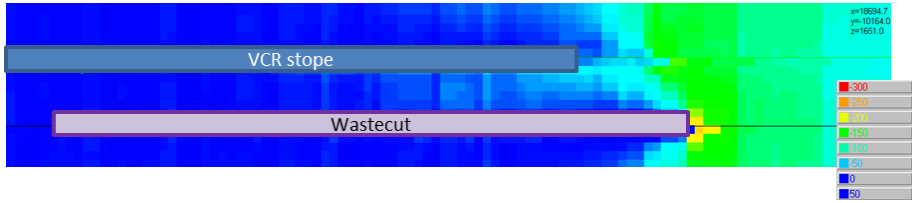
Contour plot of Step 15



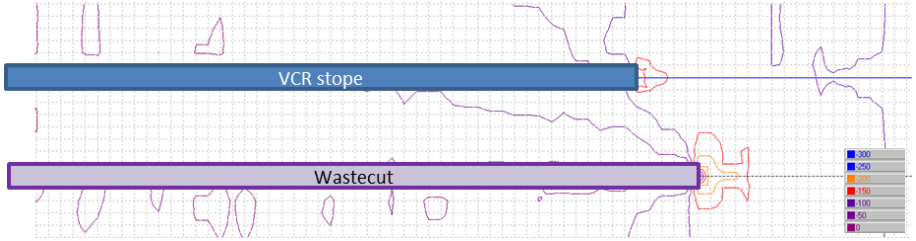
Contour map of Step 15



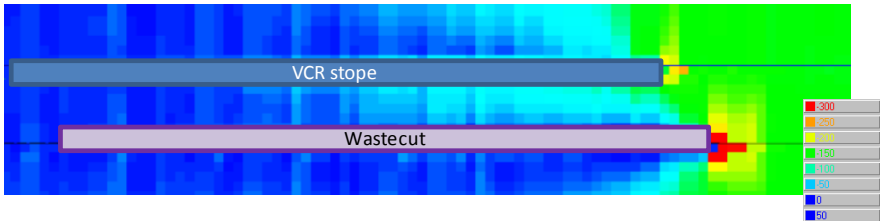
Contour plot of Step 17



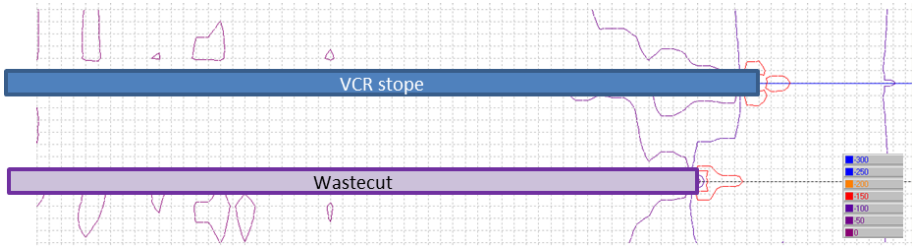
Contour map of Step 17



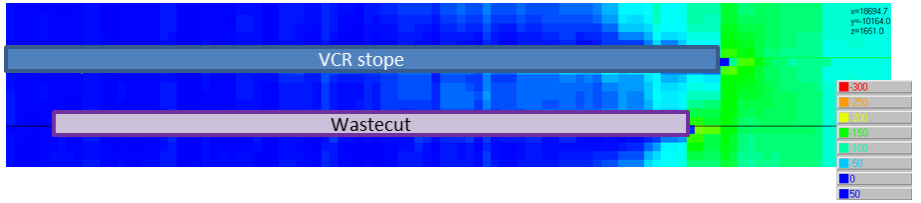
Contour plot of Step 19



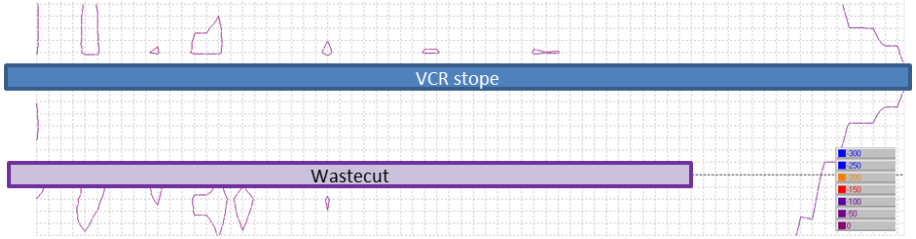
Contour map of Step 19



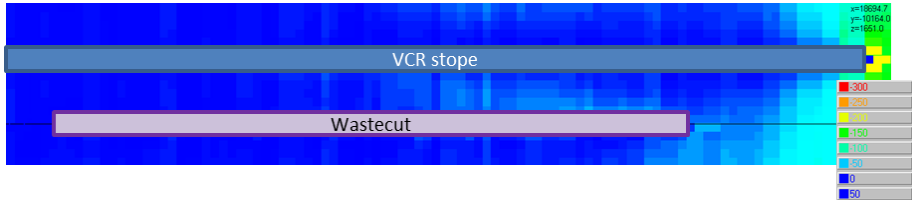
Contour plot of Step 23



Contour map of Step 23



Contour plot of Step 29



Contour map of Step 29